A Membrane-based Flat-plate Liquid Desiccant Dehumidification Air-conditioning System

Hongyu Bai

B.Eng Architectural Environment Engineering

8th August 2019

Thesis submitted in partial fulfilment of the requirement leading to the award of

Doctorate of Philosophy in Building Technology

Table of Contents

Table of Contents i

Abstract vii

Acknowledgements ix

Publication Lists x

List of Figures xii

List of Tables xix

Nomenclature xxi

Chapter 1: Introduction 1

1.1 Research background 1

1.2 Research aim and objectives 7

1.3 Thesis structure 8

Chapter 2: Literature Review 10

2.1 Introduction 10

2.2 Dehumidifier 11

2.2.1 Direct contact type dehumidifier 11

2.2.1.1 Adiabatic type 11

2.2.1.2 Internally cooled type 14

2.2.2 Membrane-based type dehumidifier 20

2.2.2.1 Flat-plate type 21

2.2.2.2 Hollow-fiber type 32

2.3 Regenerator 41

2.3.1 Direct contact type regenerator 41

2.3.2 Membrane-based type regenerator 48

2.4 The complete membrane-based dehumidification system 51

2.5 Desiccant and membrane materials 56
2.5.1 Desiccant materials 56
2.5.1.1 Halide salts 57
2.5.1.2 Organic acid 58
2.5.1.3 Mixed and composite desiccant 59
2.5.2 Membrane materials 62
2.6 Mathematical modelling methods 65
2.6.1 Simplified method 65
2.6.2 Effectiveness NTU ($\varepsilon - NTU$) method 69
2.6.3 Finite difference method 73
2.6.4 Conjugate heat and mass transfer method 78
2.7 Summary 85
Chapter 3: Investigation of a membrane-based flat-plate liquid desiccant dehumidifier 91
3.1 Introduction 91
3.2 Numerical modelling 92
3.2.1 Governing equations 92
3.2.1.1 Solution side governing equations 93
3.2.1.2 Air side governing equations 96
3.2.2 Normalization of governing equations 98
3.2.3 Boundary conditions 99
3.2.3.1 Heat transfer boundary conditions on membrane surfaces 100
3.2.3.2 Mass transfer boundary conditions on membrane surfaces 100
3.2.4 Air and solution property calculations 100
3.2.5 Simulation procedure 104
3.2.5.1 Discretization of governing equations 104
3.2.5.2 Numerical solving procedure 105

3.3 Performance evaluation indices 107
3.4 Experimental set-up 107
3.5 Numerical model validation 111
3.6 Results and discussion 114
3.6.1 Temperature and humidity (concentration) fields 114
3.6.2 Effects of dimensionless parameters 116
3.6.3 Effects of solution properties 121
3.6.4 Effects of inlet air condition 127
3.7 Summary 133
Chapter 4: Investigation of a membrane-based flat-plate liquid desiccant regenerator 135
4.1 Introduction 135
4.2 Numerical modelling 136
4.2.1 Governing equations 136
4.2.2 Normalization of governing equations 137
4.2.3 Boundary conditions 137
4.2.3.1 Heat transfer boundary conditions on membrane surfaces 137
4.2.3.2 Mass transfer boundary conditions on membrane surfaces 138
4.2.4 Air and solution property calculations 138
4.2.5 Simulation procedure 139
4.2.5.1 Discretization of governing equations 139
4.2.5.2 Numerical solving procedure 139
4.3 Performance evaluation indices 140
4.3.1 Solution side effectiveness for regenerator 140
4.3.2 Solution side moisture flux rate (MFR) 141
4.3.3 Solution temperature decrease rate (TDR) 142
4.4 Experimental set-up 142
4.5 Numerical model validation 143

4.6 Results and discussion 145
4.6.1 Temperature and humidity fields 145
4.6.2 Effects of dimensionless parameters 146
4.6.3 Effects of desiccant solution properties 153
4.6.4 Effects of air properties 158
4.7 Summary 161
Chapter 5: Investigation of a complete membrane-based flat-plate liquid desiccant dehumidification system 163
5.1 Introduction 163
5.2 Numerical modelling 164
5.2.1 Dehumidifier and regenerator 165
5.2.1.1 Governing equations 165
5.2.1.2 Boundary conditions 166
5.2.2 Heat exchangers 166
5.2.3 Simulation procedure 168
5.3 Performance evaluation indices 170
5.3.1 Effectiveness for the complete system 170
5.3.2 Moisture flux rate MFR 170
5.3.3 Total cooling output $Qcooling$ 171
5.3.4 Coefficient of performance COP 171
5.4 Experimental set-up 172
5.5 Numerical model validation 174
5.6 Results and discussion 177
5.6.1 Temperature and humidity (concentration) fields 177
5.6.2 Effects of dimensionless parameters 180
5.6.2.1 Effects of dehumidifier side $NTUde$ 180
5.6.2.2 Effects of regenerator side $NTUre$ 186

5.6.2.3 Effects of mass flow rate ratio $m*$ 190
5.6.3 Effects of solution inlet property 194
5.7 Summary 198
Chapter 6: Parametric analysis of mixed LiCl-$CaCl_2$ solution and optimum mixing ratio selection 200
6.1 Introduction 200
6.2 Mixed liquid desiccant properties calculation 201
6.3 Numerical modelling 204
6.4 Performance evaluation indices 204
6.4.1 Effectiveness of dehumidifier 204
6.4.2 Moisture flux rate 205
6.4.3 Coefficient of performance (COP) 205
6.5 Experimental set-up 206
6.6 Numerical model validation 207
6.7 Results and discussion 209
6.7.1 Specific humidity of the mixed desiccant solution 209
6.7.2. Impact of the mixed solution property on cooling effect 212
6.7.3 Impact of the mixed solution property on dehumidification effect 214
6.7.4 Impact of the solution mixing ratio on system COP 220
6.8 Summary 224
Chapter 7: Conclusions and future work 226
7.1 Introduction 226
7.2 Main conclusions 226
7.3 Recommendations for future work 231
References 233
Appendices 257

Appendix A: Normalization Methods for Governing Equations of Numerical Modelling 257

Appendix B: Matlab Script for Dehumidifier or Regenerator Simulation 261

Appendix C: Matlab Script for the Complete System Simulation.....266

Appendix D: Matlab Script for the Mixed LiCl-$CaCl_2$ Solution Properties Calculation...275

Abstract

The enormous increase of energy consumption for building indoor environment, specifically for indoor thermal comfort has brought numerous state-of-art technologies as alternatives to the traditional vapour compression air-conditioning system. The membrane-based liquid desiccant dehumidification has gain wide attention for good feasibility, high energy efficiency and no desiccant carry-over problem. As a matter of fact, the membrane-based liquid desiccant system is still under research and development stage with limited number of literatures.

The main aim of this thesis is to develop and evaluate a novel membrane-based liquid desiccant dehumidification air-conditioning system. The research scope mainly covers system design, numerical modelling, simulation programme development, experimental testing and system performance evaluation. The first step in the study is to develop a numerical model for a cross flow flat-plate type membrane-based dehumidifier and validate model by experimental data. Following this, a single regenerator with the similar structure as the dehumidifier is investigated numerically and experimentally. With models for single dehumidifier and regenerator, a numerical model for a more realistic complete membrane-based dehumidification system, which consists of two membrane-based heat and mass contractors, three heat exchangers, cooling water and hot water supply units is developed and validated experimentally. Finally, influences of using mixed LiCl-$CaCl_2$ solution with different mixing ratios on the system performance are analysed.

The results show that the number of heat transfer unit NTU and mass flow rate ratio m^* have the most significant effects on the performance of the dehumidifier and regenerator, and their effects are interacted with each other. The increasing gradients of dehumidifier and regenerator effectiveness hardly change when NTU and m^* exceed their critical values NTU_{crit} and m^*_{crit}, which are 4 and 1 for the dehumidifier, and 4 and 2 for the regenerator. The dehumidifier

sensible effectiveness is insensitive to both solution inlet temperature T_{sol} and concentration C_{sol}, while the latent effectiveness increases significantly with C_{sol} at a high solution temperature. The dehumidifier shows broad adaptability in different weather conditions by providing relative stable state supply air, in particular at high NTU, while neither $T_{air,in}$ nor $W_{air,in}$ has remarkable influence on the regenerator performance, though the solution re-concentration ability can be enhanced slightly by applying drier and warmer air. Regenerator can benefit from increased solution temperature as enhanced re-concentration (0.8% increase of moisture flux rate MFR) and cooling effects (13.7% increase of temperature decrease rate TDR). However this means more cooling energy is required for the high temperature desiccant solution. For the complete system, NTU_{de} and m^* have the most considerable impact on the overall system effectiveness. The critical values of m^* vary under different NTUs, and it is preferable to keep m^* at or below the critical values as further increasing solution flow rate would reduce the system coefficient of performance COP. The latent cooling output Q_{lat} is normally two times higher than the sensible cooling output Q_{sen} under all circumstances meaning further cooling, such as indirect evaporative cooling is required after the dehumidification. Compared with the pure LiCl solution system, the mixed solution system COP can be raised up to 30.23% by increasing $CaCl_2$ content. The optimum mixing ratio varies with the solution concentration. For the LiCl-$CaCl_2$ solution, the highest COPs appear at the mixing ratios of 3:1, 2:1 and 1:1 for 20%, 30% and 40% concentrations respectively.

Acknowledgements

I would like to express my deep appreciation to my supervisors Dr. Jie Zhu and Prof. Yuying Yan for their help and inspiration throughout the project. Their enthusiasms towards the project were contagious and their guidance was invaluable, I really look forward to collaborate with them again.

This research would not have been possible without the technical support from the Marmont Laboratory, the Department of Architecture and Built Environment. Special mention goes to, Tony Gospel, Dave Oliver, Andrew Matthew and Jonny Moss for their professional and enthusiastic help and support with my experimental work. I am also grateful to my dear colleagues, especially Miss. Yuqi Pan and Mr. Ke Qu for discussing problems I encountered with me during my research.

Last but not the least, I would like to thank my family: my parents and grandparents for supporting me spiritually throughout the whole journey, and of course my girlfriend Yinglin Zhou, thank you for all the joys and treasured moments we shared together. You guys mean the world to me.

Publication Lists

Journal Publications

1. HY Bai, J Zhu, JZ Chu, XJ Chen, YY Yan, Influences of the mixed LiCl-$CaCl_2$ liquid desiccant solution on a membrane-based dehumidification system: parametric analysis and mixing ratio selection, Energy and Buildings, Volume 183, 2019, Pages 592-606.
2. JZ Chu, ZZ Chen, HY Bai, J Zhu, Experimental study of liquid to air membrane energy exchanger (LAMEE) performance by measuring its temperature fields, Thermal Science and Engineering Progress, Volume 10, 2019, Pages 163-168.
3. HY Bai, J Zhu, ZW Chen, JZ Chu, YW Liu, Performance evaluation of a membrane-based flat-plate heat and mass exchanger used for liquid desiccant regeneration, Applied Thermal Engineering, Volume 139, 2018, Pages 569-584.
4. HY Bai, J Zhu, ZW Chen, JZ Chu, State-of-art in modelling methods of membrane-based liquid desiccant heat and mass exchanger: A comprehensive review, International Journal of Heat and Mass Transfer, Volume 125, 2018, Pages 445-470.
5. XJ Chen, YH Su, D Aydin, HY Bai, H Jarimi, XX Zhang, S Riffat, Experimental investigation of a polymer hollow fibre integrated liquid desiccant dehumidification system with aqueous potassium formate solution, Applied Thermal Engineering, Volume 142, 2018, Pages 632-643.
6. HY Bai, J Zhu, ZW Chen, JZ Chu, Parametric analysis of a cross-flow membrane-based parallel-plate liquid desiccant dehumidification system: Numerical and experimental data, Energy and Buildings, Volume 158, 2018, Pages 494-508.
7. HY Bai, J Zhu, ZW Chen, LN Ma, RZ Wang, TX Li, Performance testing of a cross-flow membrane-based liquid desiccant dehumidification system, Applied Thermal Engineering, Volume 119, 2017, Pages 119-131.

8. ZW Chen, J Zhu, HY Bai, YY Yan, LZ Zhang, Experimental study of a membrane-based dehumidification cooling system, Applied Thermal Engineering, Volume 115, 2017, Pages 1315-1321.
9. ZW Chen, J Zhu, HY Bai, Performance assessment of a membrane liquid desiccant dehumidification cooling system based on experimental investigations, Energy and Buildings, Volume 139, 2017, Pages 665-679.

Conference Papers

1. JZ Chu, J Zhu, ZW Chen, HY Bai, Parametric study of a membrane based liquid desiccant dehumidifier by CFD model, The 8th International Conference on Compressors and Refrigeration 2017, Xi'an, China.
2. JZ Chu, ZW Chen, HY Bai, J Zhu, Experimental study of liquid to air membrane energy exchanger (LAMEE) performance by measuring its temperature field, The 3rd International Symposium of Fluid and Thermal Engineering 2017, Ningbo, China.
3. HY Bai, ZW Chen, HJ Xu, J Zhu, Theoretical analysis of a membrane-based cross-flow liquid desiccant system, International Heat Transfer Symposium (IHTS) and Heat Powered Cycles (HPC) Conference 2016, Nottingham, United Kingdom.
4. ZW Chen, HY Bai, ZH Ye, J Zhu, Experimental study of a membrane-based dehumidification cooling system, International Heat Transfer Symposium (IHTS) and Heat Powered Cycles (HPC) Conference 2016, Nottingham, United Kingdom.

List of Figures

Fig 1- 1 World energy consumption for each fuel [3] 2

Fig 1- 2 UK final energy consumption by source 2011[14] 3

Fig 1- 3 Psychometric chart for the process of cooling and dehumidification in a cooling coil [31] 5

Fig 1- 4 Psychometric chart for simplified liquid desiccant dehumidifier combined with sensible cooler [31] 6

Fig 2- 1 Schematic of adiabatic structured packing dehumidifier [52] 14

Fig 2- 2 Schematic diagram of a packed column with cooling pipe dehumidifier [36, 53] 15

Fig 2- 3 Schematic of parallel-plate internally cooled dehumidifier [55] 16

Fig 2- 4 Schematic diagram of fin-coil type internally cooled dehumidifier [59] 18

Fig 2- 5 Schematic of a internally cooled cross flow type dehumidifier [61] 19

Fig 2- 6 Schematic diagram of flat-plate air-to-air heat and mass exchanger [63, 64] 21

Fig 2- 7 Schematic diagram of small-scale single panel LAMEE: flow arrangement for the unit (a); cross section view of the unit (b) [67, 68] 22

Fig 2- 8 Schematic diagram of a flat-plate counter-cross flow heat and mass exchanger [70, 78] 26

Fig 2- 9 The structure of a cross flow IMLDD [83, 84] 28

Fig 2- 10 The structure of a quasi-counter flow parallel-plate membrane contractor with cooling tubes [85] 29

Fig 2- 11 Schematic diagram of 3-fluid LAMEE: prototype of 3-fluid LAMEE (a); solution channel with cooling tubes (b); cross-section view (c) [87, 88] 30

Fig 2- 12 Schematic of IHPMC: 3-D structure (a); plan view (b); calculation domain (c) [89] 31
Fig 2- 13 Structure and dimensions of a hollow-fiber module prototype [93] 33
Fig 2- 14 Structure of the counter-flow hollow fiber membrane module [99, 100] 34
Fig 2- 15 Structure of the cross-flow hollow fiber membrane module [102, 103] 36
Fig 2- 16 Schematic of an elliptical hollow-fiber membrane contractor [110-113] 38
Fig 2- 17 Schematic of a conventional straight module (a); coiled module (b); secondary flow in a curved tube (c) [117] 40
Fig 2- 18 Schematic diagram of direct contact regenerator tower [125] 43
Fig 2- 19 Schematic diagram of a ultrasonic atomization liquid desiccant regeneration system (UARS) [127, 128] 45
Fig 2- 20 Different flow configurations between air flow and liquid film [129] 46
Fig 2- 21 Pictorial view of the regenerator [140] 50
Fig 2- 22 Schematic diagram of a run-around heat and mass recovery system [71] 52
Fig 2- 23 Schematic diagram of a counter-cross flow RAMEE [145] 54
Fig 2- 24 Schematic diagram of counter-flow heat and mass transfer process in packed-type liquid desiccant dehumidifier [197] 67
Fig 2- 25 Schematic diagram of heat and mass transfer in a packed column [198] 68
Fig 2- 26 Two-dimensional schematic of the computational domain [206] 74
Fig 2- 27 Free surface models for axial flow [212] 81
Fig 3- 1 Structure of membrane-based parallel-plate dehumidifier (a), and coordinate system used for numerical modelling (b)..... 92
Fig 3- 2 Control volume used for the energy conservation in solution side 93
Fig 3- 3 Control volume used for the moisture conservation in solution side 95
Fig 3- 4 Control volume used for the energy conservation in air side 96

Fig 3- 5 Control volume used for the moisture conservation in air side.....97
Fig 3- 6 Psychometric chart of LiCl for dehumidifier.....103
Fig 3- 7 Flow chart for the solution procedure for dehumidifier.....106
Fig 3- 8 Schematic diagram of the laboratory test rig 108
Fig 3- 9 Comparisons among numerical modelling, experimental data and analytical solutions for sensible and latent effectiveness under different NTU values: NTU=2(a); NTU=4(b); NTU=8(c). 113
Fig 3- 10 Air temperature field (a); air humidity ratio field (b); temperature field on membrane surface (c); humidity ratio field on membrane surface (d) 115
Fig 3- 11 Variations of effectiveness: (a) sensible effectiveness; (b) latent effectiveness; (c) total effectiveness with $m*$and NTU.....116
Fig 3- 12 Sensible effectiveness variations with $m*$ under different NTUs.....117
Fig 3- 13 Latent effectiveness variations with $m*$ under different NTUs. 118
Fig 3- 14 Total effectiveness variations with $m*$ under different NTUs.....118
Fig 3- 15 Variations of effectiveness with NTU under $m*= 4.$.....120
Fig 3- 16 Variations of effectiveness: (a) sensible effectiveness; (b) latent effectiveness; (c) total effectiveness with $Tsol$ and $Csol$.....122
Fig 3- 17 Sensible effectiveness variations with $Tsol$ under different $Csol.$.....123
Fig 3- 18 Latent effectiveness variations with $Tsol$ under different $Csol.$ 124
Fig 3- 19 Total effectiveness variations with $Tsol$ under different $Csol.$.....124
Fig 3- 20 Variations of effectiveness with $Csol$ under $Tsol = 18℃$.....126
Fig 3- 21 Variations of effectiveness: (a) sensible effectiveness; (b) latent effectiveness; (c) total effectiveness with $Tair, in$ and $RHair, in.$.....128
Fig 3- 22 Sensible effectiveness variations with $Tair, in$ under different $RHair, in$....129
Fig 3- 23 Latent effectiveness variations with $Tair, in$ under different $RHair, in.$.....130

Fig 3- 24 Total effectiveness variations with $Tair, in$ under different $RHair, in$.....130
Fig 3- 25 Inlet and outlet air conditions on the psychrometric chart for numerical modelling. 132
Fig 4- 1 Psychometric chart of LiCl for regenerator.....138
Fig 4- 2 Flow chart for the solution procedure for regenerator 140
Fig 4- 3 (a) Solution temperature field; (b) Solution concentration field; (c) Air temperature field; (d) Air humidity ratio field; (e) Temperature field on membrane surface; (f) Humidity ratio field on membrane surface 146
Fig 4- 4 Sensible effectiveness variations with NTU under different $m*$ 147
Fig 4- 5 Latent effectiveness variations with NTU under different $m*$.....147
Fig 4- 6 Total effectiveness variations with NTU under different $m*$ 148
Fig 4- 7 Influences of NTU on TDR, MFR and $Csol, out$ 149
Fig 4- 8. Variations of effectiveness with $m*$ under $NTU = 6$.....150
Fig 4- 9 Influences of $m*$ on TDR, MFR and $Csol, out$ 151
Fig 4- 10 Sensible effectiveness variations with $Tsol, in$ under different $Csol, in$.....153
Fig 4- 11 Latent effectiveness variations with $Tsol, in$ under different $Csol, in$ 153
Fig 4- 12 Total effectiveness variations with $Tsol, in$ under different $Csol, in$.....154
Fig 4- 13 Influences of $Tsol, in$ on TDR, MFR and $Csol, out$.....154
Fig 4- 14 Variations of effectiveness with $Csol, in$ under $Tsol, in = 60$℃.....156
Fig 4- 15 Influences of $Csol, in$ on TDR, MFR and $Csol, out$.....156
Fig 4- 16 Variations of effectiveness with $Tair, in$ under $Wair, in = 12\ gkg\ dry\ air$ 158
Fig 4- 17 Influences of $Tair, in$ on TDR, MFR and $Csol, out$ 158
Fig 4- 18 Variations of effectiveness with $Wair, in$ under $Tair, in = 30$℃.....160
Fig 4- 19 Influences of $Wair, in$ on TDR, MFR and $Csol, out$ 160

Fig 5- 1 Concept diagram of the complete dehumidification system……...167

Fig 5- 2 Flow chart of the numerical solving scheme for the complete system 169

Fig 5- 3 Schematic of a complete liquid desiccant dehumidification system.....172

Fig 5- 4 Air temperature and humidity ratio fields in dehumidifier (a) (b); solution temperature and concentration fields in regenerator (c) (d); temperature and humidity ratio fields on membrane surface in dehumidifier (e) (f); temperature and humidity ratio fields on membrane surface in regenerator (g) (h) 178

Fig 5- 5 System sensible effectiveness variations against $NTUde$ under various $msol$181

Fig 5- 6 System latent effectiveness variations against $NTUde$ under various $msol$ ...181

Fig 5- 7 Moisture flux rate variations against $NTUde$ under various $msol$.....182

Fig 5- 8 Total cooling output $Qcooling$ variations against $NTUde$ under various $msol$ 184

Fig 5- 9 COP variations against $NTUde$ under various $msol$ 184

Fig 5- 10 System sensible effectiveness variations against $NTUre$ under various $msol$ 186

Fig 5- 11 System latent effectiveness variations against $NTUre$ under various $msol$..186

Fig 5- 12 Moisture flux rate variations against $NTUre$ under various $msol$ 187

Fig 5- 13 Total cooling output $Qcooling$ variations against $NTUre$ under various $msol$ 188

Fig 5- 14 COP variations against $NTUre$ under various $msol$ 189

Fig 5- 15 System sensible effectiveness variations against $m*$ under various NTU 190

Fig 5- 16 System latent effectiveness variations against $m*$ under various NTU 191

Fig 5- 17 Moisture flux rate variations against $m*$ under various NTU.....191

Fig 5- 18 Total cooling output $Qcooling$ variations against $m*$ under various NTU.193

Fig 5- 19 COP variations against $m*$ under various NTU 193

Fig 5- 20 Variations of effectiveness and moisture flux rate against $Csol, in$.....195

Fig 5- 21 Total cooling output $Qcooling$ variations against $Csol, in$.....195

Fig 5- 22 COP variations against $Csol, in$.....196

Fig 6- 1 Schematic diagram of the mixed solution dehumidification system…….. 206

Fig 6- 2 Mixed solution specific humidity variations with temperature for different mixing ratios under $Csol = 15\%$.....209

Fig 6- 3 Mixed solution specific humidity variations with temperature for different mixing ratios under $Csol = 30\%$.....210

Fig 6- 4 Mixed solution specific humidity variations with temperature for different mixing ratios under $Csol = 42\%$.....210

Fig 6-5 Mixed solution specific humidity variations for pure LiCl and $CaCl_2$ solutions under different concentrations 212

Fig 6-6 Sensible effectiveness changes with the mixing ratio under different solution concentrations 212

Fig 6-7 Sensible effectiveness changes with the mixing ratio under different solution temperatures.....213

Fig 6-8 Latent effectiveness changes with mixing ratio for different solution concentrations 215

Fig 6- 9 Impact of solution concentration on MFR and $Wair, out$.....216

Fig 6-10 Latent effectiveness changes with mixing ratio for different solution temperatures.....217

Fig 6- 11 Impacts of solution temperature on MFR and $Wair, out$.....217

Fig 6- 12 Influences of solution mixing ratio on MFR and $Wair, out$ 219

Fig 6- 13 Variations of $Qreg$ with contents of LiCl and $CaCl_2$ at 16℃.....220

Fig 6- 14 Variations of COP with contents of LiCl and $CaCl_2$ at 16℃.....221

Fig 6- 15 Variations of $Tsol, out$, $Tair, out$ and MFR with $CaCl_2$ mass fraction.....222

Fig 6- 16 Variations of total cooling output and $Qreg$ with $CaCl_2$ mass fraction for 30% desiccant solution.....223

List of Tables

Table 2- 1 Fully developed (fRe), Nusselt and Sherwood numbers for different aspect ratios.....79

Table 2- 2 Comparison of fully developed (fRe), Nuseelt and Sherwood numbers for different aspect ratios with and without considering developing entrance.....80

Table 2- 3 Comparison of different modelling methods for liquid desiccant heat and mass exchanger.....84

Table 3- 1 Electrolyte parameters for $CaCl_2$ and LiCl solutions [216]……..102

Table 3- 2 Air and desiccant solution transport properties……..104

Table 3- 3 Dehumidifier specifications and membrane physical properties……....109

Table 3- 4 Measurement devices and uncertainties…….110

Table 3- 5 Comparisons between numerical results and experimental data…….111

Table 4- 1 Comparisons between numerical and experimental results for solution side effectiveness…….143

Table 4- 2 Comparisons between numerical and experimental results for TDR and MFR 144

Table 5- 1 Physical and transport properties of dehumidifier and regenerator……..174

Table 5- 2 Calculated and tested performance indices under different operating conditions 175

Table 6- 1 Parameters of binary interaction energy for mixed solution activity coefficient calculation (25℃) [167]…… 203

Table 6- 2 Sensible and latent effectiveness under various designed operating conditions, comparison of numerical and experimental results 208

Table 6- 3 Moisture flux rates under different designed operating conditions, comparison of numerical and experimental results 208

Nomenclature

a_w	activity of water
A	membrane surface area (m^2)
A_ϕ	Debye-Huckel constant
c_p	specific heat capacity (J/kgK)
C	concentration (%)
COP	coefficient of performance
C_r^*	thermal capacity ratio
d	width of the rectangular channel (m)
D	diffusivity (m^2/s)
f_w	activity coefficient of water
h	convective heat transfer coefficient (W/m^2K)
h_{fg}	condensation heat of water (J/kg)
h^*	operating factor
H	height of the dehumidifier unit (m)
I_x	ionic strength in mole fraction scale
k	thermal conductivity ($W/m\,K$)
L	length of the dehumidifier unit (m)
LRC	long range interaction
MFR	moisture flux rate
MRR	moisture removal rate (kg/s)
M_w	molecular weight of water ($kg/kmole$)
m^*	solution to air mass flow rate ratio

$\dot{m}$	mass flow rate (kg/s)
NRTL	electrolyte non-random two-liquid method
NTU	number of heat transfer units
NTU_m	number of mass transfer units
P	atmospheric pressure (pa)
P_v	equilibrium vapour pressure of desiccant solution (pa)
Q	energy power (kW)
Re	Reynolds number
Sh	Sherwood number
SMR	simple mixing rules
SRC	short range interaction
T	temperature (℃)
U	overall heat transfer coefficient ($\mathrm{W/m^2K}$)
U_m	overall mass transfer coefficient ($\mathrm{kg/m^2s}$)
$\dot{V}$	volumetric flow rate (l/min)
W	humidity ratio (kg/kg dry air)
X	solution mass fraction
x	mole concentration

Greeks

ε	effectiveness
δ	thickness of membrane (m)
η	efficiency
ρ	density ($\mathrm{kg/m^3}$)

τ	binary interaction energy parameter
χ	closest approach parameter of the Pitzer-Debye-Huckel equation

Superscripts

$*$	dimensionless

Subscripts

air	air flow
$crit$	critical value
d	duct
de	dehumidifier
$desi$	desiccant
exp	experimental
fan	fan
in	inlet
lat	latent
m	mass transfer
mem	membrane
$moisture$	moisture
num	numerical
out	outlet
$pump$	pump
re	regenerator
reg	regeneration

sen	sensible
sol	solution flow
sys	system
tol	total
w	water

Chapter 1: Introduction

Chapter 1 is structured in the following sections: Section 1.1 gives a brief introduction to the background of this research; Section 1.2 provides with aims and objectives of this research; Section 1.3 presents the detailed research methodology and Section 1.4 is the summary of the thesis structure.

1.1 Research background

Energy is the engine driving for human activities, development and sustainability [1]. The global energy consumption has increased dramatically in past decades as a result of growing population and rapidly developing economy. The world's total energy consumption has increased by 38% between 1998 and 2011. World primary energy consumption raised by 2.2% in 2017, up from 1.2% in 2016 and the highest since 2013. The energy consumption growth was below average only in Asia Pacific, the Middle East and South & Central America but above average in other regions [2]. Between 1990 and 2010, the energy consumption in Canada increased by 23%, and it raised by more than three times between 1980 and 2005 in Mediterranean region [1]. Until today fossil fuels still remain the dominant source for global energy consumption as observed in Fig 1-1 [3], and this situation is expected to last for the next decades [4].

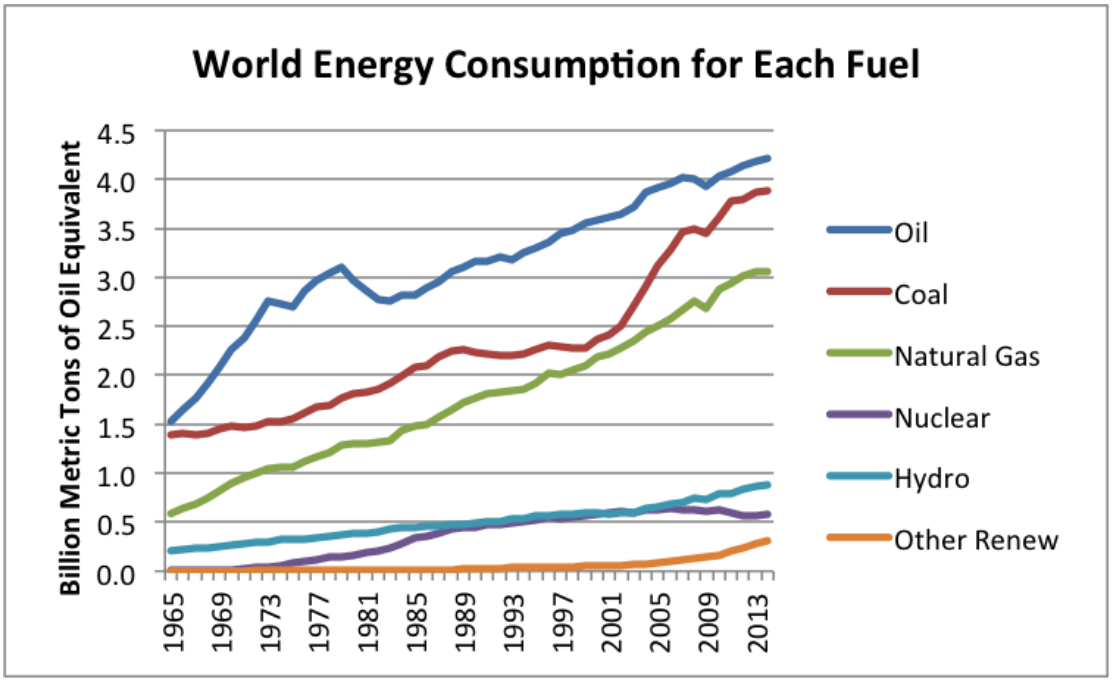


Fig 1- 1 World energy consumption for each fuel [3]

The global energy demand is predicted to rise from 87.4 million barrel/day in 2011, to 99.7 million barrel/day in 2035. This would cause the dramatic increase of petroleum oil price from 125 $/ barrel in 2011, to more than 215 $/ barrel in 2035 [5]. In the meantime, exponential global atmospheric carbon dioxide and ocean acidification rises are very likely to cause a significant shift, conserving energy and reducing fossil fuel consumption are needed [5].

Under these circumstances, many countries and international organizations in general have ambitious targets for the reduction of greenhouse gas emissions and global warming [4]. For the UK, the government committed to decreasing the levels of carbon dioxide and five other greenhouse gases by 12.5% below 1990 levels by 2008–2012. A longer climate changer target, which is to reduce the carbon dioxide emission by 80% by 2050 has also been set [6, 7]. Besides, the European Commission proposed three specific targets to be achieved by 2020: to decrease greenhouse gas emission by 20%, to increase the energy efficiency by 20% and to increase the contribution of renewable energy to the final energy consumption to 20% [8]. Chinese

government aimed to control its primary energy consumption within 5 billion tonnes of coal equivalent (tce) by 2020, and within 6 billion tce by 2030 [9].

Buildings are responsible for around 40% of the total global energy consumption [10-12]. According to [13] the U.S. building sectors account for 41% of national primary energy consumption, and specifically residential buildings are 22% nationally while commercial buildings are 19%. For UK, based on statistic from department of energy and climate change [14], between 38% to 42% of UK energy consumption is mostly spent in buildings, which is illustrated in Fig 1-2. In particular, heating, ventilation and air-conditioning (HVAC) systems are responsible for 40%-60% of total energy consumption in buildings in China [15], 55% in Malaysia [16]. By and large, in developed countries HVAC systems are responsible for half of the building energy consumption [17], and predictions also indicate a dramatic growth in HVAC energy consumption in EU for the next 15 years, rising approximately in 50% [18].

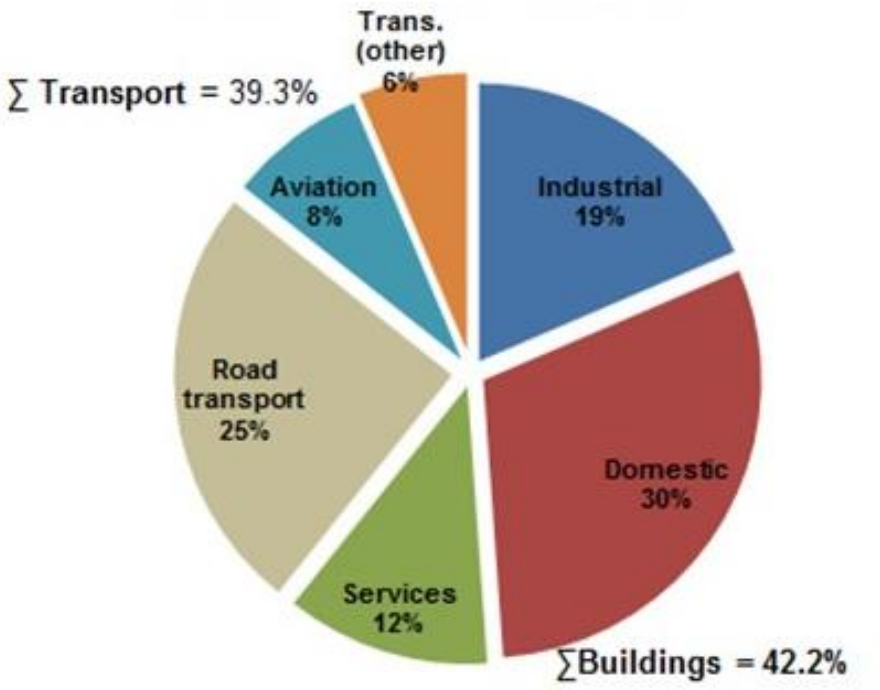


Fig 1- 2 UK final energy consumption by source 2011[14]

People spend approximately 90% of their time in the indoor environment [19]. Thus human thermal comfort and health can be significantly influenced by building indoor environmental parameters such as temperature, humidity level and air quality [20, 21]. Ventilation, which is the continuous replacement of contaminated indoor air with fresh outdoor air is of vital importance for the improvement of indoor air quality and human's health, comfort level and performance [22]. Buildings with insufficient ventilation rate are characterized by high concentrations of pollutants and occupants may suffer different health problems. For example: irritations, asthma, headaches, dizziness and allergy, which would reduce occupants' living qualities and production qualities as well [23]. It is reported that the performances of people in an office building could be decreased by 6-9% as the result of poor indoor air quality [10].

Indoor humidity is of critical importance on assuring human sensations, indoor air quality and dryness feeling, and low level of relative humidity could cause skin dryness, eye dryness, nasal dryness and associated with SBS (sick building syndrome) symptoms [24-28]. Besides, too high humidity level could be harmful to occupants as well. In many costal countries where humidity levels are relatively high, occupants would feel uncomfortable and mildew would grow on the building surfaces. Both production safety and quality can be badly affected [29]. As the result, air ventilation and dehumidification are of vital importance in the air conditioning system. As a matter of fact, the demand of energy for air conditioning system is expected to increase dramatically due to the increase in population and higher standards of living. It is expected that the energy consumed for indoor environment will rise by 120% from 2002 to 2030, and the energy required for indoor thermal comfort accounts for about 50% of the building total energy consumption which in most cases is in the form of electrical energy [30]. For the traditional vapour compression technology, which uses cooling coil to dehumidify moist air to a temperature lower than its dew point has several problems. For example, it has relatively weak ability and low efficiency of dealing with latent cooling load, which leads to

low coefficient of performance (COP) in humid areas. Additional energy may be required for reheating the dehumidified air to supply temperature. The psychrometric chart showing the process of cooling and dehumidification in a cooling coil is given in Figs 1-3[31].

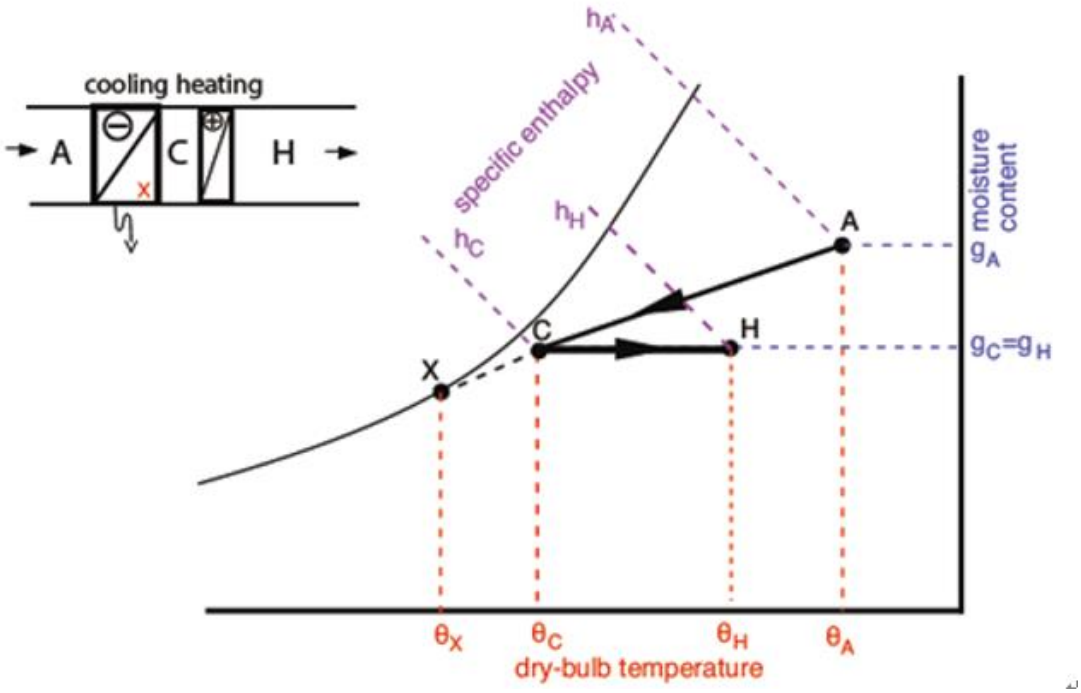


Fig 1- 3 Psychometric chart for the process of cooling and dehumidification in a cooling coil [31]

It also has problems of growths of mould and bacteria, surface corrosion etc, which can cause health issues by affecting indoor air quality [17, 32, 33]. In recent years, comprehensive researches have been conducted on reducing the consumption of energy for cooling and dehumidification in buildings, without compromising thermal comfort and indoor air quality. Alternative systems have been studied for air cooling and dehumidification such as absorption cooling, jet cooling, electrochemical dehumidification, solid desiccant cooling and liquid desiccant cooling [33-37]. Among these technologies, liquid desiccant cooling has gain much progress for its advantages: it is feasible, highly efficient, cost effective and has no liquid water condensation problem. The system can be regenerated by low grade energy such as solar energy,

and regenerated solution can be used as energy storage medium [29]. A liquid desiccant dehumidifier is typically used in serious with a sensible cooler to reduce its temperature. The psychrometric chart of simplified liquid desiccant dehumidifier combined with sensible cooler is given in Figs 1-4[31].

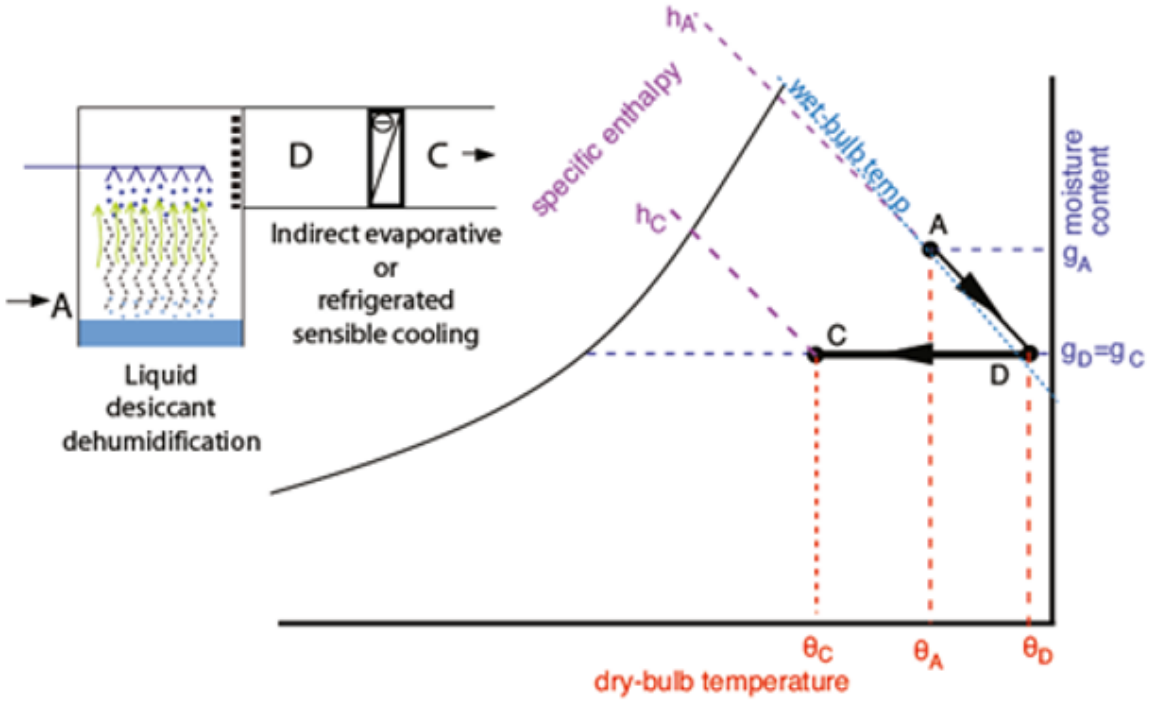


Fig 1- 4 Psychometric chart for simplified liquid desiccant dehumidifier combined with sensible cooler [31]

Packed beds or packed columns are normally used for liquid desiccant dehumidification systems, where liquid desiccant solution and air are in direct contact. However the problem with packed beds and packed columns is that the small droplets of desiccant solution could be carried over by the dehumidified air and supplied to the conditioned rooms, which is harmful for not only occupants but also building structure. As a result, the cost of maintenance of building is increased because of corrosion [38]. As the alternative, semi-permeable membranes are combined with liquid desiccant dehumidification system to form a novel type of system, so called membrane-based liquid desiccant dehumidification system. In this system, semi-

permeable membranes are used to separate solution and air flows to avoid carry-over problems [29, 39]. The biggest difference between this new system and the traditional one is that semi-permeable membranes are applied as alternatives to packed beds or columns as heat and moisture transfer medium where air and liquid desiccant are separated by membranes. Only water vapour can be transferred through membranes so the carryover problem can be solved. This system can also be powered by renewable energy sources so the performance could be even higher [29]. Moreover, other harmful gases are prevented from permeating to supply air so air quality is improved as well.

1.2 Research aim and objectives

The main aim of this thesis is to develop and evaluate a novel membrane-based liquid desiccant dehumidification air-conditioning system. The research scope mainly covers system design, numerical modelling, simulation programme development, experimental testing and system performance evaluation. With refer to different parts within the system, dehumidifier, regenerator and the complete system are investigated. With regard to the working fluid, both pure desiccant solution and the mixed solution are studied. Consequently, six objectives have been established for achieving the thesis aim:

1) Literature review on technologies related to the liquid desiccant dehumidification system to give a comprehensive background and evaluation of current available literature on the topic. More importantly, to highlight the research gaps in the existing literature of the membrane-based liquid desiccant dehumidification system.
2) Numerical and experimental analysis of the membrane-based dehumidifier under various conditions and the performance evaluation based on the simulation and experimental results.

3) Numerical and experimental analysis of the membrane-based regenerator under different conditions and the performance evaluation based on the simulation and experimental results.
4) Development of a complete membrane-based liquid desiccant dehumidification system by integrating both dehumidifier and regenerator, and to investigate effects of various operating conditions on the complete system performance through simulation and experimental data.
5) Investigation on effects of mixed LiCl-$CaCl_2$ solution on the system performance, and to provide an optimum mixing ratio selection method based on the mathematical model and experimental data.
6) Recommendations for future work.

1.3 Thesis structure

The thesis is mainly organized to seven chapters and four additional appendices for addressing the thesis aim and six thesis objectives.

Chapter 1 gives the brief introduction to the thesis, by providing the research background, research aim, objectives and the thesis structure.

Chapter 2 is the in-depth systematic review of the existing literature on technologies related to the liquid desiccant dehumidification system. In this chapter, the research gaps between published literatures and current research are identified.

Chapter 3 presents the numerical and experimental analysis for the performance of a membrane-based flat-plate liquid desiccant dehumidifier, while chapter 4 gives the numerical and experimental analysis for the performance of a regenerator with similar structure of dehumidifier.

Chapter 5 presents numerical and experimental investigations of a complete membrane-based liquid desiccant dehumidification system that include a dehumidifier, a regenerator, and hot and cooling water supply systems.

Chapter 6 presents the investigation of effects of using mixed LiCl-$CaCl_2$ solution on the membrane-based dehumidification system, and the optimum mixing ratio selection method is also provided in this chapter.

Finally, chapter 7 concludes the thesis by listing main conclusions as well as recommendations for future work.

Last but not least, supplementary materials such as normalization methods for governing equations, and Matlab scripts for simulation are provided in Appendices.

Chapter 2: Literature Review

2.1 Introduction

This chapter presents a comprehensive literature review on technologies related to the liquid desiccant dehumidification system. The following main topics have been covered in critically reviewed literatures:

1) Dehumidifier in section 2.2, including direct contact type and membrane-based type.
2) Regenerator in section 2.3, including direct contact type and membrane-based type.
3) The complete membrane-based dehumidification type in section 2.4.
4) Materials of liquid desiccant and membranes in section 2.5.
5) Different mathematical methods for numerical modelling in section 2.6.
6) The main findings and identified research gaps from the literature review in section 2.7.

The purposes of the literature review are: (1) to provide a comprehensive background and evaluation of current available literature on the topic, document detailed start-of-art development with regard to the related technology; (2) to specify the methodological approach for the research; (3) to identify the research gaps between published literatures and current research. To implement these purposes, extensive reviews are conducted from a variety of disciplines including different parts within the complete liquid desiccant dehumidification system, materials used for liquid desiccant and membrane, and different developed mathematical methods for the numerical modelling. A brief summary containing main findings from the review, and novelty of this research and identified research gaps between previous studies and current study is presented in Section 2.7.

2.2 Dehumidifier

The dehumidifier is the most important unit in a liquid desiccant dehumidification system. In the dehumidifier, water vapour in the humid air is absorbed by liquid desiccant. Thus the literature review starts from the different types of dehumidifier. Generally they can be divided into two main types: direct contact type and membrane-based type. They will be introduced in Sections 2.2.1 and 2.2.2 respectively.

2.2.1 Direct contact type dehumidifier

Packed beds or packed columns are normally applied as dehumidifiers for heat and mass transfer in traditional liquid desiccant dehumidification system. There's two main types of direct contact dehumidifier: adiabatic type and internally cooled type. The difference between these types is whether the internal heat source in the liquid desiccant is cooled inside the dehumidifier. These two types are explained in Sections 2.2.1.1 and 2.2.1.2 respectively.

2.2.1.1 Adiabatic type

Adiabatic type dehumidifiers have been widely used for industrial and residential applications for various advantages:

1) The contact area between air and liquid desiccant are usually very large so they have relatively high heat and moisture transfer efficiency [29].
2) The geometry of this type is normally simple, so the maintenance is usually low [29].

However, due to the fact that there is no additional cooling for the liquid desiccant, during the process of dehumidification in the dehumidifier, the temperature of liquid desiccant would increase as the result of latent heat release, and this would exert an adverse influence on the dehumidifier performance. As a result, both moisture and temperature control of the processed

air are less effective. Besides, adiabatic type has the disadvantage of imposing large pressure drop for the processed air flowing through the dehumidifier [29]. There is various structures for adiabatic type dehumidifiers, such as spray tower, packed beds or columns and wetted wall columns.

In the spray tower, the liquid desiccant is broken into small droplets by the nozzle in the spray chamber, so the contact area between air and liquid desiccant can be increased. The advantages of such type are: simple geometry and relatively lower pressure drop in air side. However, its dehumidification effectiveness is not high, and the pressure drop is high in the solution side [40]. Finned coils, flat plate heat exchangers and heat pipes are some designs that haven been used in spray towers to provide simultaneous cooling [41-43].

Packed beds and packed columns are most widely used adiabatic direct contact dehumidifier types. They have many advantages such as: high compactness, high liquid-air contacting area, long liquid-air contact air and high dehumidification effectiveness [40].

Numerous researches have been carried out for packed beds and packed columns. Zurigat et al [44] experimentally tested the performance of an air dehumidifier using triethylene glycol (TEG) as desiccant. Packed bed column (dehumidifier) was applied, with low packing density (77 m^2/m^3), to provide direct contact between the air and the TEG. Two different structured packings were used, wood and aluminium. Authors compared their experimental results with different theoretical correlations and found that many of them [45, 46] could not predict the effectiveness.

Thus more accurate correlation was given by Zurigat et al [44], and they found that the effectiveness of the column was improved by increasing the TEG mass flow rate and inlet TEG temperature for both wood and aluminium packings.

Babakhani and Soleymani [47] proposed an analytical solution for air dehumidification by liquid desiccant in an adiabatic packed column, based on the consumption of constant

equilibrium humidity level on the interface. They compared their analytical solution to experimental data and very good agreement have been achieved.

Factor and Grossman [48] used a randomly packed packed bed for solar air conditioning with liquid desiccant. A theoretical model was developed to predict the performance of packed bed. They found that the packed bed yields good results as a dehumidifier, and pressure drop can be reduced with the use of suitable packing.

Patnaik. et al [49] experimentally investigated a solar open-cycle liquid desiccant dehumidification system using randomly packed packed column as dehumidifier, and total cooling capacity of 3.5-14.0 kW (1.0 – 4.0 refrigeration tons) were achieved for the dehumidifier. However, for randomly packed type, the required desiccant solution mass flow rate for good wetting and air side pressure drop are normally very high.

Elsarrag [50] used a structured packed column dehumidifier for liquid desiccant dehumidification system. They pointed out that the structured packed columns represents the latest development in high efficiency and high packing capacity for heat and moisture transfer compared with randomly packed columns. They developed two mass transfer correlations for normal and high solution flows, and the mass transfer coefficient were predicted within 15%.

Pietruschka et al [51] presented a new liquid desiccant dehumidification system using structured packed columns to be integrated in residential mechanical ventilation systems. A theoretical model was developed for the system and compared with experimental data. According to their results the system can provide inlet air conditions with the temperature below 20 °C under the summer design conditions of 32 °C and 40% relative humidity, and in total 886 W of cooling power can be generated when the air volume flow rate is 200 $m^3 h^{-1}$.

Zhang. et al [52] experimentally investigated the moisture transfer in adiabatic structured packing dehumidifier using liquid desiccant. The test section is 500mm × 270mm transparent plastic rectangular parallel-piped, and they are packed up to 250mm deep with structured

packing as shown in Fig 2-1. They pointed out that when the air velocity changed from 0.5 to 1.5 m/s, the overall mass-transfer coefficient in the adiabatic structured packing dehumidifier increased from 4.0 to 8.5 g/m^2 s. Furthermore, higher solution temperature resulted in lower overall mass-transfer coefficients.

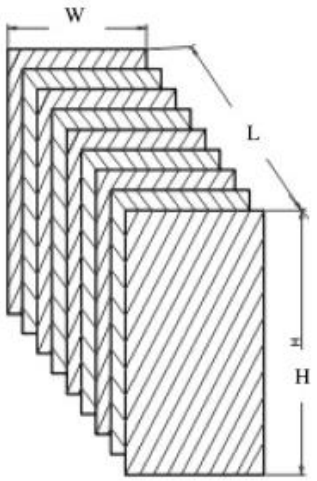


Fig 2- 1 Schematic of adiabatic structured packing dehumidifier [52]

To sum up, all researches about adiabatic type direct contact dehumidifiers were mainly focused on the structure optimisation. In fact, the improvement of the performance is limited by the temperature increase in the dehumidifier due to the latent heat release during the process of dehumidification. Internally cooled type dehumidifier is an alternative to adiabatic type, which will be discussed in next section.

2.2.1.2 Internally cooled type

Compared with adiabatic type, internally cooled type normally applies a cooling coil in the liquid side to remove the latent heat generated during dehumidification. The most critical unit for this type is the cooling pipes installed in the liquid desiccant, they must be strictly separated with the liquid desiccant. Thus the focus of such type is the structure of dehumidifier unit.

Many different structures have been designed and manufactured in previous studies. Fig 2-2 shows a typical packed column with cooling pipe, where cooling coils are embedded in the packing to remove latent heat [36, 53].

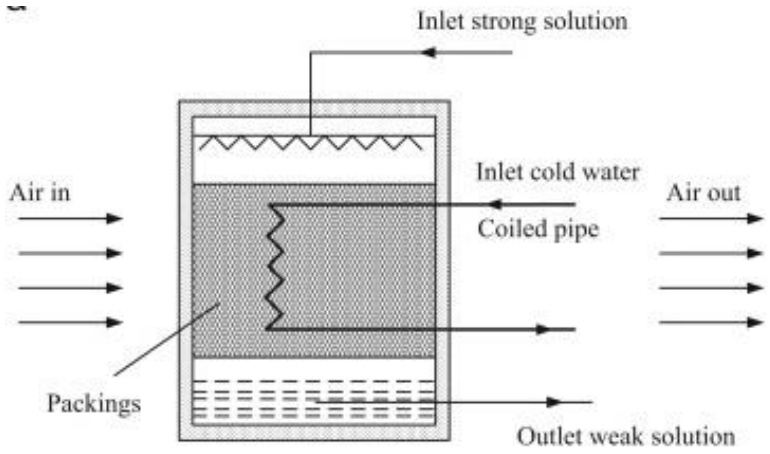


Fig 2- 2 Schematic diagram of a packed column with cooling pipe dehumidifier [36, 53]

In such type of dehumidifier, air flow and solution flow can be arranged as cross, parallel or counter flow arrangements. An outer insulation layer is applied for the dehumidifier to prevent heat gain from the environment.

Bansal et al [54] investigated an internally cooled structured packed-bed dehumidifier, which uses rigid media pads with cooling water flowing through the tubes embedded in the packing. $CaCl_2$ was used as the liquid desiccant, which flows by gravity, while air flows in a cross flow arrangement. They compared the moisture removal rate and dehumidifier effectiveness between an adiabatic dehumidifier and internally cooled dehumidifier, and found that the maximum effectiveness for an internally cooled dehumidifier is between 0.55 to 0.706, while it is between 0.38 to 0.55 for an adiabatic dehumidifier. However, the drawbacks of such structure are the embedment of cooling pipes into packing materials are very difficult to achieve. Relatively large solution flow rate is also required for optimal humidity control.

The second structure of internally cooled dehumidifier is parallel-plate type. Yin et al [55] experimentally tested an internally cooled parallel-plate type dehumidifier, which are illustrated in Fig. 2-3.

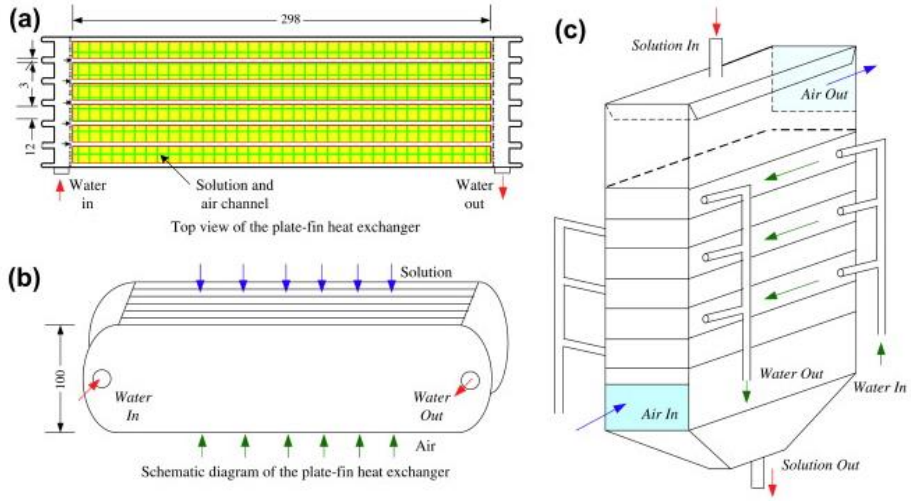


Fig 2- 3 Schematic of parallel-plate internally cooled dehumidifier [55]

It can be seen from Fig 2-3 that desiccant solution is sprayed from the top of the dehumidifier to bottom driven by gravity while humid air is blown from the bottom of the dehumidifier in a counter-flow configuration. Cooling water is pumped into cooling water pipes, which are located inside the plate to take phase change heat away. It is concluded that the desiccant with lower temperature has higher mass transfer coefficient. As the result, both desiccant with lower temperature, and desiccant with internal cooling can provide with better dehumidification effect.

Kessling et al. [56] developed and experimentally tested a internally-cooled dehumidifier with plastic plate structure. The plate dimensions are: 0.46m high, 0.98m wide and 5.5mm thick. In this dehumidifier the distance between adjacent parallel plates is 5.5 mm and the heat transfer coefficient through the plate is approximately 170 W/m^2K. The cooling water was circulated in horizontal channels within the double plates. A numerical model was developed to simulate

the performance of dehumidifier, and good agreement was achieved between numerical and experimental results. The results showed that as the thickness of the plate was rather small, the dehumidifier showed satisfactory heat transfer performance between liquid desiccant and cooling water, the dehumidification performance was satisfactory even under low desiccant flow rate.

Yoon et al. [57] developed a new internally water cooled vertical plate absorber. In their model vertical plates were lined with equal spaces. Liquid desiccant flows under the effect of gravity down each vertical plate along both sides, and the solution in falling film can be cooled by water that flows in a counter flow configuration. They also developed a numerical model for analysis, and the results showed good dehumidification results since the latent heat released in the solution channel can be effectively removed by cooling water in another neighbouring channel [29].

Another type of internally cooled dehumidifier is fin-coil dehumidifier, where cooling water flows inside the coil to cool the liquid desiccant that flows from the top of the unit. Then the air flows can be blown from either the front or the bottom side of the fin coil. Liu et al. [58] experimentally analysed an internally cooled fin-coil dehumidifier made of thermally conductive plastic. Their dehumidifier is an eight-row heat exchanger, in each raw there's eight parallel channels. Tubes with fins were installed in the dehumidifier to increase the contact area of the unit, as the result the moisture transfer between solution and air is enhanced significantly. The cooling water flows into the dehumidifier from the bottom from a water separator, then it is collected at the top of the unit. Both experimental and simulation analysis were carried out, and they concluded that the moisture removal rate m_w increases with solution flow rate, which indicates the increase of solution flow rate would enhance the heat and mass transfer coefficient considerably.

Zhang et al.[59] developed an internally cooled dehumidifier with fins made of stainless steel to improve the heat and mass transfer coefficients by increasing the contact area. The fin is 0.127 mm thick, and the distance between two adjacent fins is 2.2 mm. The schematic diagram of such type dehumidifier is given in Fig 2-4:

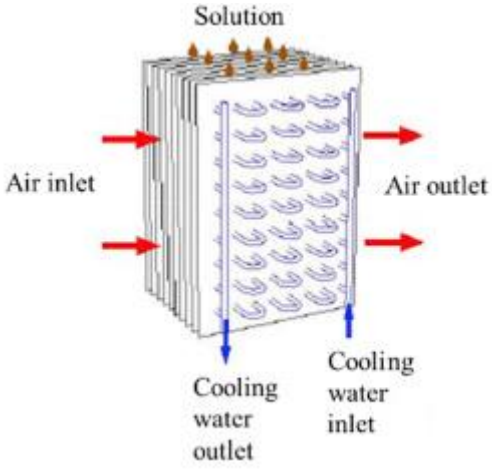


Fig 2- 4 Schematic diagram of fin-coil type internally cooled dehumidifier [59]

The dehumidifier consists of eight rows with in total 22 cooling water channels in each row. The distance between the centre of two adjacent pipes is 25.4 mm. Experimental tests were conducted under various conditions using lithium bromide as liquid desiccant. Numerical model, which was validated by experimental data was used for the prediction of such dehumidifier. According to their results the system coefficient of performance (COP) is between 4.2-6.5, and it rises with the decrease of the humidity ratio of processed air.

Detailed quantitative comparisons of three typical types of internally-cooled direct contact dehumidifiers (packed column, parallel-plate and fin-coil) were conducted by Liu et al [60]. Their results showed that among three types the packed column with internal cooling tubes performs more like an adiabatic type, its dehumidification effect shows disadvantages compared with another two types. By contrast, the fin-coil type shows the best

dehumidification performance under different inlet conditions. The difference between these three types is mainly the mass transfer ability, thus more efforts should be paid to the improvement of mass transfer between air and desiccant solution.

Apart from three main types as introduced above, Saman and Alizadeh [61] proposed another new type of internally-cooled type dehumidifier, as shown in Fig 2-5.

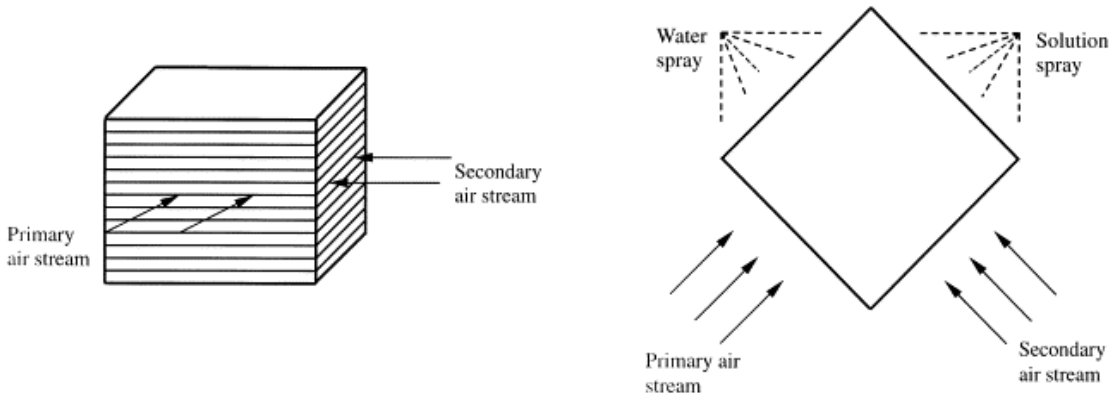


Fig 2- 5 Schematic of a internally cooled cross flow type dehumidifier [61]

As seen from the figure above, any two adjacent flow channels are separated by a flat plate where primary air is cooled and dehumidified. On one side of the plate, the primary air (humid and warm air) comes in direct contact with the liquid desiccant. On another side of the plate, a secondary air, normally return air from conditioned rooms is brought in contact with cooling water, so that the phase change heat released to the primary air can be simultaneously absorbed by secondary air. Considering that the room return air has lower humidity level than the outdoor air, it can be utilized to improve the performance in the secondary air side, then help in maintaining a nearly isothermal operation in each channel of the dehumidifier. Their experimental results indicated that the dehumidifier mass transfer coefficient increases with primary air mass flow rate, temperature and humidity level. Furthermore, the dehumidification efficiency can be improved by increasing the plate heat exchanger (PHE) angle.

Lun et al.[62] experimentally tested a novel internally-cooled dehumidifier with self-cooled liquid desiccant. The novelty of this study is that anhydrous ethanol was added into the liquid desiccant (lithium chloride in this study) for orm a hybrid solution (LiCl-ethanol-water solution) as the vaporizable coolant to control the temperature increase of the desiccant solution. The hybrid mixed solution was pumped to the top of dehumidifier, and distributed to the top surface of dehumidifier using nozzles. The surface of wire mesh of dehumidified bed was covered with hydrophilic fabric to achieve high porosity and wettability. Their experimental results suggested 25℃ 40% mixed solution as the optimum solution temperature and concentration. Compared with traditional LiCl solution, the self-cooled solution showed more than 40% of performance improvement under the same experimental conditions.

2.2.2 Membrane-based type dehumidifier

As mentioned in the previous section, semi-permeable membranes can be applied to solve desiccant carry-over problems of direct-contact type dehumidifiers. With regard to the structure of membranes, such type of dehumidifier can be further divided into flat-plate type dehumidifier and hollow-fiber type dehumidifier. As the name implies, the flat-plate type dehumidifier normally is formed by layers of flat membranes being stacked together in a plastic shell to form a complete unit. The hollow-fiber type dehumidifier is similar to a tube-and-shell heat exchanger, where the solution flows inside numerous number of hollow fiber tubes and air flows in the shell side. They are packed inside a rectangular or circular shell to form a complete hollow-fiber dehumidifier. Flat-plate type dehumidifier and hollow-fiber type dehumidifier will be discussed in sections 2.2.2.1 and 2.2.2.2 respectively.

2.2.2.1 Flat-plate type

Compared with hollow-fiber type dehumidifier, flat-plate type dehumidifier has many advantages. First of all, the pressure losses in solution and air channels are relatively low, thus less pump or fan power is required for the system. Secondly, the structure of flat-plate type is easy and clear, which makes the construction and maintenance of the system much easier [29]. The operation of the system using flat-plate type dehumidifier is more reliable. Compared with other structures, the sealing of desiccant solution is much easier for flat-plate type [36, 53]. Before being applied for the air dehumidification purpose, flat-plate membrane-based heat and mass exchangers have been analysed as air-to-air heat and mass exchangers. Zhang et al [63, 64] developed a cross-flow enthalpy exchanger as shown in Fig 2-6.

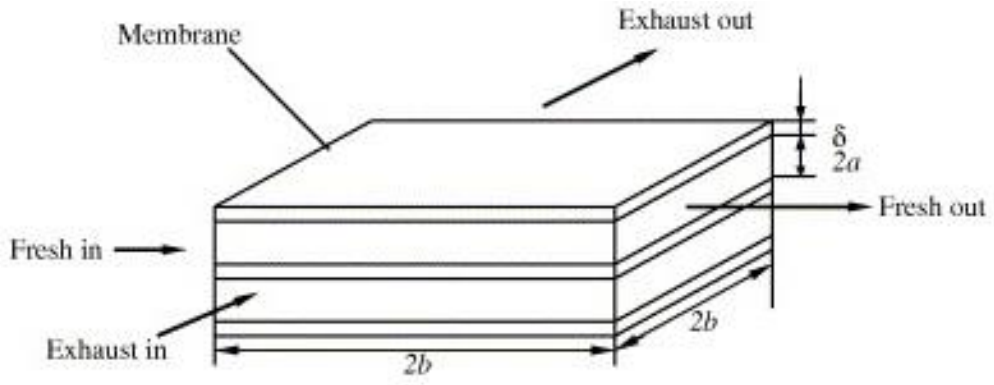


Fig 2- 6 Schematic diagram of flat-plate air-to-air heat and mass exchanger [63, 64]

As seen in Fig 2-6, the fresh air and the exhaust air flow in two adjacent channels in a cross flow configuration. The thickness of membranes is 100 μm. The fully developed Nusselt number Nu_C and the Nusselt number under uniform heat flux boundary condition, Nu_H were numerically calculated using CFD modelling. It is found that Nu_C is generally lower than Nu_H, and Nu_C is higer than the Nusselt number under constant temperature boundary condition Nu_T under large aspect ratios, but 37% less than Nu_T under small aspect ratios. Authors further

extended the research into all entry regions and calculated friction factors, Nusselt and Sherwood numbers in the entry region and in the fully developed regions for three various flow configurations: concurrent, counter and cross flows.

Niu and Zhang [65] numerically studied the effects of dimensionless parameters, membrane material and clarification of moisture resistance. Their study revealed that the membrane material with linear sorption curve performs better than other types of materials. A new coefficient of moisture diffusive resistance (CMDR) was introduced for better performance prediction of the enthalpy exchanger.

Zhang and Niu [66] proposed an analytical solution for a membrane-based heat and moisture exchanger, the effectiveness correlations were developed and validated through experimental tests.

Moghaddam et al [67, 68] proposed a small-scale single-panel membrane-based liquid-to-air membrane energy exchanger (LAMEE), and the schematic diagram of such unit is given in Fig 2-7.

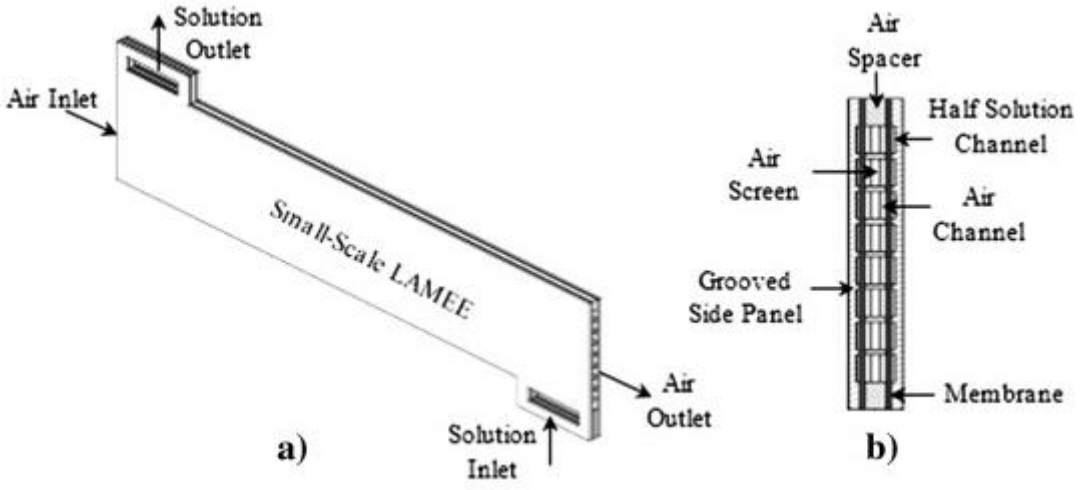


Fig 2- 7 Schematic diagram of small-scale single panel LAMEE: flow arrangement for the unit (a); cross section view of the unit (b) [67, 68]

As seen in the schematic diagram, solution flow and air flow are in counter-flow arrangement and they are separated by membrane layer. The exchanger is 0.49m long, and has 8 solution channels on each side of the panel. The thickness of air and solution channel are 0.8 mm and 5 mm respectively. The membrane they used has the thickness of 0.265 mm. SIMULINK software were used for the numerical simulation, and results were validated by experimental tests. Membrane vapour diffusion resistance (VRD) and air side convective coefficient were used to evaluate the performance, and the results revealed that reducing VRD from 56 $\mathrm{s/m}$ to 24 $\mathrm{s/m}$ would increase the latent effectiveness by 11%, while sensible effectiveness is not significantly influenced. Moreover, sensible, latent and total effectiveness would all increase by 4% with the rising of air convective coefficient.

Abdel-Salam et al [69] experimentally investigated the performance of a counter-flow membrane liquid desiccant air-conditioning system. The dehumidifier unit has the dimension of 1m high, 2m long, and 250 solution channels in total. Each solution channel is 3.17mm thick, while the thickness of air channel is 6.35mm. The material of membrane is polyethylene, which has the thickness of 0.54mm. They experimentally investigated the system performance by evaluating the effects of different parameters, such as number of heat transfer unit NTU, solution inlet temperature and thermal capacity ratio Cr^*. The results indicated that the solution inlet temperature is recommended to be set at 15-20℃ for good dehumidification performance. Optimum NTU and Cr^* are 5-10 and 3-5 respectively.

According to [36, 53], parallel flow structure is not easy for the sealing of liquid desiccants. Furthermore, the parallel flow exchanger with simple headers located next to each other is hard to construct in the limited space available in HVAC system [70]. Thus cross flow arrangement is more favourable for practical application.

Fan et al [71] developed a cross-flow plate heat and mass exchanger, where solution flow and air flows are in cross-flow arrangement. A two-dimensional steady-state numerical model was

used to simulate the heat and mass transfer in dehumidification system using Lithium Chloride (LiCl) as liquid desiccant. It was shown that up to 70% of overall effectiveness can be achieved if the size of dehumidifier and operating conditions can be selected correctly.

Das and Jain [72, 73] experimentally and numerically tested the performance characteristics of cross-flow membrane contractors for a liquid desiccant system. The membrane contractor is formed by series of alternate solution and air channels in which desiccant solution and air flow in cross-flow arrangement. Wicking material, which is made of a special type of cotton is inserted into the solution channels to soak the solution immediately so that the solution can be distributed uniformly throughout the solution channels. The results revealed that the contractor effectiveness increases at lower air channel gap, but the cost is increased due to higher pressure drop. Aspect ratio of the contractor has insignificant impact on the contractor performance.

Min and Su [74] developed a mathematical model for a cross-flow membrane enthalpy exchanger and the effects of membrane parameters on the exchanger effectiveness were investigated. It is shown in their results that sensible effectiveness does not change much with membrane parameters since membrane resistance only account for a small fraction of total resistance. In the meantime, latent effectiveness changes relatively more considerable with membrane parameters because the membrane moisture resistance decreases dramatically. Huang et al. [75] numerically investigated the fluid flow, heat and mass transfer in a cross-flow flat-plate membrane module using LiCl as liquid desiccant. In their numerical modelling the real boundary conditions on the membrane surface was calculated through simultaneous momentum, energy and humidity (concentration) governing equations for solution and air. Equal spacing was kept between two adjacent membrane layers to form solution and air channels. In their study the fluid flow was solved firstly, then the fundamental data such as Nusselt number and Sherwood number was obtained. The numerical model was validated by experimental results and satisfactory agreement was found between numerical and

experimental results. Their results showed that the fully developed Nusselt number in air side $Nu_{C,a}$ are between Nusselt number under constant temperature boundary condition Nu_T, and Nusselt number under uniform heat flux boundary condition Nu_H. The Sherwood numbers are slightly higher than Nusselt numbers. Moreover, Sherwood numbers in solution side are significantly higher than those in solution side, solution side Nu_C is approximately 15% higher than air side Nu_C.

The research was extended by considering the effects of developing entrances [76]. Their study results showed that the fluid flow, heat and mass transfer become fully developed after 30% of the air-side channel length. In solution side, fluid flow and heat transfer become fully developed after 30% of the solution-side channel length, but mass transfer was still developing even at the outlet of the duct.

The drawback of cross flow type compared with parallel flow type is that the efficiency of the cross flow exchanger is about 10% lower than that of the parallel flow exchanger [77].

A novel heat and mass exchanger that incorporates both parallel flow exchanger and cross flow exchanger were developed by Vali et al [70, 78]. The schematic diagram of a flat-plate counter-cross flow heat and mass exchanger is depicted in Fig 2-8.

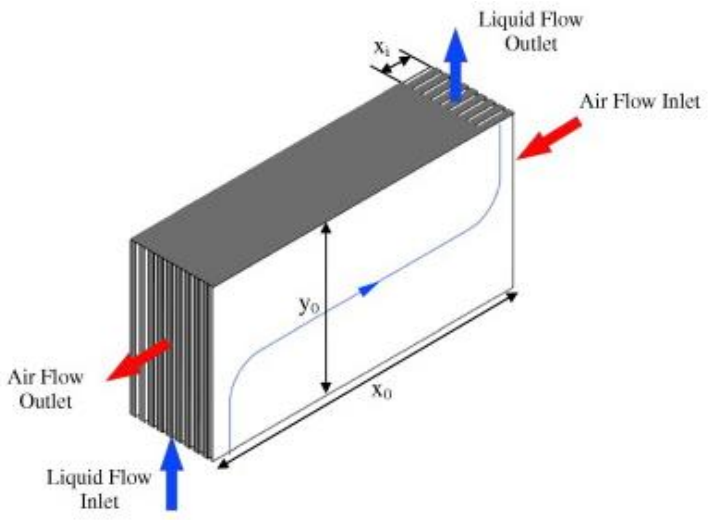


Fig 2- 8 Schematic diagram of a flat-plate counter-cross flow heat and mass exchanger [70, 78]

As seen in Fig 2-8 the air flows a uniform straight path from right side of dehumidifier to the left side, while liquid flows into the dehumidifier from the left bottom header and then leaves the dehumidifier from the right top header. The solution flows inside the dehumidifier in a S-shaped path. Their numerical simulation was verified by correlations from previous published papers. Results revealed that the effectiveness of such counter-cross heat and mass exchanger is lower than that of a parallel flow module, but higher than that of a cross flow module. For better system performance, NTU was recommended to be higher than 3, Cr^* in the ragne of 0.8-1.2. As for the geometry of the module, the aspect ratio was suggested to be less than 0.2, and the liquid channel inlet/outlet header length ratio to be less than 0.1.

Mahmud et al [79] also tested the performance of a counter-cross-flow membrane energy exchanger for HVAC applications using Magnesium Chloride ($MgCl_2$). A 200mm × 1800mm × 86mm module with 3.18mm thick air channels and 1.5mm thick solution channels was tested. The effects of Cr^* and face velocity V_{face} on the dehumidifier effectiveness were investigated, and it is found that when NTU=12 and $V_{face} = 0.55\ \mathrm{m/s}$, the maximum total effectiveness of 53% at $Cr^* = 4.5$ and 55% at $Cr^* = 2.8$ can be achieved under summer and winter testing conditions respectively.

Moghaddam [80] et al experimentally tested the steady-state performance of a small-scale counter-cross flow membrane energy exchanger for different heat and mass transfer directions, different desiccant types and concentrations. Compared to previously introduced modules, a small-scale counter-cross-flow single-panel module was manucrafted for the first time. This module offers better sealing between air and solution channels to prevent desiccant solution leaking from solution channel to air channel, as the result the sources of errors in experiment

can be minimized. Furthermore, membrane deflection as the result of pressure difference between air and solution sides inside the module can be reduced, thus flow mal-distribution caused by membrane deflections can be avoided. Results showed that effectiveness increases with Cr^* for both air cooling and dehumidifying, and air heating and humidifying testing conditions. Sensible effectiveness was proved to be insensitive to the change of solution type and concentration, while latent and total effectiveness increase with solution concentration.

Namvar et al [81] compared the steady state and transient effectiveness of a counter-cross-flow membrane energy exchanger through experimental tests under summer and winter conditions. Their results indicated that both sensible and latent effectiveness of the dehumidifier would increase during the transient period before reaching steady state value. Huang et al [82] studied a similar structure of dehumidifier, so called quasi-counter flow parallel-plate membrane contractor (QFPMC). In solution channels, the solution flows along an S-shaped path line, so the arrangement is between counter flow and cross flow. It has been found in their study that the sensible and latent effectiveness of such QFPMC are deteriorated by 5-29% and 2-13% respectively compared with a cross-flow parallel-plate membrane contractor. The pressure drop in solution side in raised by 0.15-4.84 times approximately.

All membrane-based dehumidifiers investigated in previous studies are adiabatic types, so the solution is heated by absorption heat released in solution side. So the dehumidification effect could be deteriorated as the result of the solution temperature increase. Similar to internally-cooled direct contact dehumidifiers, internally-cooled membrane-based dehumidifiers have been developed and examined.

Huang et al [83, 84] built an internally-cooled membrane-based liquid desiccant dehumidifier (IMLDD) for the improvement of dehumidification. The structure of a cross flow IMLDD is shown in Fig 2-9. As seen in the figure, channels are made by membranes and plastic plates being stacked together. The feed air (process air) and liquid desiccant divided by membranes

are in cross-flow configuration. The cooling water flows vertically along the plastic plates to for the water falling films in the water channel. Water channels are next to solution channels separated by plastic plates. The sweep air flows over water falling films, in a co-current configuration. When the heat is released to the solution channel, they are taken by the falling water through plastic plates, and then the heat is extracted by the sweep air through evaporation.

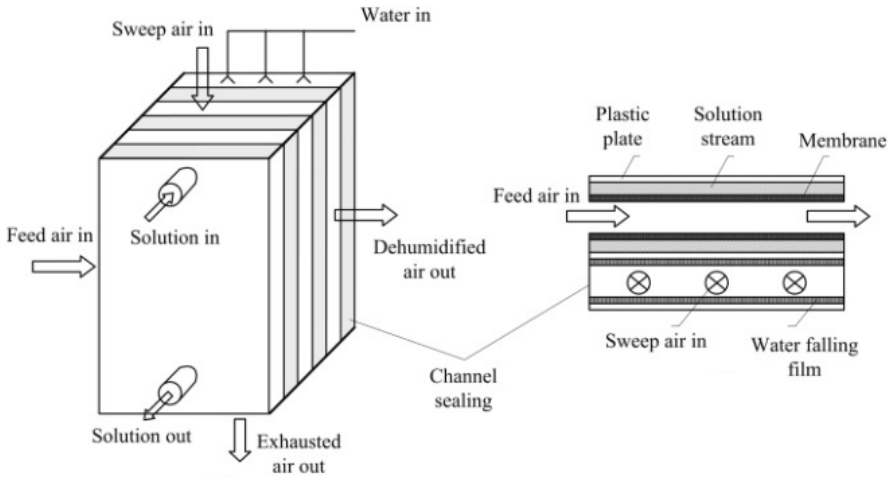


Fig 2- 9 The structure of a cross flow IMLDD [83, 84]

Through numerical modelling and experimental tests it is found that compared to an adiabatic type dehumidifier, the fully developed Nusselt and Sherwood numbers of cross flow IMLDD in feed air and solution channels are 2-3% smaller. The design used cooling channels adjacent to the solution channels, there is another type of structure, which achieve internal cooling by installing cooling tubes inside solution channels.

Huang et al [85] developed a quasi-counter flow parallel-plate membrane channels with cooling tubes (QCPMCC) as depicted in Fig 2-10.

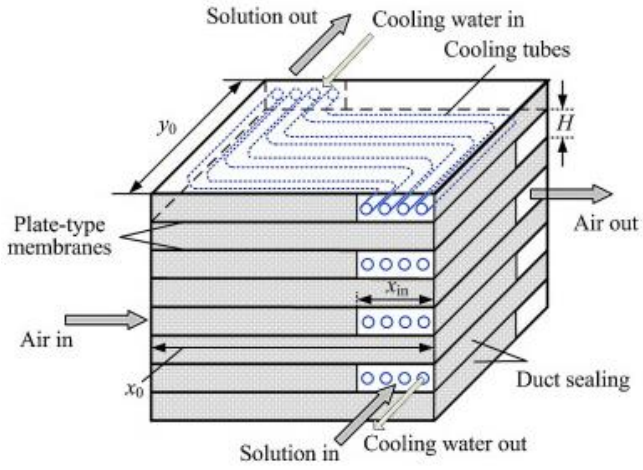


Fig 2- 10 The structure of a quasi-counter flow parallel-plate membrane contractor with cooling tubes [85]

As seen in Fig 2-10, solution flows into and out of the contractor from side openings, they and air flows are in quasi-counter flow configuration. Several Z-shaped cooling tubes with cooling water flowing inside are installed in solution channels to take absorption heat away. Each channel has the dimension of 0.1m long and 0.1m wide. Four cooling tubes with the outer diameter of 0.003mm are installed. The research mainly focused on the effects of channel structural parameters on friction factors and Nusselt numbers. It was pointed out that under the tube outer diameter of 0.003m, the mean Reynolds number $(fRe)_m$ increases with tube number N_{tub}, but the mean Nusselt number Nu_m decreases with N_{tub}. When the number of tubes is fixed (4 in their case), the $(fRe)_m$ increases with tube outer diameter, but the Nu_m decreases with tube outer dimeter.

Huang et al [86] proposed an analytical solution to a internally cooled plate membrane desiccant dehumidifier with similar structure to QCPMCC. However the cooling tubes installed in solution channels are straight rather than S-shaped. Solution flows and air flows are in counter-flow arraignment. Their analytical solution implied that the dehumidifier performance can be improved if solution inlet temperature can be controlled to a relatively low level. Abdel-

Salam et al [87, 88] designed and investigated a novel 3-fluid liquid-to-air membrane-based energy exchanger (3-fluid LAMEE) as shown in Fig 2-11.

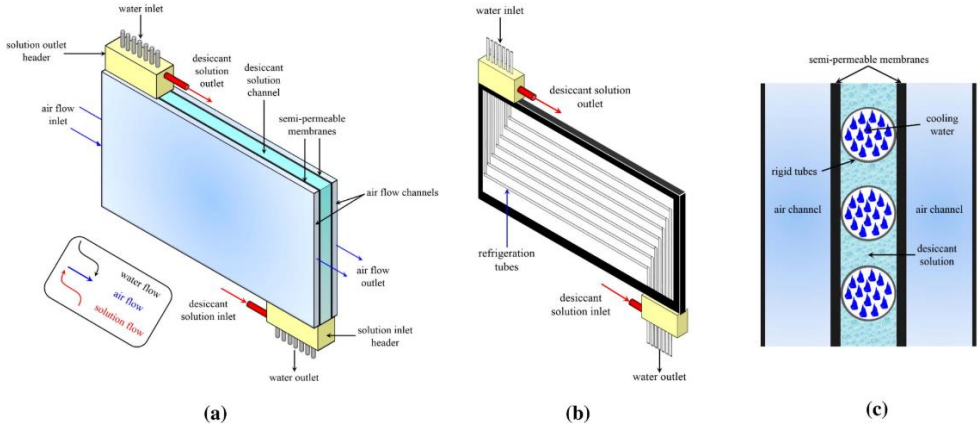


Fig 2- 11 Schematic diagram of 3-fluid LAMEE: prototype of 3-fluid LAMEE (a); solution channel with cooling tubes (b); cross-section view (c) [87, 88]

The solution flow and air flow in 3-fluid LAMEE are in counter-cross flow configuration, while solution and refrigeration (water) are in counter flow arrangement. The unit is 470mm long and 100mm high. The thickness of membranes is 0.3mm. In total 7 refrigeration tubes made from Titanium are installed in solution channel, with inner diameter of 2.362mm and outer diameter of 3.175mm. Water is used as refrigerant. 3-fluid LAMEE has shown better performance compared with 2-fluid LAMEE introduced previously (adiabatic LAMEE) as same effectiveness can be achieved under lower NTU and Cr^*, thus the size of a LAMEE can be significantly reduced if 3-fluid design is applied.

Qiu et al [89] developed another novel internally-cooled hexagonal parallel-plate membrane channel (IHPMC) used for air dehumidification. The schematic diagram of such module is given in Fig 2-12.

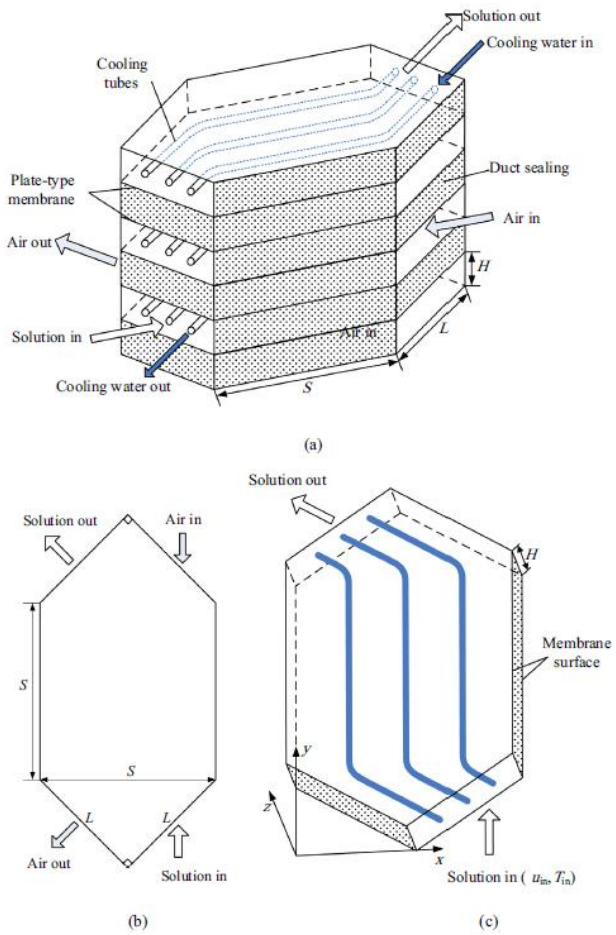


Fig 2- 12 Schematic of IHPMC: 3-D structure (a); plan view (b); calculation domain (c) [89]

Hexagonal structure is another type of quasi-counter flow membrane channels (another type is side in and side out structure as discussed previously). Compared with side in and side out type, hexagonal structure has a smaller pressure drop [90, 91]. As seen in Fig 2-12, the module is formed by layers of internally-cooled hexagonal parallel-plate membrane channels (IHPMC) and HPMC being packed together. Air and solution flows into the contractor from right inlets, and flows out of the contractor from left inlets and they are in quasi-counter flow arraignment. In total three cooling tubes with water as the refrigerant flowing inside are installed in HPMC to form IHPMC, and solution and cooling water are in counter-flow configuration. The fluid flow and heat transfer in IHPMC were studied through finite volume approach, which was solved by CFD (Fluent) software. They calculated fundamental numbers of the mean $(fRe)_m$ and mean Nusselt number Nu_m and they found that under the fixed cooling tube outer dimeter

of 0.002m, $(fRe)_m$ increases and Nu_m decreases with total tube number. By contrast, under the fixed total tube number of 3, $(fRe)_m$ increases and Nu_m decreases with tube outer diameter.

To sum up, numerous researches into flat-plate type membrane-based dehumidifiers have been carried out previously around different topics. Based on flow arrangement they can be formed as parallel-flow, cross-flow, counter-cross-flow or quasi-counter-flow. Based on the structure they can be divided into adiabatic type and internally-cooled type. With regard to internally-cooled type, two types of cooling approach: using cooling channels adjacent to solution channels and using cooling tubes inside solution channels can be applied. They are easy for fabrication due to simple structure. However the packing density of flat-plate modules is around 500 m^2/m^3, which is not large enough [29]. Thus in recent years another type of membrane-based dehumidifier so called hollow-fiber membrane module is developed for its higher packing density and better heat and mass transfer ability. This will be discussed in next section.

2.2.2.2 Hollow-fiber type

Hollow-fiber membrane contractors have similar structures of parallel tube-and-shell heat exchangers. Theoretically speaking, for a liquid-to-air hollow fiber membrane contractor the air can flow either inside (tube side) or outside (shell side) the fibers. However in most applications the air flows outside the fibers while desiccant solution flows inside the fibers. The reason for this structure is that air flows in shell side with much lower pressure drops, so the performance is better [92]. Bergero and Chiari [93] first developed a hollow fiber module prototype in 2001. The structure and dimensions of their built module are shown in Fig 2-13.

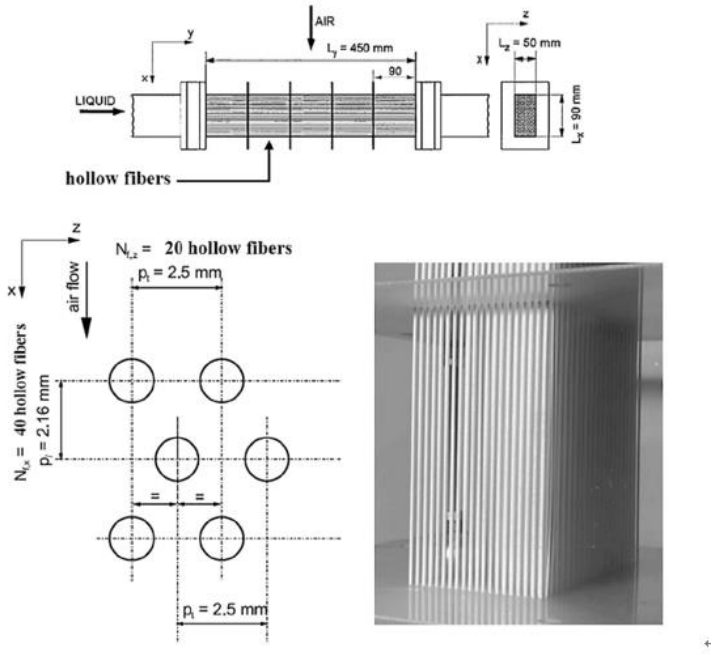


Fig 2- 13 Structure and dimensions of a hollow-fiber module prototype [93]

In total 800 polypropylene hollow fibers are assembled together in a rectangular geometry, LiCl and water are used as the working fluids for air dehumidification and humidification. Their contractor has the total hollow-fiber membrane surface area of $1.2\ m^2$, hollow polypropylene capillaries were arranged in a staggered array, and it has a mass transfer area per unit volume of $593\ m^2/m^3$. Through experimental and numerical analysis, it is found that the effectiveness of contractor decreases slightly as the air mass flow rate increases. It is illustrated in [94] that the mechanism of the common gas-liquid membrane contractors is based on the combined Knudsen and ordinary diffusions for microporous membranes. As for nonporous membranes, which are highly hydrophobic, Knudesn diffusion is the predominant mechanism for water vapour transporting through the membranes.

[95, 96] developed a Graetz-Levegue solution to predict the fiber-side mass transfer coefficient, and a general classification for Graetz-Levegue solution is given in [97] by curve fitting of Graetz and Levegue solutions, which can be applied for transition region not covered by

Graetz-Levegue solution. The heat and mass transfer outside the hollow fiber tubes is relatively more complex than that in inner fiber tubes.

With regards to the flow pattern inside the hollow-fiber membrane module, solution flow and air flow can be either parallel (longitudinal) or cross. For parallel flow, solution and air flow parallel to each other on opposite side of hollow fibers, and they can be co-current or counter-current flows.

Yang and Cussler [98] evaluated the construction design of parallel and cross type contractors. They proposed the mass transfer correlations for hollow-fiber modules under different flow types, and compared these correlations with correlations in previous literatures for heat and mass transfer problem. They concluded that although the heat transfer coefficients in such modules are not always high, the modules' surface area per volume is normally very high, which can be up to 4000 m^2/m^3. The results provided a basis for the design of hollow-fiber type membrane contractors.

Zhang et al [99, 100] analytically and numerically studied the heat and mass transfer in a counter-flow hollow-fiber membrane module used for dehumidification. The structure of the counter-flow hollow fiber membrane module is given in Fig 2-14.

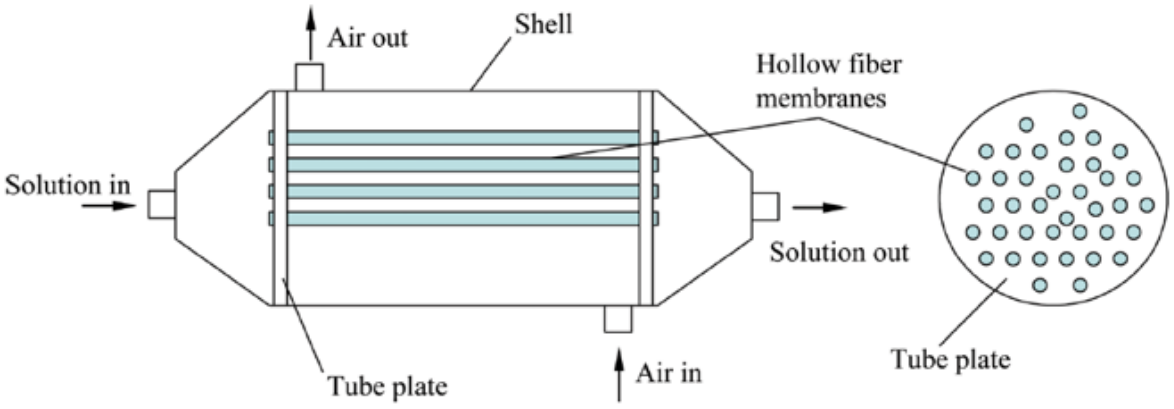


Fig 2- 14 Structure of the counter-flow hollow fiber membrane module [99, 100]

In total 200 hollow fibers were installed in a circular shell to form a complete module. Hollow fibers have the outer diameter of 750 μm and inner diameter of 600 μm. A relatively simple analytical solution was proposed first, and then the conjugate heat and mass transfer problem was solved using free surface method. Mathematical methods used for numerical modelling will be explained in more details in Section 2.6. The conjugate heat and mass transfer problems were solved by finite volume method, and velocity, temperature and concentration distributions for air flow, solution flow and membranes were obtained, the local and mean Nusselt number and Sherwood number were calculated as well.

Then the research was extended by considering the effects of the fiber-to-fiber interaction [101]. Both in-line and staggered arrangement of hollow fibers were considered in the contractor. Then the friction factor, mean and local Nusselt and Sherwood numbers were obtained and analysed. Their studies provided the fundamental data for counter flow hollow fiber membrane contractors under the conjugate heat and mass transfer boundary conditions.

Parallel flow type introduced above has the advantage of simple for manufacturing, well know fluid dynamics in tube and shell sides, and easy for moisture transfer estimation [98]. However it has its disadvantages as well: relatively large pressure loss; low Nusselt and Sherwood numbers; less number of fibers in a shell et al. It was stated that the parallel flow contractor has 200-600 fibers installed in a shell with 4cm in diameter, while there is around 200-1200 fibers in a cross flow contractor. As the result, cross flow type is more attractive than parallel flow type.

Huang et al [102, 103] developed a cross flow hollow-fiber membrane contractor as illustrated in Fig 2-15.

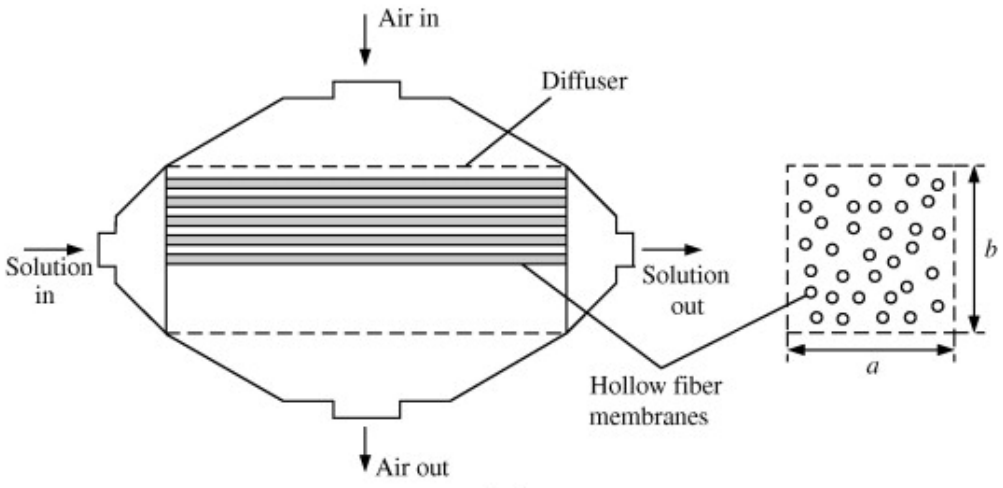


Fig 2- 15 Structure of the cross-flow hollow fiber membrane module [102, 103]

Compared with a counter-flow contractor, corss-flow contractor has a rectangular section, solution and air are flowing in cross arrangement. In total 600 fibers were installed in the rectangular shell box. The outer and inner diameters of hollow fibers are the same as those for counter-flow contractor. Free surface approach was used first to analyse the conjugate heat and mass transfer under the assumption that air flows across the fiber bank to be laminar flow. Subsequently a more realistic and complex situation was considered by assuming that the air flows across the fiber bank trends to be turbulent flow. A low-Re $k-\varepsilon$ turbulence model was used to solve the turbulence situation for air flow, while solution flow was dealt with using a laminar model. For both situations the friction factors and the Nusselt and Sherwood numbers were obtained and validated through experimental data.

The research was extended by considering the interactions between neighbouring fibers [104, 105]. Instead of free surface model, periodic unit cell model was applied to deal with both in-line and staggered fiber arrangements. The friction factors, Nusselt and Sherwood numbers were numerically calculated and validated experimentally. Their results provide fundamental data for a cross-flow hollow-fiber membrane contractor, these data is useful for future component design and structural optimization.

Dindore and Versteeg [106] investigated a cross-flow rectangular hollow-fiber gas-liquid membrane contractor used for physical gas absorption. An analytical solution was derived for the heat transfer problem under limited cases, and CO_2 absorption experiment was conducted in a single-pass cross-flow membrane contractor using water as the solution for the validation of analytical solution. It was concluded that the analytical solution can predict the performance of cross-flow hollow-fiber module under the asymptotic conditions of negligible or small volumetric flow rate changes. But if there is significant change of volumetric flow rate change, analytical solution results are slightly under the module performances.

For a better comparison of cross-flow and parallel-flow, Wickramasinghe el at [107] did a comparison of mass transfer performance in various hollow fiber structures. The performance of both parallel and cross flow contractors were investigated under equal flow per membrane area and flow per module volume, and their research results revealed that cross-flow hollow-fiber membrane contractor shows better performance and higher effectiveness than parallel-flow modules.

Above researches focused on either pure parallel or pure cross flows. However these are all very ideal flow patterns, in reality oblique or skewed flow is a more common case, in which shell side flow impinges the hollow fibers with a skewed angle. Ouyang et al [108, 109] studied the fluid flow and heat and mass transfer across a skewed flow hollow-fiber membrane bank under uniform temperature (concentration), and naturally formed boundary conditions. Authors investigate the influences of skewed angles from 0° to 90° on heat mass transfer and friction properties, and correlations for these basic data under different skewed angles were given. It was summarized that both friction factors, Nusselt and Sherwood numbers rise with skewed angle, they are higher than those for parallel flow, but lower than those of cross flow. Furthermore, staggered array arrangement has higher heat transfer coefficient and pressure drop than aligned arrangement.

Perfectly circular cross-section shapes were assumed for all hollow fibers in researched mentioned previously. However, it should be noticed that the circular cross-section shapes can be easily changed to elliptical ones during the fabrication process [110]. Huang et al [110-113] conducted a series of researches into elliptical hollow-fiber conductors. The schematic of an elliptical hollow-fiber membrane contractor is shown in Fig 2-16.

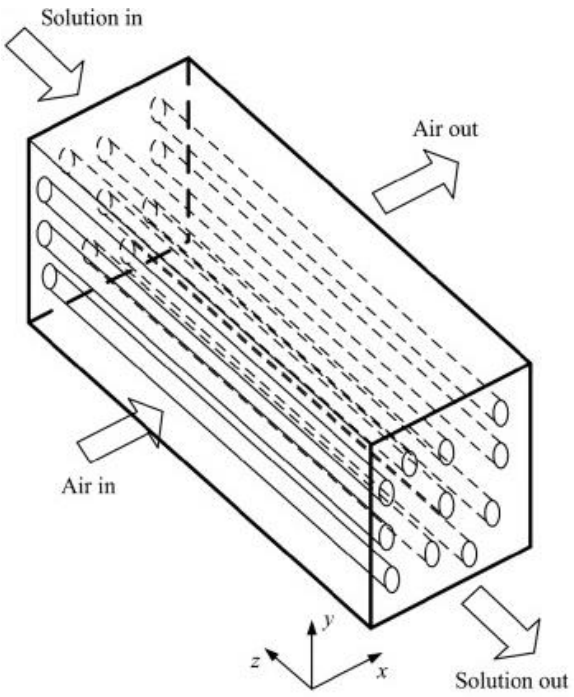


Fig 2- 16 Schematic of an elliptical hollow-fiber membrane contractor [110-113]

As seen in Fig 2-16, due to the fact that hollow fibers are weak in strength and can be easily squeezed to elliptical shapes during the fabrication, a bundle of elliptical hollow fibers are placed in a rectangular shell. Some fundamental heat mass transfer data were numerically obtained such as friction factors, Nusselt numbers and Sherwood numbers for both counter and cross flow modules, and they were validated experimentally. Results showed that heat and mass transfer were deteriorated by around 0.1-6% for the in-line arrangement, and by about 0.15-26% for staggered arrangement when semi-axis ratio in between 0.5 and 1. However when

semi-axis ratio is between 1.0-2.0%, the heat transfer is intensified by about 0.1-9% in an elliptical module compared with a normal module.

Recently, great attention has been paid to another novel structure of hollow-fiber membrane contractor, so called coiled module. Moulin et al [114] first proposed the mass transfer enhancement by secondary flows in a helically tubular hollow fiber. In their design a helically wound, or tubular hollow fiber was built to reduce the liquid-film resistance, experiments were conducted with deoxygenated water flowing inside the hollow fibers with various speeds, and the oxygen was maintained under pressure in the shell side. Is was proved that a secondary flow can be formed in a curved pipe due to the pressure difference between the internal and external wall of the fiber, which is also known as the centrifugal force.

Dean [115, 116] first investigated the complex flow pattern in a curved pipe in a concentric toroidal co-ordinate system. It was pointed out that a secondary motion due to a given pressure gradient would decrease the rate of flow and cause an outward movement of region where the primary motion is the greatest. Thus a helically tubular fiber membrane module applies this phenomena for the mass transfer enhancement.

Moulin et al [114] compared the experimental data from their design with a conventional straight hollow fiber membrans in a parallel alignment. It was found that the performance of oxygen transfer is greatly improved due to the presence of vortices, and the improvement factors were in the range of 2-4.

Liu [117] investigated the mass transfer in a coiled hollow-fiber membrane module. It is made of helical hollow fibers, which are coiled around a core that is a stainless tube with the outer dimeter of 6-12 mm at some wind angles. All fibers were laid evenly in parallel paths. The comparison between a conventional straight module and a coiled module, and a schematic of a secondary flow in curved tube are given in Fig 2-17.

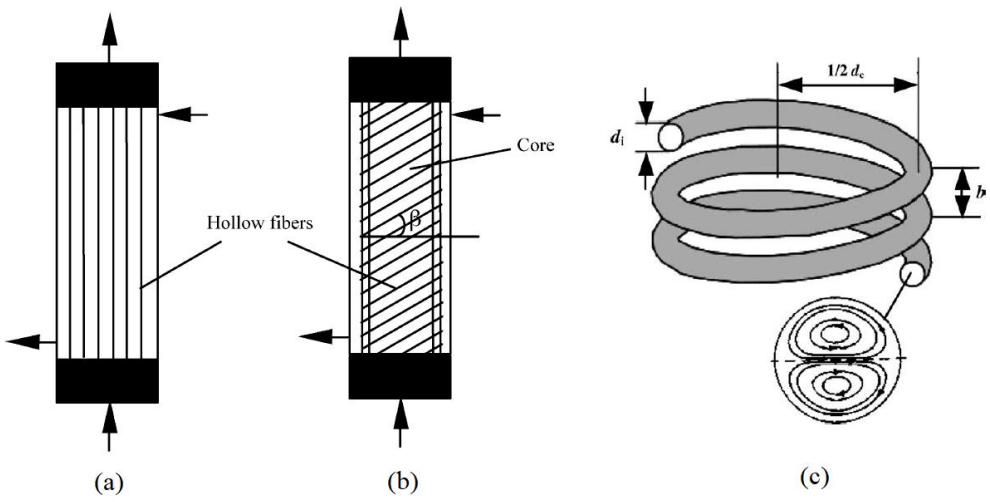


Fig 2- 17 Schematic of a conventional straight module (a); coiled module (b); secondary flow in a curved tube (c) [117]

The mass transfer performance of the module was examined for stripping dissolved oxygen from water. The results showed that the mass transfer can be significantly enhanced in a coiled hollow-fiber module in both shell and air sides, and this is attributed to dean vortices generated in secondary flow inside the helical fiber and the promoted turbulence on the shell.

To sum up, hollow-fiber membrane contractors provide larger packing density and higher performance compared with flat-plate membrane contractors. With regard to the structure they can be divided into parallel-flow, cross-flow and coil types. More realistic cases such as skewed flow and elliptical fiber shapes have been investigated. However, relatively high pressure drop in tube side and complex structure are two of the biggest drawbacks for applications of this type in practice, thus flat-plate type membrane contractors are far more widely used in practice than hollow-fiber type membrane contractors.

2.3 Regenerator

For a complete liquid desiccant dehumidification system, regeneration is considered to be one of the most critical processes in the system since the diluted solution generated in dehumidifier needs to be re-concentrated to realize the solution recycle. Similar to dehumidifiers, with regard to the module structure, regenerators can be divided into direct contact type and membrane-based. They will be discussed in Sections 2.3.1 and 2.3.2 respectively.

2.3.1 Direct contact type regenerator

Similar to direct contact dehumidifiers, packed beds or columns are the main structure of direct contact regenerators. With regard to the flow pattern of liquid desiccant and air, they can be divided into counter flow and cross flow types. Fumo and Goswami [118] studied a cross flow packed bed regenerator using $LiCl_2$ as the desiccant solution. The packing in the regenerator tower is polypropylene Rauschert Hiflow rings, there are 2.54 cm long and the specific surface area is 210 m^2/m^3. The diluted solution was distributed from the top of the regenerator tower by 3 spray heads spaced evenly in an equilateral triangular arrangement. In the regenerator tower desiccant solution and air are in direct contact, and they are in counter-flow configuration. The moisture is the weak solution was taken by air flows due to the surface pressure difference. Their results stated that the regeneration performance can be considerably affected by desiccant inlet temperature, concentration and air mass flow rate. Longo and Gasparella [119] experimentally tested the performance of a counter flow packed column regenerator with structured and random packing using LiBr solution. Two different structures: a random column with 1 Pall Ring elements and a structured column Mellapack 250Y, which uses cylindrical elements made of perforated and corrugated sheets were tested. A one-dimensional simulation code was developed in the study to simulate the packed column, and good agreements was

found between experimental and numerical results. It was indicated that the regeneration temperature is at around 50 ℃ which can be achieved using solar energy or other recovered heat from a thermal engine, and the regeneration performance of a random packed column is 20-25% higher than that of a structured packed column.

Counter flow packed beds have the advantage of high heat mass transfer effectiveness, but the structure of this type is relatively complex and hard for fabrication. By contrast, the duct arrangement and installation of cross flow packed beds are more convenient and easy compared with counter flow ones. Higher efficiency can be achieved if several cross flow packed beds are combined [120, 121].

Kim et al [122] developed a simplified first-order empirical model for cross-flow packed-bed tower regenerator using LiCl as the working fluid. In the study a honeycomb structured packed tower was used as the regenerator. The internal dimeter of the regenerator was 0.01 m, and it had the volume of 0.315 m^2 using wood fiber structured packing with 223 m^2/m^3 specific surface area. Desiccant solution was sprayed from the top of the regenerator and then distributed evenly through the packing, the intake air came into direct contact with the solution and heat mass are transferred between them. The model showed reliable agreement with experimental data, and can be used to determine the optimum regeneration temperature or desiccant mass flow rate to minimize the operating energy consumption.

Liu et al [123] built a regenerator made of CELdek structured packings and tested it using Lithium Bloride (LiBr) as the liquid desiccant. In the regenerator solution and air are in direct contact with each other, and they are in cross flow pattern. The regenerator has the dimensions of 0.55m high, 0.40m long and 0.35m wide. CELdek structured packing was applied as the packing material with specific surface area of 396 m^2/m^3 and the flute is 7mm high. Packings were made of corrugated cellulose paper sheets with various flute angles. One steep and one flat paper sheet were bonded together. They concluded that the regeneration effectiveness

would increase with solution mass flow rate and concentration, but decrease with air mass flow rate and solution temperature. A dimensionless mass transfer correlation was developed as well, and it was validated by experimental data.

Bouzenada et al [124] experimentally studied the mass transfer using LiBr as the liquid desiccant in direct contact with the air flows under various operating conditions. A dynamic vapour sorption equipment (DVS) was used in the laboratory to measure the moisture being absorbed by air flows. The experimental results showed that LiBr can be regenerated at a relatively low temperature, which can be achieved by using flat plate solar collectors. The mass transfer potential in regenerator rises linearly with the air humidity ratio, and the moisture removal rate increases with solution concentration.

Shen et al [125] investigated a liquid desiccant regenerator with heat recovery heat pipe system using Lithium Chloride as desiccant solution. The regenerator used in the system is a direct contact regenerator tower, which is given in Fig 2-18.

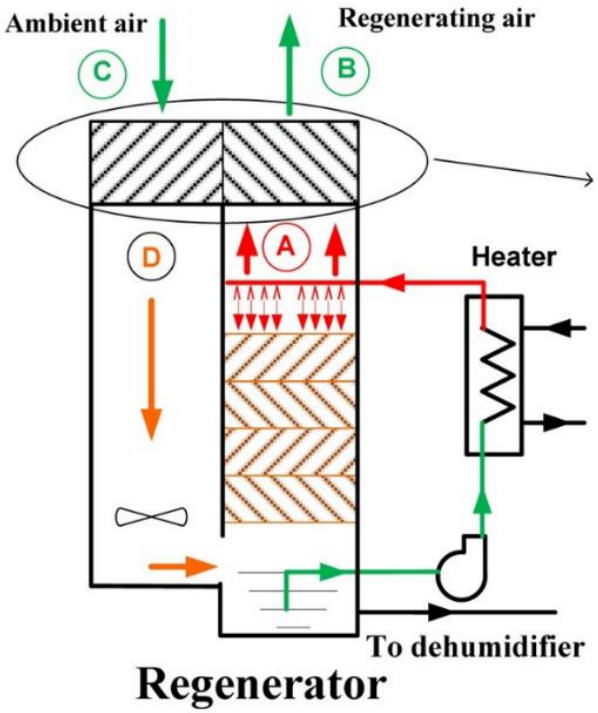


Fig 2- 18 Schematic diagram of direct contact regenerator tower [125]

In the regenerator tower, the upwind air flow and liquid desiccant are in direct contact on the surface of the structured packing in a counter-flow arrangement, and the heat mass transfer occur simultaneously between air and solution flows. The novelty of their research is that they applied a heat pipe heat exchanger for the regeneration air heat recovery. This process is achieved by the preheating of incoming air by the reutilization of the water heat in exhausting regenerating air. After this preheating process the temperature difference between regenerating air and solution in regenerator is reduced, so the solution can maintain relatively higher temperature and vapour pressure. So the mass transfer from solution to air is enhanced. They designed another type of such heat recovery system by using a fixed-plate heat exchanger [126]. The structure of regenerator tower is the same, but the heat recovery unit is replaced by a fixed-plate heat exchanger. The comparison between regenerating performance with heat recovery system and without heat recovery system was made. Results showed that for the heat pipe heat recovery system, maximum 25% and 26.5% of waste heat were recovered, which contributes to 26.5% and 27% energy saving for 4 and 8 rows. For the fixed-plate heat recovery system, maximum 16-19% of waste heat was recovered, which contributes to 14-18% of energy saving. Yang et al [127, 128] designed an ultrasonic atomization liquid desiccant dehumidification/regeneration (UARS) system. In such system the mass transfer performance is greatly enhanced by atomizing the desiccant solution into numerous tiny droplets with the diameter of about 50 μm. The system diagram is depicted in Fig 2-19.

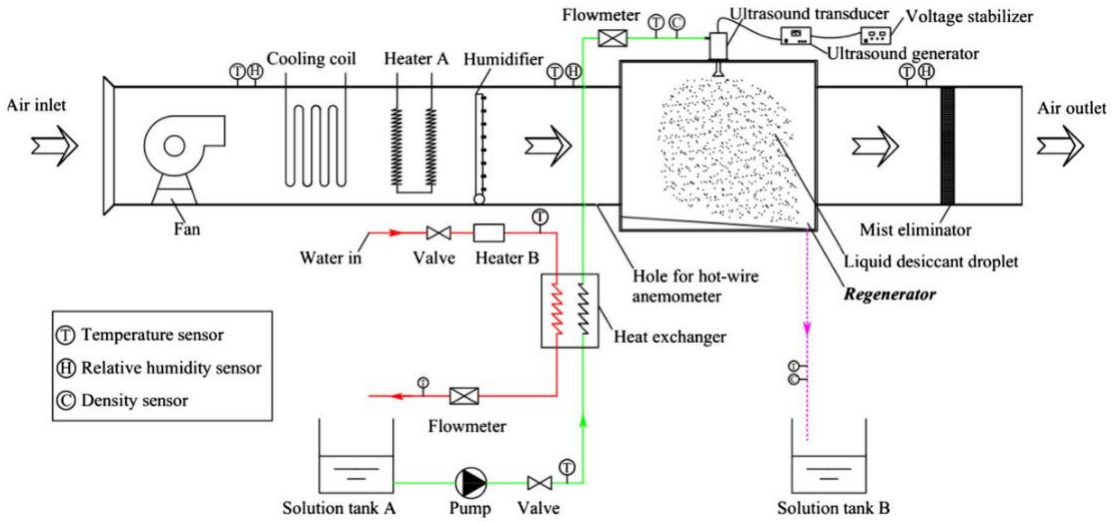


Fig 2- 19 Schematic diagram of a ultrasonic atomization liquid desiccant regeneration system (UARS) [127, 128]

The most critical unit in the system is ultrasonic atomization system, which consists of a ultrasonic generator, a ultrasonic transducer and a voltage stabilizer. Ultrasonic signals can be generated in the ultrasonic generator, and then sent to ultrasonic transducer, where high-frequency vibration can be generated. Desiccant solution can be atomized into small droplets under the effects of these vibrations and cavitation effect. The diameter of droplets can be as small as 50 μm. The results showed that UARS has many advantages over traditional packed bed regenerators. The necessary regeneration temperature can be reduced by 4.4 ℃, the potential power saving can reach up to 23.4% for regenerating a unit mass flow of desiccant solution.

Nada [129] numerically studied the air regeneration by a liquid desiccant falling on rectangular finned-tube heat exchanger for different air flow arrangement: parallel flow, counter flow and cross flow. According to their design, desiccant solution falls on a vertical rectangular fin surface, while the air flows within the gaps between adjacent fins. The air flow and film solution flow can be in different configurations: parallel flow (same direction), counter flow (opposite direction) and cross flow (perpendicular direction) as illustrated in Fig 2-20.

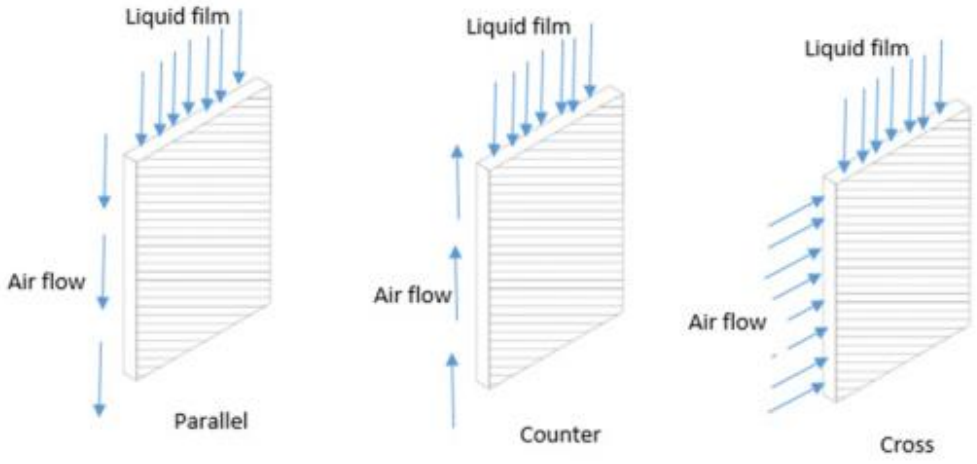


Fig 2- 20 Different flow configurations between air flow and liquid film [129]

The results showed that among all three flow configurations, parallel flow provides the highest heat and vapour transfer rates. For all three arrangements, the air outlet temperature and humidity ratio increase with air and liquid desiccant mass flow rate during the regeneration process.

Liquid desiccant can be regenerated using low-grade energy such as solar energy. Recent development about this topic mainly focused on solar thermal regeneration and solar electro-dialysis technology. In the solar thermal regeneration system weak solution absorbs the solar thermal energy and is heated in a solar collector. In the electro-dialysis system the regenerator is basically an electro-dialysis stack which consists of a multitude cells placed in parallel between two electrodes. This technology is based on the transport of ions under the influence of an electrical filed, and it is driven by photovoltaic cells.

A comprehensive comparison between these two types was carried out by Cheng and Zhang [130], it was stated that solar electro-dialysis regeneration system is more energy efficient, but the cost is relatively higher than solar thermal regeneration system.

Alosaimy and Hamed [131] theoretically and experimentally investigated a packed column regenerator regenerated by solar heating system. The regenerator was a packed column made

of honeycomb packing, and the water heated by solar heating system was circulated in a finned tube air heater to heat the air. Then hot air came into direct contact with weak solution in the packed column regenerator. The results demonstrated that the system can operate at nearly steady state condition when a storage tank in used with solar collector.

Kabeel [132] investigated the forced cross flow of the solar regenerator in the open cycle absorption solar cooling system. The regenerator has the absorption surface of 0.6 m × 1 m, and it is made of layers of black cloth. $CaCl_2$ was used as the working fluid. The forced cross flow solar regenerator was compared with the free convection solar regenerator collector, and it was found that the forced convection cross flow solar regenerator has higher efficiency than the free convection regeneration, and the regeneration rate depends on the solution concentration and mass flow rate.

Li et al [133, 134] proposed a photovoltaic-electrodialysis (PV-ED) regeneration method for desiccant cooling system. The regenerator is an electrodialysis (ED) stack, which is formed of multitude parallel cells between two electrodes. In alternating cells the desiccant solution is concentrated and diluted respectively, means the weak solution enters into the concentrate cells while the diluted solution enters into the diluted cells. So in the ED stack, the weak solution can be concentrated and the diluted solution is diluted. Concentrated solution is the strong solution and can be used for dehumidification. The primary investigation showed that regardless of the poor PV efficiency, PV-ED system performance can be higher than twice of that of the conventional solar thermal system.

Li et al [135, 136] compared the performance of single-stage and double-stage PV-ED systems. In a double-stage PV-ED system, two regenerators corresponding to stage 1 and stage 2 were used. The concentrated solution from stage 1 was further concentrated in stage 2. It is revealed in their results that compared with single-stage system, double stage PV-ED system is more energy-efficient and can save more than 50% energy under optimized working conditions.

Yang et al [137] developed a novel photovoltaic capacitive deionization, so called PV-CDI method for liquid desiccant regeneration. They proposed a photovoltaic (PV) capacitive deionization (CDI) regeneration method, which uses CDI unit to promote the adsorption of ions in the electrochemical double layer of a charged electrode surface by applying an electric potential. The regeneration system they used consists of two CDI units, one works as regenerator to produce concentrated solution and another works as deionizer to produce pure water. This system was connected to a direct current (DC)-DC converter, which transform the variable V-I curve into either constant voltage or constant current supply. As a result the CDI units could also act as a discharging capacitor and uses the stored energy to deionize the solution. The results showed that under the same cooling output, PV-CDI system consumes more solar energy than solar thermal system since the efficiency of PV system is currently significantly lower than that of solar thermal system. However it still has great potential for flexibility, stability and green air-conditioning system.

All regenerator introduced in this section have the direct-contact structure, which would inevitably cause the problem of carry-over of the regeneration air. Membrane-based regenerators, which could avoid carry-over problems have been studied in previous literatures. There will be reviewed in the next section.

2.3.2 Membrane-based type regenerator

Membrane-based regenerator is an alternative to direct-contact regenerator to solve the desiccant droplet carry-over problem. Furthermore, it also saves the liquid desiccant since considerable desiccant is lost due to carry-over.

Duong et al [138] investigated the regeneration of LiCl solution by membrane distillation for air conditioning. The regenerator was a plate-and-frame module consists of layers of flat-sheet polytetrafluoroethylene (PTFE) membranes from Porous Membrane Technology. The

membranes used were 60 μm thick, with and the nominal pore size of 0.2 μm and porosity of 80%, and the total active surface area was 138 cm^2. During the experiments, the diluted solution was heated by stainless steel coils submerged in a hot water bath. Then it entered the solution channels, the heat and mass transfer occurred through the membranes, so diluted solution was concentrated in the solution channels. The regeneration capacity ΔC and specific thermal energy consumption α were used to evaluate the regeneration performance. The results revealed that when the feed temperature is 65 ℃, the system could increase the solution concentration up to 29% without significant loss of desiccant solution. Increasing feed temperature would increase ΔC and reduce α.

Ge et al [139] compared the experimental and numerical data for heat and mass transfer of a flat-plate membrane-based heat mass transfer contractor used for regeneration. A small-scale single-panel regenerator was used, and the solution and air were in counter-cross flow configuration. The structure of the regenerator is similar to that of the dehumidifier in [67, 68] as depicted in Fig 2-7. The regenerator has the length of 0.99m, and the thickness for solution and air channels are 1.2 mm and 5 mm respectively, and the membranes are 0.265 mm thick. Then they investigated the influences of different parameters, such as NTU, Cr^*, air inlet temperature and humidity ratio, solution inlet temperature and concentration, on the regenerator effectiveness and moisture flux ratio. It is found that the dimensionless parameters NTU and Cr^* have significant impact on regenerator performance, while the impacts of solution and air properties are small. However, air side effectiveness was used in their study for the evaluation of regenerator.

Moghaddam et al [39] for the first time introduced the solution side effectiveness to evaluate regenerators as in regenerator the main focus is on the desiccant solution side rather than air side. They used the same structure of regenerator as that used in [139]. It was noticed in their experimental data that solution-side effectiveness were sensitive to the solution inlet

concentrations, and the difference between air-side and solution-side latent effectiveness were negligible. By contrast, solution-side sensible and total effectiveness should be applied for the evaluation of regenerators in most cases.

Datta et al [140] designed and experimentally investigated the multi-effect regenerator, which uses hydrophobic membranes to separate the solution and water vapour. The pictorial view of the regenerator is given in Fig 2-21.

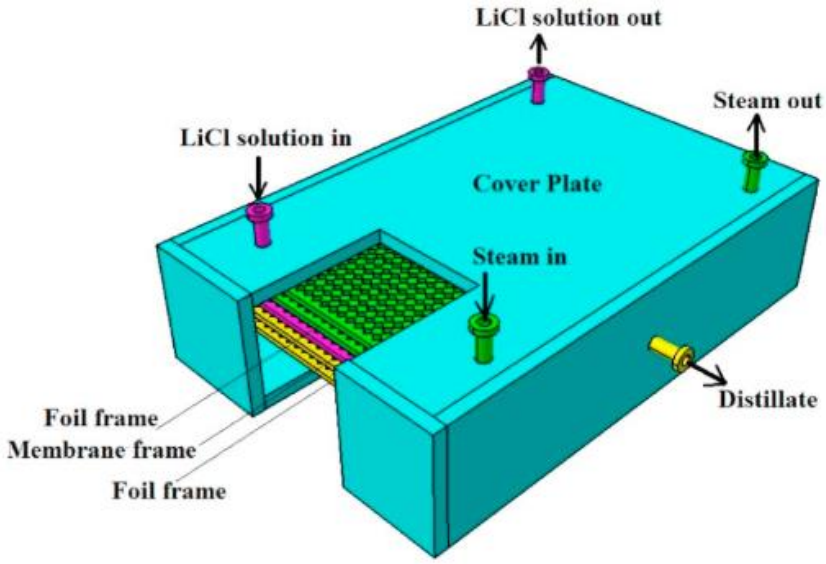


Fig 2- 21 Pictorial view of the regenerator [140]

The regenerator used layers of hydrophobic polypropylene (PTFE) membranes, which had the pore size of 0.2 μm and the thickness of 0.12-0.2 μm. The regenerator had the height of 70 cm, width of 70 cm and the thickness of 15 cm. LiCl was used as the working solution in the experiments. Performance ratio (PR), defined as the ratio of heat generation of regeneration process to the average heating energy was used for the system performance evaluation. And according to their results, PR was obtained at 2.5 under the heating water temperature of 50℃ with the inlet solution concentration of 8%. PR would improve with inlet solution temperature, but decrease significantly with inlet solution concentration.

To sum up, regenerator, as the one of the most critical units in a liquid desiccant dehumidification system have been studied in many literatures before. Based on the structure

they can be furthermore divided into direct contact type regenerators and membrane-based type regenerators. Packed bed or packed columns are the most common types of direct-contact regenerator. With regard to flow pattern, counter flow and cross flow configuration have been designed, each type has both advantages and disadvantages. The solution can be regenerated using low-grade energy, such as solar thermal (TH), photovoltaic-electrodialysis (PV-ED) or photovoltaic capacitive deionization (PV-CDI). Membrane-based type regenerators have advantages over direct-type ones of reducing desiccant loss and avoiding carry-over problems. Compared with direct-contact type, there is limited number of studies into the membrane-based type regenerators so far.

2.4 The complete membrane-based dehumidification system

Membraned-based dehumidifiers and regenerators have gain considerable attention recently. However the studied around this topic as introduced in previous two sections mainly focus on the performance of either single dehumidifier or single regenerator. For more comprehensive understanding of the system operation, studies about the complete membrane-based dehumidification system have been carried out previously in several literatures, which will be reviewed in this section.

The run-around system was firstly proposed by London and Kays [141], where they studied a liquid-coupled run-around system for gas-turbine plants. It was revealed that the system optimum performance can be achieved once the heat capacity rates of air and solution are equal under the constant NTU values.

Then Forsyth and Besant [142, 143] studied the performance of a run-around heat recovery system using two identical coil heat exchanger and aqueous glycol as the coupling fluid. A numerical model was developed for the performance prediction, but the results did not agree well with the experimental results due to several complex factors in experimental test were not

considered in the mass transfer correlations. Even though it was still found that for the optimum design of the system, the effectiveness should not be considered as the only influencing factor, and the total life cycle cost should be taken into account as well.

Fan et al [71] numerically tested the performance of a run-around heat and mass recovery system that consists of two cross flow membrane liquid-to-air heat and mass exchangers (RAMEE) as shown in Fig 2-22.

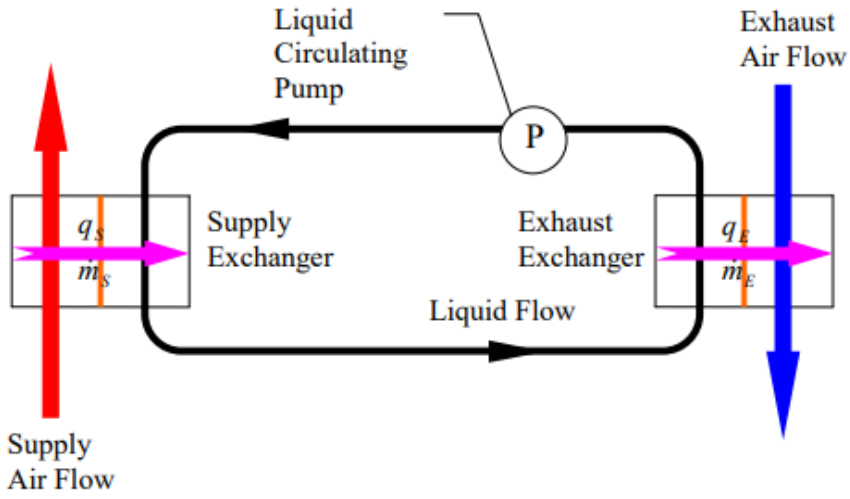


Fig 2- 22 Schematic diagram of a run-around heat and mass recovery system [71]

In the run-around system, two identical cross flow heat and mass exchangers were connected by solution flow, one as the supply exchanger (dehumidifier) and the other as the exhaust exchanger (regenerator). LiCl was used as the coupling fluid and it was running cross-flow to the exhaust and supply air flows. The solution could regenerate itself through mass exchange with supply and exhaust air flows. The steady stage operation was investigated when the total heat and moisture transfer rates in the exhaust exchanger balance the rates in the supply exchanger. As the result, neither energy nor moisture need to be added or removed from the system, and the only energy input is the pump and fan energy for operation. A numerical model was developed for the run-around system, and it was validated experimentally. They concluded that air channel size has greater impact on the run-around system performance than the solution

channel size, and the thermal entry length of two heat mass exchangers can be neglected in the run-around system.

Hemingson et al [144] presented a study of steayd-state performance of a run-around membrane heat and mass recovery system consists of two identical counter-flow RAMEE for a range of outdoor air conditions. It was found that the effectiveness of the run-around system were considerably dependent on outdoor conditions. For several outdoor conditions the effectiveness exceeded 100% or below 0%, and latent and sensible effectiveness were influenced by heat and moisture transfer respectively.

Vali et al [70] studied another run-around heat recovery system using two identical counter-cross flow flat-plate heat exchangers. Only heat transfer was considered in the two-dimensional numerical model, and the heat transfer between solution and supply exchanger, and the heat transfer between solution and exhaust exchanger were considered balanced under steady state operation conditions. It was shown that the effectiveness of this counter-cross flow run-around system is higher than the cross-flow flow run-around system but lower than counter-flow run-around system. The maximum sensible effectiveness was achieved for exchangers with a small entrance aspect ratio and small solution flow inlet and outlet lengths under the fixed total surface area.

Ge et al [145] proposed an analytical solution to a counter-cross flow run-around membrane energy exchangers system (RAMEE). The system includes two or more individual liquid-to-air membrane energy exchangers, the liquid desiccant solution is pumped in the closed loop to connect these membrane energy exchanger. The schematic diagram of such system they investigated is shown in Fig 2-23.

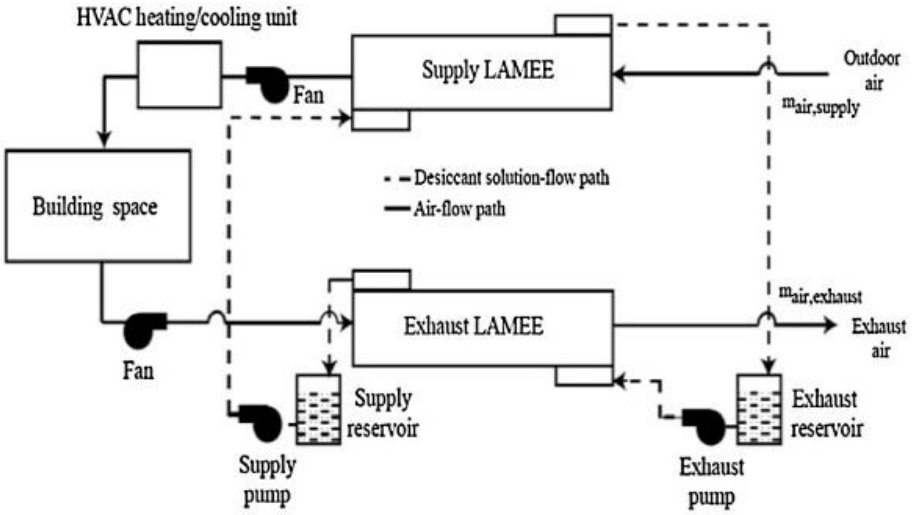


Fig 2- 23 Schematic diagram of a counter-cross flow RAMEE [145]

As seen in Fig 2-23, two liquid-to-air membrane energy exchangers (LAMEE) were connected by desiccant solution, one acts as supply LAMME and another as exhaust LAMEE.

One LAMEE was located in the outdoor supply air flow entering the building, while the other one was installed in the exhaust air flow leaving the building. There is not additional heat or cold source for the system and only electricity used by fans and pumps were added to the system. The analytical solution was based on Zhang's analytical solution to a counter-flow tube and shell liquid desiccant dehumidifier [99]. Results showed that the run-around system with equally sized heat mass exchangers can achieve the maximum effectiveness in most conditions, and the annual energy recovery rate can be improved by up to 7% if the solution mass flow rate can be properly controlled.

All literatures introduced above dealt with the steady-state performance of the run-around system. Seyed-Ahmadi et al [146] studied the transient behaviour of a run-around heat and moisture exchanger system, which consists of two identical cross-flow LAMEEs in the closed loop. Firstly they developed a theoretical model to investigate the transient performance using the finite difference method with an implicit time discretization. To study the transient performance, a new definition so called quasi-steady state was defined as the time when all

heat and mass lost in one airflow is taken by the other air flow. So the system was investigated for a sufficient period of time so that quasi-steady state has been achieved. Numerical results for heat transfer only single LAMEE were compared with an analytical solution and good agreements were obtained. The numerical model was useful for determing the transient response time of RAMEE and approaches to properly control RAMEE under various practical situations. For the second step, the transient model was applied under a range of initial conditions [147], where the transient response of the RAMEE system was presented for step changes in the air temperature and specific humidity at the inlets. Influences of several parameters on the transient responses were studied: NTU, Cr^*, storage volume ratio, and solution inlet concentration. Is was found in their results that the transient response can be dramatically affected by storage volume ratio and solution inlet concentration. Moreover, the system quasi-steady conditions can be substantially changed by the heat transfer between run-around system and its surrounding environment.

Apart from heat and mass transfer investigation, Patel et al [148] studied the contaminant transfer in run-around membrane energy exchangers. In a run-around system volatile organic compounds (VOCs) could transfer from exhaust air side to supply air side for various reason, which would have adverse health effects on occupants such as headache, drowsiness and breathing difficulties [149]. In experiments sulphur hexafluoride was used as tracer gas to test the air leakage, toluene and formaldehyde were applied for testing VOCs transfer fraction. It was concluded that for a run-around system, the transfer of low water soluble VOCs between two exchangers were negligible, but a small detectable transfer of very water soluble VOSs were traced.

Rasouli et al [150] conducted an energetic, economic and environmental analysis of a 3-storey hospital HVAC system using a RAMEE system. The RAMEE system was simulated for the hospital building under four North American climates. It is found that RAMEE has the potential

of reducing heating and cooling capacities by 50% and 25% respectively. The payback period of the RAMEE was estimated to be 0-3 years, and the application of RAMEE could reduce the greenhouse gas emission by up to 25%.

To sum up, numerous studies about complete run-around membrane energy recovery systems have been conducted regarding different aspects. However, it is assumed in these studies that the heat and mass transfer rates in supply exchanger balance those in exhaust exchanger, in other words, there is no heat or moisture added or removed from the system. As a matter of fact, the system can benefit significantly from an external heat source or cold source, in which case a hot water loop and cooling water loop are included in the configuration.

2.5 Desiccant and membrane materials

A desiccant material absorbs the water vapour towards itself, and the strength of desiccant material can be evaluated by its equilibrium surface vapour pressure, which increases with desiccant temperature and the water content in the desiccant solution. Apart from surface vapour pressure, there is some other properties that affect the performance of liquid desiccant, such as regeneration temperature, energy storage density, crystallization point, solubility, availability, cost et al [151]. Furthermore, the semi-permeable membrane is considered to be the most critical component in a membrane-based liquid desiccant dehumidification system. The characteristics of membranes may significantly influence the system performance. Thus in this section, different liquid desiccant and membrane materials will be introduced and compared.

2.5.1 Desiccant materials

Firstly, commonly used desiccant materials: halide salts such as LiCl, $CaCl_2$, LiBr, triethylene glycol, organic acids and the mixture or composite of salts will be introduced.

2.5.1.1 Halide salts

Triethylene glycol was the earliest used halide salt liquid desiccant, but its usage was strictly limited by its relatively high viscosity, which would made the system unstable due to liquid residence. It has the advantages of low toxicity and compatibility with most metals.

EIsarrag [152] pointed out that glycol is volatile since its surface vapour pressure is too low, and glycol in the dehumidification system may volatilize into the conditioned rooms, which would increase the cost dramatically and is unacceptable for air-conditioning systems.

It was also revealed in [151] that the dew point of air achieved by using the 96% triethylene glycol can be achieved by using LiCl solution with the mass concentration of 42%. This means that the molar concentration of the glycol in the air would be 1% that of the water vapour, thus the annual loss of glycol in the air conditioning systems would be very high.

Lithium Chloride (LiCl), Calcium Chloride ($CaCl_2$) and Lithium Bromide (LiBr) are three of the most commonly used halide salt solutions recently.

Ahmed et al [153], Zuber et al [154], Sun et al [155] and Morrillon et al [156] measured the thermodynamic properties of different liquid desiccants. It was found that among these halide salts LiCl solution is the most stable liquid desiccant, which offers the lowest water vapour pressure under the same temperature. Furthermore, it will not vaporize under ambient conditions and its viscosity is relatively low so that the pump energy consumption can be saved. However, the price of LiCl is relatively high.

By contrast, $CaCl_2$ is the cheapest halide salt, and it is the most readily available type. Its dehumidification potential is the lower than LiCl, and according to [151], $CaCl_2$ with the concentration of 43% would have the same dehumidification effect as the LiCl with the concentration of 34%. In the meanwhile, its usage is limited due to the fact that its stability depends on conditions of inlet air and desiccant concentration.

McNeely [157] tested the thermodynamic properties of LiBr. Kaita [158] developed an equation to predict the thermodynamic properties of LiBr at high temperatures. The developed equation was valid for concentration of 40-65 % for weight under the temperature of 40-210 ℃. The result was very helpful for the modelling and design of triple-effect LiBr chillers.

The mass transfer performance of LiBr and $CaCl_2$ solutions were analysed and compared by Lazzarin et al.[159]. The authors revealed that based on the same temperature and crystal temperature, LiBr showed better heat and mass transfer performance than that of $CaCl_2$.

Liu and Jiang [160] experimentally tested the dehumidification of air (air flow rate between 0.24-0.48kg/s and inlet temperature between 25.4-38.8 ℃) using LiBr and LiCl, and according to their results the COPs of both system are similar, with 0.45 for LiBr and 0.47 for LiCl respectively.

Kornnaki et al.[161] compared LiCl, $CaCl_2$ and LiBr through testing the performance of a counter flow dehumidifier mathematically. Under the same air outlet conditions the dehumidifier absorption efficiency was 0.145, 0.137 and 0.125 for LiCl, LiBr and $CaCl_2$ respectively. Moreover, LiBr has the highest price among three, which is approximately 20% higher than that of LiCl. Other types of halide salts have been investigate as well.

Namvar et al.[81] used magnesium chloride ($MgCl_2$) as the desiccant solution for a membrane-based liquid desiccant dehumidification system. The results showed that the $MgCl_2$ working concentration rate was less than saturation concentration (35.9%) which would avoid crystallization problems.

2.5.1.2 Organic acid

All halide salt solutions introduced above have the disadvantage of being corrosive to metal, which would negatively affect the operation of air-conditioning systems. In recent years another type of liquid desiccant so called organic acid, such as potassium formate (KCOOH),

sodium formate (KCOONa) and potassium acetate ($C_2H_3KO_2$) has gained much attention for its low corrosivity, low toxicity and low volatility [162].

Longo and Gasparelle [119] tested the performance of a packed column dehumidifier/regenerator using H_2O/LiCl, H_2O/$CaCl_2$ and H_2O/KCOOH. It was found that although conventional H_2O/LiCl and H_2O/LiBr presented a better performance than new solution H_2O/KCOOH, H_2O/KCOOH was less corrosive and much cheaper than traditional desiccants and fully compatible with the environment, which allows humidity reductions of interest for technical applications.

Furthermore, at high solution concentration KCOOH can outperform conventional liquid desiccant by promoting a high degree of vapour pressure depression while maintaining a crystallisation temperature of less than 0℃ [163]. According to [151] KCOOH, KCOONa or can dehumidify the air up to 25% of relatively humidity but maintain a high viscosity level. For example, potassium acetate ($C_2H_3KO_2$) with the temperature of 27 ℃ and mass concentration of 70% has a viscosity of around 0.028 pa, while the LiCl solution with the concentration of 43.1% and the same temperature has half of that viscosity. Last but not least, acetate formate such as $C_2H_3KO_2$ and $C_2H_3NaO_2$ have higher viscosity than potassium formats under concentrations with equivalent equilibrium relative humidity.

To sum up, despite the fact that organic acids have weaker dehumidification ability than halide salts, they are still good alternatives for many applications for several advantages,

2.5.1.3 Mixed and composite desiccant

As explained in Section 2.5.1, the prices for single desiccant material with relatively higher dehumidification ability such as LiCl are too high. Thus there has been increasing attention paid to the mixed desiccant, which have the better dehumidification efficiency, lower material cost and energy consumption [164].

Ertas et al. [165] experimentally tested the properties of the mixed LiCl-$CaCl_2$ desiccant solution under 20% of mass concentration, and proposed a mixing ratio of 1:1 for the best performance.

Ahmed et al. [153] predicted the vapour pressure of the mixed LiCl-$CaCl_2$ desiccant solution using a simple mixing rule (SMR) proposed by Nilson [166]. However by comparing the calculated results with experimental tested result, the SMR could predict the viscosity of mixed solution well, but not so well in predicting the density and vapour pressure of the mixed desiccant.

Then Chen and Evans [167] and Chen et al. [168] proposed an electrolyte non-random two-liquid (NRTL) method which uses only binary parameters.

Yao et al. [169] compared these two methods by testing the surface vapour pressure of the mixed solution under different circumstances, and found that the SMR shows the better accuracy when the mixed solution concentration is below 10%, while the NRTL method is much more accurate when the solution concentration is higher than 30%.

Zhu and Yao [170] investigated the optimum mixing ratio of LiCl-$CaCl_2$ solution to be 1:1 by NRTL method and are verified through measuring the vapour pressures of various mixture ratios and mass concentrations of mixed solution under different temperatures.

Zhao et al. [171] and Li et al. [172, 173] applied the NRTL method to investigate the optimal ratio of the mixed LiCl-$CaCl_2$ desiccant solution for a direct contact liquid desiccant dehumidification system. A new optimum ratio selection method was provided by using activity map.

Li et al [174] also proposed a novel approach for selecting a cost-effectiveness mixed desiccant solution group by combing the NRTL method with desiccant cost to obtain the mathematical form of the cost-effectiveness. It was found that the best cost-effectiveness and economy can be achieved when the total solution concentration is about 50%.

Apart from the mixed halide salt solution, several composite desiccant materials have been developed and tested. Composite desiccant usually are formed by confining salts into porous host adsorbents, thereby the limited dehumidification capacity of silica gel and the corrosive features of salt solutions could be eliminated [175].

Moreover, the composite desiccant can overcome the problem of desiccant reduction for halide salt during the operation [176]. Jia et al [177] fabricated a honeycombed desiccant wheel made of composite desicant of silica gel impregnated with LiCl and LiCl. The performance of traditional silica gel was compared with the composite silica gel-LiCl, and it was found that composite desiccant performs better than the traditional one and can remove more moisture from air by up to 50%.

Gonzalez et al [178] developed a new composite material made of sepiolite and activated carbon, or sepiolite and $CaCl_2$. The design used the fibrous and hydrophilic properties of sepiolite and the hydrophobic nature of activated carbon. The results showed that sorption capacity of sepiolite can be substantially improved when it is impregnated with $CaCl_2$.

Chua [179] investigated the heat and mass transfer performance of three different composite materials: silica gel- $CaCl_2$, silica gel-LiCl and silica gel- polyvinyl alcohol (PVOH). The author conducted experimental tests to validate the derived numerical model. It was noted in the results that the moisture removal capacity, regeneration rates and the associated pressure drops of composite desiccants could be improved by up to 11% compared with pure silica gel.

Chua et al [180] developed a hybrid system by intergrading a composite desiccant with nano-woven membranes. The composite desiccant used the silica gel and LiCl as bases, and then added $CaCl_2$ and bentonite to promote the hygroscopic nature of composite desiccant. It was found in their results that the new hybrid system could reduce the total energy consumption per unit moisture removed by up to 40% compared with pure silica gel system.

To sum up, halide salts are the most commonly used desiccant materials. LiCl has the highest dehumidification capacity, but with relatively high price. $CaCl_2$ is the cheapest halide salt, and it is the most readily available type. LiBr has the highest price, but its hygroscopic nature is between LiCl and $CaCl_2$. Organic acids have weaker dehumidification ability than halide salts, but they are good alternatives for low corrosivity, toxicity and volatility. Compared with pure desiccant, mixed desiccant may have better dehumidification efficiency, lower material cost and energy consumption. In conclusion, a good desiccant should have following properties: high hygroscopic capacity; low viscosity; low volatility; non-corrosive; non-toxic; physically stable; low regeneration temperature; inexpensive.

2.5.2 Membrane materials

In this section, different materials used to make semi-permeable membranes are introduced. Selectivity and permeability are two of the most important characteristics for membrane materials. Basically there is two main types of polymer membranes: hydrophobic microporous membranes and nonporous membranes.

Zhang et al [181] fabricated a microporous cellulose acetate (CA) membrane for heat and moisture recovery. A cheap and raw material of CA, environmentally friendly solvent acetic acid and deionized water were used during the fabrication, membranes were fabricated in a one-step approach, which was direct wet phase inversion method. A porous support layer and a dense skin layer were formed simultaneously during the solvent and coagulant medium exchange.

Zhang et al [182] fabricated a vapour-permeable composite membrane, which used porous polyethersulfone (PES) as the support layer, and dense polyvinylalcohol (PVA) as the active separating layer. During the fabrication LiCl was added to the PVA solution for the purpose of moisture permeation facilitation. The study results showed that membranes with 2.3% LiCl has

the highest moisture permeation rate, which was 70% higher than that of membranes without LiCl addition. The scanning electron micrograph (SEM) pictures showed that microporous membrane has a fractal structure with numerous macro or micro pores in various sizes in the through-plane direction. Such micro structure the membrane is normally disordered and extremely complicated [183]. The microporous membranes have the potential risk of pore-wetting by desiccant solution. Such leakage was proved to be related to the surface tension, the higher the surface tension, the lower change pore-wetting would happen, thus halide salts were added to the organic absorbents during the fabrication of membranes to increase the surface tension [29]. Apart from surface tension, many other factor could lead to leakage such as adhesion potential of hydrophobic material, adsorption as the result of electrostatic interactions [184]. As the result, the operation conditions for microporous membranes could be magnificently restricted. This problem can be solved by using nonporous membrane materials. Gabelman and Hwang [185] introduced a hollow fiber membrane contractor using nonporous polyolefin fibers that are woven into a fabric and wrapped around a central core.

Woods et al [186] developed a membrane-based absorption heat pump using microporous membrane coated with a thin layer of silica gel.

Li and Teo [187] designed and fabricated an ultrathin skinned hollow fiber module made of a bundle of hollow fibers with a dense skin layer at the outer edge. The dense skin layer would eliminate the possibility of filling membrane pores with liquid desiccant which would cause dramatic reduction of CO_2 transfer rate. For the fabrication of the outer layer, water or NaOH solution were used as the absorbent, and a gas mixture of 4% CO_2 fed to fiber lumen.

Karoor and Sirkar [188] investigated the separation of CO2 from nitrogen with water as the absorbent in a shell-and-tube hollow fiber contractor. The nonporous hollow fibers made of polydimethylsiloxane were used to absorb CO2 selectively.

Lee et al [189] numerically analysed the performance of hollow fiber membrane contractor to remove CO2 using potassium carbonate as the absorbent. In the study Polydimethylsiloxane (PDMS) were used as hollow fibers, and the pores of which were filled with gas. Thus membranes were referred as nonporous (non-wetted) mode. To avoid liquid immersing in pores, hydrophobization can be applied on the permeate side, or composite with a hydrophobic membrane layer [190].

Zhang [191] numerically studied the heat and mass transfer in an enthalpy exchanger, which used a novel membrane material so called hydrophobic-hydrophilic composite membrane. This material consisted with two layers: a hydrophobic porous support layer and a hydrophilic dense active layer. It was shown in the results that the largest moisture resistance in the composite membrane is from the support layer, while the heat resistance of both the support layer and the active layer is negligible.

Zhang [192] and Pei et al [193] designed and fabricated a polyvinylidene fluoride (PVDF) membrane material, which consisted with three layers: a sponge-like porous support layer, a porous media with finger-like macro-voids layer, and a thin denser skin layer with smaller pores. During the fabrication, the hydrophilic materials such as polyethylene glycol (PEG) and polyvinyl pyrrolidone (PVP) were added to the solution to form a hydrophilic-hydrophobic composite material.

To sum up, there is two types of membrane materials currently being used: hydrophobic microporous membranes and nonporous membranes. The former one has the potential risk of pore-wetting by desiccant solution, which can be solved by applying nonporous membranes. In conclusion, a good membrane material should have following properties: high porosity; high selectivity; low vapour transfer resistance; high strength and flexibility; high fouling resistance; high corrosion resistance; easy fabrication; inexpensive.

2.6 Mathematical modelling methods

In this section, different methods used for mathematical modelling are introduced. For the modelling of liquid desiccant dehumidification system, there is mainly four different developed approaches: Simplified method (Section 2.6.1); Effectiveness NTU ($\varepsilon - \mathrm{NTU}$) method (Section 2.6.2); Finite difference method (Section 2.6.3); Conjugate heat and mass transfer method (Section 2.6.4). For the problems of hollow-fiber contractors specifically, the modelling of randomly placed fiber and flow maldistribution will be covered in Section 2.6.5.

2.6.1 Simplified method

Liu et al [194] proposed empirical correlations for cross-flow and counter-flow packed dehumidifiers. Due to the complexity of model, the required amount of time for computer modelling is normally too long that the models based on differential elements are not possible in reality. Thus a simplified approach was developed by proposing empirical correlations for enthalpy and moisture effectiveness based on corresponding experiments. Empirical relations were compared with some already published experimental data and it was found that the maximum average differences for moisture effectiveness were 7.9% and 13.8% for cross-flow and counter-flow dehumidifiers respectively. For the enthalpy effectiveness, the maximum average differences were 6.3% and 10.8% for cross-flow and counter-flow dehumidifiers respectively.

Liu et al [195] developed an analytical solution to a cross-flow direct contact packed bed liquid desiccant dehumidifier. In their study, for the simplicity of calculation, it was assumed that liquid desiccant mass flow rate and concentration within the dehumidifier are constant because the moisture content absorbed by the desiccant solution during the dehumidification process are negligible compared with the desiccant mass flow rate. Based on the similarity between

cross flow dehumidifier and cross flow heat exchanger, they proposed the analytical solutions to air and solution parameters, enthalpy and moisture efficiencies. Results were compared with numerical and experimental results and the average absolute differences were under 8%.

Khan and Ball [196] generated a simple mathematical model to evaluate the performance of packed-type liquid desiccant dehumidifier and regenerator. The model was pure algebraic derivation based on simulation results. The simplified algebraic was developed by analysing 1700 groups of data from finite difference model. It was concluded that the model could successfully evaluate the hourly performance of each component and predict the heating and cooling requirement, but might not suitable for other conditions under which the fitting of model were not based on.

Chen et al [197] developed an integrated analytical solution to a packed-type liquid desiccant dehumidifier for counter-flow. The mathematical model was based on Khan and Ball's mathematical model [196]. The mathematical model was constructed based on the control volume:

$$\dot{m}_a dh_a = \dot{m}_1 dh_1 \tag{2-1}$$

$$d\dot{m}_1 = \dot{m}_a d\omega_a \tag{2-2}$$

$$\frac{dh_a}{dy} = \frac{NTU}{L}[Le \cdot (h_a - h_e) + (1 - Le) \cdot \lambda \cdot (\omega_a - \omega_e)] \tag{2-3}$$

$$\frac{d\omega_a}{dy} = \frac{NTU}{L}(\omega_a - \omega_e) \tag{2-4}$$

Where Le and NTU are Lewis number and number of heat transfer units; h_e and ω_e are the enthalpy and humidity ratio in equilibrium with desiccant solution; h_a and ω_a are enthalpy and humidity ratio of air flow. The schematic diagram of the counter-flow heat and mass transfer process is illustrated in Fig 2-24.

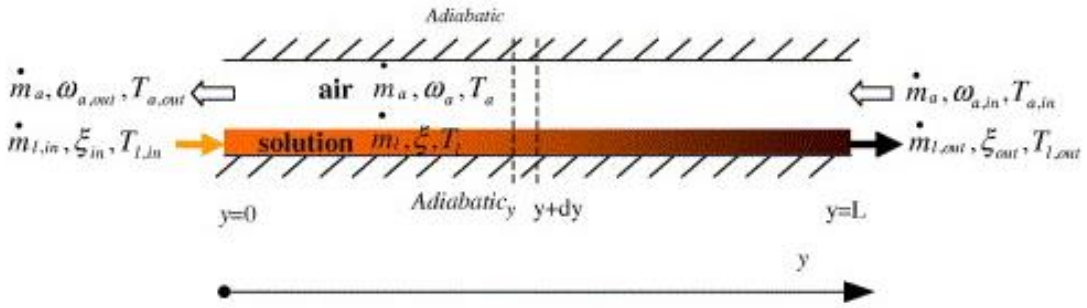


Fig 2- 24 Schematic diagram of counter-flow heat and mass transfer process in packed-type liquid desiccant dehumidifier [197]

In the study it was assumed that the concentration of desiccant solution at inlet and outlet are constant, thus the analytical solution was suitable for high desiccant solution mass flow rate conditions. For the convenience of derivation, two parameters K_a and K_e were defined, which are the enthalpy of air and equilibrium state respectively. Then the distribution of solution was obtained by the analytical solution. The results showed good agreement with the experimental data, and more importantly it can conduct seasonal performance simulation with little computing time.

Ren et al [198] further simplified the one-dimensional analytical model for packed column liquid desiccant dehumidifiers within relatively narrow range of operating conditions. Governing equations for the coupled heat and mass transfer processes were obtained following the principle of heat and mass conservation:

$$\delta W = k_{oy} a_M dV(y_a - y_{eL}) = h_D a_M dV(Y_a - Y_{eL}) \quad (2\text{-}5)$$

$$G dY_a = \delta W = dL \quad (2\text{-}6)$$

$$dL = \frac{L}{1-x} dx \quad (2\text{-}7)$$

$$\delta Q = h_{OG} a dV(T_a - T_L) \quad (2\text{-}8)$$

$$G\left(C_{pa} + Y_a C_{pv}\right) dT_a = \delta Q - G C_{pv}(T_a - T_I) dY_a \quad (2\text{-}9)$$

$$L C_L dT_L = \delta Q + G h_s dY_a \quad (2\text{-}10)$$

Where G is the dry air mass flow rate (kmol/s); T is the temperature (K); W is the mass of water species transferred (kmol/s); V is the volume of packed column (m^3); Y is the mole fraction of water in air (kmol/kmol); L is mass flow rate of solution (kmol/s) and Q is the sensible heat transferred (kW). The schematic diagram of heat and mass transfer in a packed column is shown in Fig 2-25.

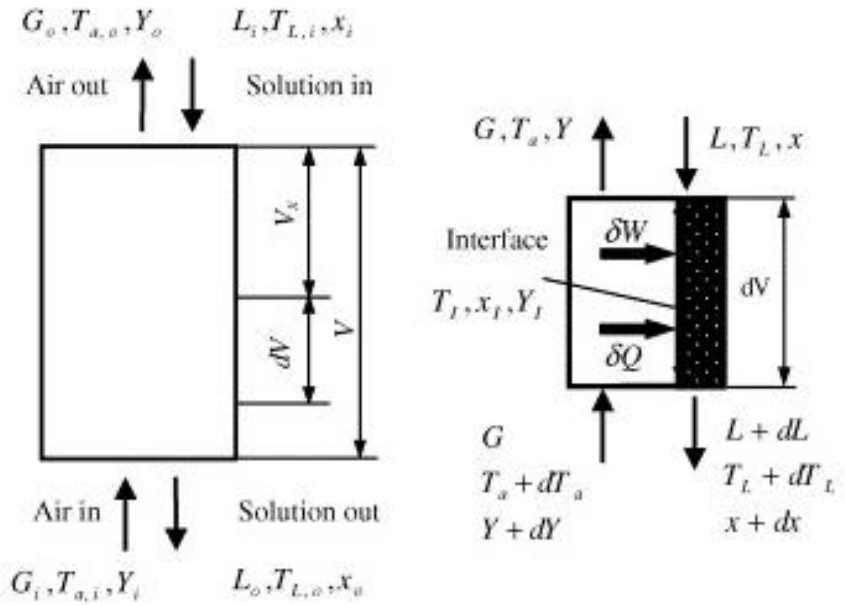


Fig 2- 25 Schematic diagram of heat and mass transfer in a packed column [198]

Based-on the one-dimensional heat and mass transfer equations for conventional packed columns, some dimensionless parameters and groups were defined and then the one-dimensional equations were normalized. Two new variables were defined as well to represent the dimensionless heat and mass transfer driving potentials: dimensionless temperature $\Delta\vartheta$ and dimensionless concentration ΔY. After the derivation one-dimensional equations were transferred to two coupled ordinary differential equations, which could be used to obtain the packed column efficiency. The obtained enthalpy efficiencies were compared with results previously published in [199] and good agreements have been found. However, the developed analytical solution may not suitable for operating conditions with large solution temperature

because the linear approximation for the dependence of equilibrium humidity ratio on solution temperature may reduce the accuracy of the analytical solution.

Babakhani and Soleymani [47, 200] developed simplified analytical solution to packed bed type dehumidifier and regenerator based the assumption that the equilibrium humidity level on the interface is constant. This assumption was made for a narrow range of operating conditions for practical dehumidification process with acceptable error to be lower than 10%. Another assumption made is the dilute gas phase, then they conducted the sensible analysis such as moisture removal rate and their results showed better predictions of outlet parameters than Chen et al [197].

In conclusion, simplified methods could perform the annual performance simulation for liquid desiccant system without costing much calculation time. These analytical models were made under several assumptions which may limit the application scope, and the accuracies of analytical solution were generally not high.

2.6.2 Effectiveness NTU ($\varepsilon - NTU$) method

Stevens et al [199] described a computationally efficient model for a packed-bed liquid desiccant heat and mass exchanger. The model was derived from an effectiveness model of a cooling tower. During the derivation it was assumed that the water loss for the solution energy balance is neglected. Furthermore, the saturation enthalpy and temperature were assumed to have linear relationship. In their study they firstly obtained the number of heat transfer units (NTU):

$$NTU = \frac{\alpha_D AV}{G_a'} \tag{2-11}$$

Then based on the similarity of packed-bed liquid desiccant dehumidifier and heat exchanger, the effectiveness of a counter-current flow dehumidifier was obtained by:

$$\varepsilon = \frac{1-e^{-NTU(1-m^*)}}{1-m^* e^{-NTU(1-m^*)}} \tag{2-12}$$

where m^* was the capacitance ratio as defined by:

$$m^* = \frac{G'_a C_{sat}}{G'_{s,i} C_{p,s}} \tag{2-13}$$

Where C_{sat} was the saturated specific heat (J/kgK); G' was the specific mass flow rate (kg/s). Then all outlet parameters, such as air temperature, humidity ratio and enthalpy were obtained based on these correlations. The results were compared with experimental and numerical results and good agreements have been found.

Then Sadasivam and Balakrishnan [201] improved Steven's method by changing the air mass flow rate to the minimum mass flow rate of solution and air. Their simplified $\varepsilon - NTU$ model was for the design of packed-bed liquid desiccant dehumidifiers, and it was found that results obtained from $\varepsilon - NTU$ model were in consonance with results calculated by more rigorous and well established but time consuming methods. Results were compared with limited amount of experimental data as well and the comparison was satisfactory.

An analytical model is presented by Shah and Sekulic [202] on pure analogy for a flat-plate heat exchanger, but only the sensible effectiveness is predicted. The model was valid for the flat-plate heat exchanger at steady-state laminar flow operating condition. Based on the study, the sensible effectiveness of pure cross and counter flow heat exchangers are given by:

$$\varepsilon_{sen,cross} = 1 - exp\left\{\frac{NTU^{0.22}}{Cr}[exp(-Cr.NTU^{0.78}) - 1]\right\} \tag{2-14}$$

$$\varepsilon_{sen,counter} = \frac{1-exp[-NTU(1-Cr)]}{1-Cr.\exp[-NTU(1-Cr)]} \tag{2-15}$$

For an innovative counter-cross flow exchanger, the sensible effectiveness can be calculated by combining Eqs. (2-14) and (2-15) [68]:

$$\varepsilon_{sen,counter-cross} = \left(\frac{A_{cross}}{A_{counter-cross}}\right)\varepsilon_{sen,cross} + \left(\frac{A_{counter}}{A_{counter-cross}}\right)\varepsilon_{sen,counter} \tag{2-16}$$

Where A is the active area of the exchanger (m^2).

However, the above analytical solution does not take mass transfer into consideration, which means this method is unable to predict the dehumidification performance. Thus the latent effectiveness for cross, counter and counter-cross flow exchangers are produced in literature [203] based on the heat and mass transfer analogy from Eqs. (2-14) - (2-16):

$$\varepsilon_{lat,cross} = 1 - exp\left\{\frac{NTU_m^{0.22}}{m^*}\left[exp(-m^*.NTU_m^{0.78}) - 1\right]\right\} \quad (2\text{-}17)$$

$$\varepsilon_{lat,counter} = \frac{1-exp[-NTU_m(1-m^*)]}{1-m^*.\exp[-NTU_m(1-m^*)]} \quad (2\text{-}18)$$

$$\varepsilon_{lat,counter-cross} = \left(\frac{A_{cross}}{A_{counter-cross}}\right)\varepsilon_{lat,cross} + \left(\frac{A_{counter}}{A_{counter-cross}}\right)\varepsilon_{lat,counter} \quad (2\text{-}19)$$

Above early-published literatures focused on heat and mass transfer for direct-contact type contractors, or traditional flat-plate heat exchangers. As for membrane-based liquid desiccant heat and mass exchanger, effectiveness correlations were introduced by Zhang and Niu [66] for a flat plate exchanger with membrane cores. In their research, some assumptions were made to build governing equations, these include: no lateral mixing of the two fluids, no heat conduction and vapour diffusion in the fluids, constant heat conductivity and water diffusivity in the membrane, and one-dimensional heat and mass transfer in the membrane. The sensible and latent effectiveness correlations were developed as:

$$\varepsilon_{sen} = 1 - exp\left[\frac{\exp(-NTU^{0.78}R_1)-1}{NTU^{-0.22}R_1}\right] \quad (2\text{-}20)$$

$$\varepsilon_{lat} = 1 - exp\left[\frac{\exp(-NTU_{lat}^{0.78}R_1)-1}{NTU_{lat}^{-0.22}R_1}\right] \quad (2\text{-}21)$$

Where

$$R_1 = \frac{(\dot{m}c_{pa})_{min}}{(\dot{m}c_{pa})_{max}} \quad (2\text{-}22)$$

$$R_2 = \frac{\dot{m}_{min}}{\dot{m}_{max}} \quad (2\text{-}23)$$

NTU_{lat} is the total number of transfer units for moisture which can be calculated by:

$$NTU_{lat} = \beta \cdot NTU \quad (2\text{-}24)$$

Where

$$\beta = \frac{1}{1+\alpha} \tag{2-25}$$

$$\alpha = \frac{\gamma_m}{\gamma_c} \tag{2-26}$$

$$\gamma_c = \frac{2}{k_s} \tag{2-27}$$

Where γ_c is the convective moisture transfer resistance, α is the ratio of diffusive resistance to convective resistance of the membrane. The empirical correlations were compared with experimentally obtained data and it was found that the correlations can predict the performance of membrane-based heat mass exchanger well.

The coupled heat and mass transfer in the hollow fiber membrane contractor was studied by Zhang [99], and an analytical solution was obtained which was convenient to use in the practice. The differential equations of heat and moisture transfer in the air and solution flows were established, then the sensible and latent effectiveness can be obtained:

$$\varepsilon_{sen} = 1 - C_1 e^{\lambda_1} - C_2 e^{\lambda_2} \tag{2-28}$$

$$\varepsilon_{lat} = 1 + K_1 C_1 e^{\lambda_1} - K_2 C_2 e^{\lambda_2} \tag{2-29}$$

Where C_1 and C_2 were coefficients that are functions of constant coefficients: $a_{11} - a_{22}$. λ_1 and λ_2 were roots of characteristic equations. K_1 and K_2 were intermedia coefficients of the analytical solution. Experiments were conducted for validation, and the maximum differences in temperature and humidity were below 5% and 12% respectively.

This analytical solution based on solely algebraic correlations was accurate and convenient to use to estimate the sensible and latent effectiveness. However the solution outlet temperature and concentration need to be assumed in order to start the calculation, which increases the calculation load. Zhang's analytical solution was extended by assuming that the desiccant solution mass flow rate and concentration are constant [145], since the moisture contents absorbed/desorbed by the solution were negligible compared with desiccant mass flow rate.

This assumption was verified by experimental results for air dehumidification and desiccant regeneration. In literature [145], a flat-plate counter-cross-flow liquid-to-air membrane energy exchanger (LAMEE) was adopted. The solution properties and its equilibrium humidity ratio were only related to the solution temperature, and the slope (E_T) was only associated with iterated solution temperature. The slope calculation method was different from Zhang's analytical solution, in which E_T was related to both iterated solution temperature and concentration. Furthermore, Zhang's analytical solution was for hollow fiber membrane contractor, thus in order to use this solution U and U_m needed to be calculated based on a flat-plate membrane contractor and substituted into Zhang's analytical correlations.

The analytical solution was validated through experimental tests under various conditions and the discrepancy between analytical and experimental effectiveness were within 10%

To conclude, compared with simplified method, $\varepsilon - NTU$ method showed better accuracy and wider scope of application. Some iteration was required but in general it is time saving and can predict the performance of heat mass exchangers rather effectively.

2.6.3 Finite difference method

Factor and Grossman [48] developed a mathematical model for a packed-bed type dehumidifier/regenerator using liquid desiccant. The numerical model used finite difference method and was based on the model for adiabatic gas absorption. The adiabatic dehumidifier/regenerator in the height was divided into n elements, the properties of air and solution were assumed to be constant across the differential elements. The differential governing equations for air temperature, humidity were developed, and they were solved through numerical integration along the unit height together with boundary conditions. The numerical results were validated through experimental data.

Following their numerical method, several more studies for packed bed or packed column were conducted: Gandhidasan et al [204] numerically investigated the heat and mass transfer for a packed tower using the finite difference method, various parameters such as the effect of liquid concentration and temperature, air temperature and humidity and solution and air mass flow rates on packed tower performance were discussed.

Oberg and Goswami [205] used a similar finite difference model to Factor and Grossman's model to simulate the performance of packed bed liquid desiccant dehumidifier.

Liu et al [206] studied the heat and mass transfer for a cross flow direct contact liquid desiccant dehumidifier/regenerator. The desiccant flowed in cross configuration with air and was distributed over the packing by gravity. To solve governing equations of heat and mass transfer in air and solution sides, the dehumidifier/regenerator was divided into an infinite number of differential elements, each with volume of dV and the computational domain was discretized into $M \times N$ meshes, as shown in Fig 2-26.

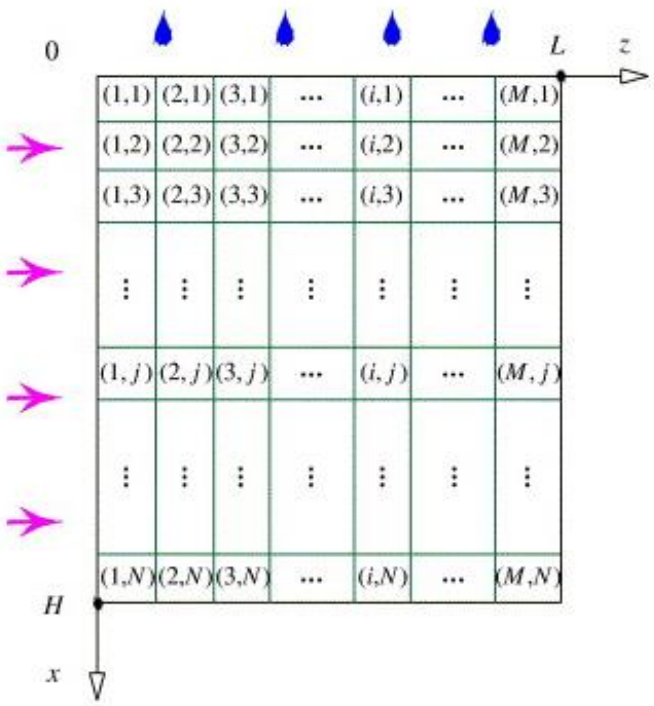


Fig 2- 26 Two-dimensional schematic of the computational domain [206]

According to their results, for the dehumidifier the average absolute differences between numerical results and 284 groups of experimental data for enthalpy and moisture effectiveness were 7.9% and 8.5% respectively, while they were 5.8% and 6.9% for regenerator under 82 groups of experimental tests.

The membrane-based contractors were also carried out in many studies. The coupled heat and mass transfer in the air, solution flows and membrane of a counter flow LAMEE is numerically modelled by Moghaddam et al [67] and the steady state effectiveness of the LAMEE was analysed. In the developed module to simplify the numerical modelling, some assumptions were made: well-insulated exchanger, steady state, fully developed flows, constant thermal properties and convective heat and mass transfer coefficients, uniform velocity and temperature at inlets, no axial conduction and phase change heat gain or loss only occur in the solution side. Solution and air side heat mass conservation governing equations were solved by finite difference method. The model was validated through experimental data, good agreements were found under summer operating conditions. But under winter operating conditions the numerical model predicted higher sensible effectiveness than experimental data, the discrepancy was up to 10%.

Fan et al [71] numerically studied the performance of a cross flow LAMEE used a similar finite difference method. Since the dehumidifier was cross flow configuration, the air flow and solution flow were in x and y direction respectively, thus the dimensionless length in x and y direction were defined as:

$$x^* = \frac{x}{x_0} \tag{2-30}$$

$$y^* = \frac{y}{y_0} \tag{2-31}$$

Vali et al [70] studied an counter-cross flow LAMEE numerically. The air temperature T_{air} and liquid solution temperature T_{sol} were obtained from heat balance equations. The bulk mean

liquid velocity was determined by applying the second-order Laplace equation for the stream function (ψ):

$$\nabla^2\psi = 0 \tag{2-32}$$

Implicit finite difference method was used to solve the governing equations. They compared the simulated results with analytical results and found the discrepancy of sensible effectiveness was within $\pm$2.5%.

Then this study was extended by considering both heat and mass transfer problems [78], and the governing equations in the air and solution sides were similar to those used in [67]. The determination of heat transfer coefficient h and mass transfer coefficient h_m were based on an approximation that heat and mass flux on the membrane are uniform. h could be derived from the correlation for Nusselt number:

$$Nu = \frac{hd_h}{k} \tag{2-33}$$

Where d_h was the hydraulic diameter (m), k was thermal conductivity ($W/m^{-1}K^{-1}$), Nu was constant and equal to 8.24 [207, 208]. Similarly, h_m could be derived from the correlation for Sherwood number [77] :

$$Sh = NuLe^{-1/3} \tag{2-34}$$

$$Sh = \frac{h_m d_h}{D} \tag{2-35}$$

Where Le was Lewis number given by the ratio of thermal diffusivity α to the mass diffusivity D. Implicit finite difference method was also used to solve the governing equations. The numerical model was validated by experimental data and the agreement was within $\pm$10%.

A similar numerical modelling for cross flow membrane contractor was produced by Das and Jain [73], but the calculation process of Nu and mass transfer resistance in the membrane was improved. Most of the previous studies only focused on the laminar regime, the approximate correlations was used to consider transition regime in literature [73]. Nusselt number was obtained from correlations for laminar, transition and turbulent conditions in literature [209].

A two-dimensional transient model was developed by Seyed-Ahmadi et al [146, 147] for the coupled heat and mass transfer in a run-around heat and moisture exchanger system (RAMEE). Compared to the steady-state modelling, the transient effect is of vital importance during the system operation since the thermal and mass capacities of the liquid are larger than that of air. In their study, governing equations were similar to those developed in literatures [67, 71, 78] . Then a characteristic dimensionless time (τ) was defined relative to the transport time for the bulk solution to flow through both LAMEEs without considering the storage tanks or connecting tubes:

$$\tau = \frac{1}{{t^*_{sol,s}}^{-1} + {t^*_{sol,e}}^{-1}} \tag{2-36}$$

τ indicates the number of complete volume circulations of the solution in both LAMEEs, which is used to interpret the transient response of the system at different operating conditions. The governing equations were discretised by applying implicit finite difference method for the time derivative and upwind scheme for the first order spatial derivative, and solved by using Gauss-Seidal iteration method. The results for both sensible and latent effectiveness showed satisfactory agreement under different operating conditions and the maximum average absolute difference between the numerically obtained and experimentally tested data for the transient effectiveness was 0.103

Following the similar method, the transient model was extended to a RAMEE system consisting two counter-cross flow LAMEEs by Namvar et al. [210]. The numerical results of latent and total effectiveness showed good agreement with the experimental data but the difference between numerically obtained and experimentally tested sensible effectiveness was up to 17%. The modelling results showed that Grashof number Gr was higher than Reynolds number under the winter testing conditions, so the buoyancy forces should not be neglected.

To sum up, the finite difference method provides better accuracy in modelling compared with simplified method and $\varepsilon - NTU$ method, its governing equations are discretised by applying

finite difference method and solved by using iteration method. The heat and mass transfer coefficients are derived from correlations of fundamental data such as Nusselt and Sherwood numbers, which are borrowed from well-known books. However, these data were obtained under the uniform temperature (heat flux) or concentration (mass flux) boundary conditions, which are unable to accurately reflect real heat and mass transfer properties in the membrane module. In order to solve this problem, conjugate heat and mass transfer modelling method is required, which will be introduced in the next section.

2.6.4 Conjugate heat and mass transfer method

As mentioned previously, the drawback of the finite difference modelling can be avoided by using the conjugate heat and mass transfer modelling method. A mathematical model was established by Huang and Zhang [75] for a cross-flow flat plate membrane module. The unit cell used for calculation consisted of one membrane and two neighbouring flow channels. Some assumptions were made in this model including: laminar flow mode for both the air and liquid solution, Newtonian fluids with constant thermophysical properties, hydrodynamically fully developed while developing both thermally and in concentration for both flows, no heat and mass diffusion along the main flow direction. The governing equations of the membrane surface were different from previous model's, the real heat and mass boundary conditions on the membrane surface were numerically obtained by simultaneous solution of momentum, energy and concentration equations for the air and solution. Governing equations and their relevant boundary conditions were solved by using the finite difference method, iterative techniques were also adopted in the process. Numerical results were validated by comparing with experimental results, the discrepancies between the numerical and experimental data were less than 6.0%. Thus generally speaking, this model predicted the heat and mass transfer well.

Fundamental data of Nusselt and Sherwood numbers under different aspect ratios (b/a) were then calculated and listed in Table 2-1.

Table 2- 1 Fully developed (fRe), Nusselt and Sherwood numbers for different aspect ratios

Aspect ratios (b/a)	Nu_H	Nu_T	Nu_C	Sh_C	$Nu_{C,a}$	$Sh_{C,a}$	$Nu_{C,s}$
References	[77, 207, 208]	[77, 207, 208]	[63]	[63]	[75]	[75]	[75]
1.0	3.61	2.98	1.88	1.89	3.12	3.30	3.41
1.43	3.73	3.08	2.49	2.52	3.23	3.41	3.64
2.0	4.12	3.39	6.06	3.10	3.48	3.65	4.05
3.0	4.79	3.96	4.06	4.00	4.15	4.28	4.74
4.0	5.33	4.44	4.64	4.52	4.61	5.11	5.35
8.0	6.49	5.60	6.06	6.03	5.79	5.83	6.41
50.0	-	-	7.78	7.81	7.54	7.74	7.91
100.0	-	-	8.07	8.05	7.70	7.98	8.08
∞	8.23	7.54	-	-	-	-	-

It was found from Table 2-1 that Nusselt number under the conjugate heat and mass transfer condition in the air side ($Nu_{C,a}$) was between that under uniform temperature condition (Nu_T) and heat flux condition (Nu_H). Furthermore, the Nusselt number under the conjugate heat and mass transfer condition in the solution side ($Nu_{C,s}$) was approximately 15% higher than that in the air side. It was assumed in previous studies that the flow was hydrodynamically fully developed to avoid difficulties in solving Navier-Stokes equations. However, this assumption would underestimate the performance seriously since the developing entrance length accounts for a huge proportion of the duct length.

A step forward to investigate the effects of the developing entrances on the fluid flow and conjugate heat and mass transfer in a cross-flow flat plate membrane module was made by Huang et al [76], the membrane module structure in this study was the same as that in literature [75]. More accurate governing equations were established and solved directly by considering the influences of the flow, heat and mass transfer developing entrances. The governing equations and conjugate heat and mass transfer boundary conditions were solved by applying

a finite volume method, iterative techniques were also used to solve interacted problems. The model was validated by comparing to the experimental data, the maximum difference between the calculated values and experimental data was 4.0%, which means this model was able to predict heat and mass transfer for the cross-flow flat plate membrane module. Then fundamental data of Nusselt and Sherwood numbers under different aspect ratios (b/a) are calculated, a comparison of these numbers and those obtained without considering developing entrance was made in Table 2-2.

Table 2- 2 Comparison of fully developed (fRe), Nuseelt and Sherwood numbers for different aspect ratios with and without considering developing entrance

Aspect ratios (b/a)	$Nu_{C,a}$	$Nu_{C,s}$	$Nu_{C,a}$	$Nu_{C,s}$	$Nu_{m,a}$	$Nu_{m,s}$
References	[75]	[75]	[76]	[76]	[76]	[76]
1.0	3.12	3.41	3.37	3.64	3.87	3.95
1.43	3.23	3.64	3.48	3.78	3.99	4.18
2.0	3.48	4.05	3.73	4.19	4.25	4.59
3.0	4.15	4.74	4.39	4.88	4.95	5.28
4.0	4.61	5.35	4.86	5.49	5.34	5.89
8.0	5.79	6.41	6.04	6.55	6.58	6.95
50.0	7.54	7.91	7.79	8.02	8.32	8.45
100.0	7.70	8.08	7.95	8.22	8.49	9.62
∞	-	-	-	-	-	-

As displayed in Table 2-2, $Nu_{C,a}$ and $Nu_{C,s}$ obtained with considering developing entrance were about 10% higher than those without this consideration. Furthermore, the mean Nusselt numbers along the complete duct ($Nu_{m,a}$ and $Nu_{m,s}$) were about 10% higher than the local values ($Nu_{C,a}$ and $Nu_{C,s}$), and approximately 20% higher than those calculated in literature [51]. This means thermally developing entrance has substantial effect on heat transfer in the duct.

An internally-cooled membrane-based liquid desiccant dehumidifier (IMLDD) was studied by Huang et al [83], which consisted of feed air, solution, cooling water and sweep air. In this

modelling, the interface between the water film and sweep air was thermodynamic equilibrium state, and the velocity of the sweeping air at interface was equal to that of water flow. Furthermore, gravitational force of the feed air was neglected, while water falling film was formed only due to its gravitational force. The governing equations of the feed air, solution, water falling film and sweep air were developed respectively and solved by a finite volume numerical scheme. Experiment tests were conducted to validate the numerical model, but only the outlet parameters of the feed air, solution, water falling film and sweep air were measured due to the difficulty in measuring parameters inside the contractor. The maximum deviation between numerical and experimental results was less than 8.0%, which means numerical model is capable of predicting the performance of IMLDD well.

Apart from the flat-plate types, hollow-fiber membrane modules was studied using conjugate heat and mass transfer approach. To model the complete bundle of a fiber-to-fiber basis directly was difficult since the number of fibers were numerous, normally 200-600 in a small shell $4cm$ in diameter. This problem could be solved by using Happel's free surface model [211]. In Happel's model, each fiber in the shell was surrounded by a fluid envelop, and there was no momentum, heat or mass transfer on the outer free surface. The fibers were assumed to be distributed homogenously and the flow was axial. The bundle consisted of a series of free surface cells, which had only one fiber in the centre and surrounded by homogeneous fluid. The free surface models in literature [211] were shown in Fig 2-27.

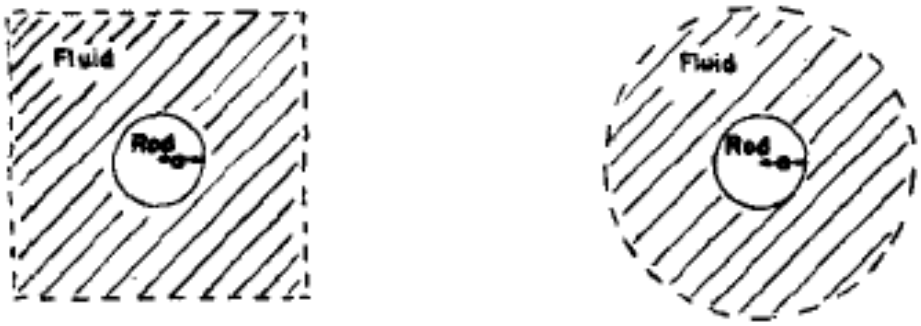


Fig 2- 27 Free surface models for axial flow [212]

Zhang et al [100, 102] numerically studied the parallel and cross flow hollow-fiber membrane modules based on Happel's free surface model under the laminar flow assumption. In their modelling, one-fourth of a cell was selected as the calculation domain for the sake of symmetry and simplicity for the parallel flow module. As for the cross flow module, only half of a cell was selected as the calculation domain. Body-fitted coordinate systems were generated to convert the physical plane into numerical one. After the set-up of boundary-fitted coordinate system, the governing equations were transformed into the corresponding governing equations, which were then discretized by using finite volume method. For the conjugate heat and mass transfer problem, alternating direction implicit (ADI) techniques were used to solve the governing equations. The local and mean Nusselt and Sherwood numbers were obtained and then experimentally validated. The experimental results showed a good agreement with calculated data. Discrepancies between the numerical and tested data were below 5% for the parallel flow module, and 6% for the cross type.

A low-Re $k-\varepsilon$ turbulent model was employed to describe the turbulent flow and heat and mass transfer in a cross flow hollow-fiber membrane module [103]. Happel's free surface model was used again to overcome the difficulty of direct modelling of numerous number of fibers. Then the overall mean Nusselt, Sherwood numbers of both flows, and total drag coefficient of the air flow were calculated and compared with the experimental results. The results showed that the maximum difference was less than 6.0% for three indices.

The free surface model illustrated previously was a coarse approximation since each single fiber was enclosed into a hypothetical concentric envelop, the effect of fiber-to-fiber interaction was not considered. Huang et al [101] [104] investigate the conjugate heat and mass transfer for counter and cross hollow fiber membrane modules using periodic unit cell model considering the fiber-to-fiber interactions. Compared with the free surface model, the free

surface radius r_f is replaced by the longitudinal pitch S_L. The governing equations were solved by using finite volume method via a self-built code developed by FORTRAN. It was found that the friction factor and Nusselt number from the free surface model deviated 8-50% from the periodic unit cell model for the counter flow contractor, and 20% for the cross flow contractor. The free surface model was only applicable when the packing fraction is less than 0.25. The periodic unit cell model was developed by Zhang et al [105] based on the same structure of the cross flow hollow fiber module, the low-Re $k-\varepsilon$ model was adopted rather than the laminar model to investigate the hollow fiber module performance. They compared the laminar and turbulent models with experimental data. It was found that when $Re_a < 300$, the results from both the laminar and turbulent models agreed with the experimental data well, the maximum difference was less than 7.0%. However, when $Re_a > 300$, the turbulent model showed a better fitting than the laminar model.

The heat and mass transfer in a skewed flow fiber bank was investigated in [108, 109]. The interactions between fibers were considered and the governing equations were solved by finite volume method. The validation showed that the maximum difference of the validation was less than 1.5% for periodically mean Nusselt number $Nu_{c,a}$, 1.4% for Sherwood number under naturally formed boundary conditions $Sh_{c,a}$ and 1.1% for friction factors f_a.

To sum up, the conjugate heat and mass transfer method provided the highest accuracy in modelling compared with simplified, $\varepsilon - NTU$ and finite difference methods. Fundamental heat and mass transfer data could be obtained directly from the conjugate heat and mass transfer governing equations. However the disadvantage of this method is that extensive iteration were required for solving governing equations, which made it unsuitable for efficient performance prediction or annual assessment for the dehumidification system. As a matter of convenience, a detail comparison of three different modelling methods is summarized in Table 2-3.

Table 2- 3 Comparison of different modelling methods for liquid desiccant heat and mass exchanger

Modelling method	exchanger type	Flow pattern	System stability	Fiber-fiber interaction (for hollow fiber exchangers only)	Air flow assumption (for hollow fiber exchangers only)	Solutions to solve governing equations	Experimental validation	References	Characteristics
Simplified method	Direct-contact	Cross and counter	Steady-stage	-		Analytical	≤ 7.9% (cross) ≤ 13.8% (counter)	[194]	Pros: 1. No iteration 2. Fastest calculation 3.Suitable for annual performance simulation Cons: 1. Lowest accuracy 2. Limited application
		Cross					≤ 8%	[195]	
		-					-	[196]	
		Counter					Good agreements	[197]	
		Counter					Good agreement	[198]	
		-					-	[200]	
$\varepsilon - NTU$ method	Direct-contact	-	Steady-state	-		Analytical	Good agreement	[199]	Pros: 1. Some iterations 2. Generally time saving Cons: 1. Accuracy not high
		-					Good agreement	[201]	
	Flat plate	Cross					-	[202, 203]	
	Flat plate	Cross					≤ 7.3% (sensible) ≤ 8.6% (latent)	[66]	
		Counter-cross					≤ 10%	[145]	
	Hollow fiber	Cross					≤ 5% (sensible) ≤ 12% (latent)	[99]	
Finite difference method	Direct-contact	Cross	Steady state	-		Finite difference	-	[48]	Pros: 1. Not complex iteration 2. Better accuracy 3.Suitable for dehumidifier performance prediction Cons: 1. Not suitable for the heat and mass transfer mechanism analysis
		Counter						[204]	
		Counter						[205]	
		Cross					≤ 7.9% (dehumidifier enthalpy effectiveness) ≤ 8.5% (dehumidifier moisture effectiveness) ≤ 5.8% (regenerator enthalpy effectiveness) ≤ 6.9% (regenerator moisture effectiveness)	[206]	
	Flat plate	Counter	Steady state				≤ 10%	[67]	
		Cross	Steady state				Good agreement	[71]	
			transient				Absolute difference: 0.103	[146, 147]	
		Counter-cross	Steady state				Within ±2.5% (heat transfer only) Within ±10% (heat and mass transfer)	[70] [78]	
		Counter-cross	Steady state				≤ 17%	[210]	
Conjugate heat and mass transfer method	Flat plate	Cross	Steady-state	-		Finite volume	≤ 6.0% (hydrodynamically fully developed) ≤ 4.0% (Consider effects of developing entrances)	[75] [76]	Pros: 1. Highest accuracy 2. Suitable for the heat and mass transfer mechanism analysis Cons: 1. Extensive iteration 2. Least efficiency
		Cross (Internally-cooled)					≤ 8%	[83]	
	Hollow fiber	Counter		Free-surface method	laminar		≤ 5%	[100]	
		Cross					≤ 6%	[102]	
		Cross			Turbulent (low-Re $k-\varepsilon$ model)		≤ 6%	[103]	
		Counter		Periodic unit cell method	laminar		≤ 5%	[101]	
		Cross					≤ 7.5%	[104]	
		Skewed					For heat transfer ≤ 1.5% For mass transfer ≤ 1.4% For friction factor ≤ 1.1%	[108, 109]	
		Cross			Turbulent (low-Re $k-\varepsilon$ model)		≤ 7% (when $Re_a < 300$)	[105]	

2.7 Summary

A comprehensive literature review on technologies related to the liquid desiccant dehumidification system is presented in this chapter. First of all, major findings from literature review are listed:

1) Dehumidifier is the most important unit in a liquid desiccant dehumidification system. Generally they can be divided into two main types: direct contact type and membrane-based type. For the first type, packed beds or packed columns are normally applied as heat and mass transfer media. For the second type, semi-permeable membranes are applied to solve desiccant carry-over problems of direct-contact type dehumidifiers.
2) With regard to the structure of membranes, membrane-based dehumidifier can be further divided into flat-plate type dehumidifier and hollow-fiber type dehumidifier. Flat-plate type dehumidifier has low pressure losses in solution and air channels, easier construction and maintenance of the system and more reliable system operation; while hollow-fiber type dehumidifier has more complicated structure but higher heat and mass transfer ability.
3) With regard to the flow pattern, the solution and air flows in dehumidifier can be arranged into parallel, cross or counter-cross configurations. Parallel structure has higher efficiency but the sealing of solution is difficult and the construction in the limited space is hard. By contrast the cross structure is more favourable for practical application. Recently, a counter-cross structure is developed to integrate both parallel and cross configurations.
4) Regenerator is another critical unit in such system since the diluted solution generated in dehumidifier needs to be re-concentrated to realize the solution recycle. Similar to dehumidifiers, with regard to the module structure, regenerators can be divided into

direct contact type and membrane-based. The solution can be regenerated using low-grade energy, such as solar thermal (TH), photovoltaic-electrodialysis (PV-ED) or photovoltaic capacitive deionization (PV-CDI).

5) A complete run-around membrane energy recovery system consists of both dehumidifier and regenerator linked by solution. It is assumed in previous studies that the heat and mass transfer rates in supply exchanger balance those in exhaust exchanger, in other words, there is no heat or moisture added or removed from the system.
6) Many materials have been used as liquid desiccant, for example halide salts, triethylene glycol, organic acids and the mixture or composite of salts all have both advantages and disadvantages. The most commonly used materials are LiCl, $CaCl_2$ and LiBr. Among them LiCl solution is the most stable liquid desiccant, which offers the lowest water vapour pressure and viscosity under the same temperature. However, the price of LiCl is relatively high. By contrast, $CaCl_2$ is the cheapest halide salt, and it is the most readily available type. Using mixed desiccant could have better dehumidification efficiency, lower material cost and energy consumption.
7) For the prediction of property of mixed solution, simple mixing rule (SMR) and electrolyte non-random two-liquid (NRTL) have been developed. The former one has the advantage of simple and time-saving, while the later one provides better prediction of mixed solution surface vapour pressure, especially when the solution concentration is higher than 30%.
8) There is two types of membrane materials currently being used: hydrophobic microporous membranes and nonporous membranes. The former one has the potential risk of pore-wetting by desiccant solution, which can be solved by applying nonporous membranes.

9) There are four predominant modelling methods for the membrane-based liquid desiccant heat and mass exchanger: simplified, effectiveness $NTU(e-NTU)$, finite difference and conjugate heat and mass transfer methods.
10) Simplified method could perform the annual performance simulation for liquid desiccant system without costing much calculation time. But the accuracy is the lowest. effectiveness $NTU\,(e-NTU)$ is generally time saving but with wider scope of application compared to the simplified method. Finite difference method is the most commonly used one, it provides better accuracy in modelling and its governing equations are discretised by applying finite difference method and solved by using iteration method. Conjugate heat and mass transfer method has the highest accuracy, but extensive iteration are required for solving governing equations, which make it unsuitable for efficient performance prediction or annual assessment for the dehumidification system.

Based on literature review, the novelty of this research and identified research gaps between previous studies and current study are presented:

1) As discussed previously, many experimental studies have been carried out to investigate the performance of a membrane-based dehumidifier. Several numerical investigations use conjugate heat and mass transfer methods that solve momentum equation and continuity equation to obtain velocity field, energy and mass equation to obtain concentration and temperature distributions. These studies focus on the basic heat and mass transfer mechanism of plate membrane-based contractor. A few studies evaluate the performance of liquid desiccant system numerically by examining the effects of several operating and design parameters. However, limited researches have been carried out to evaluate the performance of a cross-flow membrane-based parallel

plate liquid desiccant system numerically by considering comprehensive operating parameters. In this thesis, the heat and mass transfer in a membrane-based dehumidifier is investigated by using both numerical and experimental methods in Chapter 3, the influences of three groups of main parameters (i.e. dimensionless parameters: NTU and solution to air mass flow rate ratio m^*, solution properties: temperature T_{sol} and concentration C_{sol}, and inlet air conditions: temperature $T_{air,in}$ and relative humidity $RH_{air,in}$) are assessed. Moreover, the interactions of different parameters on the system performance are also investigated. This thesis provides a comprehensive parametric study on the membrane-based liquid desiccant dehumidifier performance, which supplies valuable data for the optimum design in the dehumidification and air-conditioning systems in practice.

2) Most of the previous literatures mainly focused on the analysis of dehumidifier. Limited number of researches into regenerator focused on the direct contact type, such as packed beds or packed columns. Researches on membrane-based regenerator, especially numerical modelling have not been conducted widely. In this thesis, the heat and mass transfer in a membrane-based regenerator is investigated numerically and experimentally in Chapter 4. The effects of main operating parameters, such as dimensionless parameters (i.e. NTU and m^*), solution inlet properties (i.e. temperature $T_{sol,in}$ and concentration $C_{sol,in}$) and air inlet conditions (i.e. temperature $T_{air,in}$ and humidity ratio $W_{air,in}$) on the performance of regenerator are investigated. Solution-side effectiveness, together with another two indicators: solution side temperature decrease rate (TDR) and moisture flux rate (MFR) are applied to evaluate the regeneration performance. This thesis presents a comprehensive parametric analysis on membrane-based liquid desiccant regenerator.

3) The majority of previous literatures focused on either single dehumidifier or single regenerator in a system. In limited number of literatures about run-around systems, it is assumed that the heat and mass transfer rates in supply exchanger balance those in exhaust exchanger, in other words, there is no heat or moisture added or removed from the system. However, the system can benefit significantly from an external heat source or cold source, in which case a hot water loop and cooling water loop are included in the configuration. Thus in this thesis a complete membrane-based liquid desiccant dehumidification system that includes a dehumidifier, a regenerator, and a hot and a cooling water supply systems is investigated in Chapter 5. The numerical model for the complete system containing both dehumidifier and regenerator is developed for the first time, experimental tests are conducted to validate the numerical model. The effects of parameters that are controllable in reality such as dimensionless parameters (i.e. dehumidifier and regenerator side $NTUs$ and m^*) and solution inlet properties (i.e. temperature $T_{sol,in}$ and concentration $C_{sol,in}$), and outdoor air conditions (i.e. temperature $T_{air,in}$ and humidity ratio $W_{air,in}$) on the performance of the complete system are investigated. Energy analysis is conducted through COP and total cooling energy output $Q_{cooling}$. It presents a comprehensive parametric analysis on the complete membrane-based liquid desiccant dehumidification system, and provides valuable data for HVAC engineers to design and operate the complete system in reality.
4) Many literatures used a simple mixing rule (SMR) to investigate the properties of mixed desiccant solution. Compared to SMR method, electrolyte non-random two-liquid (NRTL) method provides better prediction of mixed solution surface vapour pressure, especially when the solution concentration is higher than 30%. Previous literatures on NRTL method only focuse on direct contact systems, while there are few studies on the influences of different mixing ratios and the optimum mixing ratio for the membrane-

based system using NRTL method. Chapter 6 investigates the effects of the mixed LiCl-$CaCl_2$ desiccant solution properties (i.e. temperature T_{sol}, concentration C_{sol} and mixing ratio of LiCl and $CaCl_2$) on the performance of a membrane-based liquid desiccant dehumidification system by numerical modelling and experimental tests. The optimum mixing ratio of the LiCl-$CaCl_2$ desiccant is determined based on dehumidification capacity and COP analyses. By comparing with the experimental results, this thesis comes out a method to predict the system performance with the mixed solution by combining the NRTL method and numerical modelling. It presents a comprehensive investigation on the effects of the mixed LiCl-$CaCl_2$ desiccant properties on the membrane-based liquid desiccant dehumidification system, and provides an approach for the optimum mixing ratio selection through the system performance and COP analyses.

Chapter 3: Investigation of a membrane-based flat-plate liquid desiccant dehumidifier

3.1 Introduction

Based on the literature review presented in the previous chapter, limited researches have been carried out to evaluate the performance of a cross-flow membrane-based parallel plate liquid desiccant system numerically by considering comprehensive operating parameters. In this chapter, the conjugate heat and mass transfer in a cross-flow membrane-based parallel-plate liquid desiccant (using lithium chloride as desiccant) dehumidification system is investigated by numerical modelling, the influences of three groups of main parameters (i.e. dimensionless parameters: NTU and solution to air mass flow rate ratio m^*, solution properties: temperature T_{sol} and concentration C_{sol}, and inlet air conditions: temperature $T_{air,in}$ and relative humidity $RH_{air,in}$) are assessed. In order to validate the developed numerical model, experimental investigations are implemented with a test rig developed in the laboratory. Moreover, the interactions of different parameters on the system performance are also investigated. This chapter is structured in the following sections: Section 3.2 presents the numerical modelling method; Section 3.3 introduces the performance evaluation indices; Section 3.4 demonstrates the experimental investigation method; Section 3.5 presents the validation of numerical model; Section 3.6 investigates the performance of the dehumidifier and Section 3.7 shows the main conclusions from this chapter.

This work provides a comprehensive parametric study on the membrane-based liquid desiccant dehumidifier performance, which supplies valuable data for the optimum design in the dehumidification and air-conditioning systems in practice.

3.2 Numerical modelling

3.2.1 Governing equations

The structure of the membrane-based parallel-plate dehumidifier is depicted in Fig 3-1(a), and its air and solution flows are in a cross-flow arrangement. The air and solution channels are separated by semi-permeable membranes, thus heat and vapour can be transferred through membranes while the desiccant solution is prevented from going through them. The coordinate system used in numerical modelling is given in Fig 3-1(b). As can be seen, the air and solution flow in x and y directions respectively, while heat and mass are exchanged in z direction. One air channel and one neighbouring solution channel are selected as the calculating domain.

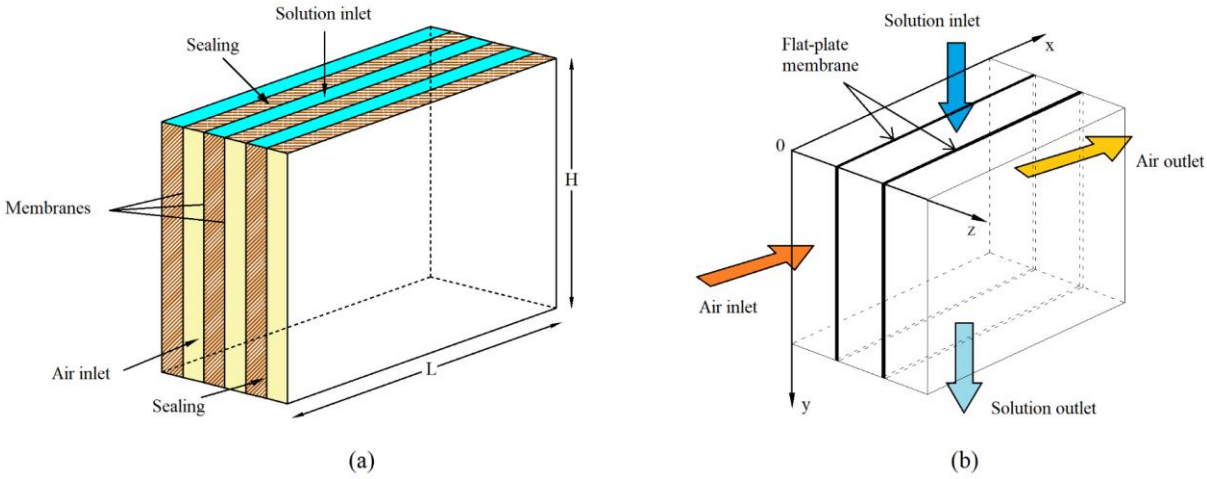


Fig 3- 1 Structure of membrane-based parallel-plate dehumidifier (a), and coordinate system used for numerical modelling (b).

Heat and mass transfer phenomena of the dehumidifier are complicated, many factors have the influences on heat and mass transfer characteristics, such as the fluid thermal properties, vapour condensation, fluid flow rate, etc. In order to develop the numerical model, the following assumptions for simplification in this study are made:

1) The dehumidifier is well-insulated, which means heat transfer between the dehumidifier and environment is not considered.
2) Heat and mass transfer through membrane is normal to the membrane in z direction.
3) Axial conductions in both air and solution channels are neglected since Peclet numbers (pe) in the air and solution channels are much larger than 20 [70, 147].
4) Absorption heat is released to solution side only since the solution side convective heat transfer coefficient is much higher than that in the air side.
5) Both the air and solution flows are treated as laminar flows since their Reynolds numbers (Re) are much lower than 2300 in most cases [67] .
6) Both the air and solution flows are fully developed, while their temperature and concentration vary along channel length only.

3.2.1.1 Solution side governing equations

Solution side governing equations are developed based on the energy and moisture conservations in the solution channel. For solution channel, the control volume used for the energy conservation is illustrated in Fig 3-2.

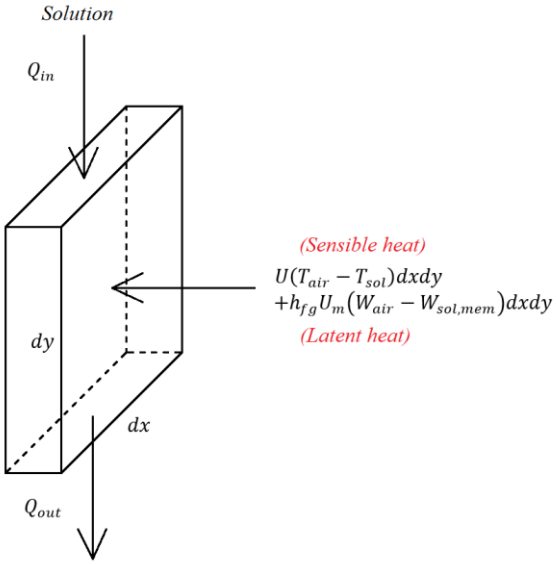


Fig 3- 2 Control volume used for the energy conservation in solution side

The energy flows in the control volume Q_{in} and out from the control volume Q_{out} are:

$$Q_{in} = \frac{\dot{m}_{sol}}{L} dx \cdot C_{p,sol} T_{sol} \tag{3-1}$$

$$Q_{out} = \frac{\dot{m}_{sol}}{L} dx \cdot C_{p,sol} T_{sol} + \frac{\dot{m}_{sol}}{L} dx \cdot C_{p,sol} \cdot \frac{\partial T_{sol}}{\partial y} dy \tag{3-2}$$

Where $\dot{m}_{sol}$ is solution mass flow rate (kg/s); L is the length of dehumidifier (m); dx and dy are length and height of control volume respectively; T_{sol} is solution temperature (℃); T_{air} is air temperature (℃); $C_{p,sol}$ is solution specific heat capacity (J/kgK).

Then the energy addition to the control volume ΔQ can be obtained:

$$\Delta Q = Q_{out} - Q_{in} = \left(\frac{\dot{m}_{sol}}{L} \cdot \frac{\partial T_{sol}}{\partial y} \cdot C_{p,sol}\right) \cdot dxdy \tag{3-3}$$

Then based on the heat transfer, the energy addition to the control volume can also be derived:

$$\Delta Q = U(T_{air} - T_{sol})dxdy + h_{fg} \cdot U_m\left(W_{air} - W_{sol,mem}\right)dxdy \tag{3-4}$$

Where the first term is the sensible heat addition, and the second term is the latent heat addition, or the adsorption heat. W_{air} is air humidity ratio (kg/kg dry air); $W_{sol,men}$ is humidity ratio of membrane surface on solution side ($kg/kg\ \ dry\ air$);h_{fg} is water condensation heat (J/kg); U (W/m^{2}K) and U_m (kg/m^{2}s) are heat transfer and mass transfer coefficients respectively, which are given by:

$$U = \left(\frac{1}{h_{air}} + \frac{\delta}{k_{mem}} + \frac{1}{h_{sol}}\right)^{-1} \tag{3-5}$$

$$U_m = \left(\frac{1}{h_{m,air}} + \frac{\delta}{k_{m,mem}}\right)^{-1} \tag{3-6}$$

Where h_{air} and h_{sol} are convective heat transfer coefficients in air and solution sides respectively (W/m^{2}K); $h_{m,air}$ is air side mass transfer coefficient (kg/m^{2}s); δ is membrane thickness (m); k_{mem} (W/mK) and $k_{m,mem}$(kg/ms) are membrane thermal conductivity and mass transfer conductivity respectively.

It should be noticed in Eq. 3-6 that the solution side mass transfer is neglected since the solution side mass transfer coefficient $h_{m,sol}$ is much higher than that in air side $h_{m,air}$.

Subsequently, by combining Eq, 3-3 and 3-4, the solution side heat balance equation can be calculated as:

$$\left(\frac{\dot{m}_{sol}}{L}\cdot\frac{\partial T_{sol}}{\partial y}\cdot C_{p,sol}\right)\cdot dxdy = \left[U(T_{air}-T_{sol})+h_{fg}\cdot U_m\left(W_{air}-W_{sol,mem}\right)\right]dxdy \quad (3\text{-}7)$$

Then the control volume used for the moisture conservation in solution side is illustrated in Fig 3-3.

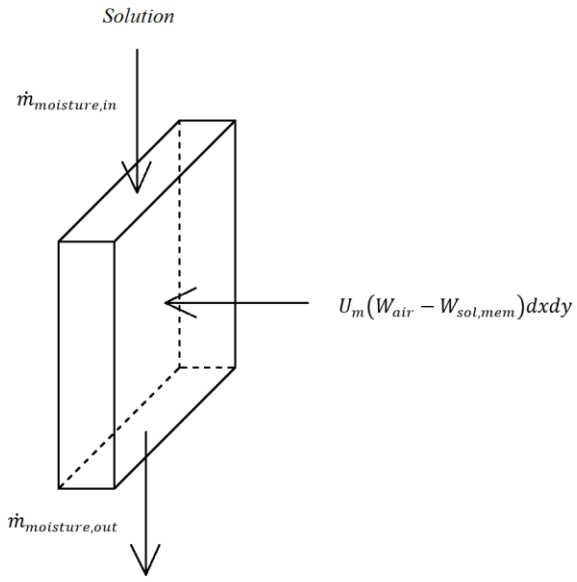


Fig 3- 3 Control volume used for the moisture conservation in solution side

The moisture flows in the control volume $\dot{m}_{moisture,in}$ and out from the control volume $\dot{m}_{moisture,out}$ are:

$$\dot{m}_{moisture,in} = \frac{\dot{m}_{desi}}{L}dx\cdot\frac{\dot{m}_{moisture}}{\dot{m}_{desi}} = (\frac{\dot{m}_{desi}}{L}X_{sol})dx \quad (3\text{-}8)$$

$$\dot{m}_{moisture,out} = (\frac{\dot{m}_{desi}}{L}X_{sol})dx + \frac{\dot{m}_{desi}}{L}dx\cdot\frac{\partial X_{sol}}{\partial y}dy \quad (3\text{-}9)$$

Where $\dot{m}_{desi}$ is desiccant mass flow rate (kg/s); W_{air} is air humidity ratio (kg/kg dry air); $W_{sol,men}$ is humidity ratio of membrane surface on solution side (kg/kg dry air); X_{sol} is solution mass fraction, which is calculated as:

$$X_{sol} = \frac{\dot{m}_{moisture}}{\dot{m}_{desi}} = \frac{1-C_{sol}}{C_{sol}} \quad (3\text{-}10)$$

Where C_{sol} is solution mass concentration:

$$C_{sol} = \frac{\dot{m}_{desi}}{\dot{m}_{sol}} \tag{3-11}$$

So the moisture addition to the control volume $\Delta\dot{m}_{moisture}$ can be obtained:

$$\Delta\dot{m}_{moisture} = \dot{m}_{moisture,out} - \dot{m}_{moisture,in} = \frac{\dot{m}_{desi}}{L} \cdot \frac{\partial X_{sol}}{\partial y} \cdot dxdy \tag{3-12}$$

Based on the mass transfer, $\Delta\dot{m}_{moisture}$ can also be derived:

$$\Delta\dot{m}_{moisture} = U_m \cdot \left(W_{air} - W_{sol,men}\right)dxdy \tag{3-13}$$

Subsequently, the solution side mass balance equation is given as:

$$\frac{\dot{m}_{desi}}{L} \cdot \frac{\partial X_{sol}}{\partial y} \cdot dxdy = U_m \cdot \left(W_{air} - W_{sol,men}\right)dxdy \tag{3-14}$$

3.2.1.2 Air side governing equations

The control volume used for the energy conservation in air side is illustrated in Fig 3-4.

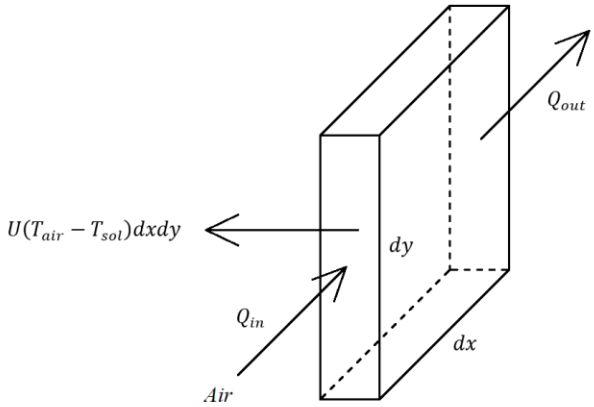


Fig 3- 4 Control volume used for the energy conservation in air side

The energy flows in the control volume Q_{in} and out from the control volume Q_{out} are:

$$Q_{in} = \frac{\dot{m}_{air}}{H} dy \cdot C_{p,air} T_{air} \tag{3-15}$$

$$Q_{out} = \frac{\dot{m}_{air}}{H} dy \cdot C_{p,air} T_{air} + \frac{\dot{m}_{air}}{H} dy \cdot C_{p,air} \cdot \frac{\partial T_{air}}{\partial x} dx \tag{3-16}$$

Where H is height of the dehumidifier (m); $C_{p,air}$ is air specific heat capacity (J/kgK).

So the energy adduction to the control volume ΔQ can be obtained:

$$\Delta Q = Q_{out} - Q_{in} = \left(\frac{\dot{m}_{air}}{H} \cdot \frac{\partial T_{air}}{\partial x} \cdot C_{p,air}\right) \cdot dxdy \tag{3-17}$$

Then based on the heat transfer, the deduction from the control volume is derived:

$$\Delta Q = -U(T_{air} - T_{sol})dxdy \tag{3-18}$$

So the air side energy balance equation is given as:

$$\frac{\dot{m}_{air}}{H} \cdot \frac{\partial T_{air}}{\partial x} \cdot C_{p,air} + U(T_{air} - T_{sol}) = 0 \tag{3-19}$$

The control volume used for the moisture conservation in air side is illustrated in Fig 3-5.

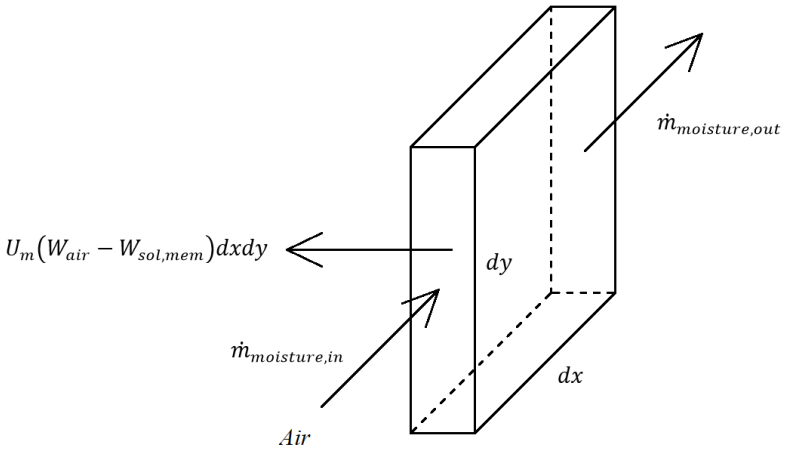


Fig 3- 5 Control volume used for the moisture conservation in air side

The moisture flows in the control volume $\dot{m}_{moisture,in}$ and out from the control volume $\dot{m}_{moisture,out}$ are:

$$\dot{m}_{moisture,in} = \frac{\dot{m}_{air}}{H} dy \cdot \frac{\dot{m}_{moisture}}{\dot{m}_{air}} = \frac{\dot{m}_{air}}{H} W_{air} dy \tag{3-20}$$

$$\dot{m}_{moisture,out} = \frac{\dot{m}_{air}}{H} W_{air} dy + \frac{\dot{m}_{air}}{H} dy \cdot \frac{\partial W_{air}}{\partial x} dx \tag{3-21}$$

So the moisture deduction from the control volume $\Delta\dot{m}_{moisture}$ can be obtained:

$$\Delta\dot{m}_{moisture} = \left(\frac{\dot{m}_{air}}{H} \frac{\partial W_{air}}{\partial x}\right) dxdy \tag{3-22}$$

Based on the mass transfer, $\Delta\dot{m}_{moisture}$ can also be derived:

$$\Delta\dot{m}_{moisture} = -U_m \cdot \left(W_{air} - W_{sol,men}\right)dxdy \tag{3-23}$$

Subsequently, the air side mass balance equation is given as:

$$\frac{\dot{m}_{air}}{H}\frac{\partial W_{air}}{\partial x} + U_m \cdot \left(W_{air} - W_{sol,men}\right) = 0 \quad (3\text{-}24)$$

To sum up, Eqs. (3-7), (3-14), (3-19) and (3-24) are governing equations of heat and mass balance in solution and air sides respectively.

3.2.2 Normalization of governing equations

Governing equations: Eqs. (3-7), (3-14), (3-19) and (3-24) are normalized as:

$$\frac{\partial {T_{sol}}^*}{\partial y^*} - NTU_m h^* \frac{1}{Cr^*}\left({W_{air}}^* - {W_{sol,mem}}^*\right) - NTU\frac{1}{Cr^*}({T_{air}}^* - {T_{sol}}^*) = 0 \quad (3\text{-}25)$$

$$\frac{\partial X_{sol}}{\partial y^*} - NTU_m \frac{1}{m^*} W_0 (1 + X_{sol})({W_{air}}^* - {W_{sol,mem}}^*) = 0 \quad (3\text{-}26)$$

$$\frac{\partial {T_{air}}^*}{\partial x^*} + NTU({T_{air}}^* - {T_{sol}}^*) = 0 \quad (3\text{-}27)$$

$$\frac{\partial {W_{air}}^*}{\partial x^*} + NTU_m\left({W_{air}}^* - {W_{sol,mem}}^*\right) = 0 \quad (3\text{-}28)$$

Where in the above equations, the following dimensionless properties have been defined. Dimensionless length is defined by:

$$x^* = \frac{x}{L} \quad (3\text{-}29)$$

Dimensionless height is defined by:

$$y^* = \frac{y}{H} \quad (3\text{-}30)$$

Dimensionless temperature is defined by:

$$T^* = \frac{T - T_{air,in}}{T_0} \quad (3\text{-}31)$$

Where T_0 is equal to $(T_{sol,in} - T_{air,in})$. $T_{sol,in}$ and $T_{air,in}$ are solution and air temperatures at the dehumidifier inlet respectively (℃).

Dimensionless humidity ratio is defined by:

$$W^* = \frac{W - W_{air,in}}{W_0} \quad (3\text{-}32)$$

Where W_0 is equal to ($W_{sol,in} - W_{air,in}$). $W_{sol,in}$ and $W_{air,in}$ are solution and air humidity ratio at the dehumidifier inlet respectively (kg/kg dry air).

m^* is mass flow rate ratio, which is defined by:

$$m^* = \frac{\dot{m}_{sol}}{\dot{m}_{air}} \tag{3-33}$$

Cr^* is thermal capacity ratio, which is defined by:

$$Cr^* = \frac{(\dot{m}c_p)_{sol}}{(\dot{m}c_p)_{air}} \tag{3-34}$$

h^* is operating factor, which is a dimensionless number defined by:

$$h^* = \frac{W_0}{T_0}\frac{h_{fg}}{c_{p,air}} \tag{3-35}$$

NTU and NTU_m are numbers of heat and mass transfer respectively, which are defined by:

$$NTU = \frac{UA}{(\dot{m}c_p)_{air}} \tag{3-36}$$

$$NTU_m = \frac{U_m A}{\dot{m}_{air}} \tag{3-37}$$

Where A is total membrane area (m^2).

The detailed normalization methods for governing equations are given in Appendix A.

3.2.3 Boundary conditions

Boundary conditions for the solution side are:

$T_{sol}{}^* = 1$, at y^*=0 (3-38)

$X_{sol} = X_{sol,in}$, at y^*=0 (3-39)

While the air side boundary conditions are:

$T_{air}{}^* = 0$, at x^*=0 (3-40)

$T_{air}{}^* = 0$, at x^*=0 (3-41)

3.2.3.1 Heat transfer boundary conditions on membrane surfaces

To solve the governing equations, heat and mass transfer boundary equations on membrane surfaces need to be established. Heat transfer boundary conditions are based on thermal energy balance through the membrane:

$$h_{sol}\left(T_{sol,mem}-T_{sol}\right)=U\left(T_{air}-T_{sol,mem}\right)+h_{fg}U_{m}\left(W_{air}-W_{sol,mem}\right) \quad (3\text{-}42)$$

Eq. (3-42) can be normalized as:

$$NTU_{sol}\left({T_{sol,mem}}^{*}-{T_{sol}}^{*}\right)=NTU\left({T_{air}}^{*}-{T_{sol,mem}}^{*}\right)+NTU_{m}h^{*}\left({W_{air}}^{*}-{W_{sol,mem}}^{*}\right) \quad (3\text{-}43)$$

Where NTU_{sol} is number of heat transfer unit in solution side and defined by:

$$NTU_{sol}=\frac{h_{sol}A}{\left(\dot{m}c_{p}\right)_{air}} \quad (3\text{-}44)$$

3.2.3.2 Mass transfer boundary conditions on membrane surfaces

Similarly, mass transfer boundary conditions are based on mass balance through the membrane:

$$U_{m}\left(W_{air}-W_{sol,mem}\right)=h_{m,sol}\left(C_{sol}-C_{sol,mem}\right) \quad (3\text{-}45)$$

Eq. (3-45) can be normalized as:

$$NTU_{m}W_{0}\left({W_{air}}^{*}-{W_{sol,mem}}^{*}\right)=NTU_{m.sol}\left(C_{sol}-C_{sol,mem}\right) \quad (3\text{-}46)$$

Where $C_{sol,mem}$ is solution concentration in the interface between the solution and membrane surface; $NTU_{m.sol}$ is number of mass transfer unit in the solution side, which is defined by:

$$NTU_{m.sol}=\frac{h_{m,sol}A}{\dot{m}_{air}} \quad (3\text{-}47)$$

Where $h_{m,sol}$ is solution side mass transfer coefficient ($\mathrm{kg/m^2s}$).

3.2.4 Air and solution property calculations

In numerical modelling, the air absolute humidity AH ($\mathrm{kg/m^3}$) is derived from its relative humidity RH (%) by applying the correlation [213]:

$$AH(\mathrm{kg/m^3}) = 10^{-3} \times \frac{6.112 \times e^{\left(\frac{17.67 \times T_{air}}{T_{air}+243.5}\right) \times RH \times 2.1674}}{273.15+T_{air}} \quad (3\text{-}48)$$

Subsequently the air specific humidity, or humidity ratio W_{air} (kg/kg dry air) can be obtained by:

$$W_{air}(\mathrm{kg/kg\ dry\ air}) = \frac{AH}{\rho_{air}} \quad (3\text{-}49)$$

Where ρ_{air} is the air density ($\mathrm{kg/m^3}$).

The solution equilibrium specific humidity W_{sol} is used to calculate both the sensible and latent effectiveness, the relationship between the specific humidity and vapour pressure is given by [214]:

$$W_{sol} = 0.62198 \frac{P_v}{P - P_v} \quad (3\text{-}50)$$

Where P is atmospheric pressure (Pa) and P_v is vapour pressure of desiccant solution (Pa).

The equilibrium vapour pressure of desiccant solution is a function of T_{sol} and C_{sol} ($P_v = f(T_{sol}, C_{sol})$), the correlation is given by [215]:

$$Log\ P_v = KI\left[A - \frac{B}{T - E_s}\right] + \left[C - \frac{D}{T - E_s}\right] \quad (3\text{-}51)$$

Where P_v is solution equilibrium vapour pressure (kPa), T is the temperature (K); A, B, C, D can be calculated as:

$$A = A_s + 3.60591 \times 10^{-4} \times I + M_s/2303 \quad (3\text{-}52)$$

$$B = B_s + 1.382982 \times I - 0.031185 \times I^2 \quad (3\text{-}53)$$

$$C = C_s - 3.99334 \times 10^{-3} \times I - 1.11614 \times 10^{-4} \times I^2 + M_s I(1 - \chi)/2303 \quad (3\text{-}54)$$

$$D = D_s - 0.138481 \times I + 0.027511 \times I^2 - 1.79277 \times 10^{-3} \times I^3 \quad (3\text{-}55)$$

Where A_s, B_s, C_s, D_s, E_s and K are electrolyte parameters related to solute and solvent. For $CaCl_2$ and LiCl solutions that use water as solvent, these parameters as given in Table 3-1 [215].

Table 3- 1 Electrolyte parameters for $CaCl_2$ and LiCl solutions [216]

	A_s	B_s	C_s	D_s	E_s	K
$CaCl_2$	-0.021302	-5.390915	7.192959	1730.2857	39.53	0.32138
LiCl	-0.021302	-5.390915	7.192959	1730.2857	39.53	0.72567

I is the ionic strength (mol/kg) which can be obtained by [215]:

$$I = \frac{1}{2}\sum b_{(i)} {Z_{(i)}}^2 \tag{3-56}$$

Where $b_{(i)}$ is the molality of electrolyte i; $Z_{(i)}$ is the valence of electrolyte i.

M_s is the molecular weight of the solvent (kg/mol). For water solvent, $M_s = 0.018$ kg/mol.

χ is another electrolyte property related to the solute as calculated by [215]:

$$\chi = 2(v_+ + v_-)/(v_+ {Z_+}^2 + v_- {Z_-}^2) \tag{3-57}$$

Where v_+ and v_- are number of models of cation and anion produced by the dissociation of one moles of the electrolyte respectively; Z_+ and Z_+ are valence of cation and anion respectively;

As the result, once the temperature and concentration of solution are given, the equilibrium vapour pressure can be obtained through Eqs. (3-51)-(3-57). Subsequently the solution equilibrium specific humidity W_{sol} can be calculated by Eq. (3-50). In this study the LiCl is selected as the working solution, so a psychometric chart of LiCl solution is plotted and shown in Fig 3-6.

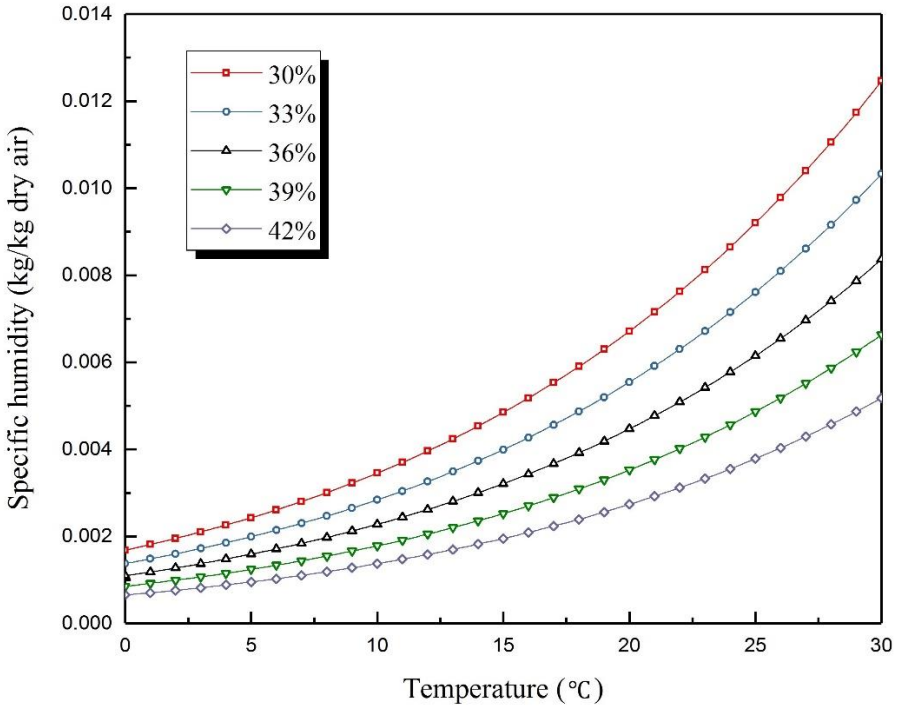


Fig 3- 6 Psychometric chart of LiCl for dehumidifier

Specific heat capacity, density, conductivity and diffusivity for air and solution flows are obtained from heat and mass transfer reference books [213, 217]. For the Nusselt number and Sherwood number in air and solution side, Huang et al. [75, 76] presented the relationship between aspect ratio and Nusselt number and Sherwood number. For the membrane unite used in this study, the aspect ratios for air channel and solution channel are calculated as 27 and 48 respectively, and their corresponding Nusselt numbers for air side and solution side are 6.58 and 7.74 respectively, and the Sherwood number for air side is 6.7.

The desiccant solution and air transport properties used in the mathematical modelling are listed in Table 3-2.

Table 3- 2 Air and desiccant solution transport properties.

Description	Symbol	Unit	Value
Air specific heat capacity	$c_{p,air}$	*J/kgK*	1020
Solution specific heat capacity	$c_{p,sol}$	*J/kgK*	3200
Air density	ρ_{air}	kg/m^3	1.29
Solution density	ρ_{sol}	kg/m^3	1247
Air side diffusivity	D_{air}	m^2/s	2.46×10^{-5}
Solution side diffusivity	D_{sol}	m^2/s	0.892×10^{-2}
Air side heat conductivity	k_{air}	*W/Mk*	0.03
Solution side heat conductivity	k_{sol}	*W/Mk*	0.53
Air side Nusselt number	Nu_{air}	-	6.58
Solution side Nusselt number	Nu_{sol}	-	7.74
Air side Sherwood number	Sh_{air}	-	6.7

3.2.5 Simulation procedure

3.2.5.1 Discretization of governing equations

Governing equations in Section 3.2.1 are solved by finite difference method, and discretized by a forward difference scheme. Discretization equations are given below:

$$T_{sol\,(m+1,n)}{}^{*} - T_{sol\,(m,n)}{}^{*} - dy^{*}NTU_{m}h^{*}Cr\left[W_{air\,(m+1,n)}{}^{*} - W_{sol,mem\,(m+1,n)}{}^{*}\right] - dy^{*}NTUCr\left[T_{air\,(m+1,n)}{}^{*} - T_{sol\,(m+1,n)}{}^{*}\right] = 0 \quad (3\text{-}58)$$

$$X_{sol\,(m+1,n)} - X_{sol\,(m,n)} - dy^{*}m^{*}W_{0}NTU_{m}\left[1 + X_{sol\,(m+1,n)}\right]\left[W_{air\,(m+1,n)}{}^{*} - W_{sol,mem\,(m+1,n)}{}^{*}\right] = 0 \quad (3\text{-}59)$$

$$T_{air\,(m,n+1)}{}^{*} - T_{air\,(m,n)}{}^{*} + dx^{*}NTU\left[T_{air\,(m,n+1)}{}^{*} - W_{sol\,(m,n+1)}{}^{*} = 0\right. \quad (3\text{-}60)$$

$$W_{air\,(m,n+1)}{}^{*} - W_{air\,(m,n)}{}^{*} + dx^{*}NTU_{m}\left[W_{air\,(m,n+1)}{}^{*} - W_{sol,mem\,(m,n+1)}{}^{*}\right] = 0 \quad (3\text{-}61)$$

Where m is number of grids in x direction, and n is number of grids in y direction.

Since the air and desiccant solution are closely interacted with each other, the governing equations are solved in Matlab iteratively until converged. In order to guarantee the accuracy of numerical results, numerical tests have been conducted to determine the grid size. It has been found that 30×60 grids are adequate in this study, the result difference is less than 1.0% compared with 50×100 grids. The numerical uncertainty is 1.0%.

3.2.5.2 Numerical solving procedure

The numerical solution procedure used to solve interacted governing equations are given below:

1) Set the initial temperature and concentration fields for air and solution as boundary conditions.
2) Assume the initial humidity ratio on the membrane surface as the solution inlet equilibrium specific humidity.
3) Solve the energy equation (3-25) to get the solution temperature field ($T_{sol}{}^{*}$).
4) Solve the mass equation (3-26) to obtain the solution concentration field (X_{sol}).
5) Solve the energy equation (3-27) to acquire the air temperature field ($T_{air}{}^{*}$).
6) Solve the mass equation (3-28) to get the air humidity field ($W_{air}{}^{*}$).
7) Based on the temperature and humidity fields for air and solution flows, solve heat and mass transfer boundary conditions on the membrane surface (3-43) and (3-46) to obtain the membrane surface temperature and concentration fields in the solution side ($T_{sol,mem}{}^{*}$ and $C_{sol,mem}$).
8) Calculate the membrane surface humidity field in the solution side ($W_{sol,mem}{}^{*}$) based on $T_{sol,mem}{}^{*}$ and $C_{sol,mem}$.
9) Adopt new $W_{sol,mem}{}^{*}$ as a default value and return to step 7 until $W_{sol,mem}{}^{*}$ is converged.
10) Return to step 3 with the new $W_{sol,mem}{}^{*}$ until$T_{sol}{}^{*}$, X_{sol}, $T_{air}{}^{*}$ and $W_{air}{}^{*}$ are converged.

For better illustration, the solution procedure used to solve interacted governing equations is shown in Fig 3-7.

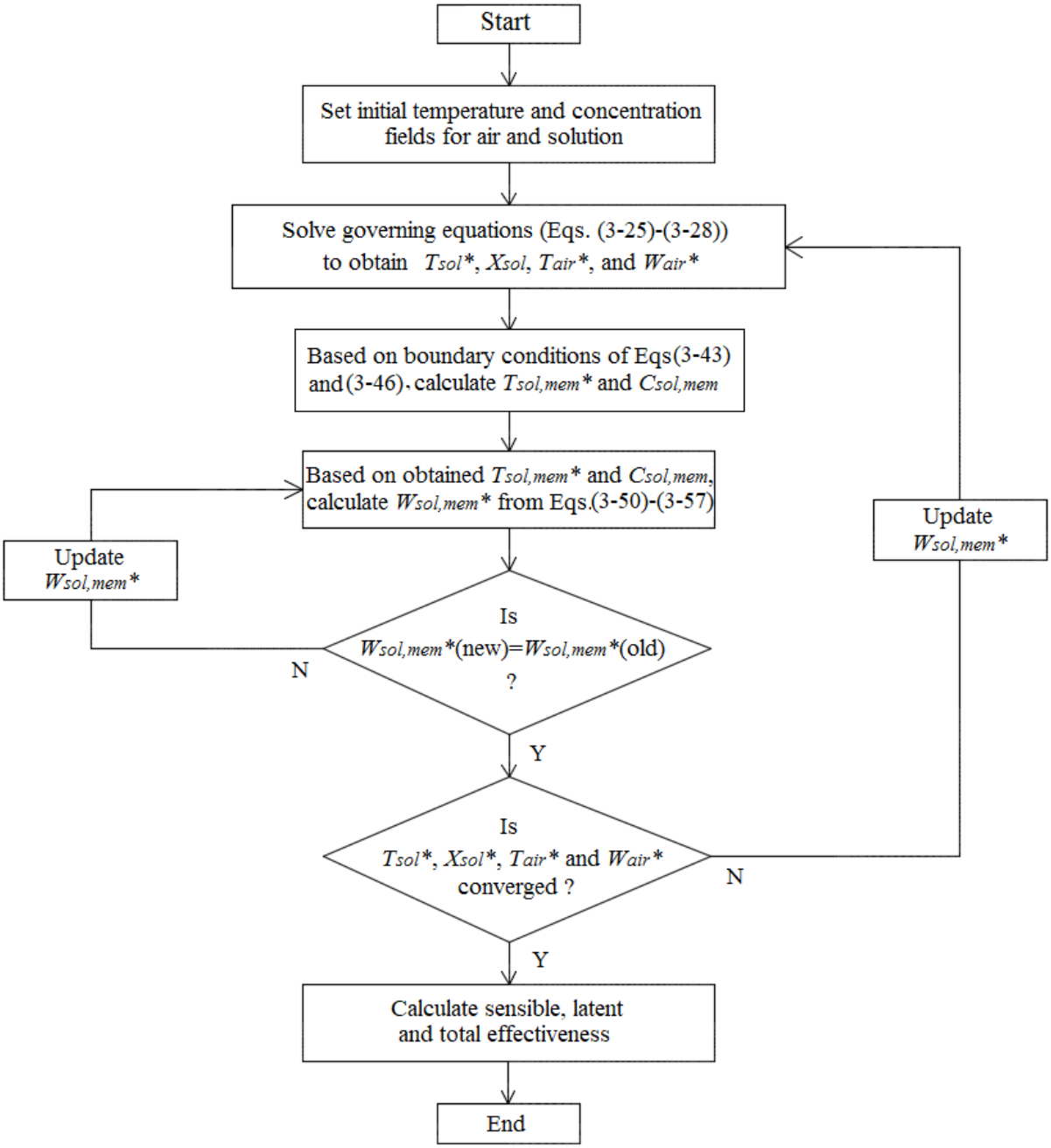


Fig 3- 7 Flow chart for the solution procedure for dehumidifier

3.3 Performance evaluation indices

Effectiveness is the most important parameter used to evaluate the performance of a heat and mass exchanger [216]. Three types of effectiveness have been defined in this study: sensible effectiveness (ε_{sen}), latent effectiveness (ε_{lat}) and total effectiveness (ε_{tot}). ε_{sen} is the ratio between the actual and maximum possible rates of sensible heat transfer in a heat exchanger. ε_{lat} is the ratio between the actual and maximum possible moisture transfer rates in a mass exchanger. ε_{tot} is the ratio between the actual and maximum possible energy (enthalpy) transfer rates in a heat and mass exchanger. The capacity rate of desiccant solution is higher than that of the air, which means $Cr^* \geq 1$, then the sensible, latent and total effectiveness are defined by Eqs. (3-62) - (3-64) [218].

$$\varepsilon_{sen} = \frac{T_{air,in} - T_{air,out}}{T_{air,in} - T_{sol,in}} \tag{3-62}$$

$$\varepsilon_{lat} = \frac{W_{air,in} - W_{air,out}}{W_{air,in} - W_{sol,in}} \tag{3-63}$$

$$\varepsilon_{tol} = \frac{\varepsilon_{sen} + H^* \varepsilon_{lat}}{1 + h^*} \tag{3-64}$$

Where $T_{air,out}$ is air temperature at the outlet (℃) and $W_{air,out}$ is air humidity ratio at the outlet (kg/kg dry air).

3.4 Experimental set-up

In order to assess the performance of a membrane-based parallel-plate liquid desiccant dehumidification system, a test facility is designed and built in the laboratory, which is depicted in Fig 3-8.

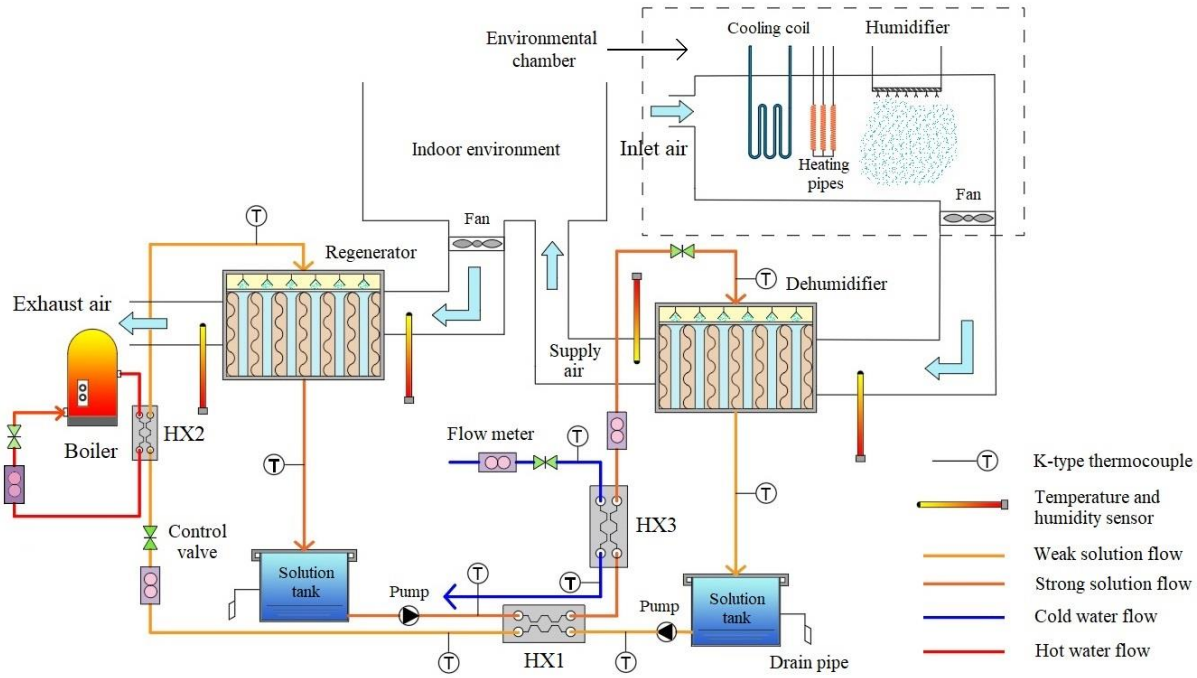


Fig 3- 8 Schematic diagram of the laboratory test rig

The test rig mainly consists of a dehumidifier, a regenerator, two solution tanks and three heat exchange units. The outdoor air with high temperature and relative humidity is generated in the environmental chamber, and it flows into the dehumidifier where both its moisture content and temperature are reduced by cold desiccant solution, then it leaves the dehumidifier unit at a dry and cool state. Its flow rate is controlled by adjusting an AC axial fan rotation speed (ebm-papst Mulfingen GmbH & Co. KG). The dehumidifier has a dimension of 410mm (L) × 186mm (W) × 230mm (H) with 11 air channels and 11 solution channels. The regenerator has the same structure as the dehumidifier. Three gauze layers are paved on the top surface of the dehumidifier unit to ensure even solution distribution. The dehumidifier specifications and membrane physical properties are given in Table 3-3.

Table 3- 3 Dehumidifier specifications and membrane physical properties

Description	Symbol	Unit	Value
Length of dehumidifier unit	L	m	0.41
Width of dehumidifier unit	W	m	0.23
Height of dehumidifier unit	H	m	0.21
Number of air channels	-	-	11
Number of solution channels	-	-	11
Air channel thickness	d_{air}	m	0.0077
Solution channel thickness	d_{sol}	m	0.0043
Membrane thickness	δ_{mem}	m	0.5×10^{-3}
Membrane conductivity	k_{mem}	W/mK	0.3
Membrane mass transfer conductivity	$k_{m,mem}$	kg/ms	3.87×10^{-6}

Lithium chloride (LiCl) is used as the desiccant in the system. The desiccant solution is circulated in the system by two identical pumps (15W centrifugal magnetically driven type with flow rate range of 0-10L/min) and their flow rates are measured by two liquid flow indicators (Parker UCC PET 1-15 L/min).

Air velocities through the dehumidifier and regenerator are measured at the air duct outlets by a thermo-anemometer (Testo 405) with a measuring range up to 10m/s. All fans at the inlets of the dehumidifier and regenerator are equipped with infinitely variable speed controllers to adjust air flow rates. All air inlets and outlets are instrumented with humidity and temperature sensors (Sensirion Evaluation KIT EK-H4). The desiccant solution and water temperatures are measured with K-type thermocouples, and all sensors are connected to a DT500 data logger. The dehumidifier, regenerator, heat exchangers, storage tanks and pipes are well insulated to reduce the environment influence. All measurement devices and their accuracies are listed in Table 3-4.

Table 3- 4 Measurement devices and uncertainties

Device	Measurement	Range	Uncertainty
Testo thermos-anemometer	Air velocity	0-10 m/s	$\pm 5\%$
Sensiron Evaluation KIT EK-H4	Temperature	-40-125 ℃	$\pm 0.4\%$
	Relative humidity	0-100 %	$\pm 3\%$
K-type thermocouple probe	Temperature	0-1100 ℃	$\pm 0.75\%$
DT500 Datalogger	Data acquisition	-	$\pm 0.15\%$
Parker UCC PET liquid flow indicator	Solution flow rate	1-15 L/min	$\pm 5\%$
Parker liquid flow indicator	Water flow rate	2-22 L/min	$\pm 2\%$

Uncertainty analysis has been conducted for all experimental data by applying a method of propagation introduced by Taylor [219] to estimate uncertainties for experimental data. For the uncertainty in sums and differences, or in products and quotients, the uncertainty in the computed value of q can be calculated by:

$$Sums\ and\ differences:\ \delta q \approx \sqrt{(\delta x)^2 + \cdots + (\delta z)^2} \tag{3-65}$$

$$Products\ and\ quotients:\ \frac{\delta q}{|q|} \approx \sqrt{\left(\frac{\delta x}{|x|}\right)^2 + \cdots + \left(\frac{\delta z}{|z|}\right)^2} \tag{3-66}$$

Where $x, \cdots, z$ are measured quantities.

If q is any function of several variables $x, \cdots, z$, the uncertainty of q can be obtained by:

$$\delta q = \sqrt{\left(\frac{\partial q}{\partial x}\delta x\right)^2 + \cdots + \left(\frac{\partial q}{\partial z}\delta z\right)^2} \tag{3-67}$$

By applying Eqs. (3-65) - (3-67), the absolute uncertainties of calculated values can be obtained. Error bars are included in all experimental data.

3.5 Numerical model validation

Analytical solutions and experimental data are used to validate the numerical results. 12 groups of experimental data under different operating conditions are used to validate numerical results. Under each operating condition, the numerical calculation and experimental results of sensible effectiveness (ε_{sen}) and latent effectiveness (ε_{lat}) are compared, as shown in Table 3-5. It can be seen that generally numerical modelling results of both ε_{sen} and ε_{lat} agree well with experimental data. The maximum discrepancy between numerical results and experimental data for ε_{sen} is 8.756%, while the maximum discrepancy for ε_{lat} is 9.822%.

Table 3- 5 Comparisons between numerical results and experimental data

Operating conditions				Comparisons					
NTU	m^*	m_{air} (kg/s)	m_{sol} (kg/s)	$\varepsilon_{sen,num}$	$\varepsilon_{sen,exp}$	Error (%)	$\varepsilon_{lat,num}$	$\varepsilon_{lat,exp}$	Error (%)
2	1	0.1216	0.1216	0.5699	0.520	8.756	0.5101	0.460	9.822
2	2	0.1216	0.2431	0.7113	0.671	5.665	0.5311	0.500	5.856
2	3	0.1216	0.3647	0.7608	0.708	6.940	0.5380	0.508	5.576
2	4	0.1216	0.4862	0.7861	0.735	6.500	0.5413	0.511	5.597
4	1	0.0608	0.0608	0.6276	0.576	8.221	0.7226	0.653	9.632
4	2	0.0608	0.1216	0.8116	0.753	7.220	0.7632	0.742	2.778
4	3	0.0608	0.1823	0.8704	0.810	6.940	0.7756	0.756	2.527
4	4	0.0608	0.2432	0.8990	0.849	5.562	0.7816	0.750	4.043
8	1	0.0304	0.0304	0.7376	0.686	6.996	0.8778	0.818	6.812
8	2	0.0304	0.0608	0.9043	0.857	5.231	0.9270	0.916	1.187
8	3	0.0304	0.0912	0.9440	0.894	5.297	0.9396	0.918	2.299
8	4	0.0304	0.1216	0.9608	0.918	4.455	0.9452	0.928	1.820

Analytical solutions to the model of an enthalpy exchanger with membrane core have been presented in several literatures. According to these literatures, the sensible effectiveness is a function of two dimensionless parameters (NTU and Cr^*) for an unmixed cross flow, and given as [66, 202]:

$$\varepsilon_s = 1 - exp\left[\frac{\exp\left(-NTU^{0.78}{C_r}^{*-1}\right)-1}{NTU^{-0.22}{C_r}^{*-1}}\right] \tag{3-68}$$

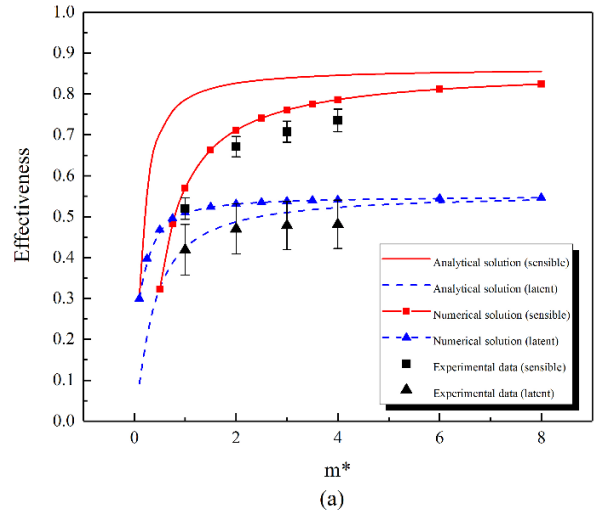
Similar to the sensible effectiveness, the latent effectiveness is calculated as [71]:

$$\varepsilon_l = 1 - exp\left\{\frac{{NTU_m}^{0.22}}{m^{*-1}}\left[\exp\left(-m^{*-1}{NTU_m}^{0.78}\right) - 1\right]\right\} \quad (3\text{-}69)$$

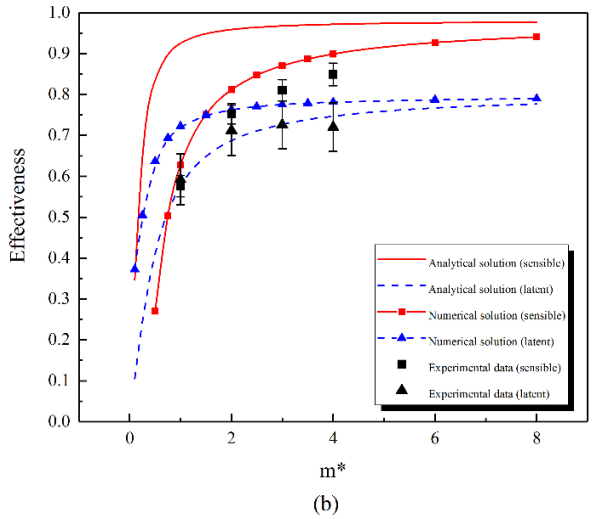
Results of the analytical solution are also given in Fig 3-9. The numerical modelling and analytical solution results have similar variation trends, an acceptable agreement between them is achieved.

The numerical modelling results and experimental data are presented in Fig 3-9, the numerical modelling results follow the same trends of experimental data for both the sensible and latent effectiveness under different NTUs. For sensible effectiveness, the maximum discrepancy between numerical and experimental results is 8.756%. In the meanwhile, the highest discrepancy between numerical experimental results for latent effectiveness is 9.822%. Based on the uncertainty analysis, which is shown as error bars for experimental data, it can be seen that numerical modelling results are within the tolerance range of experimental data. So it can be concluded that the agreements between the numerical modelling and experimental data for both the sensible and latent effectiveness are satisfied. It should be emphasized that under each NTU, the discrepancy reduces with the solution mass flow rate. This is because that the lower of solution mass flow rate, the greater influence of solution mal-distribution on the effectiveness.

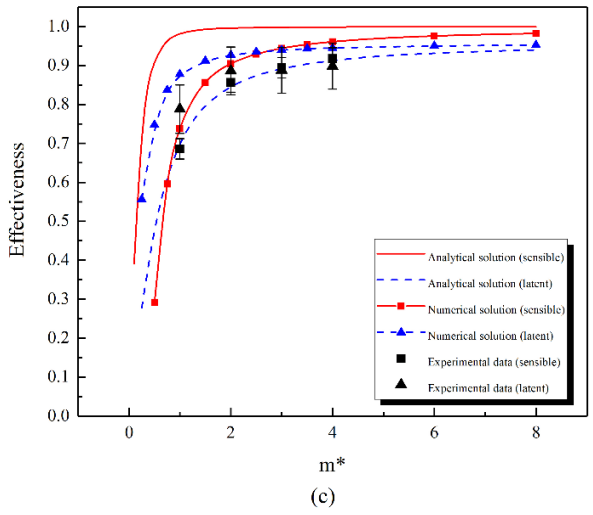
Based on the comparisons, it is valid to predict the performance of the membrane-based cross-flow dehumidifier by the numerical model.



(a)



(b)



(c)

Fig 3- 9 Comparisons among numerical modelling, experimental data and analytical solutions for sensible and latent effectiveness under different NTU values: NTU=2(a); NTU=4(b); NTU=8(c).

3.6 Results and discussion

3.6.1 Temperature and humidity (concentration) fields

Temperature and humidity fields of the air and solution channels, and the membrane surface are obtained based on the numerical model. The distributions of temperature and humidity ratio in the air channel and membrane surface under $NTU = 8$ and $m^* = 2$ are plotted in Fig 3-10. The inlet temperatures of the air and solution are 30℃ and 20℃ respectively, while the inlet air relative humidity and solution concentration are set as 70% and 39% respectively. It is observed that the air has the lowest temperature (20.00 ℃) and humidity ratio (0.0042 kg/kg dry air) at the right top corner of the air outlet. This is because the air at the top side of the dehumidifier interacts with stronger and cooler desiccant solution. Furthermore, the air becomes cooler and drier along the air channel length. It is noticed that the air temperature at left bottom corner of the dehumidifier is slightly higher than its inlet temperature. This is owing to the increase of the solution temperature during the dehumidification process.

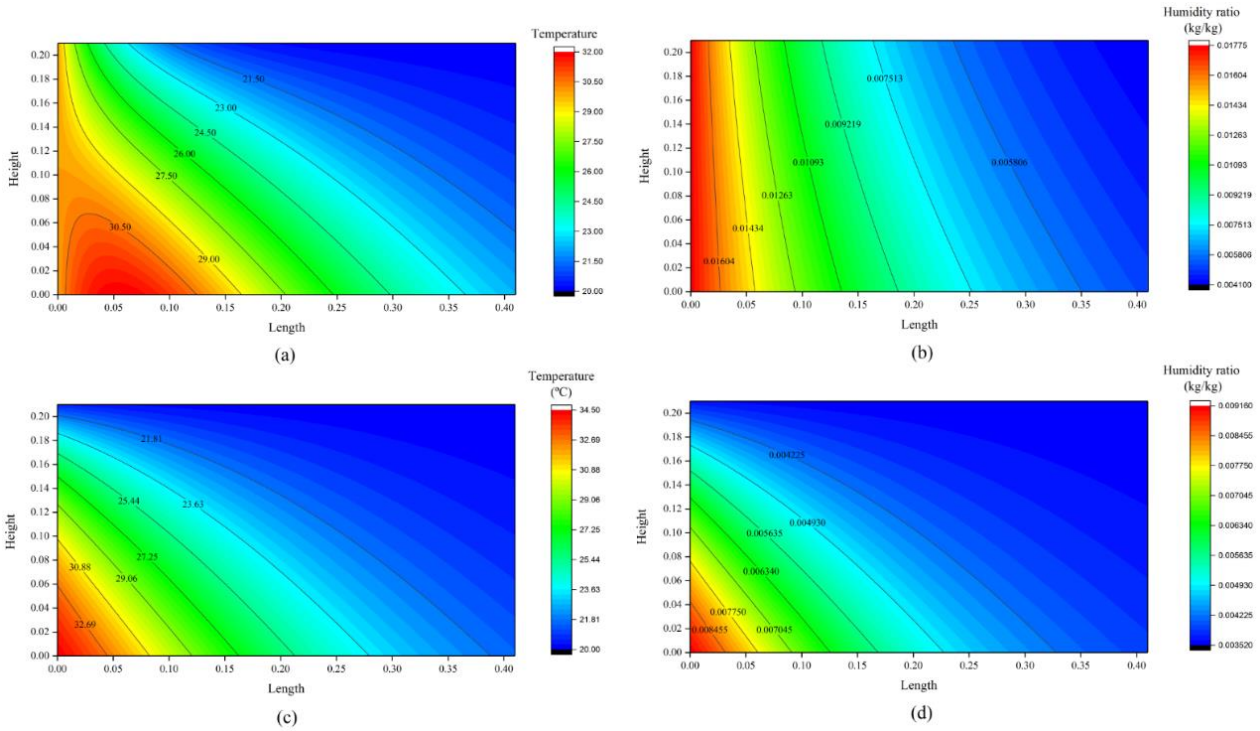


Fig 3- 10 Air temperature field (a); air humidity ratio field (b); temperature field on membrane surface (c); humidity ratio field on membrane surface (d)

Furthermore, Fig. 3-10 (c) and (d) reflect the temperature and humidity boundary conditions on the membrane surface, it is clear that the boundary condition is neither uniform temperature nor uniform humidity ratio. They are both non-uniform and two-dimensional profiles, the temperature and humidity ratio decrease along the diagonal line of the membrane surface.

3.6.2 Effects of dimensionless parameters

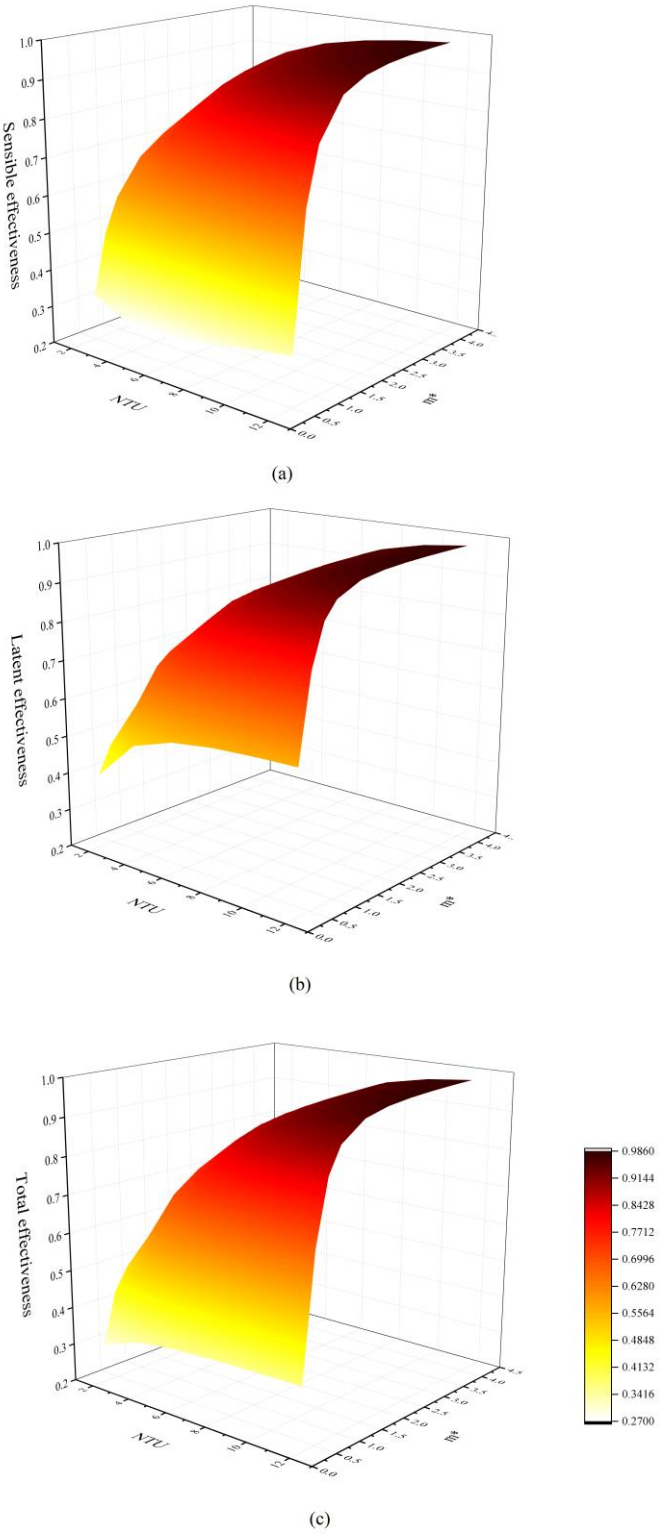


Fig 3- 11 Variations of effectiveness: (a) sensible effectiveness; (b) latent effectiveness; (c) total effectiveness with $m^*$and NTU.

The variations of sensible, latent and total effectiveness with m^* and NTU are given in Fig 3-11. The maximum values of sensible, latent and total effectiveness are 0.9849, 0.9845 and 0.9846 respectively when $m^* = 4$ and $NTU = 12$. The minimum values of sensible, latent and total effectiveness are 0.3232, 0.4682 and 0.4353 when $m^* = 0.5$ and $NTU = 2$. Separate effects of m^* and NTU are discussed then.

m^* is the relative mass flow rate of two fluids in the dehumidifier, and changed by adjusting solution mass flow rate while keeping air mass flow rate under each NTU. The variations of sensible, latent and total effectiveness with m^* at different NTUs are depicted in Figs. 3-12 – 3-14.

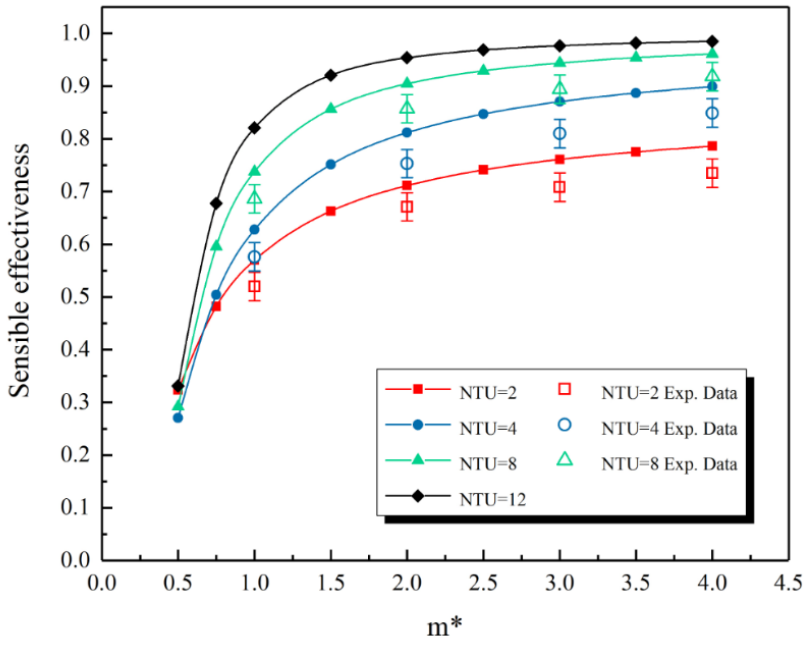


Fig 3- 12 Sensible effectiveness variations with m^* under different NTUs.

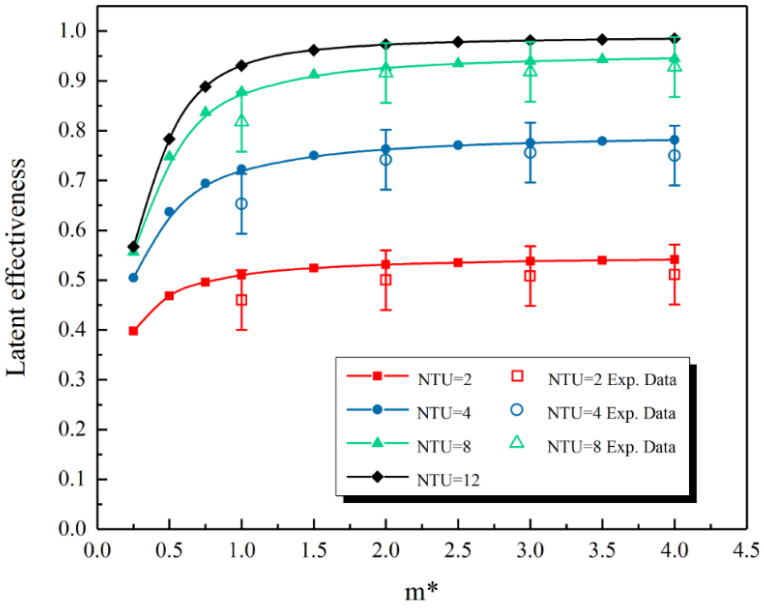


Fig 3- 13 Latent effectiveness variations with m^* under different NTUs.

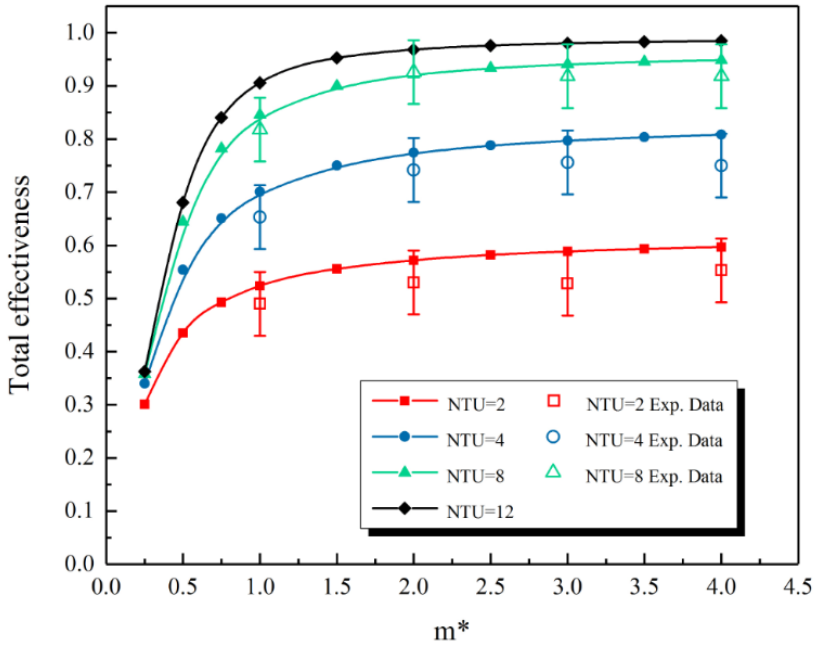


Fig 3- 14 Total effectiveness variations with m^* under different NTUs.

It is evident that m^* has significant influences on sensible, latent and total effectiveness, which all increase with m^*. The gradient of change for the sensible effectiveness is more considerable than that for latent and total effectiveness. For instance, at NTU =8, the sensible effectiveness

rises from 0.2917 to 0.9608 as m^* increases from 0.5 to 4. In the meanwhile, the latent and total effectiveness vary from 0.7476 to 0.9452 and from 0.6441 to 0.9487 respectively. However, the gradients of their changes become moderate gradually and only a slight variation is observed once m^* exceeds 1. Take the latent effectiveness as an example, under $NTU = 4$, the effectiveness increases by 43.15% as m^* rises from 0.25 to 1.0, while the effectiveness only increases by 8.16% when m^* rises from 1.0 to 4.0. Therefore a critical value of m^* can be defined as m^*_{crit}, and the effectiveness are more sensitive to m^* when m^* is lower than m^*_{crit}. Once m^* exceeds m^*_{crit}, there is not much significant change any more. Similar trends can be found in literatures [71], in which their results show that both sensible and latent effectiveness increase with m^* when $m^* < 1$, and they are nearly constant when $m^* \geq 1$. Similar to m^*_{crit}, another important indicator Cr^*_{crit} has been introduced in literatures [65, 81], as all effectiveness increase with Cr^* and are more sensitive before Cr^* reaching a critical value. This is easily explainable since Cr^* is proportional to m^*. Compared to Cr^*, m^* is a more straightforward parameter for the system. As a result, it is desirable to maintain the dehumidification system operating at a condition where m^* is close to m^*_{crit}. It is also worth mentioning that the gradient of change with m^* gets smoothly at low NTU. This is more obvious for the latent and total effectiveness. For example, the latent effectiveness increases by 36.21% (i.e. from 0.3974 to 0.5413) when m^* varies from 0.25 to 4 under $NTU = 2$, while under $NTU = 12$, an growth of 73.63% (i.e. from 0.5670 to 0.9845) is observed for the same m^* range. This means there is hardly benefit by increasing m^* at low NTU to improve the system performance.

On the other hand, NTU is another important dimensionless parameter affecting the effectiveness. In literature [65], NTU is treated as the most important parameter with the most significant impact on the dehumidification system. Compared to the flow rate, the non-dimensional group NTU is a comprehensive indicating parameter because it eliminates the

impact of channel geometric properties. In numerical modelling, NTU is changed by adjusting air mass flow rate, while the solution mass flow rate is changed proportionally to maintain a constant m^* accordingly. Variations of effectiveness with NTU under $m^* = 4$ are shown in Fig 3-15.

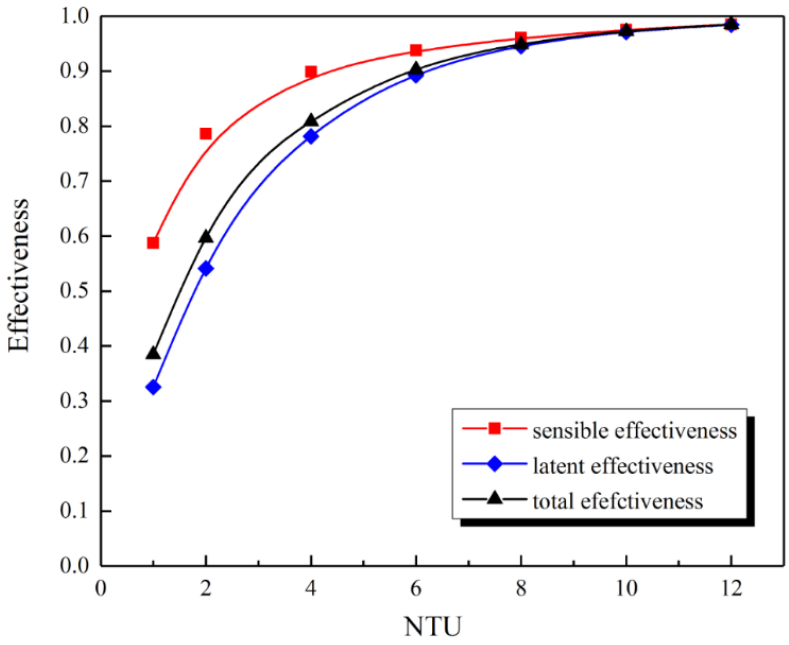


Fig 3- 15 Variations of effectiveness with NTU under $m^* = 4$.

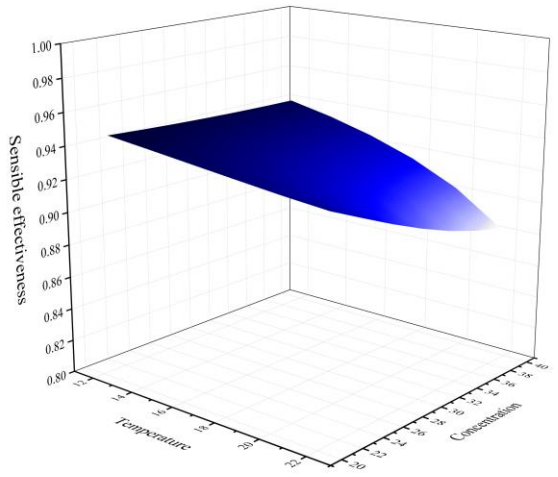
All effectiveness are seriously affected by NTU as indicated in Fig 3-15. Under the same m^*, the sensible effectiveness is the highest while the latent effectiveness is the lowest among the three effectiveness. Similar to the influences of m^*, the three effectiveness vary more remarkably when NTU is in the range of 1 to 4. Once NTU exceeds 4, variations of these effectiveness tend to level off. For instance, under $m^* = 4$, the sensible effectiveness increases by 53.02% (i.e. from 0.5875 to 0.899) when NTU changes from 1 to 4, conversely it only increases by 9.56% (i.e. from 0.899 to 0.9849) when NTU varies from 4 to 14. Cases are similar for the latent and total effectiveness. Thus similar to m^*_{crit} or Cr^*_{crit}, a critical value of NTU exists and is defined as NTU_{crit}. Increasing NTU beyond NTU_{crit} would not enhance the

system efficiency. Furthermore, it is observed from Figs. 3-12 – 3-14 that when m^* is low, there is hardly benefit to improve these effectiveness by increasing NTU. This is more obvious for the sensible effectiveness. For instance, under $m^* = 0.5$, increasing NTU from 2 to 12 will only slightly enhance the sensible effectiveness from 0.3232 to 0.3311. However, under $m^* = 4$, the sensible effectiveness improves from 0.7861 to 0.9849 when NTU increases from 2 to 12. Therefore there is hardly significance to increase NTU at low m^* for performance improvement.

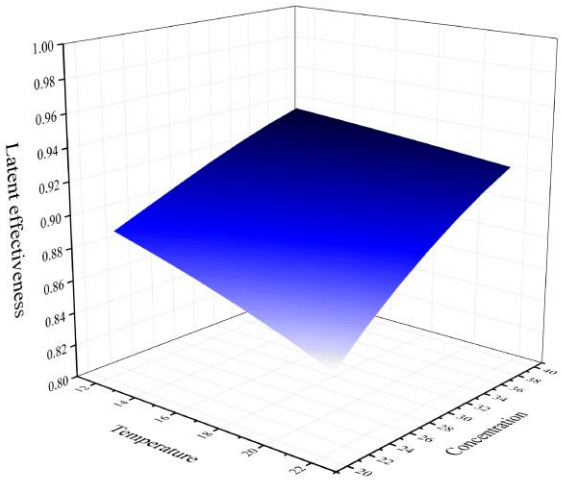
To sum up, these effectiveness increase with m^* and NTU, but their increase gradients are limited as $m^* > m^*_{crit}$ (i.e. 1 in this study) and $NTU > NTU_{crit}$ (i.e. 4 in this case). Effects of m^* and NTU are interacted on each other. Under a relatively low NTU there is hardly benefit to increase m^*, especially for the latent effectiveness. By contrast, with low m^*, no obvious performance improvement could be achieved by increasing NTU, especially for the sensible effectiveness.

3.6.3 Effects of solution properties

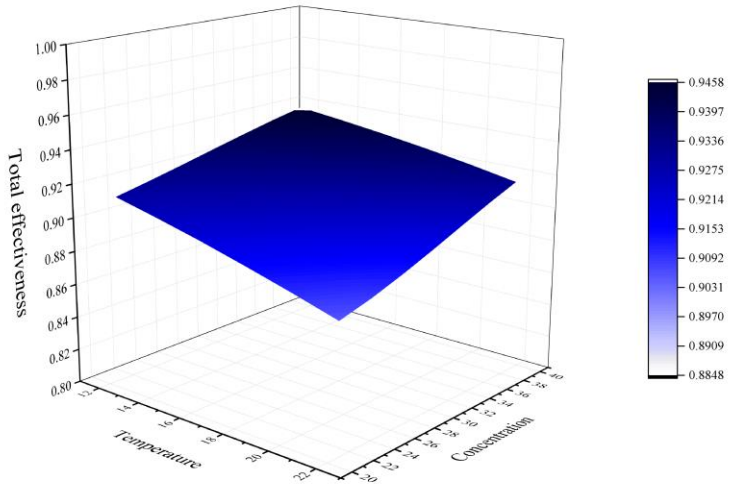
Solution temperature (T_{sol}) and concentration (C_{sol}) affect the system performance, variations of sensible, latent and total effectiveness with T_{sol} and C_{sol} are presented in Fig 3-16, while NTU and m^* are set as 8 and 2 respectively.



(a)



(b)



(c)

Fig 3- 16 Variations of effectiveness: (a) sensible effectiveness; (b) latent effectiveness; (c) total effectiveness with T_{sol} and C_{sol}.

The sensible effectiveness reaches the maximum value of 0.9458 when $T_{sol} = 12℃$ and $C_{sol} = 21\%$, while its minimum value is 0.8848 when $T_{sol} = 22℃$ and $C_{sol} = 39\%$. The maximum latent effectiveness is 0.9366 when $T_{sol} = 12℃$ and $C_{sol} = 39\%$, and its minimum value is 0.8449 when $T_{sol} = 22℃$ and $C_{sol} = 21\%$. For the total effectiveness, it reaches the maximum value of 0.9380 when $T_{sol} = 12℃$ and $C_{sol} = 39\%$, while the minimum value is 0.8757 when $T_{sol} = 22℃$ and $C_{sol} = 21\%$. Effects of T_{sol} and C_{sol} on the system performance are discussed separately then.

Solution temperature has a great influence on the system performance since it is closely related to the solution surface vapour pressure. The variations of the effectiveness with T_{sol} under different C_{sol} are shown in Figs. 3-17 – 3-19.

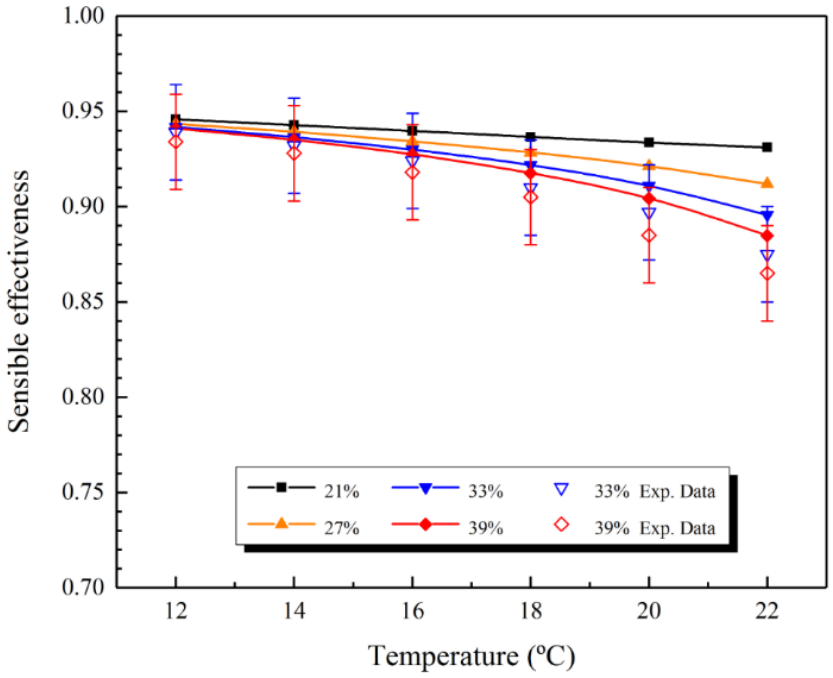


Fig 3- 17 Sensible effectiveness variations with T_{sol} under different C_{sol}.

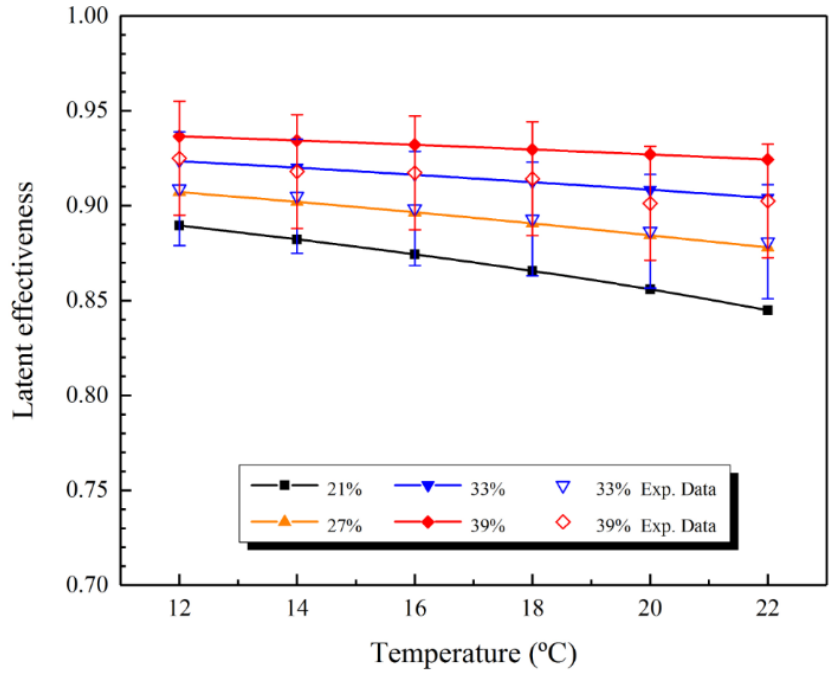


Fig 3- 18 Latent effectiveness variations with T_{sol} under different C_{sol}.

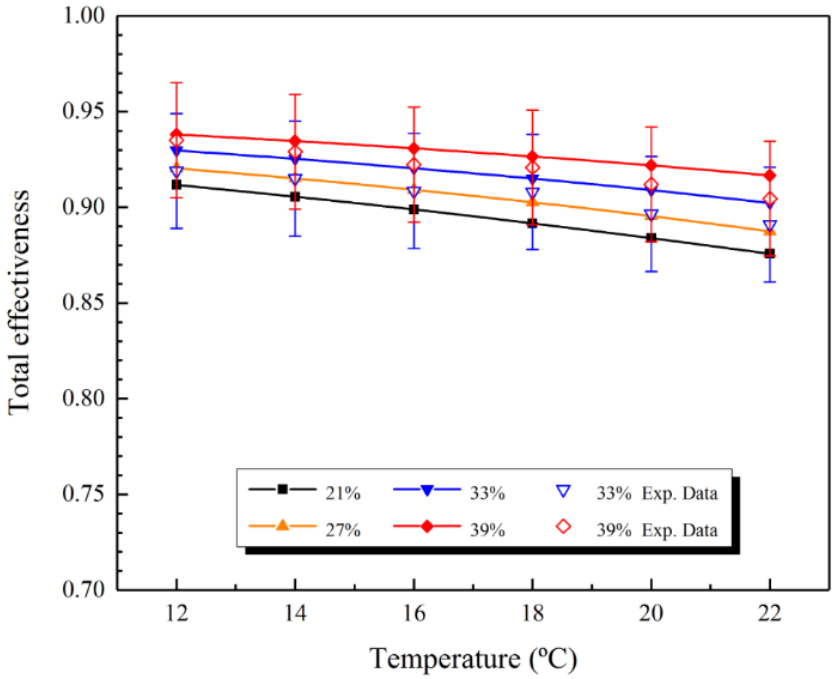


Fig 3- 19 Total effectiveness variations with T_{sol} under different C_{sol}.

It is clearly reflected in Figs. 3-17 – 3-19 that all effectiveness decrease accordingly with the solution temperature. The decrease of sensible effectiveness is easily understood since the increase of solution temperature narrows the temperature difference between the solution and air. The decrease of latent effectiveness is because vapour pressure in the solution side increases with the solution temperature, which weakens the dehumidification potential. Although decreasing the solution temperature can improve the sensible effectiveness, the improvement is not significant. The sensible effectiveness is weakened by increasing dehumidification effect since more latent heat released to the solution side would increase the solution temperature, which would affect the sensible effectiveness negatively. It also should be mentioned that at a low solution concentration, the sensible effectiveness variation is almost negligible. For instance, the sensible effectiveness increases by only 1.58 % (i.e. from 0.9311 to 0.9458) when the solution temperature decreases by 10℃ under $C_{sol} = 21\%$. Thus when the solution concentration is low, decreasing solution temperature will not improve the sensible effectiveness significantly. The case is opposite for the latent effectiveness as it is more sensitive to T_{sol} when C_{sol} is low. For example, under $C_{sol} = 21\%$, the latent effectiveness increases by 5.3% (i.e. from 0.8449 to 0.8896) when the solution temperature decreases from 22℃ to 12℃. By contrast, it only increases by 1.33% (i.e. from 0.9243 to 0.9366) under $C_{sol} = 39\%$. This indicates that the latent effectiveness is more sensitive to solution temperature at a low solution concentration. Nevertheless, the effect of T_{sol} on the latent effectiveness is insignificant compared to C_{sol} as discussed subsequently.

Solution concentration affects the system performance as it is directly related to surface vapour pressure. However, increasing C_{sol} has different impacts on the sensible, latent and total effectiveness, which can be observed from Fig 3-20.

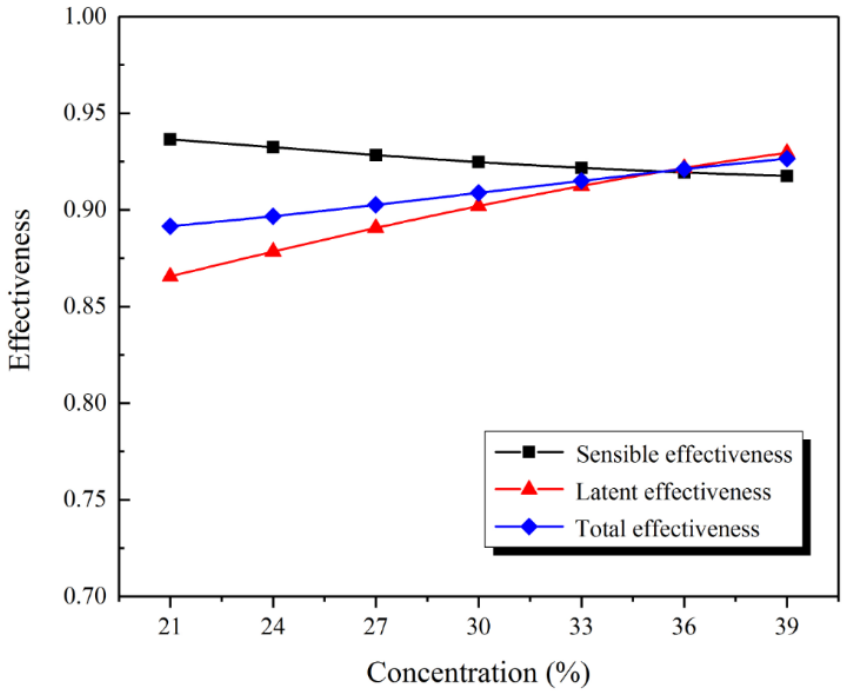


Fig 3- 20 Variations of effectiveness with C_{sol} under $T_{sol} = 18℃$

As presented in Fig 3-20, increasing solution concentration from 21% to 39% would decrease the sensible effectiveness from 0.9366 to 0.9176, and increase the latent and total effectiveness from 0.8656 to 0.9296 and from 0.8916 to 0.9266 respectively. Similar to the effects of T_{sol}, increasing solution concentration will decrease the solution surface vapour pressure, thus the solution absorption ability will be enhanced and the latent effectiveness will be increased. The increased dehumidification ability will negatively affect the sensible effectiveness since more latent heat will be released to the solution side. The total effectiveness is mainly dominated by the latent effectiveness since they have the same variation trends. It can be observed in Fig 3-17 that the sensible effectiveness is neither sensitive to T_{sol} nor C_{sol}. For the latent effectiveness, the effect of solution concentration is far more obvious than that on the sensible effectiveness. For instance, at $T_{sol} = 12℃$, the sensible effectiveness decreases by 0.51% (i.e. from 0.9458 to 0.941) when C_{sol} changes from 21% to 39%, while the latent effectiveness increases by 5.28% (i.e. from 0.8896 to 0.9366). The latent effectiveness improvement is more

significant at a higher solution temperature. For example, at $T_{sol} = 22℃$, the latent effectiveness increases by 9.40% (i.e. from 0.8449 to 0.9243) when C_{sol} varies from 21% to 39%.

To sum up, the sensible effectiveness is insensitive to both T_{sol} and C_{sol}, while the latent effectiveness is comparatively more sensitive. Thus in practical applications, a low solution temperature is not necessary since it is energy consuming and no significant performance improvement could be achieved. In the meanwhile, at a relatively high solution temperature, increasing C_{sol} will improve dehumidification ability more considerably. It implies that increasing solution concentration is a better approach to improve the latent effectiveness without decreasing the sensible effectiveness.

3.6.4 Effects of inlet air condition

Inlet air condition (i.e. temperature $T_{air,in}$ and relative humidity $RH_{air,in}$) is of vital importance to evaluate the adaptivity of the system. Variations of the sensible, latent and total effectiveness with $T_{air,in}$ and $RH_{air,in}$ are presented in Fig 3-21, while NTU and m^* are set as 8 and 2 respectively.

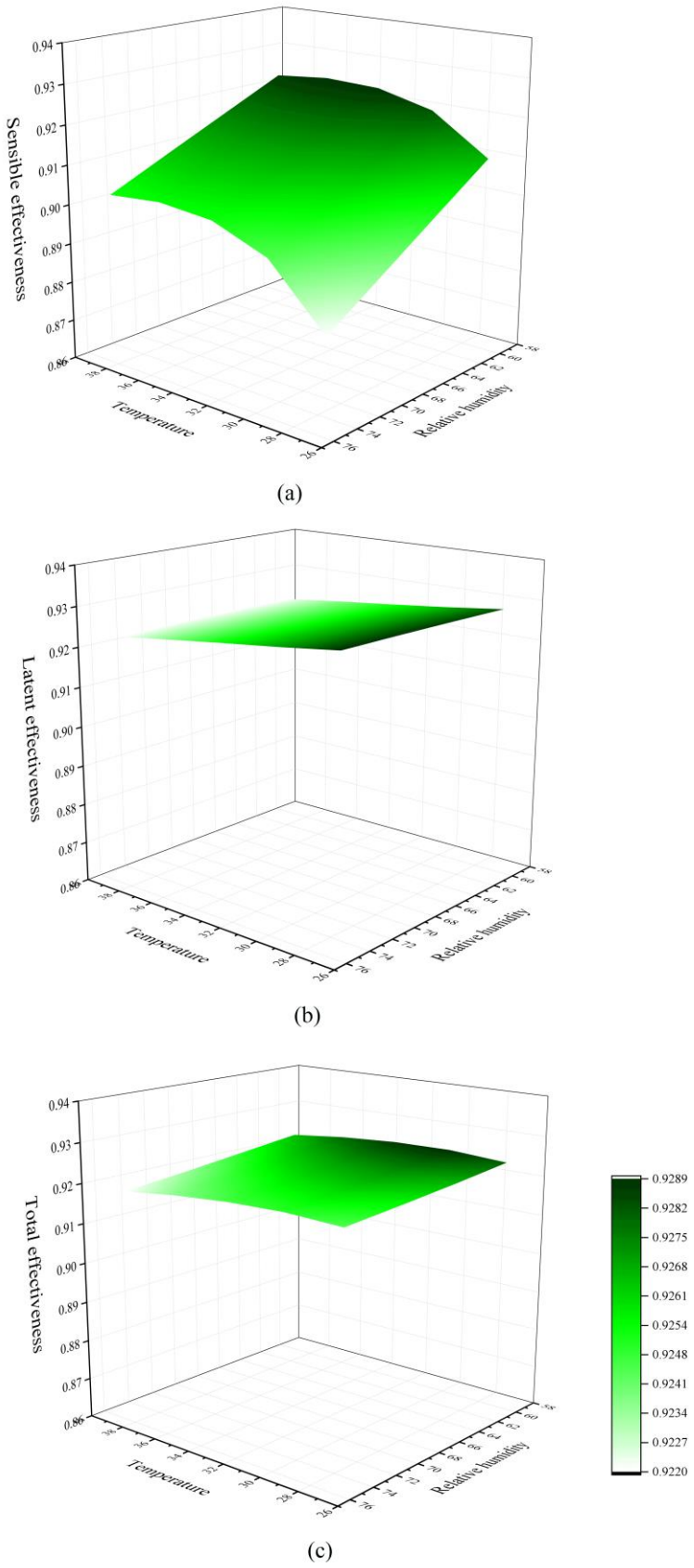


Fig 3- 21 Variations of effectiveness: (a) sensible effectiveness; (b) latent effectiveness; (c) total effectiveness with $T_{air,in}$ and $RH_{air,in}$.

The maximum sensible effectiveness is 0.924 when $T_{air,in} = 36℃$ and $RH_{air,in} = 60\%$, while the minimum value is 0.8818 when $T_{air,in} = 27℃$ and $RH_{air,in} = 75\%$. Comparatively, the latent effectiveness reaches the maximum value of 0.9289 when $T_{air,in} = 27℃$ and $RH_{air,in} = 75\%$, while the minimum value is 0.9222 when $T_{air,in} = 39℃$ and $RH_{air,in} = 60\%$. For the total effectiveness, the maximum value is 0.9249 when $T_{air,in} = 33℃$ and $RH_{air,in} = 60\%$, while its minimum value is 0.9174 when $T_{air,in} = 39℃$ and $RH_{air,in} = 75\%$. Then effects of $T_{air,in}$ and $RH_{air,in}$ on the system performance are discussed separately.

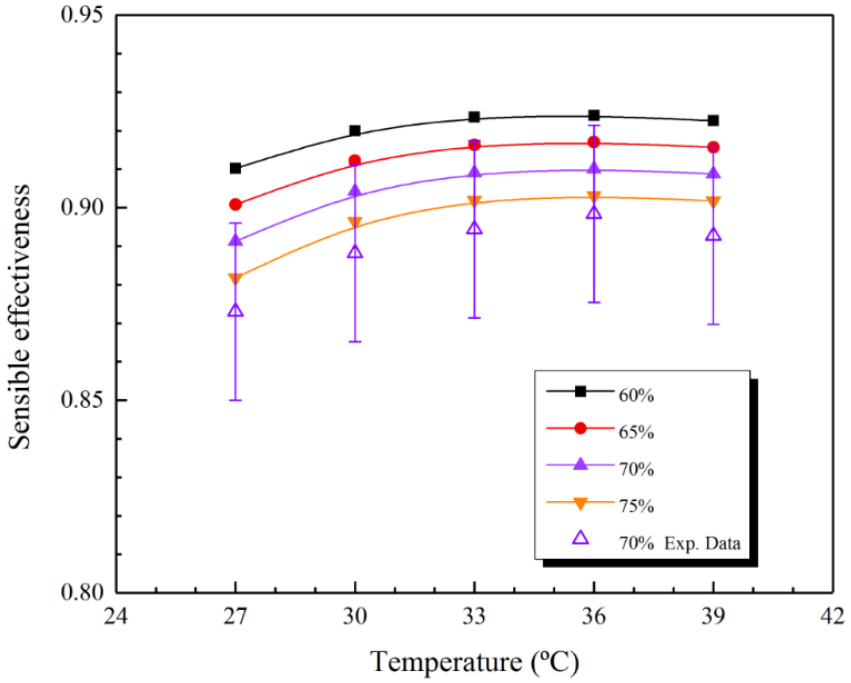


Fig 3- 22 Sensible effectiveness variations with $T_{air,in}$ under different $RH_{air,in}$.

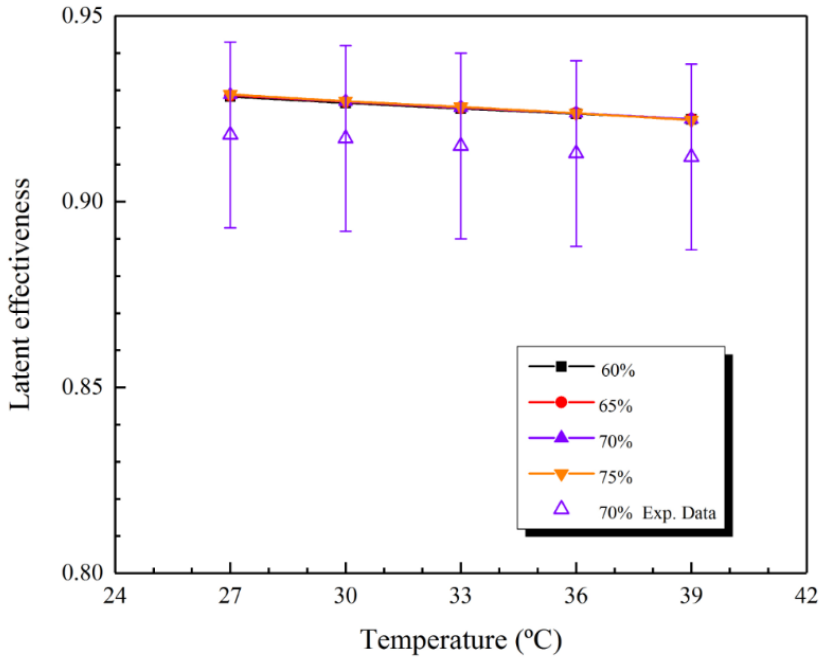


Fig 3- 23 Latent effectiveness variations with $T_{air,in}$ under different $RH_{air,in}$.

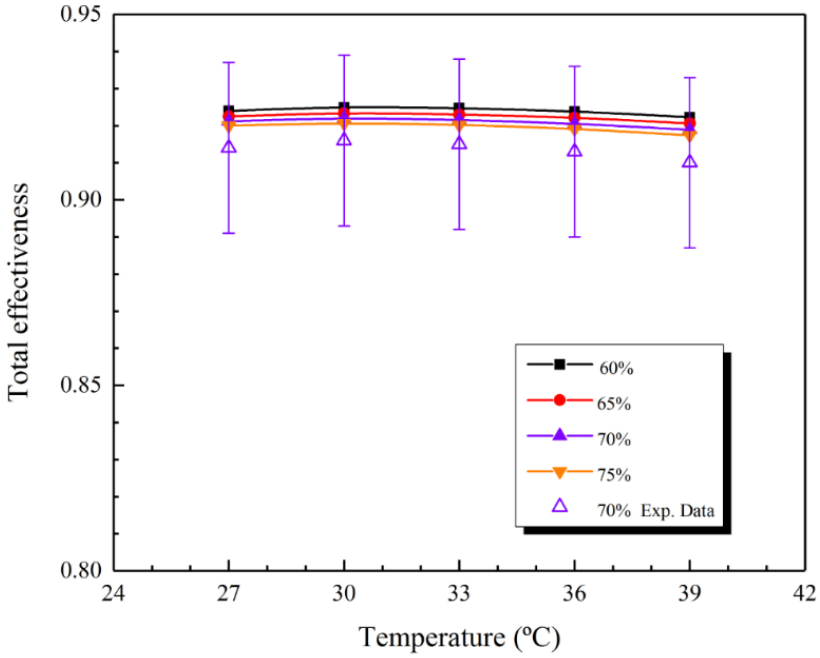


Fig 3- 24 Total effectiveness variations with $T_{air,in}$ under different $RH_{air,in}$.

The effectiveness variations with $T_{air,in}$ under different $RH_{air,in}$ are shown in Figs. 3-22 – 3-24, it can be seen that the sensible effectiveness is more sensitive to $T_{air,in}$ and $RH_{air,in}$

compared with the latent and total effectiveness. When $T_{air,in}$ increases from 27℃ to 36℃, the sensible effectiveness gradually rises and reaches the peak value at 36℃. This is because that increasing $T_{air,in}$ at a constant $RH_{air,in}$ will enhance the heat transfer potential [69]. However the sensible effectiveness starts to decrease slightly when $T_{air,in}$ is higher than 36℃. For instance, under $RH_{air,in} = 75\%$, the sensible effectiveness rises by 2.42% (i.e. from 0.8818 to 0.9031) when $T_{air,in}$ increases from 27 ℃ to 36 ℃. From 36 ℃ to 39 ℃, the sensible effectiveness decreases slightly (i.e. from 0.9031 to 0.9018). For the latent effectiveness, the effect of $T_{air,in}$ is negligible, for example, under $RH_{air,in} = 75\%$, the latent effectiveness decreases by 0.74% (i.e. from 0.9289 to 0.9220) when $T_{air,in}$ rises from 27℃ to 39℃. This is attributed to the increased membrane moisture resistance [65]. The case is similar for the total effectiveness, an obvious relationship between the total effectiveness and $T_{air,in}$ can hardly be found. Effect of $RH_{air,in}$ on the sensible effectiveness is clear, the lower $RH_{air,in}$, the higher sensible effectiveness. Furthermore, the improvements of the sensible effectiveness by decreasing $RH_{air,in}$ at different inlet air temperatures are basically similar. For example, by decreasing $RH_{air,in}$ from 75% to 60%, the sensible effectiveness improvements are 3.22%, 2.63%, 2.39%, 2.31% and 2.31% respectively at $T_{air,in}$ of 27℃, 30℃, 33℃, 36℃ and 39℃. For the latent and total effectiveness, similar to the effects of $T_{air,in}$, they can barely be affected by $RH_{air,in}$ as well. In other words, the latent and total effectiveness are insensitive to both $T_{air,in}$ and $RH_{air,in}$.

In fact, the inlet air state depends on the local weather condition, thus $T_{air,in}$ and $RH_{air,in}$ are input parameters for the system rather than controllable ones. Fig 3-25 illustrates inlet and outlet air conditions on the psychometric chart.

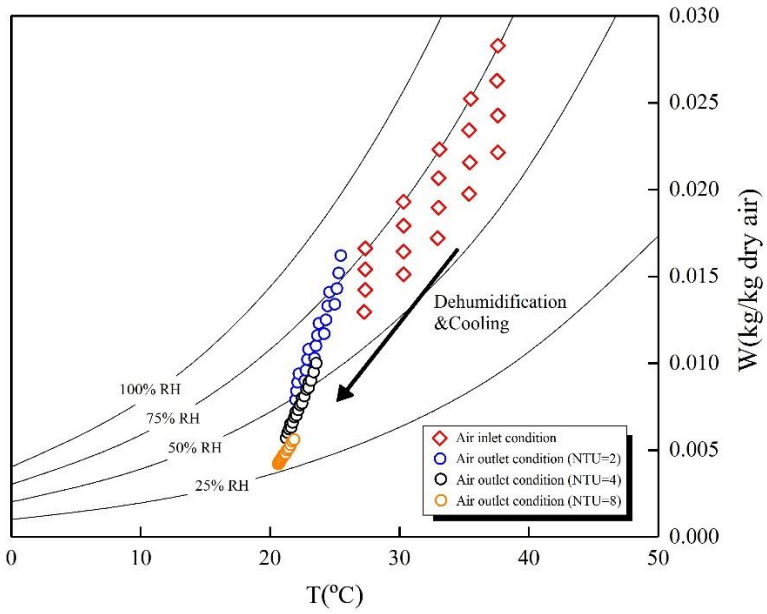


Fig 3- 25 Inlet and outlet air conditions on the psychrometric chart for numerical modelling.

In traditional cooling coil air-conditioning system, the inlet air is dehumidified by reducing its temperature below its dew point temperature, afterwards the air relative humidity is normally high, which means its temperature is too low for the supply air requirement, and subsequently re-heating is required and more energy is consumed. As seen in Fig 3-25, both inlet air temperature and humidity content are reduced after passing through the dehumidifier, and the system outlet air has relatively low temperature and relative humidity. Furthermore, the outlet air is at the very similar condition in spite of different inlet conditions with the same NTU, and this is more obvious at high NTU. This means this system has broad adaptability in different weather conditions, and can produce relative stable state supply air.

To sum up, the influences of $T_{air,in}$ and $RH_{air,in}$ on the latent and total effectiveness are negligible, while their effects on the sensible effectiveness are weak as well but evident. The cross-flow membrane-based parallel-plate liquid desiccant dehumidification system has better air-conditioning ability to provide the supply air with relatively stable condition despite diverse outdoor conditions.

3.7 Summary

In this chapter, a numerical model is developed to investigate the performance of a cross-flow membrane-based parallel-plate liquid desiccant dehumidification system, the interaction between the solution and air through membranes is studied by solving heat and mass governing equations in Matlab. Experimental and analytical solutions are used to validate the numerical model, and the highest discrepancy for sensible and latent effectiveness between numerical and experimental results are 8.756% and 9.822% respectively.

The influences of main parameters on dehumidification effectiveness (sensible, latent and total effectiveness) are assessed respectively, which include: number of heat transfer units (NTU), solution to air mass flow rate ratio (m^*), solution temperature (T_{sol}), solution concentration (C_{sol}), inlet air temperature ($T_{air,in}$) and relative humidity ($RH_{air,in}$). The conclusions can be drawn as follows:

- $m^*$and NTU are two of the most important parameters influencing the dehumidifier effectiveness. Although all effectiveness increase with $m^*$and NTU, their increasing gradients hardly change when $m^*$and NTU exceed m^*_{crit} and NTU_{crit} respectively.
- It is desirable to operate the system at the critical condition where m^*_{crit} and NTU_{crit} are 1 and 4 respectively in this study.
- Effects of m^* and NTU on the system performance are interacted with each other. There is hardly benefit to the system performance improvement by increasing m^* at low NTU, especially for the latent effectiveness. By contrast, no obvious performance enhancement is achieved by increasing NTU at low m^*, especially for the sensible effectiveness.
- There is no obvious improvement in the sensible effectiveness with low temperature and high concentration solution, which is insensitive to both T_{sol} and C_{sol}.

- The latent effectiveness increases significantly with C_{sol} at a high solution temperature, while the system sensitive effectiveness does not decrease observably.
- The system has broad adaptability in different weather conditions by providing relative stable state supply air, in particular at high NTU.

In general, the work presented in this chapter contributes to a progress in the field of membrane-based liquid desiccant dehumidification system. It provides a comprehensive parametric study on the membrane-based liquid desiccant dehumidifier performance, which supplies valuable data for the optimum design in the dehumidification and air-conditioning systems in practice.

Chapter 4: Investigation of a membrane-based flat-plate liquid desiccant regenerator

4.1 Introduction

Based on the literature review, most of the previous literatures focused on the dehumidification process. However, within the liquid desiccant dehumidification system, regeneration process is considered to be one of the most crucial processes since the diluted desiccant solution after dehumidification needs to be re-concentrated to realize the solution recycle. Literatures that have been carried out regarding regeneration dealt with direct contact regeneration between the desiccant solution and air. Thus the main objective of this chapter is to investigate the effects of main operating parameters, such as dimensionless parameters (i.e. NTU and m^*), solution inlet properties (i.e. temperature $T_{sol,in}$ and concentration $C_{sol,in}$) and air inlet conditions (i.e. temperature $T_{air,in}$ and humidity ratio $W_{air,in}$) on the performance of a membrane-based heat and mass exchanger used for desiccant regeneration by numerical simulation and experimental test. Solution-side effectiveness, together with another two indicators: solution side temperature decrease rate (TDR) and moisture flux rate (MFR) are applied to evaluate the regeneration performance. Section 4.2 presents the numerical modelling method; Section 4.3 introduces the performance evaluation indices; Section 4.4 shows the experimental set-up; Section 4.5 validates the numerical modelling; Section 4.6 investigates the regenerator performance and Section 4.7 is the summary of this chapter. This chapter presents a comprehensive parametric analysis on membrane-based liquid desiccant regenerator, and provides valuable data for the development and operation of liquid desiccant dehumidification air-conditioning system.

4.2 Numerical modelling

4.2.1 Governing equations

The structure of regenerator is identical to that of the dehumidifier, which has been illustrated in Section 3.2.1, Fig 3-1. Assumptions made for the sake of simplification in numerical modelling are the same as those made for dehumidifier modelling which includes: well-insulated regenerator assumption; heat and mass transfer normal to the membrane; neglected heat conductions in air and solution channels; laminar flow assumptions in air and solution channels et al.

Compared to the dehumidifier, the directions of heat and mass transfer are conversed in the regenerator. In dehumidifier, heat and mass are transferred from the warm and moist air to cold and concentrated solution, while in regenerator, heat and mass are transferred from hot and diluted solution to dry air. It should be noticed that the evaporative heat is taken from the solution side only since the solution side mass transfer coefficient is much higher than that in the air side. Then the governing equations for heat and mass transfer are given as:

Solution side heat balance equation:

$$\left(\frac{\dot{m}_{sol}}{L}\cdot\frac{\partial T_{sol}}{\partial y}\cdot C_{p,sol}\right)\cdot dxdy=-\left[U(T_{sol}-T_{air})+h_{fg}\cdot U_m\left(W_{sol,mem}-W_{air}\right)\right]dxdy \quad (4\text{-}1)$$

Solution side mass balance equation:

$$\frac{\dot{m}_{desi}}{L}\cdot\frac{\partial X_{sol}}{\partial y}\cdot dxdy=-U_m\cdot\left(W_{sol,mem}-W_{air}\right)dxdy \quad (4\text{-}2)$$

Air side heat balance equation:

$$\left(\frac{\dot{m}_{air}}{H}\cdot C_{p,air}\cdot\frac{\partial T_{air}}{\partial x}\right)\cdot dxdy=U(T_{sol}-T_{air})dxdy \quad (4\text{-}3)$$

Air side mass balance equation:

$$\left(\frac{\dot{m}_{air}}{H}\cdot\frac{\partial W_{air}}{\partial x}\right)\cdot dxdy=U_m\left(W_{sol,mem}-W_{air}\right)dxdy \quad (4\text{-}4)$$

4.2.2 Normalization of governing equations

Governing equations Eqs. (4-1) – (4-4) are normalized as:

$$\frac{\partial T_{sol}^*}{\partial y^*} + NTU_m h^* \frac{1}{Cr^*}\left(W_{sol,mem}^* - W_{air}^*\right) + NTU \frac{1}{Cr^*}\left(T_{sol}^* - T_{air}^*\right) = 0 \quad (4\text{-}5)$$

$$\frac{\partial X_{sol}}{\partial y^*} + NTU_m \frac{1}{m^*} W_0 (1 + X_{sol})(W_{sol,mem}^* - W_{air}^*) = 0 \quad (4\text{-}6)$$

$$\frac{\partial T_{air}^*}{\partial x^*} - NTU(T_{sol}^* - T_{air}^*) = 0 \quad (4\text{-}7)$$

$$\frac{\partial W_{air}^*}{\partial x^*} - NTU_m\left(W_{sol,mem}^* - W_{air}^*\right) = 0 \quad (4\text{-}8)$$

4.2.3 Boundary conditions

Boundary conditions for the solution side are:

$T_{sol}{}^* = 1$, at y^*=0 (4-9)

$X_{sol} = X_{sol,in}$, at y^*=0 (4-10)

While the air side boundary conditions are:

$T_{air}{}^* = 0$, at x^*=0 (4-11)

$T_{air}{}^* = 0$, at x^*=0 (4-12)

4.2.3.1 Heat transfer boundary conditions on membrane surfaces

To solve the governing equations, heat and mass transfer boundary equations on membrane surfaces need to be established. Heat transfer boundary conditions are based on thermal energy balance through the membrane:

$$h_{sol}\left(T_{sol} - T_{sol,mem}\right) = U\left(T_{sol,mem} - T_{air}\right) + h_{fg} U_m \left(W_{sol,mem} - W_{air}\right) \quad (4\text{-}13)$$

Eq. (4-13) can be normalized as:

$$NTU_{sol}\left(T_{sol}^* - T_{sol,mem}^*\right) = NTU\left(T_{sol,mem}^* - T_{air}^*\right) + NTU_m h^* (W_{sol,mem}^* - W_{air}^*) \quad (4\text{-}14)$$

4.2.3.2 Mass transfer boundary conditions on membrane surfaces

Similarly, mass transfer boundary conditions are based on mass balance through the membrane:

$$U_m\left(W_{sol,mem} - W_{air}\right) = h_{m,sol}(C_{sol,mem} - C_{sol}) \tag{4-15}$$

Eq. (4-15) can be normalized as:

$$NTU_m W_0\left(W^*_{sol,mem} - W^*_{air}\right) = NTU_{m.sol}(C_{sol,mem} - C_{sol}) \tag{4-16}$$

4.2.4 Air and solution property calculations

The calculation methods for air and solution properties have been explained in Section 3.2.4. It should be noticed that compared with investigation into dehumidifier, the solution concentration and temperature of interest for regenerator performance investigation in this chapter are different. Thus the equilibrium specific humidity of LiCl under different conditions are calculated, and another psychometric chart of LiCl solution is given in Fig 4-1.

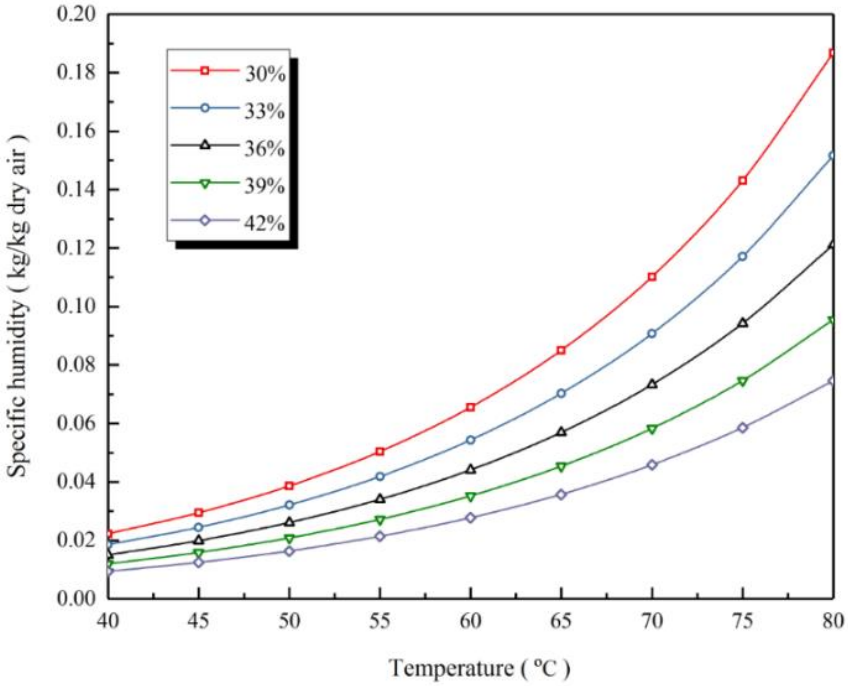


Fig 4- 1 Psychometric chart of LiCl for regenerator

4.2.5 Simulation procedure

4.2.5.1 Discretization of governing equations

Finite difference method is used to solve governing equations which are discretized by a forward difference scheme:

$$T^*_{sol\,(m+1,n)} - T^*_{sol\,(m,n)} + dy^* NTU_m h^* Cr\left[W^*_{sol,mem\,(m+1,n)} - W^*_{air\,(m+1,n)}\right] + dy^* NTUCr\left[T^*_{sol\,(m+1,n)} - T^*_{air\,(m+1,n)}\right] = 0 \quad (4\text{-}17)$$

$$X_{sol\,(m+1,n)} - X_{sol\,(m,n)} + dy^* m^* W_0 NTU_m\left[1 + X_{sol\,(m+1,n)}\right]\left[W^*_{sol,mem\,(m+1,n)} - W^*_{air\,(m+1,n)}\right] = 0 \quad (4\text{-}18)$$

$$T^*_{air\,(m,n+1)} - T^*_{air\,(m,n)} - dx^* NTU[T^*_{sol\,(m,n+1)} - T^*_{air\,(m,n+1)} = 0 \quad (4\text{-}19)$$

$$W^*_{air\,(m,n+1)} - W^*_{air\,(m,n)} - dx^* NTU_m\left[W^*_{sol,mem\,(m,n+1)} - W^*_{air(m,n+1)}\right] = 0 \quad (4\text{-}20)$$

Where m is number of grids in x direction, and n is number of grids in y direction. Governing equations are solved in Matlab iteratively until converged. Numerical tests have been conducted to determine the grid size for guaranteeing the accuracy of numerical results. It has been found that 30×60 grids are adequate in this study, the result difference is less than 1.0% compared with 50×100 grids. The numerical uncertainty is 1.0%.

4.2.5.2 Numerical solving procedure

The solution procedure applied for solving interacted governing equations for regenerator is similar to that used for dehumidifier as shown in Section 3.2.5.2. Here the solution procedure for regenerator is depicted in Fig 4-2.

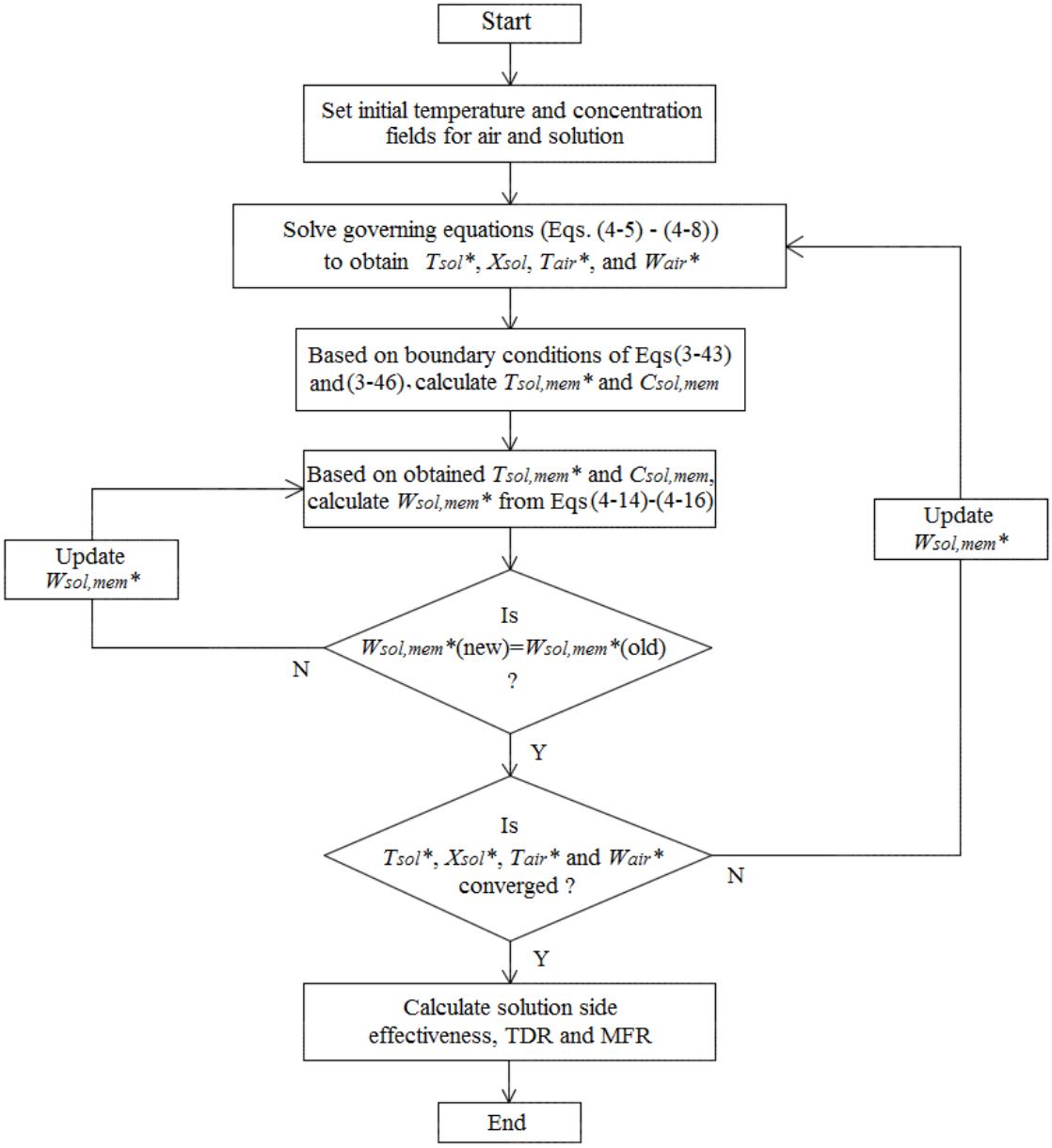


Fig 4- 2 Flow chart for the solution procedure for regenerator

4.3 Performance evaluation indices

4.3.1 Solution side effectiveness for regenerator

Effectiveness is the most important parameter used to evaluate the performance of a heat and mass exchanger. Air side effectiveness have been widely used for the dehumidification

performance evaluation. They are used for the dehumidifier performance evaluation in last chapter. However in the regeneration process where the main focus is on desiccant solution, the air side effectiveness cannot reflect the regenerator performance correctly, thus the solution side effectiveness for regenerator are introduced referring to literature [39]:

$$\varepsilon_{sol,sen} = \frac{(\dot{m}c_p)_{sol}(T_{sol,in}-T_{sol,out})-\dot{m}_{desi}h_{fg}(X_{sol,in}-X_{sol,out})}{(\dot{m}c_p)_{min}(T_{sol,in}-T_{air,in})} \quad (4\text{-}21)$$

$$\varepsilon_{sol,lat} = \frac{\dot{m}_{desi}h_{fg}(X_{sol,in}-X_{sol,out})}{\dot{m}_{min}h_{fg}(W_{sol,in}-W_{air,in})} \quad (4\text{-}22)$$

$$\varepsilon_{sol,tol} = \frac{(\dot{m}c_p)_{sol}(T_{sol,in}-T_{sol,out})}{(\dot{m}c_p)_{min}(T_{sol,in}-T_{air,in})+\dot{m}_{min}h_{fg}(W_{sol,in}-W_{air,in})} \quad (4\text{-}23)$$

Where $\dot{m}_{desi}$ is desiccant flow rate (kg/s), which can be obtained by:

$$\dot{m}_{desi} = \frac{\dot{m}_{sol}}{1+X_{sol}} \quad (4\text{-}24)$$

4.3.2 Solution side moisture flux rate (MFR)

Moisture removal rate (MRR) has been used to evaluate the amount of moisture being removed by the air from diluted liquid desiccant solution, or the amount of moisture being absorbed by concentrated solution from humid air. In this study with the main focus on desiccant solution, a similar index so called solution side moisture removal rate is introduced and expressed as:

$$MRR = \dot{m}_{desi}(X_{sol,in} - X_{sol,out}) \quad (4\text{-}25)$$

Then, another important index so called solution side moisture flux rate is defined:

$$MFR = \frac{MRR}{U_m A} = \frac{\dot{m}_{desi}(X_{sol,in}-X_{sol,out})}{U_m A} \quad (4\text{-}26)$$

As can been seen from the above equation, MFR is the ratio between moisture removal rate MRR and membrane overall mass transfer conductance. MFR is generally used for performance evaluation rather than MRR, because it is independent of the size of the regenerator. It only depends on the inlet condition, which would make results more general [139]

4.3.3 Solution temperature decrease rate (TDR)

Apart from re-concentration of the liquid desiccant solution, the lower solution temperature is preferred. Lower solution temperature would make dehumidification more effective. Thus, the index so called solution temperature decrease rate (TDR) is applied to evaluate the sensible performance of regeneration, which is defined as:

$$TDR = \frac{T_{sol,in} - T_{sol,out}}{T_{sol,in}} \quad (4\text{-}27)$$

4.4 Experimental set-up

Experimental tests are conducted using the same membrane-based heat and mass exchanger test facility built in the laboratory as introduced in Section 3.4. The regenerator and its membranes have the same physical properties as dehumidifier, those are given in Table 3-3. The weak desiccant solution temperature is controlled by a hot water supply system with the supply water temperature range of 20℃ to 80℃. The hot water flow rate is controlled and measured by a liquid flow indicator (Parker FM 26 122 212 0.5-4.5 L/min). All measurement devices and their accuracies have been listed in Table 3-4. Uncertainty analysis has been conducted for all experimental data by applying the method of propagation as explained in last chapter to estimate uncertainties for experimental data. Extensive experiments have been carried out to investigate the regeneration performance under different operating conditions. Detailed validation data are given in the next section.

4.5 Numerical model validation

The experimental data are used to validate the numerical simulation results. 44 groups of experimental data under different operating conditions are adopted in this study. The experiment consists of two stages. In the first stage, 22 groups of tests are conducted to validate the solution side effectiveness (solution side sensible effectiveness $\varepsilon_{sol,sen}$, latent effectiveness $\varepsilon_{sol,lat}$, and total effectiveness $\varepsilon_{sol,tot}$). The operating conditions (i.e. NTU, m^* et al.), as well as numerically calculated and measured results of effectiveness are listed in Table 4-1. In the second stage, another 22 groups of tests are carried out to validate the solution side temperature decrease rate (TDR) and moisture flux rate (MFR). The comparisons between numerical and experimental results are given in Table 4-2.

Table 4- 1 Comparisons between numerical and experimental results for solution side effectiveness

Operating conditions								Comparisons								
NTU	m*	m_{air} (kg/s)	m_{sol} (kg/s)	$T_{sol,in}$ (℃)	$C_{sol,in}$ (%)	$T_{air,in}$ (℃)	$W_{air,in}$ (kg/kg)	$\varepsilon_{sol,sen,num}$	$\varepsilon_{sol,sen,exp}$	Error (%)	$\varepsilon_{sol,lat,num}$	$\varepsilon_{sol,lat,exp}$	Error (%)	$\varepsilon_{sol,tot,num}$	$\varepsilon_{sol,tot,exp}$	Error (%)
2	1	0.1234	0.1234	60	35	30	12.6	0.6628	0.622	6.156	0.2893	0.246	14.967	0.3881	0.342	11.878
6	1	0.0411	0.0411	60	35	30	12.6	0.7594	0.710	6.505	0.4311	0.388	9.998	0.5179	0.470	9.249
10	1	0.0247	0.0247	60	35	30	12.6	0.7752	0.719	7.250	0.4835	0.429	11.272	0.5606	0.508	9.383
2	2	0.1234	0.2469	60	35	30	12.6	0.7553	0.729	3.482	0.3767	0.334	11.335	0.4769	0.435	8.786
6	2	0.0411	0.0822	60	35	30	12.6	0.8968	0.860	4.103	0.6079	0.566	6.893	0.6843	0.636	7.058
10	2	0.0247	0.0494	60	35	30	12.6	0.9293	0.898	3.368	0.6963	0.658	5.501	0.7580	0.729	3.826
2	3	0.1234	0.3703	60	35	30	12.6	0.7914	0.785	0.809	0.4166	0.392	5.905	0.5157	0.472	8.474
6	3	0.0411	0.1234	60	35	30	12.6	0.9482	0.927	2.236	0.6905	0.671	2.824	0.7587	0.741	2.333
10	3	0.0247	0.0741	60	35	30	12.6	0.9852	0.955	3.065	0.7918	0.757	4.395	0.8430	0.825	2.135
8	2	0.0309	0.0617	50	35	30	12.6	0.9502	0.926	2.547	0.7386	0.706	4.414	0.8130	0.778	4.305
8	2	0.0309	0.0617	55	35	30	12.6	0.9329	0.909	2.562	0.7024	0.669	4.755	0.7724	0.741	4.065
8	2	0.0309	0.0617	60	35	30	12.6	0.9156	0.887	3.124	0.6602	0.623	5.635	0.7278	0.695	4.507
8	2	0.0309	0.0617	65	35	30	12.6	0.8981	0.861	4.131	0.6136	0.573	6.617	0.6792	0.639	5.919
8	2	0.0309	0.0617	70	35	30	12.6	0.8803	0.849	3.556	0.5636	0.512	9.155	0.6272	0.583	7.047
8	2	0.0309	0.0617	60	35	26	12	0.8335	0.813	2.460	0.4617	0.421	8.815	0.5679	0.529	6.850
8	2	0.0309	0.0617	60	35	28	12	0.8319	0.808	2.873	0.4635	0.417	10.032	0.5643	0.522	7.496
8	2	0.0309	0.0617	60	35	30	12	0.8302	0.756	8.938	0.4654	0.425	8.681	0.5606	0.520	7.242
8	2	0.0309	0.0617	60	35	32	12	0.8282	0.762	7.993	0.4672	0.398	14.812	0.5567	0.510	8.389
8	2	0.0309	0.0617	60	35	34	12	0.8258	0.779	5.667	0.4691	0.414	11.746	0.5527	0.508	8.088
8	2	0.0309	0.0617	60	35	30	9	0.8280	0.753	9.058	0.4680	0.419	10.470	0.5564	0.495	11.035
8	2	0.0309	0.0617	60	35	30	12	0.8302	0.756	8.938	0.4654	0.425	8.681	0.5606	0.510	9.026
8	2	0.0309	0.0617	60	35	30	15	0.8324	0.761	8.578	0.4623	0.397	14.125	0.5653	0.509	9.959

Table 4- 2 Comparisons between numerical and experimental results for TDR and MFR

Operating conditions								Comparisons					
NTU	m*	m_{air} (kg/s)	m_{sol} (kg/s)	$T_{sol,in}$ (℃)	$C_{sol,in}$ (%)	$T_{air,in}$ (℃)	$W_{air,in}$ (kg/kg)	TDR_{num}	TDR_{exp}	Error (%)	MFR_{num}	MFR_{exp}	Error (%)
2	2	0.1234	0.2469	60	35	30	12.6	0.1437	0.131	8.838	0.0162	0.015	7.407
6	2	0.0411	0.0822	60	35	30	12.6	0.2062	0.196	4.947	0.0087	0.008	8.046
10	2	0.0247	0.0494	60	35	30	12.6	0.2283	0.220	3.636	0.0056	0.005	10.254
2	1	0.1234	0.1234	60	35	30	12.6	0.2338	0.221	5.475	0.0124	0.011	11.290
2	2	0.1234	0.2469	60	35	30	12.6	0.1437	0.127	11.797	0.0162	0.015	7.407
2	3	0.1234	0.3703	60	35	30	12.6	0.1036	0.092	11.197	0.0179	0.017	5.028
8	2	0.0309	0.0617	50	35	30	12.6	0.1474	0.132	10.448	0.0035	0.003	14.286
8	2	0.0309	0.0617	55	35	30	12.6	0.1843	0.176	4.504	0.0057	0.005	12.281
8	2	0.0309	0.0617	60	35	30	12.6	0.2192	0.198	9.672	0.0068	0.006	11.493
8	2	0.0309	0.0617	65	35	30	12.6	0.2525	0.242	4.158	0.0092	0.009	2.174
8	2	0.0309	0.0617	70	35	30	12.6	0.2843	0.266	6.437	0.0115	0.010	13.043
8	2	0.0309	0.0617	60	33	26	12	0.2411	0.232	3.774	0.0082	0.008	2.439
8	2	0.0309	0.0617	60	35	28	12	0.2192	0.196	10.584	0.0069	0.006	13.493
8	2	0.0309	0.0617	60	37	30	12	0.1957	0.178	9.044	0.0057	0.005	12.667
8	2	0.0309	0.0617	60	35	26	12	0.0598	0.056	6.355	0.0202	0.019	5.941
8	2	0.0309	0.0617	60	35	28	12	0.0584	0.055	5.822	0.0203	0.019	6.404
8	2	0.0309	0.0617	60	35	30	12	0.0571	0.054	5.429	0.0203	0.019	6.404
8	2	0.0309	0.0617	60	35	32	12	0.0557	0.053	4.847	0.0204	0.020	1.961
8	2	0.0309	0.0617	60	35	34	12	0.0543	0.051	6.077	0.0205	0.019	7.317
8	2	0.0309	0.0617	60	35	30	9	0.0602	0.057	5.316	0.0222	0.021	5.405
8	2	0.0309	0.0617	60	35	30	12	0.0571	0.054	5.429	0.0203	0.019	6.404
8	2	0.0309	0.0617	60	35	30	15	0.0539	0.048	10.946	0.0185	0.018	2.703

It can be seen in Table 4-1 that the numerical modelling results of ε_{sen}, ε_{lat} and ε_{tot} generally agree well with the experimental data. The maximum discrepancies between numerical results and experimental data for $\varepsilon_{sol,sen}$, $\varepsilon_{sol,lat}$ and $\varepsilon_{sol,tot}$ are 9.058%, 14.967% and 11.878% respectively. The maximum differences for TDR and MFR are 11.797% and 14.286% respectively, as indicated in Table 4-2. It should be emphasized that under the same NTU, the discrepancy reduces with the solution mass flow rate. For instance, under $NTU = 6$, the differences between numerical and experimental results decrease from 6.505% to 2.236% for $\varepsilon_{sol,sen}$, 9.998% to 2.824% for $\varepsilon_{sol,lat}$, and 9.249% to 2.333% for $\varepsilon_{sol,tot}$ respectively when the solution mass flow rate increases from 0.0411 kg/s to 0.1234 kg/s. This is because the lower of solution mass flow rate, the greater influence of solution mal-distribution on the effectiveness. The numerical modelling results and experimental data have similar variation trends, an acceptable agreement between them is achieved, meaning the developed model

predicts the performance rather accurately and is successful to simulate the operating characteristics of the cross-flow flat-plate membrane-based regenerator.

4.6 Results and discussion

4.6.1 Temperature and humidity fields

Under each operating condition, temperature and humidity fields of the air and solution channels and the membrane surface are obtained after all governing equations are converged. The distributions of temperature and concentration in the solution channel, and the temperature and humidity ratio fields in the air channel and membrane surface under $NTU = 8$ and $m^* = 2$ are plotted in Fig 4-3. The inlet temperatures of the diluted solution and air are 60 ℃ and 30 ℃ respectively, while the inlet solution concentration and air relative humidity are set as 35% and 50% ($W_{air,in} = 12.6\,\mathrm{g/kg\ dry\ air}$) respectively. It can be observed in Fig 4-3 (a) and (b) that the solution has the lowest temperature (35.4℃) and highest concentration (35.51%) at the left bottom corner of the regenerator. This is due to the fact that the hot and diluted solution at the left bottom side interacts with the cooler and dryer supply air. Similar case can be found in the air channel, the air reaches its highest temperature (60 ℃) and humidity ratio ($45.7\mathrm{g/kg\ dry\ air}$) at the right top corner since the air is heated and humidified along the length of the regenerator. Moreover, Fig 4-3 (e) and (f) illustrate the temperature and humidity boundary conditions on the membrane surface, it is clear that the boundary condition is neither uniform temperature nor uniform humidity ratio. The temperature and humidity ratio are non-uniform and two-dimensional profiles, both of them increase along the diagonal line of the membrane surface.

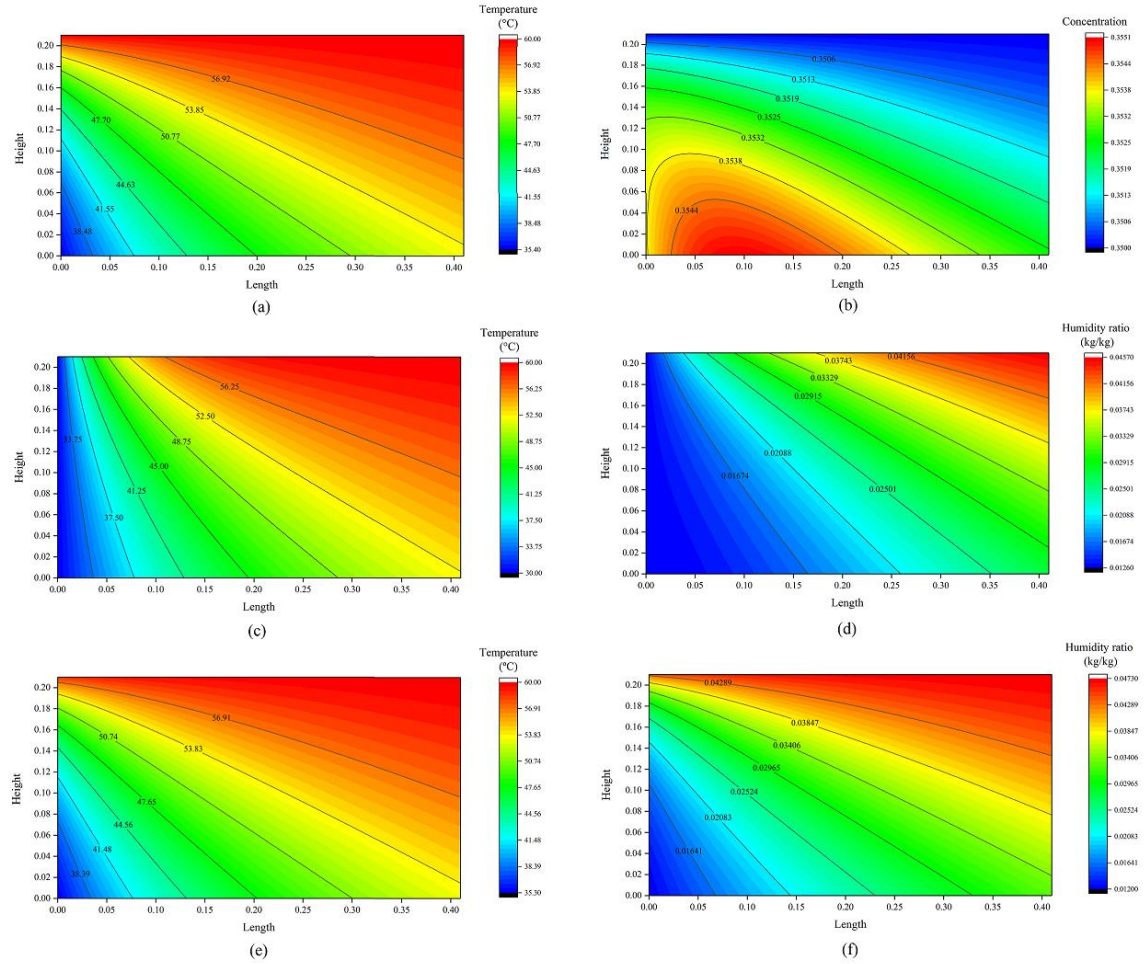


Fig 4- 3 (a) Solution temperature field; (b) Solution concentration field; (c) Air temperature field; (d) Air humidity ratio field; (e) Temperature field on membrane surface; (f) Humidity ratio field on membrane surface

4.6.2 Effects of dimensionless parameters

In this section, influences of two dimensionless parameters: NTU and m^* on the regeneration performance are addressed. NTU has been considered as a critical parameter with the most significant impact on the dehumidification system. Compared to the flow rate, the non-dimensional group NTU is a comprehensive indicating parameter because it is independent of the channel geometric properties. In numerical simulation, NTU is changed by adjusting air

mass flow rate, while the solution mass flow rate is changed proportionally to maintain a constant m^* accordingly.

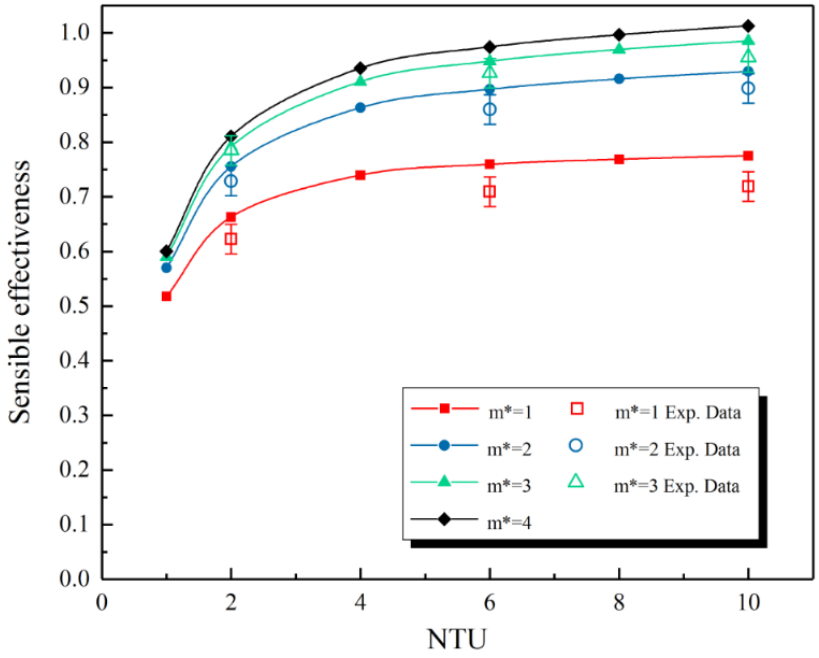


Fig 4- 4 Sensible effectiveness variations with NTU under different m^*

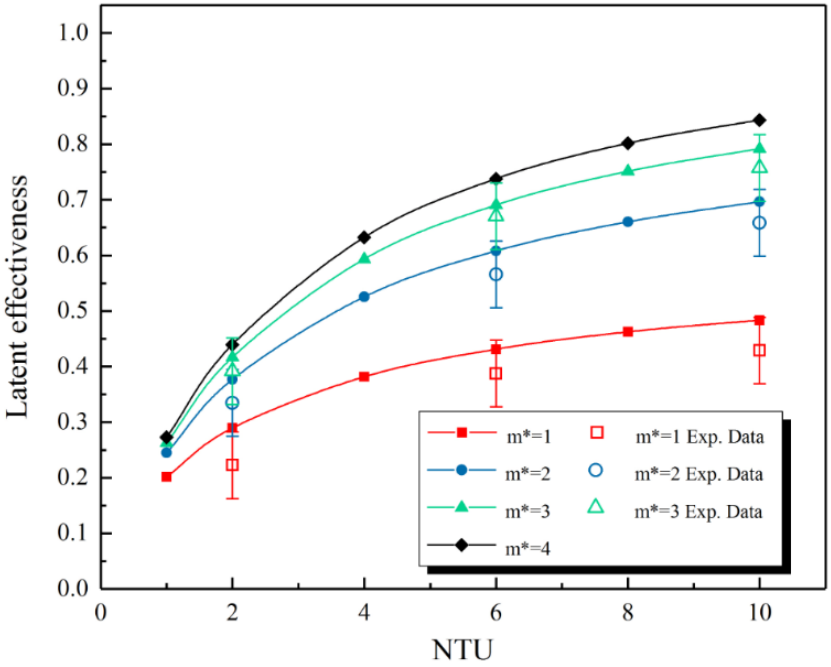


Fig 4- 5 Latent effectiveness variations with NTU under different m^*

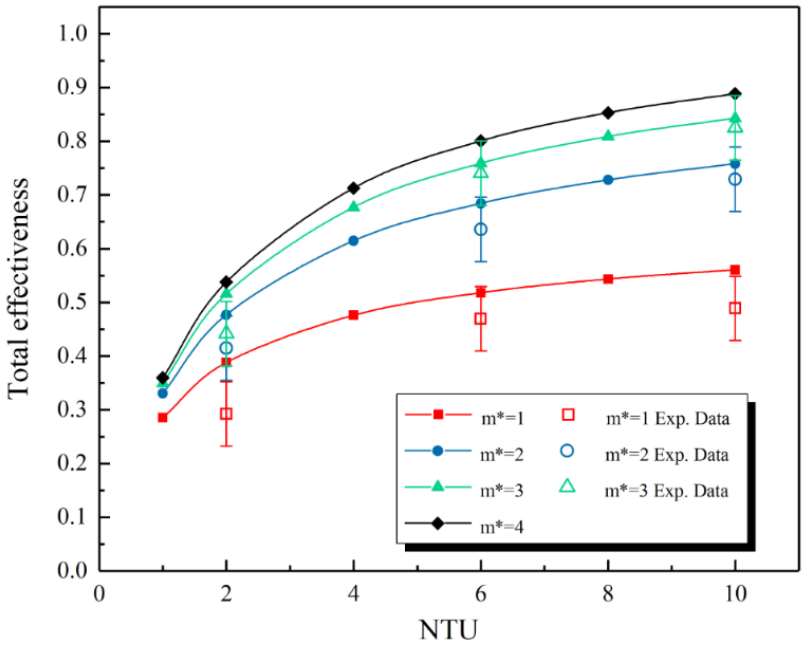


Fig 4- 6 Total effectiveness variations with NTU under different m^*

Influences of NTU on the regenerator effectiveness are analysed at first. Variations of the effectiveness with NTU under $m^* = 1,2,3,4$ are plotted in Figs. 4-4 – 4-6. It can be seen in these figures that under the same m^*, the sensible effectiveness always has the highest value among three effectiveness, while the latent effectiveness is the lowest one and the total effectiveness is the middle one. For example, under $m^* = 1$, the sensible effectiveness varies from 0.5179 to 0.7752 when NTU rises from 1 to 10. In the meanwhile, the latent effectiveness changes from 0.2017 to 0.4835 and the total effectiveness increases from 0.2854 to 0.5606. It is obvious that all effectiveness are significantly affected by NTU, and can be improved by increasing NTU. A critical value of NTU exists and is defined as NTU_{crit}, which is equal to 4 in this case. Increasing NTU beyond NTU_{crit} would not enhance the regeneration performance efficiently. For instance, under $m^* = 1$, the sensible effectiveness is increased by 42.79% (from 0.5179 to 0.7395) when NTU changes from 1 to 4. After NTU exceeding 4 the variation of the sensible effectiveness trends to level off, and it is only increased by 4.83% (from 0.7395 to 0.7752) when NTU rises from 4 to 10. Therefore increasing NTU beyond NTU_{crit} would

not enhance the effectiveness effectively. This effect is relatively inconspicuous for the latent and total effectiveness. Take the latent effectiveness as an example, under $m^* = 1$, it is increased by 89.09% and 26.77% when NTU rises from 1 to 4 and from 4 to 10 respectively. Furthermore, when m^* is relatively low, the growth extent of the effectiveness with NTU is not as obvious as that when m^* is high. Take the latent effectiveness as an example, under $m^* = 1$, the latent effectiveness is increased by 0.2818 (from 0.2017 to 0.4835) when NTU changes from 1 to 10, while it is increased by 0.5707 (from 0.2728 to 0.8435) under $m^* = 4$, almost twice as that under $m^* = 1$. Similar cases can also be found for the sensible and total effectiveness.

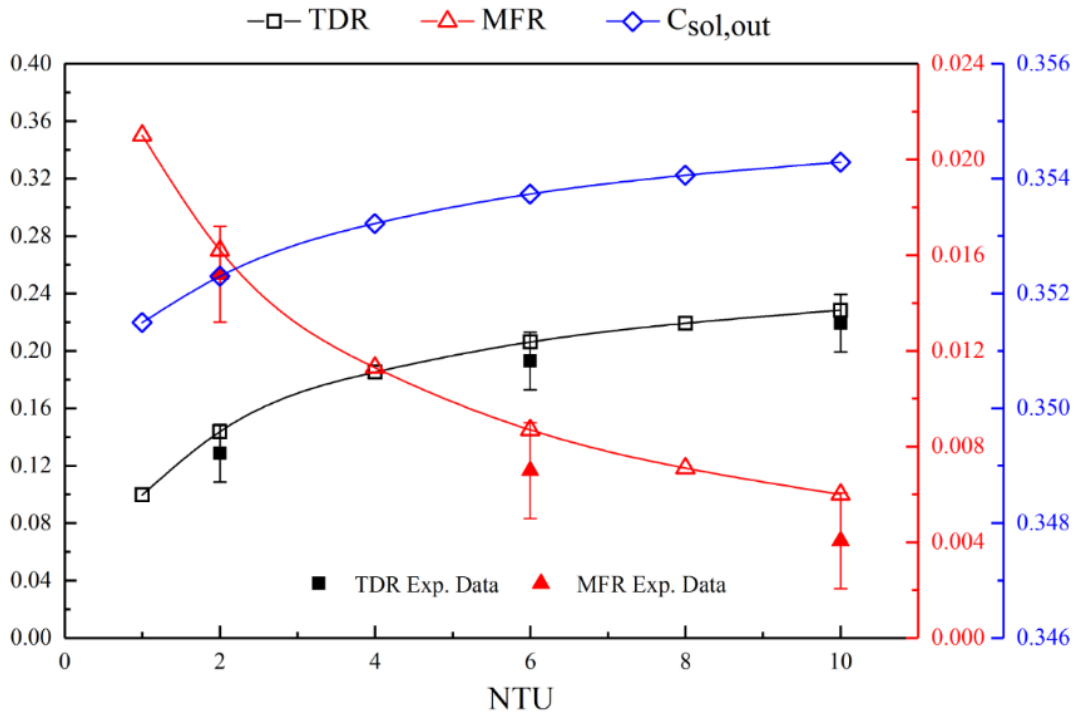


Fig 4- 7 Influences of NTU on TDR, MFR and $C_{sol,out}$

Apart from the solution side effectiveness, the solution side TDR and MFR have also been applied for regeneration performance evaluation. The variations of TDR, MFR and solution outlet concentration $C_{sol,out}$ with NTU under $m^* = 2$ are shown in Fig 4-7. According to this

figure, TDR increases from 0.0997 to 0.2283 when NTU changes from 1 to 10, meaning the solution cooling effect is enhanced. Meanwhile, MFR is dramatically decreased from 0.021 to 0.006. This is because the air mass rate decreases (from 0.2469 kg/s to 0.0247 kg/s) with NTU. When m^* remains unchanged, the corresponding solution flow rate should decrease as well. Based on Eq. (4-24), the desiccant mass flow rate is then decreased significantly (from 0.1728 kg/s to 0.0173 kg/s), and as a result MFR is deteriorated. However, $C_{sol,out}$ is increased from 0.351 to 0.355. The low vapour pressure in the air channel would be nearly constant as the air and solution flow rates decrease. Consequently, the mass transfer between the air and solution is enhanced, which leads to the increase of the solution outlet concentration.

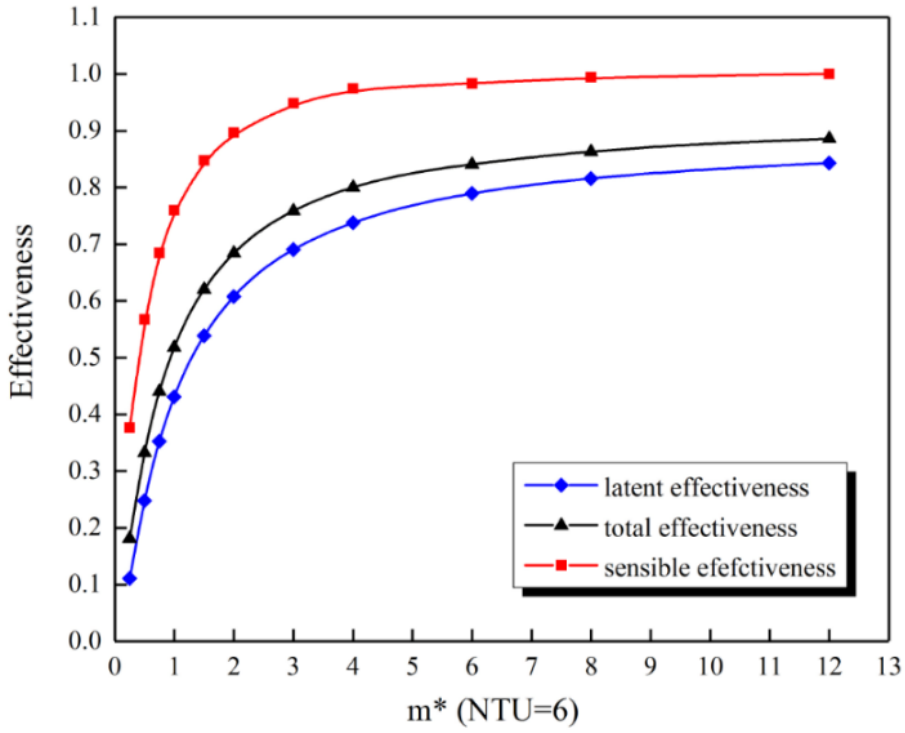


Fig 4- 8. Variations of effectiveness with m^* under $NTU = 6$

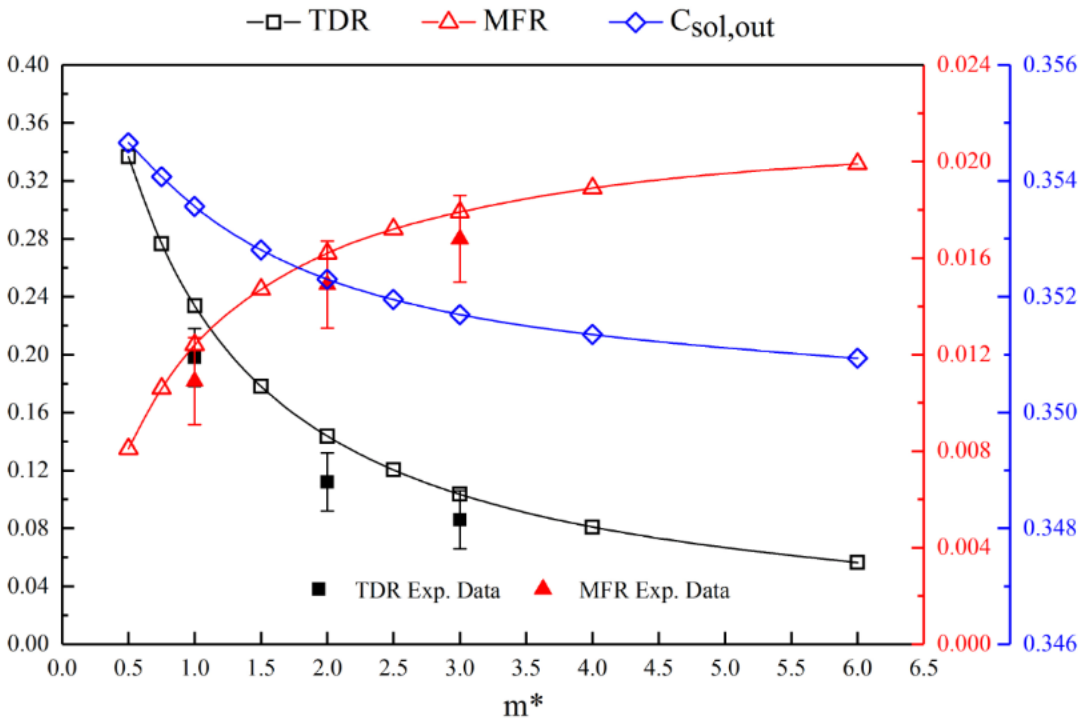


Fig 4- 9 Influences of m^* on TDR, MFR and $C_{sol,out}$

m^* is another important dimensionless parameter affecting regeneration performance, which is the relative mass flow rate of two fluids in the regenerator. m^* can be controlled by adjusting the solution mass flow rate while keeping the air mass flow rate constant under each NTU. Variations of the effectiveness, TDR, MFR and $C_{sol,out}$ with m^* under $NTU = 6$ are shown in Figs. 4-8 and 4-9. Clearly, under the same NTU, the sensible effectiveness is continuously the highest one, while the latent effectiveness is the lowest one and the total effectiveness is the middle one. A critical indicator Cr^*_{crit} has been introduced [65, 81], all effectiveness increase with Cr^* and are more sensitive before Cr^* reaching Cr^*_{crit}. Similarly a critical value of m^* is defined as m^*_{crit}. m^* is proportional to Cr^*, but it is a more straightforward parameter for the system. The effectiveness are more sensitive to m^* when m^* is lower than m^*_{crit}. As shown in Fig. 4-8, m^*_{crit} is 2 in this study, and once m^* exceeds m^*_{crit}, the gradients of all effectiveness changes become moderate gradually and only a slight variation can be observed. For example,

the sensible effectiveness is improved by 0.5198 (from 0.377 to 0.8968) when m^* changes from 0.25 to 2. However, it is only increased by 0.0997 (from 0.8968 to 0.9965) when m^* keeps increasing to 12. Besides, as mentioned previously, the effects of NTU and m^* are interacted with each other. It can also be observed from Figs.4-4 – 4-6 that the effectiveness variations with m^* are more significant under high NTU, meaning the effectiveness cannot be improved effectively by increasing m^* when NTU is too low. For instance, the sensible, latent and total effectiveness are raised by 0.0825, 0.0711 and 0.0741 individually as m^* increases from 1 to 4 under $NTU = 1$. By contrast, these effectiveness are increased by 0.2376, 0.36 and 0.3277 respectively under $NTU = 10$.

Effects of m^* on TDR, MFR and $C_{sol,out}$ are demonstrated in Fig 4-9. Compared with the effects of NTU as shown in Fig 4-7, m^* has opposite influences on TDR, MFR and $C_{sol,out}$. Heat capacity rate of the solution become higher with the solution flow rate, which would cause less temperature reduction of the desiccant solution during the phase change process [127], meaning the solution outlet temperature is increased and TDR is reduced. For example, under $NTU = 6$, $T_{sol,out}$ rises from 41.28 ℃ to 50.86 ℃ as m^* increases from 1 to 3, resulting in the TDR decreases from 0.3120 to 0.1524. So the solution cooling effect is deteriorated. In the meanwhile, the solution outlet concentration is decreased as well. It can be noticed in Fig 4-9 that $C_{sol,out}$ reduces slightly from 0.356 to 0.352. However, according to Eq. (4-24), increasing the solution mass flow rate would raise desiccant mass flow rate as well, which eventually improves MFR from 0.0035 to 0.0113. It is also noteworthy that similar to the effects of m^*_{crit} on the effectiveness, the variations of TDR, MFR and $C_{sol,out}$ also become steady after m^* reaching m^*_{crit}.

4.6.3 Effects of desiccant solution properties

Two solution properties: solution inlet temperature $T_{sol,in}$ and concentration $C_{sol,in}$ are investigated to clarify their influences on the regenerator effectiveness, TDR, MFR and $C_{sol,out}$. Variations of the regenerator effectiveness, TDR, MFR and $C_{sol,out}$ with $T_{sol,in}$ under different $C_{sol,in}$ are displayed in Figs. 4-10 - 4-13.

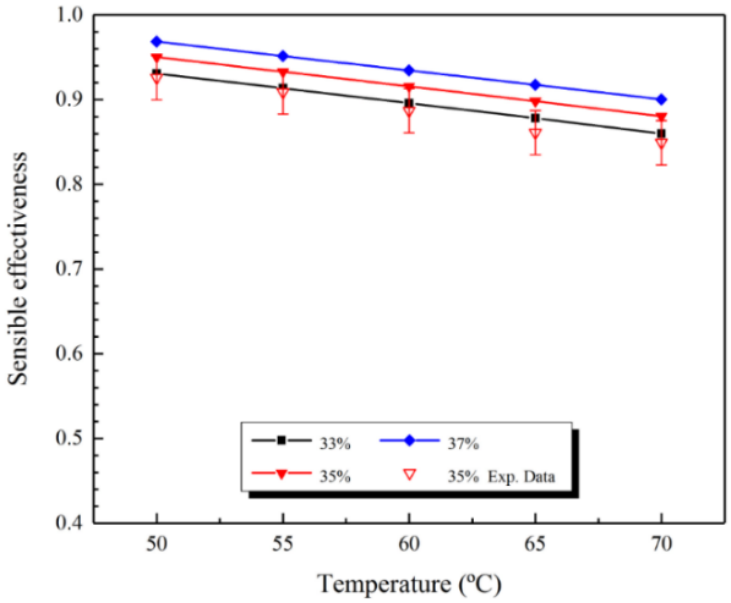


Fig 4- 10 Sensible effectiveness variations with $T_{sol,in}$ under different $C_{sol,in}$

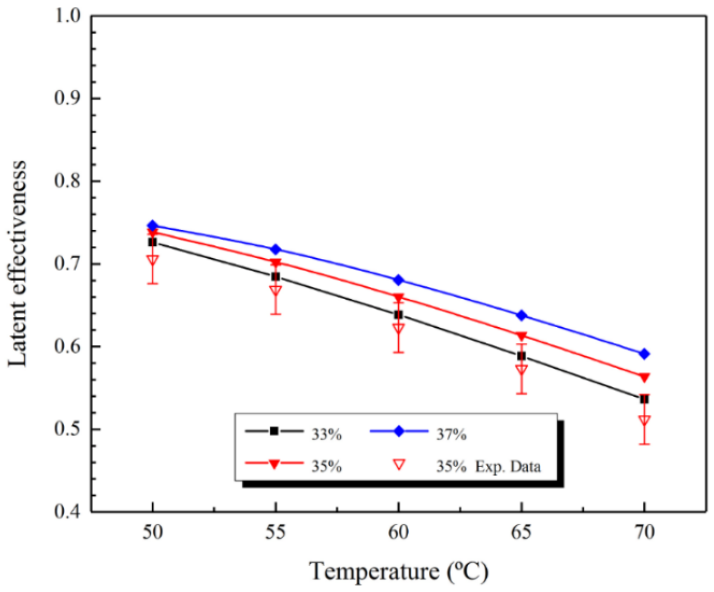


Fig 4- 11 Latent effectiveness variations with $T_{sol,in}$ under different $C_{sol,in}$

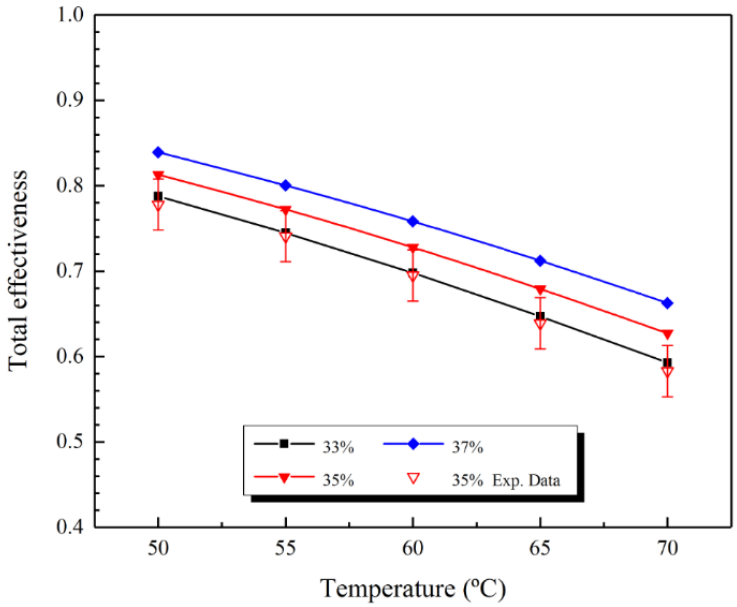


Fig 4- 12 Total effectiveness variations with $T_{sol,in}$ under different $C_{sol,in}$

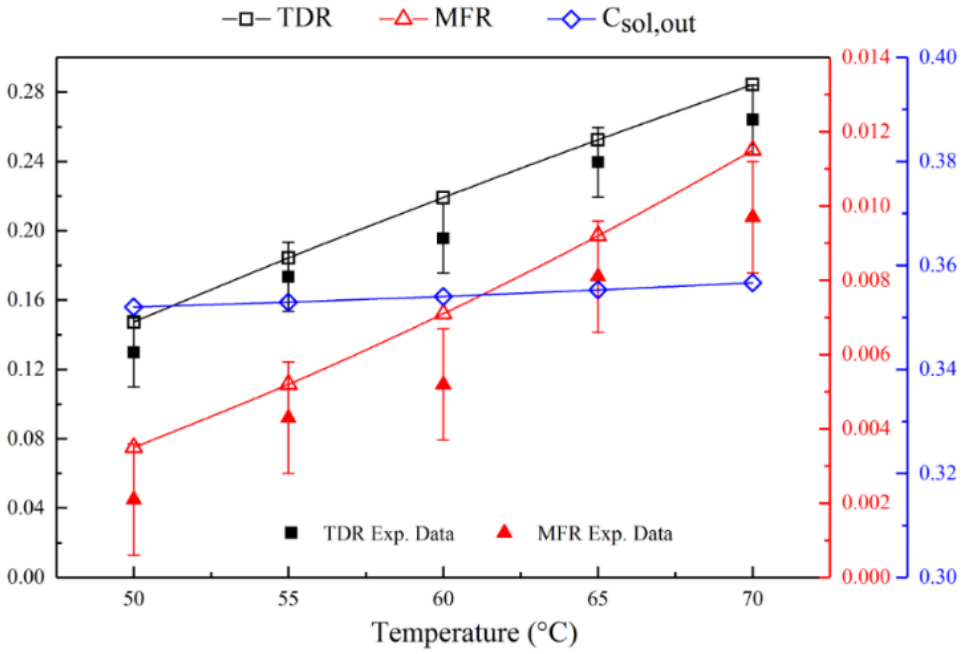


Fig 4- 13 Influences of $T_{sol,in}$ on TDR, MFR and $C_{sol,out}$

Solution temperature has great influence on the system performance as it is closely related to the solution surface vapour pressure. For the purpose of variable separation, NTU and m^* are set as 8 and 2 respectively. As shown in Figs. Figs. 4-10 - 4-12, under the same solution concentration, the sensible effectiveness is the highest among three effectiveness, while the

latent effectiveness is the lowest and the total effectiveness is the middle. For example, under $C_{sol,in} = 33\%$, the sensible effectiveness varies from 0.9308 to 0.86 when $T_{sol,in}$ rises from 50 ℃ to 70 ℃. In the meanwhile, the latent effectiveness decreases from 0.7263 to 0.5362 and the total effectiveness changes from 0.7877 to 0.5931 respectively. All effectiveness decrease with $T_{sol,in}$. According to the definition of the solution side sensible effectiveness (as given in Eq. (4-21)), the absolute value of denominator in Eq. (4-21) increases with $T_{sol,in}$, so the sensible effectiveness is reduced moderately. Besides, as indicated in Fig 4-1, the increase of $T_{sol,in}$ under the same $C_{sol,in}$ would result in high solution equilibrium humidity ratio. Based on the definition of the solution side latent effectiveness (as given in Eq. (4-22)), the absolute value of denominator in Eq. (4-22) increases with $T_{sol,in}$, this leads to the decrease of the latent effectiveness. Compared to the latent and total effectiveness, the sensible effectiveness is relatively less sensitive to $T_{sol,in}$. For instance, under $C_{sol,in} = 37\%$, increasing $T_{sol,in}$ from 50 ℃ to 70 ℃ would reduce the sensible effectiveness by 7.05% (from 0.9686 to 0.9003). By contrast, the latent and total effectiveness are reduced by 20.80% (from 0.7463 to 0.5911) and 21.05% (from 0.8393 to 0.6626) respectively. Despite the deterioration of all effectiveness with increasing $T_{sol,in}$, the higher $T_{sol,in}$, the higher solution equilibrium humidity ratio and vapour pressure. Consequently both heat and mass transfer potentials are strengthened, and these have been reflected clearly in Fig. 4-13, where TDR, MFR and $C_{sol,out}$ are all improved with $T_{sol,in}$.

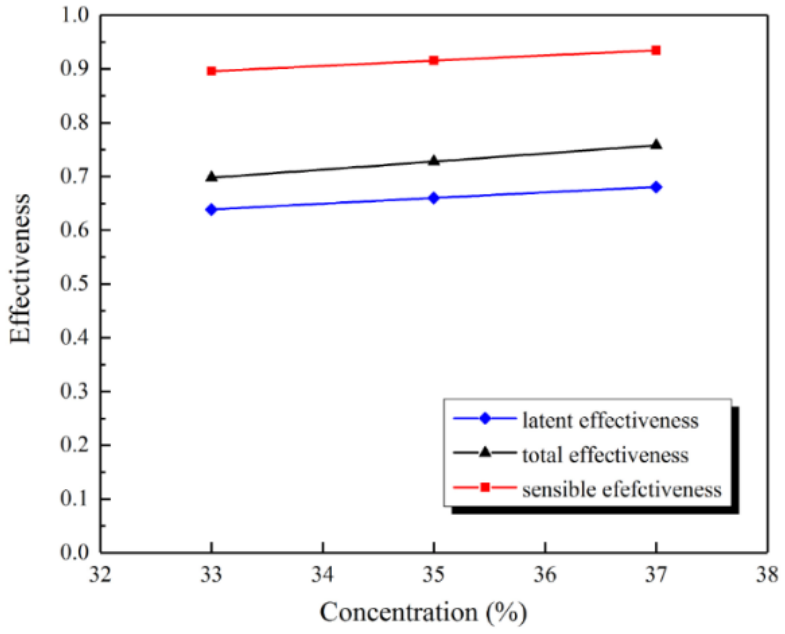


Fig 4- 14 Variations of effectiveness with $C_{sol,in}$ under $T_{sol,in} = 60℃$

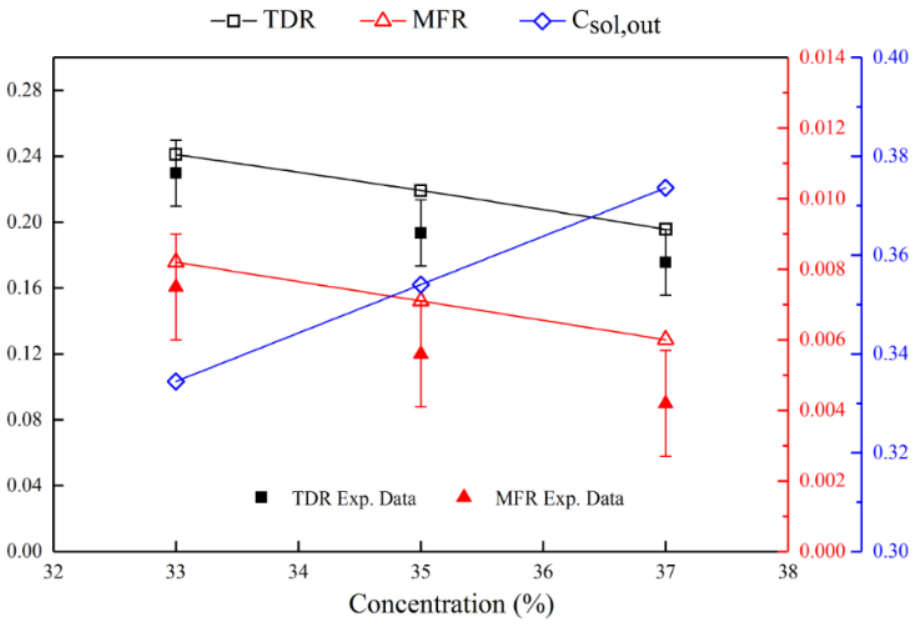


Fig 4- 15 Influences of $C_{sol,in}$ on TDR, MFR and $C_{sol,out}$

Apart from the solution inlet temperature, the solution inlet concentration also affects the regeneration performance since it is directly related to surface vapour pressure as well. Variations of the effectiveness, TDR, MFR and $C_{sol,out}$ with $C_{sol,in}$ under $T_{sol,in} = 60℃$ are

shown in Figs 4-14 and 4-15. As indicated in Fig 4-14, the sensible effectiveness is again the highest among three, while the latent effectiveness is the lowest and the total effectiveness is the middle under the same $T_{sol,in}$. All effectiveness increase with $C_{sol,in}$ slightly. However the increase rates are insignificant compared with the effects of decreasing $T_{sol,in}$, meaning the regenerator is less sensitive to $C_{sol,in}$. For example, the sensible, latent and total effectiveness are only changed by 4.3%, 6.58% and 8.64% respectively when $C_{sol,in}$ rises from 33% to 37%. Based on Fig 4-1, increasing the solution inlet concentration would decrease the solution equilibrium humidity ratio. Thus both the solution inlet mass fraction $X_{sol,in}$ and equilibrium humidity ratio $W_{sol,in}$ in Eq. (4-22) are decreased. These effects offset with each other and eventually the latent effectiveness increases slightly. However, the decrease of the solution vapour pressure would reduce mass transfer potential. As a result, MFR is decreased as illustrated in Fig 4-15. On the other hand, the reduction of mass transfer (latent heat transfer) would decrease heat absorption during the evaporation process in the solution channel. Thus $T_{sol,out}$ is increased and TDR is decreased as reflected in Fig 4-15. As for the slight increase of the sensible effectiveness, this can be explained by the definition in Eq. (4-21), increasing $T_{sol,out}$ would decrease the absolute value of the total heat transfer, which is the first term in the numerator. In the meanwhile, the second term in the numerator is deteriorated as well, which represents the latent heat transfer. Consequently, the sensible effectiveness increases slightly by the offset effect. It is noticed that although the regenerator has better regenerating and cooling effects with more diluted solution at the inlet, the solution inlet concentration is more of a non-controllable parameter since it is from dehumidifier directly. By contrast, the regenerator benefits from the high solution temperature owing to enhanced re-concentration and cooling effects. But the high solution outlet temperature means more cooling is needed before the solution enters the dehumidifier. Thus more follow up studies on optimization design for the complete system are required.

4.6.4 Effects of air properties

Compared with the solution inlet properties, the air inlet properties are easier to be controlled in practice. The influences of the inlet air temperature $T_{air,in}$ and humidity ratio $W_{air,in}$ on the regenerator effectiveness, TDR, MFR and $C_{sol,out}$ are analysed in this section. Variations of the effectiveness, TDR, MFR and $C_{sol,out}$ with $T_{air,in}$ under $W_{air,in} = 12\ g/kg\ dry\ air$ are shown in Figs. 4-16 and 4-17.

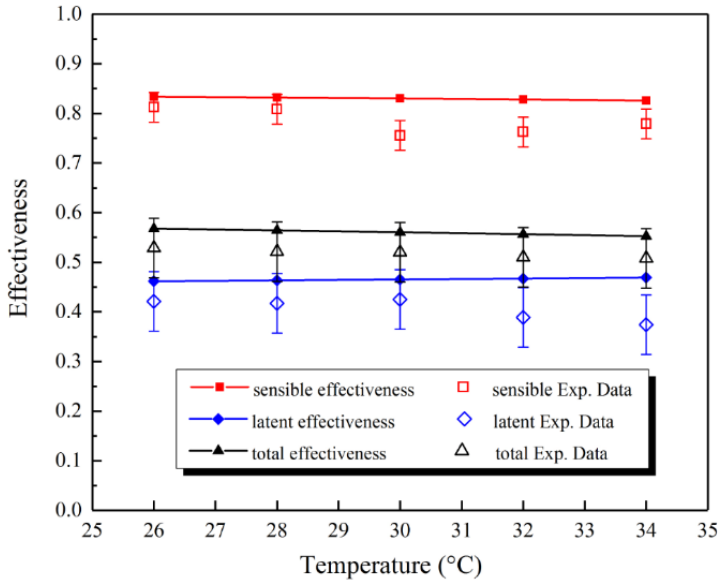


Fig 4- 16 Variations of effectiveness with $T_{air,in}$ under $W_{air,in} = 12\ g/kg\ dry\ air$

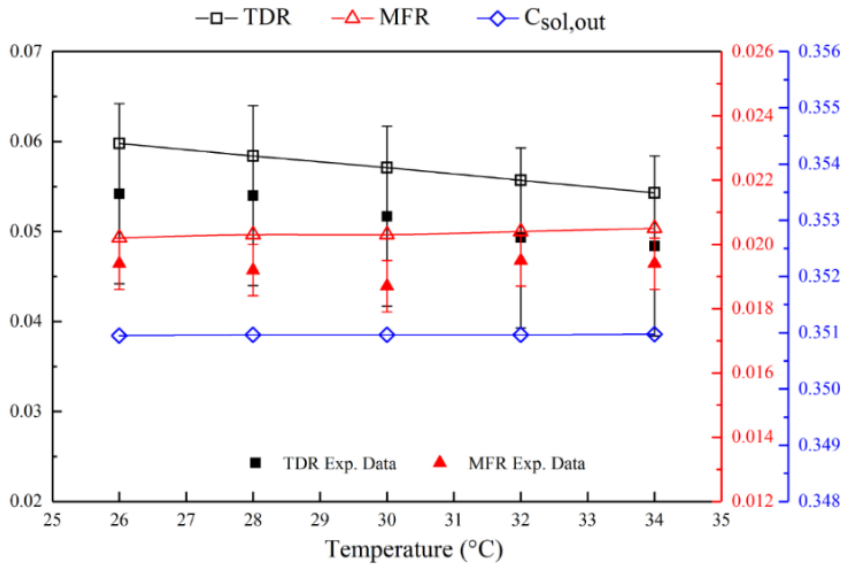


Fig 4- 17 Influences of $T_{air,in}$ on TDR, MFR and $C_{sol,out}$

Under the same $W_{air,in}$, the sensible effectiveness has the highest value, which is approximately twice of the latent effectiveness, while the total effectiveness is still in the middle as shown in Fig 4-16. All effectiveness hardly vary with $T_{air,in}$ in the temperature range of 26℃ to 34℃, and only change by 0.92%, 1.61% and 2.68% for the sensible, latent and total effectiveness respectively. For the latent heat transfer, air vapour pressure is only determined by air humidity ratio $W_{air,in}$ based on Eq. (3-50), and little impact on air vapour pressure would be imposed by changing air temperature only. Therefore, the mass transfer potential between the air and solution would remain constant in this case. Despite this, the latent effectiveness, MFR and $C_{sol,out}$ still increase slightly with $T_{air,in}$ as shown in Figs 4-16 and 4-17. A possible explanation has been given in literature [128], the significant sensible heat transfer would occur between the air and solution when the solution temperature is higher than the air temperature. The cooling of the solution when contacting with the air would decrease the air vapour pressure, which restrains the regeneration. With higher temperature inlet air, there would be less sensible heat transfer from the solution to the air. Consequently, the vapour pressure difference between the air and solution sides can be maintained at a high level, and the latent heat transfer can still be enhanced slightly. On the other hand, the high $T_{air,in}$ would narrow the temperature difference between the air and solution, which deteriorates the sensible heat transfer potential. As a result, the sensible effectiveness and TDR are reduced to a small degree as illustrated in Figs 4-16 and 4-17. Therefore, the effect of the air inlet temperature on the regeneration performance can be neglected, no obvious improvement can be achieved by adjusting $T_{air,in}$.

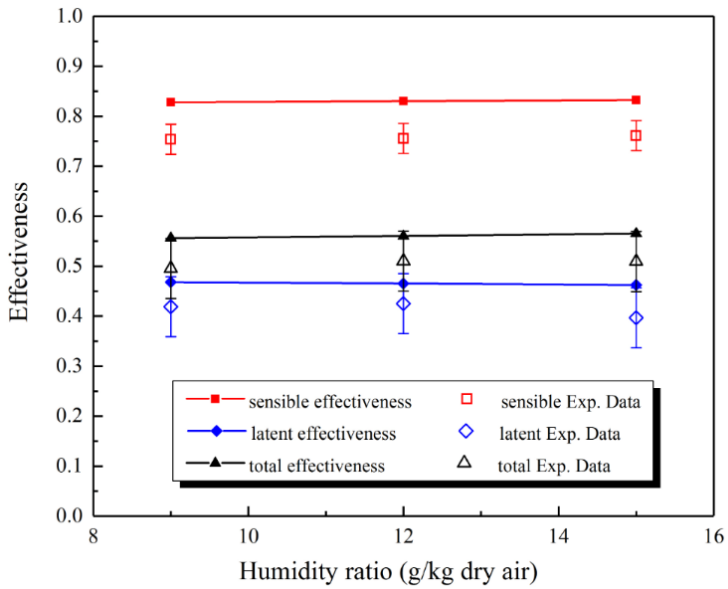


Fig 4- 18 Variations of effectiveness with $W_{air,in}$ under $T_{air,in} = 30℃$

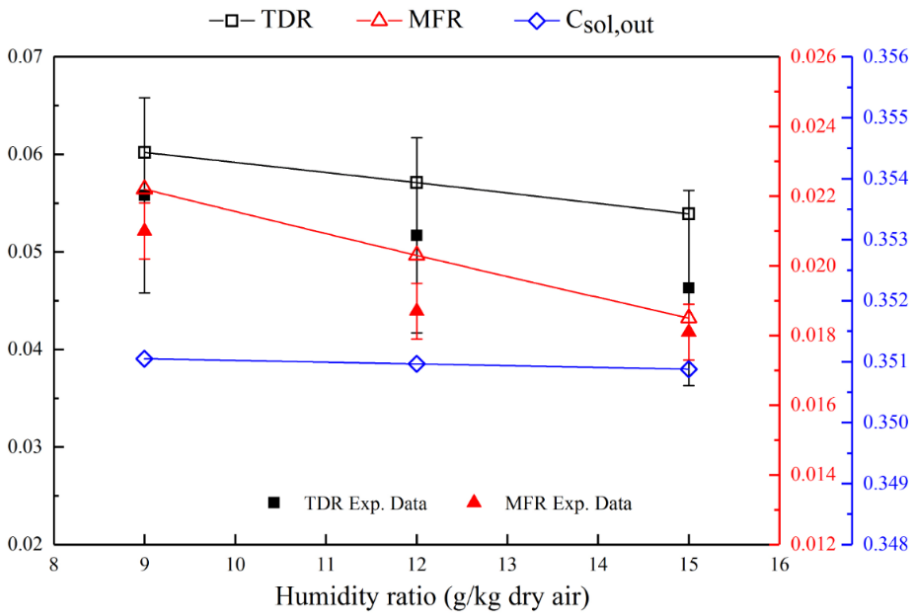


Fig 4- 19 Influences of $W_{air,in}$ on TDR, MFR and $C_{sol,out}$

Variations of the effectiveness, TDR, MFR and $C_{sol,out}$ with $W_{air,in}$ under $T_{air,in} = 30℃$ are shown in Figs 4-18 and 4-19. Similar to all cases discussed previously, the sensible effectiveness has the highest value, followed by the latent and total effectiveness. Based on Eq. (3-50), the air vapour pressure increases with its humidity ratio. With the remarkable reduction of vapour pressure difference between the air and solution sides, the mass transfer potential is

reduced significantly as well. As a result, MFR is decreased considerably as displayed in Fig 4-19. This trend is in accordance with those in previous studies [128, 139]. Nevertheless, the latent effectiveness decreases significantly as well in the previous studies, this can be regarded as an effectiveness difference between the air and solution sides. As shown in Fig 4-19, $C_{sol,out}$ decreases slightly with $W_{air,in}$. As the result solution outlet mass fraction $X_{sol,out}$ is increased. With refer to the definition of the solution side latent effectiveness as given in Eq. (4-22), both the numerator and denominator are reduced, and the combined effect causes the ignorable reduction of the latent effectiveness. Regarding the sensible heat transfer, it is slightly affected by reduced heat absorption during the evaporation process when the mass transfer is weakened. So the air outlet temperature $T_{sol,out}$ would increase to a small extent, which results in the decrease of TDR. Furthermore, according to the definition of the solution side sensible effectiveness in Eq. (4-26), the denominator would remain constant while both $T_{sol,out}$ and $X_{sol,out}$ are increased. Consequently, the sensible effectiveness is almost independent of $W_{air,in}$ as the result of the combined effect. To sum up, despite all effectiveness barely change with $W_{air,in}$, the regenerator moisture removal and cooling effects can still be improved by drier air.

4.7 Summary

In this chapter, the regeneration performance of a membrane-based parallel-plate heat and mass exchanger is investigated, heat and moisture transfer characteristics between the solution and air through membranes are studied by numerical simulation and experimental test. Solution side effectiveness, temperature decrease rate (TDR) and moisture flux rate (MFR) are applied to evaluate the regeneration performance.

Experimental tests are used to validate the numerical model, and the maximum discrepancies between numerical results and experimental data for $\varepsilon_{sol,sen}$, $\varepsilon_{sol,lat}$ and $\varepsilon_{sol,tot}$ are 9.058%, 14.967% and 11.878% respectively. The maximum differences for TDR and MFR are 11.797% and 14.286% respectively. The influences of main parameters are assessed respectively, which include: number of heat transfer units (NTU), solution to air mass flow rate ratio (m^*), solution inlet temperature ($T_{sol,in}$), solution inlet concentration ($C_{sol,in}$), air inlet temperature ($T_{air,in}$) and humidity ratio ($W_{air,in}$). The conclusions can be drawn as follows:

- The boundary conditions of the membrane surface are neither uniform temperature nor uniform humidity ratio, and they change along the diagonal line of the membrane.
- NTU and m^* have the most significant effects on the regeneration performance, and their effects are interacted with each other. There is hardly benefit to the performance improvement by increasing NTU at low m^*(e.g. lower than 1). By contrast, no obvious performance enhancement is achieved by increasing m^* at low NTU (e.g. lower than 2).
- Although the regeneration performance can be improved by increasing NTU and m^*, their increasing gradients hardly change when NTU and m^* exceed NTU_{crit} and m^*_{crit}, which are 4 and 2 respectively in this study.
- Regenerator benefits from increased solution temperature as enhanced re-concentration (0.8% increase of MFR) and cooling effects (13.7% increase of TDR). However more cooling energy is required for the high temperature desiccant solution.
- Neither $T_{air,in}$ nor $W_{air,in}$ has remarkable influence on the regeneration performance, though the solution re-concentration ability can be enhanced slightly by applying drier and warmer air.

Chapter 5: Investigation of a complete membrane-based flat-plate liquid desiccant dehumidification system

5.1 Introduction

Last two chapters discussed the performance of single dehumidifier and regenerator respectively. In most literatures about complete membrane-based dehumidification system as reviewed in Section 2.4, supply and exhaust side exchangers are coupled with aqueous salt solution flowing in a closed loop. It is assumed in these literatures that the heat and mass transfer rates in supply exchanger balance those in exhaust exchanger, in other words, there is no heat or moisture added or removed from the system. However, the system can benefit significantly from an external heat source or cold source, in which case a hot water loop and cooling water loop are included in the configuration. The heat and mass transfer rates in dehumidifier and regenerator may not be equal. Thus in this chapter a complete membrane-based liquid desiccant dehumidification system that include a dehumidifier, a regenerator, and hot and cooling water supply systems is investigated. The numerical model for the complete system is firstly developed (Section 5.2 and 5.3), experimental tests are conducted to validate the numerical model (Section 5.4 and 5.5). The effects of parameters that are controllable in reality such as dimensionless parameters (i.e. dehumidifier and regenerator side $NTUs$ and m^*) and solution inlet properties (i.e. solution inlet concentration in dehumidifier $C_{sol,in}$) on the performance of the complete system are investigated. Energy analysis is conducted through COP and total cooling energy output $Q_{cooling}$ (Section 5.6).

5.2 Numerical modelling

The developed numerical model mainly consists of three parts: dehumidifier, regenerator and heat exchanger. The structures of the dehumidifier and regenerator are similar, only their heat and mass transfer directions are converse, thus the numerical models for the dehumidifier and regenerator are explained in one sub-section. First of all, the assumptions made for the numerical model are given as follows:

1) All components are well-insulated, including the dehumidifier, regenerator, heat exchangers, pipes and ducts, there is no heat and mass transfer between the component and the ambient environment.
2) The directions of heat and mass transfer through membrane are normal to the membrane plane.
3) Both the liquid desiccant solution and air flows in the dehumidifier and regenerator are considered as the laminar flow because their Reynolds numbers (Re) are much lower than 2300 in most cases [67].
4) Condensation or evaporative heat is released to, or taken from the solution channels only since mass transfer coefficient in the solution side is much higher than that in the air side.
5) The physical properties of the solution and air, and their convective heat transfer coefficients are assumed to be constant at the steady operating condition.
6) Both the solution and air flows in the dehumidifier and regenerator are fully-developed flows, while their temperature and humidity ratio (or concentration) vary along the channel length.

In consequence, the numerical modelling methods for dehumidifier and regenerator, and for heat exchangers will be introduced in Section 5.2.1 and 5.2.2 respectively; Simulation procedure will be introduced in Section 5.2.3.

5.2.1 Dehumidifier and regenerator

The structure of dehumidifier and regenerator, and the unit cell applied for the numerical modelling for these two heat and mass exchangers have been given in Fig 3-1. For the dehumidifier, hot and humid air from outside flows along the x-axis, while strong and cold solution inversely flows along the y-axis. For the regenerator, return air from room flows along the x-axis, while weak and hot solution flows along the y-axis.

5.2.1.1 Governing equations

Governing equations after normalization of heat and mass conservation for dehumidifier and regenerator have been introduced in Chapter 3 and Chapter 4 respectively, and they are summarized here:

Dehumidifier solution side:

$$\frac{\partial {T_{sol}}^*}{\partial y^*} - NTU_m h^* \frac{1}{Cr^*}\left({W_{air}}^* - {W_{sol,mem}}^*\right) - NTU \frac{1}{Cr^*}({T_{air}}^* - {T_{sol}}^*) = 0 \quad (5\text{-}1)$$

$$\frac{\partial X_{sol}}{\partial y^*} - NTU_m \frac{1}{m^*} W_0 (1 + \omega_{sol})({W_{air}}^* - {W_{sol,mem}}^*) = 0 \quad (5\text{-}2)$$

Dehumidifier air side:

$$\frac{\partial {T_{air}}^*}{\partial x^*} + NTU({T_{air}}^* - {T_{sol}}^*) = 0 \quad (5\text{-}3)$$

$$\frac{\partial {W_{air}}^*}{\partial x^*} + NTU_m\left({W_{air}}^* - {W_{sol,mem}}^*\right) = 0 \quad (5\text{-}4)$$

Regenerator solution side:

$$\frac{\partial T_{sol}^*}{\partial y^*} + NTU_m h^* \frac{1}{Cr^*}\left(W_{sol,mem}^* - W_{air}^*\right) + NTU \frac{1}{Cr^*}(T_{sol}^* - T_{air}^*) = 0 \quad (5\text{-}5)$$

$$\frac{\partial X_{sol}}{\partial y^*} + NTU_m \frac{1}{m^*} W_0 (1 + \omega_{sol})(W_{sol,mem}^* - W_{air}^*) = 0 \quad (5\text{-}6)$$

Regenerator air side:

$$\frac{\partial T_{air}^*}{\partial x^*} - NTU(T_{sol}^* - T_{air}^*) = 0 \quad (5\text{-}7)$$

$$\frac{\partial W_{air}^*}{\partial x^*} - NTU_m\left(W_{sol,mem}^* - W_{air}^*\right) = 0 \quad (5\text{-}8)$$

5.2.1.2 Boundary conditions

For both dehumidifier and regenerator, boundary conditions of temperature and humidity ratio (or concentration) are:

Solution side

$T_{sol}{}^* = 1$, at y^*=0 (5-9)

$X_{sol} = X_{sol,in}$, at y^*=0 (5-10)

Air side

$T_{air}{}^* = 0$, at x^*=0 (5-11)

$W_{air}{}^* = 0$, at x^*=0 (5-12)

Boundary conditions of heat and moisture conservations on the membrane surface are:

$$NTU_{sol}\left(T_{sol,mem}{}^* - T_{sol}{}^*\right) = NTU\left(T_{air}{}^* - T_{sol,mem}{}^*\right) + NTU_m h^*\left(W_{air}{}^* - W_{sol,mem}{}^*\right) \quad (5\text{-}13)$$

$$NTU_m W_0\left(W_{air}{}^* - W_{sol,mem}{}^*\right) = NTU_{m.sol}\left(C_{sol} - C_{sol,mem}\right) \quad (5\text{-}14)$$

5.2.2 Heat exchangers

There are three liquid-to-liquid plate heat exchangers installed in the complete system. The concept diagram of the complete system is given in Fig 5-1. The concentrated (strong) solution is cooled by cold water in heat exchanger 3 (HX3) before entering the dehumidifier. By contrast, the diluted (weak) solution is heated by hot water in heat exchanger 2 (HX2) before entering the regenerator. Furthermore, there is heat recovery between the strong and weak solutions in heat exchanger 1 (HX1). For the parallel-flow heat exchanger, the effectiveness ε is defined as the ratio of the actual heat transfer rate over the maximum possible heat transfer rate [213]:

$$\varepsilon \equiv \frac{q}{q_{max}} = \frac{C_h\left(T_{h,i} - T_{h,o}\right)}{C_{min}\left(T_{h,i} - T_{c,i}\right)} = \frac{C_c\left(T_{c,o} - T_{c,i}\right)}{C_{min}\left(T_{h,i} - T_{c,i}\right)} \quad (5\text{-}15)$$

Where C_h and C_c are heat capacity rates of hot and cold fluid respectively; $T_{h,i}$, $T_{h,o}$, $T_{c,i}$ and $T_{c,o}$ are temperatures of hot and cold fluids at inlets and outlets. For HX1-3, their effectiveness can be expressed as:

$$\varepsilon_1 = \frac{\dot{m}_{sol}c_{p,sol}(T_{sol,out,re}-T_{sol,1})}{\dot{m}_{sol}c_{p,sol}(T_{sol,out,re}-T_{sol,out,de})} = \frac{\dot{m}_{sol}c_{p,sol}(T_{sol,2}-T_{sol,out,de})}{\dot{m}_{sol}c_{p,sol}(T_{sol,out,re}-T_{sol,out,de})} \tag{5-16}$$

$$\varepsilon_2 = \frac{\dot{m}_{sol}c_{p,sol}(T_{sol,1}-T_{sol,out,de})}{\min(\dot{m}_{sol}c_{p,sol},\dot{m}_{cooling,w}c_{p,w})(T_{sol,1}-T_{cooling,w,in})} \tag{5-17}$$

$$\varepsilon_3 = \frac{\dot{m}_{sol}c_{p,sol}(T_{sol,in,re}-T_{sol,2})}{\min(\dot{m}_{sol}c_{p,sol},\dot{m}_{hot,w}c_{p,w})(T_{hot,w,in}-T_{sol,2})} \tag{5-18}$$

Where subscripts "de" and "re" represent dehumidifier and regenerator respectively. $T_{cooling,w,in}$ and $T_{hot,w,in}$ are temperatures of cooling water and hot water at inlets respectively (℃); $T_{sol,1}$ and $T_{sol,2}$ are temperatures of strong and weak solutions after HX1(℃), as illustrated in Fig 5-1. $\dot{m}_{cooling,w}$ and $\dot{m}_{hot,w}$ are mass flow rates of cooling water and hot water respectively (kg/s).

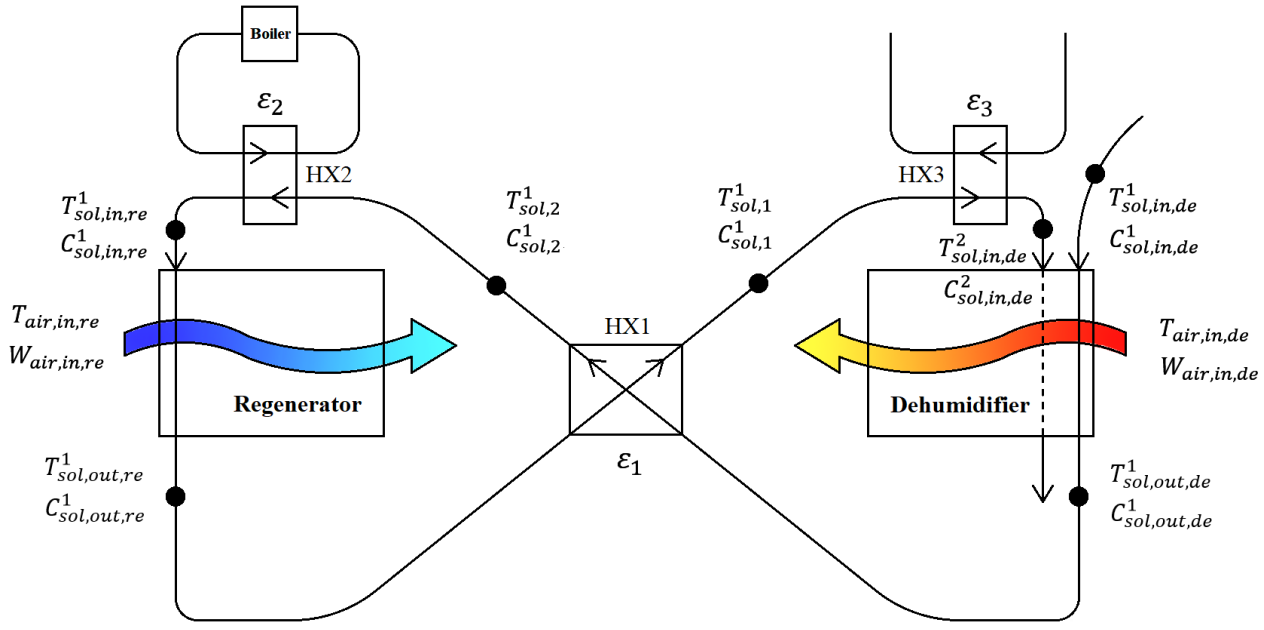


Fig 5- 1 Concept diagram of the complete dehumidification system

5.2.3 Simulation procedure

The finite difference method is applied for the solving of governing equations. Eqs. (5-1)-(5-8) are discretized by forward difference scheme to:

$$T_{sol\,(i+1,j)}{}^{*} - T_{sol\,(i,j)}{}^{*} - dy^{*}NTU_{m}h^{*}\Upsilon^{*}\left[W_{air\,(i+1,j)}{}^{*} - W_{sol,mem\,(i+1,j)}{}^{*}\right] - dy^{*}NTU\Upsilon^{*}\left[T_{air\,(i+1,j)}{}^{*} - T_{sol\,(i+1,j)}{}^{*}\right] = 0 \quad (5\text{-}19)$$

$$\omega_{sol\,(i+1,j)} - \omega_{sol\,(i,j)} - dy^{*}m^{*}W_{0}NTU_{m}\left[1 + \omega_{sol\,(i+1,j)}\right]\left[W_{air\,(i+1,j)}{}^{*} - W_{sol,mem\,(i+1,j)}{}^{*}\right] = 0 \quad (5\text{-}20)$$

$$T_{air\,(i,j+1)}{}^{*} - T_{air\,(i,j)}{}^{*} + dx^{*}NTU[T_{air\,(i,j+1)}{}^{*} - W_{sol\,(i,j+1)}{}^{*} = 0 \quad (5\text{-}21)$$

$$W_{air\,(i,j+1)}{}^{*} - W_{air\,(i,j)}{}^{*} + dx^{*}NTU_{m}\left[W_{air\,(i,j+1)}{}^{*} - W_{sol,mem\,(i,j+1)}{}^{*}\right] = 0 \quad (5\text{-}22)$$

$$T^{*}_{sol\,(i+1,j)} - T^{*}_{sol\,(i,j)} + dy^{*}NTU_{m}h^{*}Y^{*}\left[W^{*}_{sol,mem\,(i+1,j)} - W^{*}_{air\,(i+1,j)}\right] + dy^{*}NTUY^{*}\left[T^{*}_{sol\,(i+1,j)} - T^{*}_{air\,(i+1,j)}\right] = 0 \quad (5\text{-}23)$$

$$\omega_{sol\,(i+1,j)} - \omega_{sol\,(i,j)} + dy^{*}m^{*}W_{0}NTU_{m}\left[1 + \omega_{sol\,(i+1,j)}\right]\left[W^{*}_{sol,mem\,(i+1,j)} - W^{*}_{air\,(i+1,j)}\right] = 0 \quad (5\text{-}24)$$

$$T^{*}_{air\,(i,j+1)} - T^{*}_{air\,(i,j)} - dx^{*}NTU[T^{*}_{sol\,(i,j+1)} - T^{*}_{air\,(i,j+1)} = 0 \quad (5\text{-}25)$$

$$W^{*}_{air\,(i,j+1)} - W^{*}_{air\,(i,j)} - dx^{*}NTU_{m}\left[W^{*}_{sol,mem\,(i,j+1)} - W^{*}_{air(i,j+1)}\right] = 0 \quad (5\text{-}26)$$

where m and n are numbers of grids in x and y directions respectively. The above equations for the air and solution flows are solved in Matlab iteratively until the required convergence has been achieved. The numerical solving scheme is illustrated in flow chart as shown in Fig. 5-2. It has been tested that the difference of obtained results between 30×60 grids and 50×100 grids is less than 1.0% meaning 30×60 grids are sufficient for the modelling, and the numerical uncertainty is less than 1.0%.

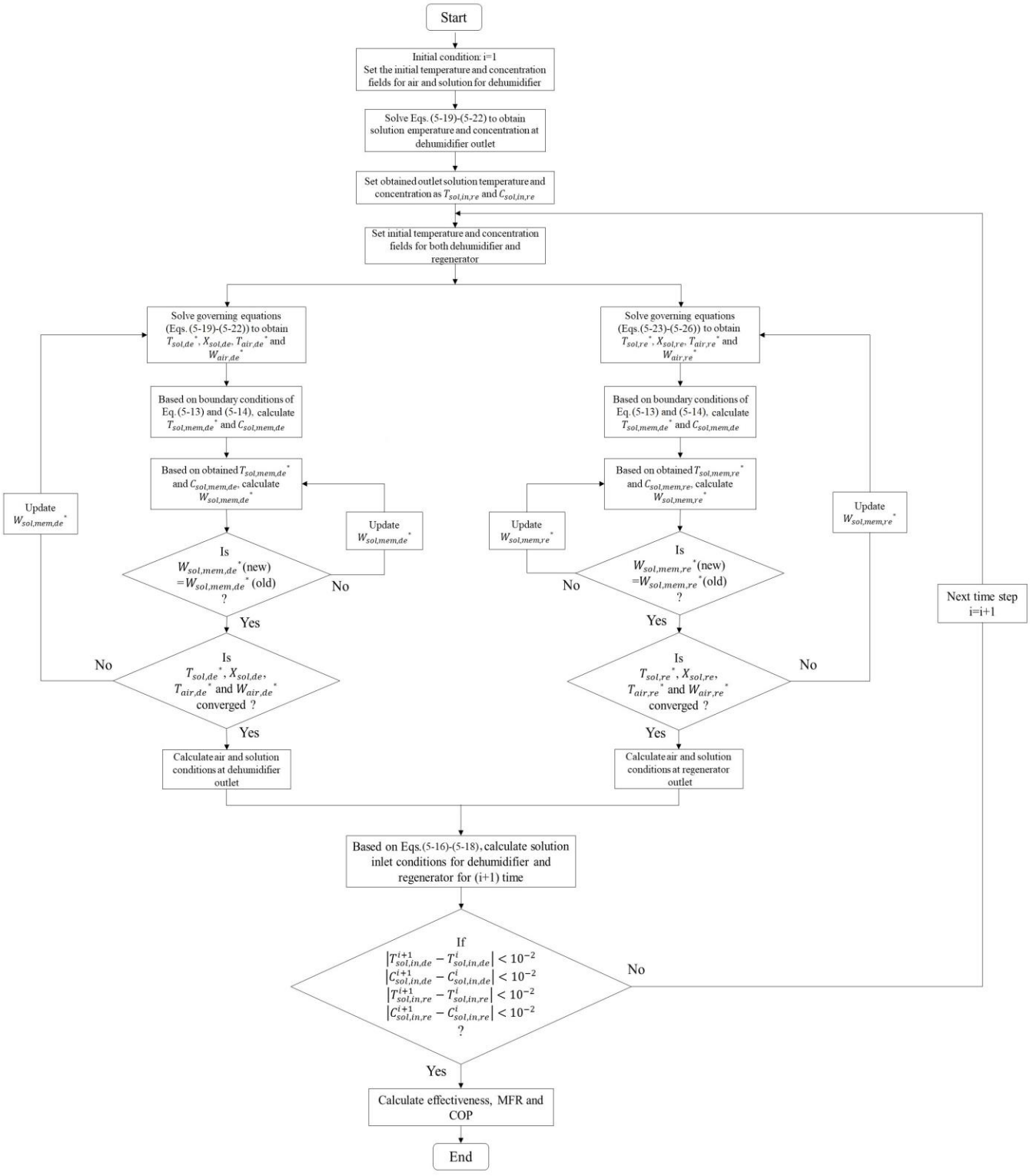


Fig 5- 2 Flow chart of the numerical solving scheme for the complete system

5.3 Performance evaluation indices

5.3.1 Effectiveness for the complete system

Effectiveness is an important dimensionless parameter applied for the performance evaluation of the heat and mass exchanger. Effectiveness for a single dehumidifier or regenerator have been defined and illustrated in previous chapters. For the complete system, the overall system sensible effectiveness, $\varepsilon_{sen,sys}$, can be defined as the ratio of actual sensible heat transfer rate between two fluids over the maximum possible sensible heat transfer rate in the system. The overall system latent effectiveness, $\varepsilon_{lat,sys}$, can be defined as the ratio of actual latent heat transfer rate between two fluids over the maximum possible latent heat transfer rate in the system. When $Cr^* > 1$, they can be expressed as:

$$\varepsilon_{sen,sys} = \frac{(\dot{m}c_p)_{air,de}(T_{air,in,de} - T_{air,out,de})}{min\left((\dot{m}c_p)_{air,de}, (\dot{m}c_p)_{sol}\right)(T_{air,in,de} - T_{air,in,re})} \tag{5-27}$$

$$\varepsilon_{lat,sys} = \frac{\dot{m}_{air,de}h_{fg}(W_{air,in,de} - W_{air,out,de})}{min(\dot{m}_{air,de}h_{fg}, \dot{m}_{sol}h_{fg})(W_{air,in,de} - W_{air,in,re})} \tag{5-28}$$

5.3.2 Moisture flux rate MFR

Moisture removal rate $\dot{m}_{moisture}$ $(\mathrm{kg/s})$ is an index of the quantity of moisture being absorbed by desiccant solution in the dehumidifier, which has be obtained by:

$$\dot{m}_{moisture} = \dot{m}_{air,de}\left(W_{air,in,de} - W_{air,out,de}\right) \tag{5-29}$$

Then moisture flux rate MFR is defined as a dimensionless parameter that represents the ratio of moisture removal rate $\dot{m}_{moisture}$ over the membrane overall mass transfer conductance. It is preferred compared to $\dot{m}_{moisture}$ as it is independent of the dehumidifier's geometric properties and only related to inlet state. MFR can be calculated by:

$$MFR = \frac{\dot{m}_{moisture}}{U_m A} = \frac{\dot{m}_{air,de}(W_{air,in,de} - W_{air,out,de})}{U_m A} \tag{5-30}$$

5.3.3 Total cooling output $Q_{cooling}$

For the dehumidification system, the most critical functions are absorbing the moisture from the moist air (latent cooling), and reduce its temperature as well (sensible cooling). Thus it is important to evaluate its total cooling output, $Q_{cooling}$ (kW), which is the sum of system sensible and latent cooling output:

$$Q_{cooling} = Q_{sen} + Q_{lat} \tag{5-31}$$

Q_{sen} and Q_{lat} are system total sensible and latent cooling output respectively (kW):

$$Q_{sen} = \dot{m}_{air,de} c_{p,air} (T_{air,in,de} - T_{air,out,de}) \tag{5-32}$$

$$Q_{lat} = \dot{m}_{moisture} \times h_{fg} = \dot{m}_{air,de} h_{fg} \left(W_{air,in,de} - W_{air,out,de}\right) \tag{5-33}$$

5.3.4 Coefficient of performance COP

To evaluate the energy efficiency of the system, coefficient of the performance, COP is defined:

$$COP = \frac{Q_{cooling}}{Q_{reg} + W_{fan} + W_{pump}} = \frac{Q_{sen} + Q_{lat}}{Q_{reg} + W_{fan} + W_{pump}} \tag{5-34}$$

Where Q_{reg} is the regeneration heat input (kW), which can be obtained by:

$$Q_{reg} = \dot{m}_{sol} c_{p,sol} (T_{sol,in,re} - T_{sol,out,re}) \tag{5-35}$$

Where W_{pump} is pump power consumption (kW); W_{fan} is fan power consumption (kW), which can be obtained by:

$$W_{fan} = \frac{W_{output}}{\eta_{fan}} = \frac{Q_{fan} \Delta P}{\eta_{fan}} = \frac{\dot{m}_{air} \Delta P}{\rho_{air} \eta_{fan}} \tag{5-36}$$

Where W_{output} is the fan power output, in other words it is the useful power output applied to the air (kW); η_{fan} is the fan efficiency; Q_{fan} is the air volumetric flow rate through the fan (m^3/s); ΔP is the drop of total pressure across the dehumidifier or regenerator, which can be calculated by:

$$\Delta P = \frac{1}{2}\rho_{air}{u_{air}}^2\left(\frac{A_{de,re}}{A_d}\right)^2\left(\frac{A_d}{A_{de,re}}-1\right)^2 \quad (5\text{-}37)$$

Where u_{air} is the air velocity ($\mathrm{m/s}$); $A_{de,re}$ is the windward area of dehumidifier or regenerator ($\mathrm{m^2}$); A_d is the cross area of the duct connected to the dehumidifier or regenerator ($\mathrm{m^2}$).

5.4 Experimental set-up

A real test rig for the complete liquid desiccant dehumidification system is set up in the laboratory as illustrated in Fig 5-3.

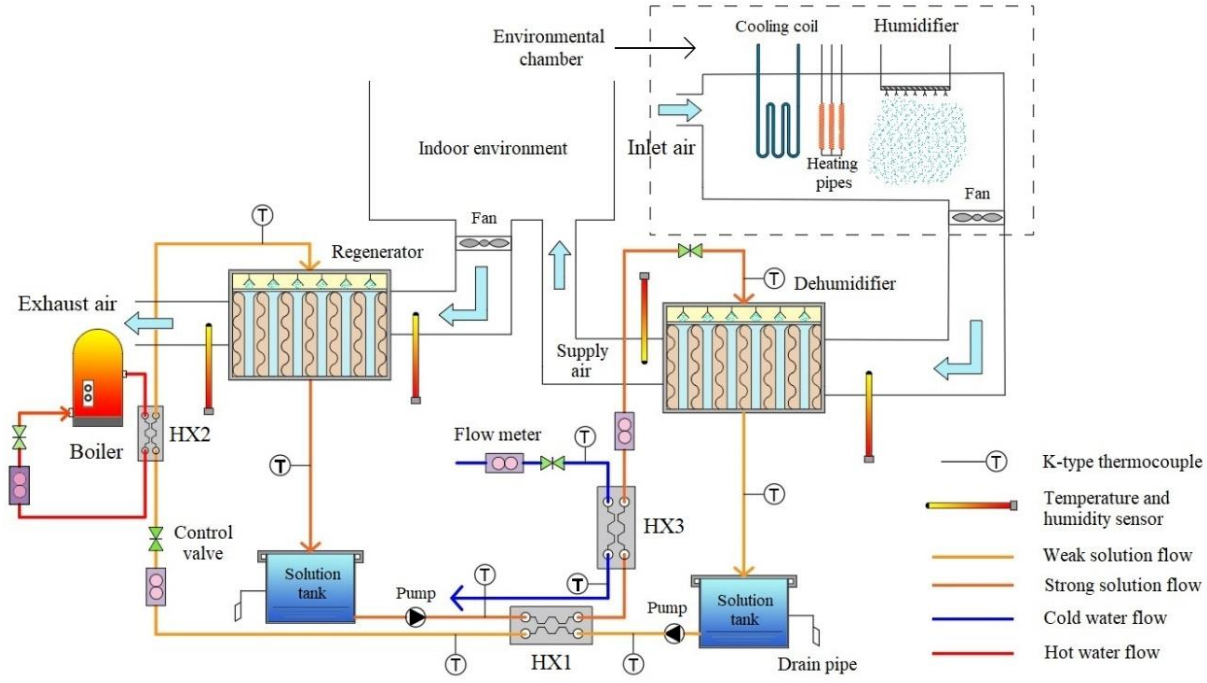


Fig 5- 3 Schematic of a complete liquid desiccant dehumidification system

It can be seen from Fig 5-3 that the complete system is comprised of one air dehumidifier, one solution regenerator, two solution tanks, three liquid-to-liquid heat exchangers, one hot water and one cold water supply units. Strong solution is cooled by cold water before entering the dehumidifier, in which both temperature and humidity ratio of the air are reduced. The air from

the dehumidifier is supplied to the indoor environment. The air from the indoor environment is returned to the regenerator, where the air is humidified and heated, and then exhausted to outdoor eventually. The diluted solution is heated by hot water before entering the regenerator. A solution heat exchanger (HX1) is used between the diluted and re-concentrated solutions for heat recovery. Two solution tanks are used to collect the solutions. With regards to experimental set-up, air flow rates through the dehumidifier and regenerator are controlled by two variable speed fans and measured by Testo thermos-anemometer (0-10m/s) with the accuracy of $\pm 5\%$. The solution is circulated by two 15W centrifugal magnetically driven pumps, and its flow rates in the dehumidifier and regenerator are adjusted by two liquid flow indicators (1-15L/min) with accuracy of $\pm 5\%$ to make sure the system runs at the steady condition. The solution concentration is obtained by measuring its density using Brannan hydrometer with accuracy of $\pm 2\%$. The hot water is provided by electrical boiler with temperature range of 20℃ to 80℃, and the cold water is from the main supply pipe with temperature of 14℃. Temperatures of the solution and water are measured by K-type thermocouples (0-1100℃) with the accuracy of $\pm 0.75\%$. Humidity of air is measured by Sensiron Evaluation KIT (0-100 %) with accuracy of $\pm 3\%$. All sensors are connected to a data logger (DT500) with accuracy of $\pm 0.15\%$ for data acquisition. Physical and transport properties of the dehumidifier and regenerator are listed in Table 5-1.

Table 5- 1 Physical and transport properties of dehumidifier and regenerator

Description	Notation	Unit	Value
Length of dehumidifier (regenerator)	L	m	0.41
Width of dehumidifier (regenerator)	W	m	0.186
Height of dehumidifier (regenerator)	H	m	0.23
Air channel thickness	d_{air}	m	0.0077
Solution channel thickness	d_{sol}	m	0.0043
Membrane thickness	δ_{mem}	m	0.5×10^{-3}
Membrane conductivity	k_{mem}	kW/mK	3×10^{-4}
Membrane mass transfer conductivity	$k_{m,mem}$	kg/ms	3.87×10^{-6}
Air specific heat capacity	$c_{p,air}$	J/kgK	1020
Solution specific heat capacity	$c_{p,sol}$	J/kgK	3200
Air side diffusivity	D_{air}	m^2/s	2.46×10^{-5}
Solution side diffusivity	D_{sol}	m^2/s	0.892×10^{-2}
Air side heat conductivity	k_{air}	W/Mk	0.03
Solution side heat conductivity	k_{sol}	W/Mk	0.53
Air side Nusselt number	Nu_{air}	-	6.58
Solution side Nusselt number	Nu_{sol}	-	7.74
Air side Sherwood number	Sh_{air}	-	6.7

5.5 Numerical model validation

The numerical model for the complete system is validated by experimental data. In total 30 groups of tests under various operating conditions have been conducted. Both the hot water and cold water flow rates are set as 0.006 kg/s, and their temperatures are set as 60℃ and 14℃ respectively. Room exhaust air is used in the regenerator for regeneration. The effects of the dehumidifier side NTU number NTU_{de}, regenerator side NTU number NTU_{re}, mass flow rate

ratio m^*, solution temperature $T_{sol,in,de}$ and concentration $C_{sol,in,de}$ at the inlet of the dehumidifier, and air temperature $T_{air,in,de}$ and humidity ratio $W_{air,in,de}$ at the inlet of the dehumidifier are evaluated. The system sensible effectiveness $\varepsilon_{sen,sys}$, latent effectiveness $\varepsilon_{lat,sys}$ and moisture flux rate MFR are adopted for the comparison between numerically obtained and experimentally tested data. The comparison results are given in Table 5−2. It is found that the maximum relative errors are 13.29%, 12.72% and 12.96% for $\varepsilon_{sen,sys}$, $\varepsilon_{lat,sys}$ and MFR. Generally speaking, the calculated results and experimental data have similar variation trends, a good agreement between them has been achieved. This means the numerical model can be used to predict the performance of the complete membrane-based liquid desiccant dehumidification system.

Table 5- 2 Calculated and tested performance indices under different operating conditions

Operating conditions								Comparisons		
NTU_{de}	NTU_{re}	m_{sol} (kg/s)	m*	$T_{sol,in,de}$ (℃)	$C_{sol,in,de}$ (%)	$T_{air,in}$ (℃)	$W_{air,in,de}$ (kg/kg)	$\varepsilon_{sen,num}$	$\varepsilon_{sen,exp}$	Error (%)
1	4	0.009	-	25	39	28	0.012	0.3184	0.281	11.746
4	4	0.009	-	25	39	28	0.012	0.7817	0.749	4.183
8	4	0.009	-	25	39	28	0.012	0.9379	0.883	5.854
1	4	0.012	-	25	39	28	0.012	0.2769	0.251	9.354
4	4	0.012	-	25	39	28	0.012	0.6991	0.667	4.592
8	4	0.012	-	25	39	28	0.012	0.8525	0.798	6.393
4	1	0.009	-	25	39	28	0.012	0.8014	0.764	4.667
4	4	0.009	-	25	39	28	0.012	0.7817	0.759	2.904
4	8	0.009	-	25	39	28	0.012	0.7711	0.732	5.071
4	1	0.012	-	25	39	28	0.012	0.7442	0.718	3.521
4	4	0.012	-	25	39	28	0.012	0.6991	0.667	4.592
4	8	0.012	-	25	39	28	0.012	0.6778	0.637	6.020
4	4	0.0056	1	25	39	28	0.012	0.7244	0.688	5.025
4	4	0.0112	2	25	39	28	0.012	0.7309	0.768	-5.076
4	4	0.0224	4	25	39	28	0.012	0.3356	0.291	13.290
6	6	0.0037	1	25	39	28	0.012	0.7659	0.724	5.470
6	6	0.0074	2	25	39	28	0.012	0.9063	0.870	4.005
6	6	0.0148	4	25	39	28	0.012	0.6678	0.629	5.810
4	4	0.0056	1	25	30	28	0.012	0.8263	0.811	1.852
4	4	0.0056	1	25	36	28	0.012	0.7898	0.769	3.743
4	4	0.0056	1	25	42	28	0.012	0.7732	0.738	4.553
4	4	0.0056	1	25	39	28	0.01	0.8449	0.862	-2.024
4	4	0.0056	1	25	39	30	0.01	0.8674	0.819	5.580
4	4	0.0056	1	25	39	34	0.01	0.8897	0.913	-2.619
4	4	0.0056	1	25	39	28	0.015	0.7505	0.718	4.330
4	4	0.0056	1	25	39	30	0.015	0.7856	0.739	5.932
4	4	0.0056	1	25	39	34	0.015	0.8254	0.791	4.168
4	4	0.0056	1	25	39	28	0.02	0.6462	0.598	7.459
4	4	0.0056	1	25	39	30	0.02	0.6968	0.712	-2.181
4	4	0.0056	1	25	39	34	0.02	0.757	0.704	7.001

Operating conditions								Comparisons		
NTU_{de}	NTU_{re}	m_{sol} (kg/s)	m*	$T_{sol,in,de}$ (℃)	$C_{sol,in,de}$ (%)	$T_{air,in}$ (℃)	$W_{air,in,de}$ (kg/kg)	$\varepsilon_{lat,num}$	$\varepsilon_{lat,exp}$	Error (%)
1	4	0.009	-	25	39	28	0.012	0.2837	0.251	11.526
4	4	0.009	-	25	39	28	0.012	0.7436	0.708	4.788
8	4	0.009	-	25	39	28	0.012	0.9342	0.850	9.013
1	4	0.012	-	25	39	28	0.012	0.2853	0.249	12.723
4	4	0.012	-	25	39	28	0.012	0.7353	0.682	7.249
8	4	0.012	-	25	39	28	0.012	0.9230	0.833	9.751
4	1	0.009	-	25	39	28	0.012	0.7466	0.702	5.974
4	4	0.009	-	25	39	28	0.012	0.7436	0.698	6.132
4	8	0.009	-	25	39	28	0.012	0.7433	0.678	8.785
4	1	0.012	-	25	39	28	0.012	0.7411	0.699	5.681
4	4	0.012	-	25	39	28	0.012	0.7353	0.702	4.529
4	8	0.012	-	25	39	28	0.012	0.7346	0.676	7.977
4	4	0.0056	1	25	39	28	0.012	0.7247	0.689	4.926
4	4	0.0112	2	25	39	28	0.012	0.7421	0.718	3.248
4	4	0.0224	4	25	39	28	0.012	0.7066	0.667	5.604
6	6	0.0037	1	25	39	28	0.012	0.8253	0.790	4.278
6	6	0.0074	2	25	39	28	0.012	0.8722	0.831	4.724
6	6	0.0148	4	25	39	28	0.012	0.8433	0.807	4.305
4	4	0.0056	1	25	30	28	0.012	0.7167	0.674	5.958
4	4	0.0056	1	25	36	28	0.012	0.7402	0.697	5.836
4	4	0.0056	1	25	42	28	0.012	0.7552	0.720	0.661
4	4	0.0056	1	25	39	28	0.01	0.7616	0.728	4.412
4	4	0.0056	1	25	39	30	0.01	0.7548	0.719	4.743
4	4	0.0056	1	25	39	34	0.01	0.7403	0.695	6.120
4	4	0.0056	1	25	39	28	0.015	0.7530	0.715	5.047
4	4	0.0056	1	25	39	30	0.015	0.7482	0.708	5.373
4	4	0.0056	1	25	39	34	0.015	0.7380	0.687	6.911
4	4	0.0056	1	25	39	28	0.02	0.7446	0.687	7.738
4	4	0.0056	1	25	39	30	0.02	0.7407	0.700	5.495
4	4	0.0056	1	25	39	34	0.02	0.7322	0.674	0.949

Operating conditions								Comparisons		
NTU_{de}	NTU_{re}	m_{sol} (kg/s)	m*	$T_{sol,in,de}$ (℃)	$C_{sol,in,de}$ (%)	$T_{air,in}$ (℃)	$W_{air,in,de}$ (kg/kg)	$MFR_{moisture,num}$	$MFR_{moisture,exp}$	Error (%)
1	4	0.009	-	25	39	28	0.012	0.0082	0.0073	10.976
4	4	0.009	-	25	39	28	0.012	0.0055	0.0048	12.727
8	4	0.009	-	25	39	28	0.012	0.0035	0.0031	11.429
1	4	0.012	-	25	39	28	0.012	0.0078	0.0068	12.821
4	4	0.012	-	25	39	28	0.012	0.0052	0.0046	11.539
8	4	0.012	-	25	39	28	0.012	0.0033	0.0029	12.121
4	1	0.009	-	25	39	28	0.012	0.0056	0.0049	12.500
4	4	0.009	-	25	39	28	0.012	0.0055	0.0048	12.727
4	8	0.009	-	25	39	28	0.012	0.0055	0.0049	10.910
4	1	0.012	-	25	39	28	0.012	0.0053	0.0048	9.434
4	4	0.012	-	25	39	28	0.012	0.0052	0.0046	11.539
4	8	0.012	-	25	39	28	0.012	0.0051	0.0045	11.765
4	4	0.0056	1	25	39	28	0.012	0.0055	0.0049	10.910
4	4	0.0112	2	25	39	28	0.012	0.0052	0.0051	1.923
4	4	0.0224	4	25	39	28	0.012	0.0045	0.0046	-2.223
6	6	0.0037	1	25	39	28	0.012	0.0041	0.0038	7.317
6	6	0.0074	2	25	39	28	0.012	0.0044	0.0039	11.364
6	6	0.0148	4	25	39	28	0.012	0.0038	0.0034	10.526
4	4	0.0056	1	25	30	28	0.012	0.0042	0.0037	11.905
4	4	0.0056	1	25	36	28	0.012	0.0051	0.0046	9.804
4	4	0.0056	1	25	42	28	0.012	0.0058	0.0053	8.621
4	4	0.0056	1	25	39	28	0.01	0.0033	0.0029	12.121
4	4	0.0056	1	25	39	30	0.01	0.0032	0.0029	9.375
4	4	0.0056	1	25	39	34	0.01	0.0032	0.0028	12.500
4	4	0.0056	1	25	39	28	0.015	0.0055	0.0051	7.273
4	4	0.0056	1	25	39	30	0.015	0.0054	0.0048	11.112
4	4	0.0056	1	25	39	34	0.015	0.0054	0.0047	12.963
4	4	0.0056	1	25	39	28	0.02	0.0077	0.0072	6.494
4	4	0.0056	1	25	39	30	0.02	0.0076	0.0070	7.895
4	4	0.0056	1	25	39	34	0.02	0.0075	0.0070	6.667

5.6 Results and discussion

5.6.1 Temperature and humidity (concentration) fields

For each operating condition, temperature and humidity fields in the air channel, and temperature and concentration fields in the solution channel can be obtained once all governing equations have converged. It is important to clarify temperature and humidity fields for the air and solution in the dehumidifier, temperature and concentration fields for the solution in the regenerator, and temperature and humidity fields on the membrane surfaces in both the dehumidifier and regenerator as these fields reflect the internal processes. These fields are shown in Fig 5-4.

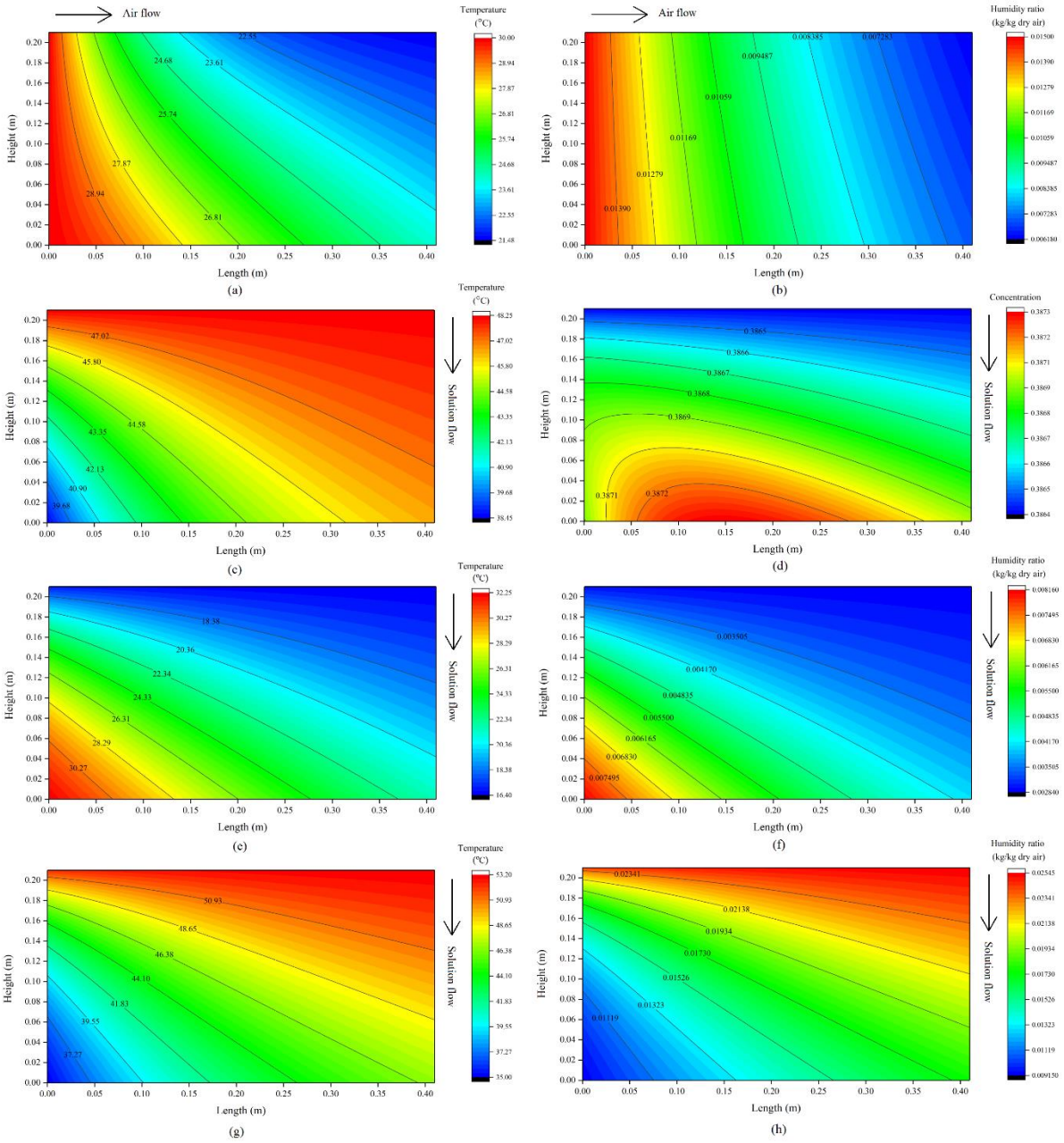


Fig 5- 4 Air temperature and humidity ratio fields in dehumidifier (a) (b); solution temperature and concentration fields in regenerator (c) (d); temperature and humidity ratio fields on membrane surface in dehumidifier (e) (f); temperature and humidity ratio fields on membrane surface in regenerator (g) (h)

Fig 5-4 is plotted under $NTU_{de} = NTU_{re} = 4$ and $m^* = 1$ ($\dot{m}_{sol} = 0.0056\,\mathrm{kg/s}$) condition. The solution inlet temperature and concentration in the dehumidifier are 25 ℃ and 39%

respectively, the air inlet temperature and humidity ratio in the dehumidifier are 30℃ and 0.015 kg/kg dry air respectively, the return air from indoor environment for regeneration is at state of 28℃ and 0.012 kg/kg dry air. It can be observed from Fig. 5−4(a) and (b) that the air temperature and humidity ratio have similar distribution in the dehumidifier as they both decrease diagonally from the left bottom corner to the right upper corner. This is because the air is cooled and dehumidified when contacting with the solution along the length of the dehumidifier. Moreover, the solution is warmed and humidified by the air along the height of the dehumidifier, thus the air has the lowest temperature and humidity ratio at the right upper corner. For the solution temperature distribution in the regenerator as illustrated in Fig. 5−4(c), the solution enters the regenerator with a relatively high temperature (48.25℃ under this operating condition) as it is heated by hot water, then it is cooled by the return air, and its average outlet temperature is 41.01℃. The solution temperature decreases along the diagonal line of the regenerator, from the right upper corner to the left bottom corner. With regard to the solution concentration distribution as shown in Fig. 5−4(d), the solution enters the regenerator with a relatively low concentration after the dehumidification process, it is re-concentrated in the regenerator. Unlike the diagonal change for other property distributions, there is a nearly semicircle zoom at the bottom of the solution concentration field. This is caused by the effects of moisture transfer and phase change in the regenerator as the latent heat is taken away from the solution channel in the process of water evaporation. The latent heat is assumed to be taken only from the solution side since convective mass transfer coefficient of the desiccant solution ($h_{m,sol}$) is much higher than that of the air ($h_{m,air}$). Based on the governing equations for the regenerator, heat transfer and mass transfer are closely related to each other, this leads to the semi-circular contour lines in the solution concentration field. The temperature and equilibrium humidity ratio boundary conditions on the membrane surfaces of the dehumidifier and regenerator are displayed in Fig. 5−4(e) (f) (g) and (h), they are neither uniform temperature

nor uniform humidity ratio distribution. The temperature and equilibrium humidity ratio increase from the right upper corner to the left bottom corner in the dehumidifier, by contrast, they decrease along the same direction in the regenerator. To sum up, the contours are both two-dimensional and non-uniform, and they all vary along the diagonal line of the membrane surface.

5.6.2 Effects of dimensionless parameters

In this section the effects of system dimensionless parameters (the dehumidifier side NTU_{de}, regenerator side NTU_{re}, and mass flow rate ratio m^*) on the complete system dehumidification performance are evaluated by the system sensible and latent effectiveness $\varepsilon_{sen,sys}$, $\varepsilon_{lat,sys}$ and moisture flux rate MFR, while the system energy performance is assessed by the total cooling output $Q_{cooling}$ and coefficient of performance COP.

5.6.2.1 Effects of dehumidifier side NTU_{de}

The variations of $\varepsilon_{sen,sys}$, $\varepsilon_{lat,sys}$ and MFR with NTU_{de} under different solution mass flow rates are plotted in Figs 5-5 – 5-7.

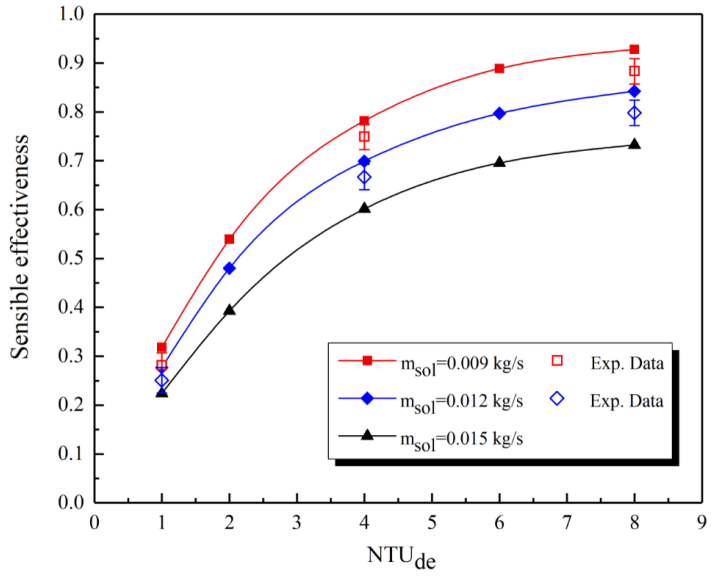


Fig 5- 5 System sensible effectiveness variations against NTU_{de} under various $\dot{m}_{sol}$

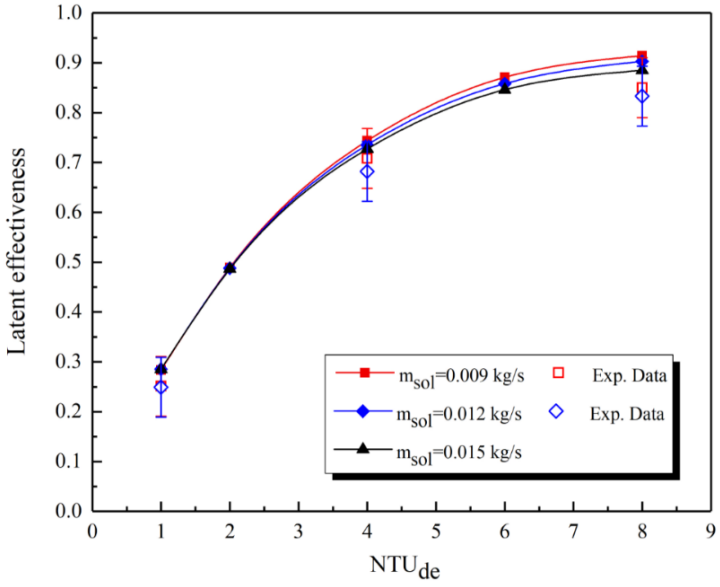


Fig 5- 6 System latent effectiveness variations against NTU_{de} under various $\dot{m}_{sol}$

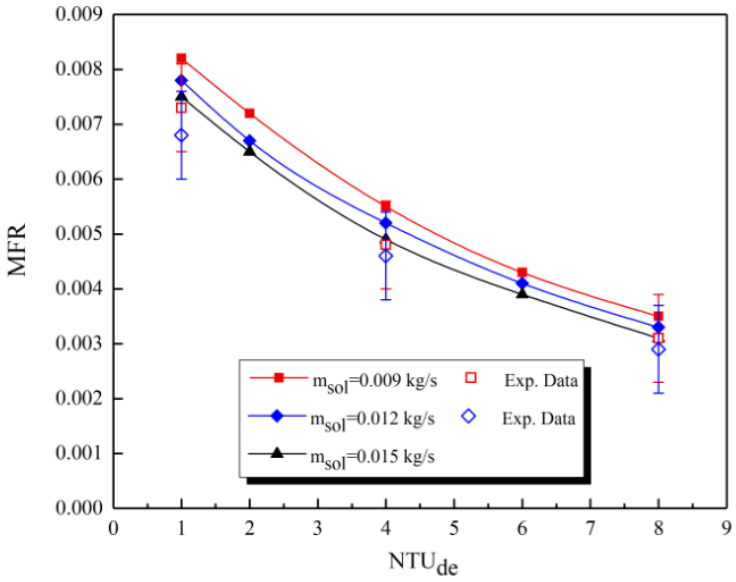


Fig 5- 7 Moisture flux rate variations against NTU_{de} under various $\dot{m}_{sol}$

NTU has been used in many literatures previously to evaluate the performance of heat and mass exchanger. In this study, according to Eq. (3-36) for a given system with the fixed sizes of the dehumidifier and regenerator, NTU_{de} is adjusted by changing air mass flow rate through the dehumidifier. NTU_{de} is inversely proportional to $\dot{m}_{air,de}$, for example, $\dot{m}_{air,de}$ decreases from 0.0224 kg/s to 0.0028 kg/s when NTU_{de} increases from 1 to 8. In the meanwhile, NTU_{re} is kept at 4 ($\dot{m}_{air,re} = 0.0056$ kg/s).

As shown in Figs. 5-5 and 5-6, both $\varepsilon_{sen,sys}$ and $\varepsilon_{lat,sys}$ increase with NTU_{de}. For example, under $\dot{m}_{air,re} = 0.015$ kg/s, $\varepsilon_{sen,sys}$ increases from 0.2237 to 0.7422 when NTU_{de} changes from 1 to 8, while $\varepsilon_{lat,sys}$ increases from 0.2852 to 0.9049. However, their increase gradients reduce with NTU_{de} gradually, and finally level off. For example, under $\dot{m}_{sol} = 0.009$ kg/s, $\varepsilon_{sen,sys}$ increases by 179.11% from 0.3184 to 0.8887 when NTU_{de} changes from 1 to 6. When NTU_{de} further increases from 6 to 8, $\varepsilon_{sen,sys}$ only raises by 5.54% from 0.8887 to 0.9379. The same situation is for $\varepsilon_{lat,sys}$, under $\dot{m}_{sol} = 0.009$ kg/s, $\varepsilon_{lat,sys}$ raises by 207.01% from 0.2837 to 0.871 when NTU_{de} changes from 1 to 6. And it only increases by 7.26% from 0.871

to 0.9342 when NTU_{de} varies from 6 to 8. Thus similar to single dehumidifier or regenerator, a critical dehumidifier side NTU does exist and can be defined as $NTU_{de,crit}$. In this case $NTU_{de,crit}$ is equal to 6. Before NTU_{de} reaches 6, both $\varepsilon_{sen,sys}$ and $\varepsilon_{lat,sys}$ can be improved by increasing NTU_{de}, but increasing NTU_{de} beyond $NTU_{de,crit}$ would not enhance $\varepsilon_{sen,sys}$ and $\varepsilon_{lat,sys}$.

It is also noticed from Figs. 5-5 and 5-6 that $\varepsilon_{sen,sys}$ is not always higher than $\varepsilon_{lat,sys}$. Under $\dot{m}_{sol} = 0.009$ kg/s and 0.012 kg/s, $\varepsilon_{sen,sys}$ are higher than $\varepsilon_{lat,sys}$ for all NTU_{de}. For instance, under $\dot{m}_{sol} = 0.012$ kg/s, $\varepsilon_{sen,sys}$ increases from 0.2769 to 0.8525 when NTU_{de} varies from 1 to 8, , while $\varepsilon_{lat,sys}$ changes from 0.2853 to 0.9230. However, once $\dot{m}_{sol}$ is increased to 0.015 kg/s, $\varepsilon_{lat,sys}$ is higher than $\varepsilon_{sen,sys}$ for all NTU_{de}. For instance, under $\dot{m}_{sol} = 0.015$ kg/s, $\varepsilon_{sen,sys}$ only increases from 0.2237 to 0.7422 when NTU_{de} changes from 1 to 8, while $\varepsilon_{lat,sys}$ increases from 0.2852 to 0.9049.

The moisture flux rate MFR is another dimensionless parameter used to evaluate the dehumidification ability. It reflects the total moisture being absorbed by the solution. As indicated in Fig. 5-7, MFR decreases with NTU_{de} under all $\dot{m}_{sol}$. This is because NTU_{de} is inversely proportional to $\dot{m}_{air,de}$, the increase of NTU_{de} is achieved by reducing the air flow rate through the dehumidifier. Although the dehumidification effectiveness is improved, and the air humidity ratio at the outlet of the dehumidifier is reduced (for instance, under $\dot{m}_{sol} = 0.009$ kg/s, $W_{air,out,de}$ is reduced from 0.0136 to 0.0041 kg/kg dry air when NTU_{de} changes from 1 to 8) , the total amount of moisture being absorbed is still decreased.

Apart from dehumidification effect, it is of our interest to evaluate the energy performance of the complete system as well. The relationships among NTU_{de}, $Q_{cooling}$ and COP under different solution mass flow rates are given in Fig 5-8 and 5-9.

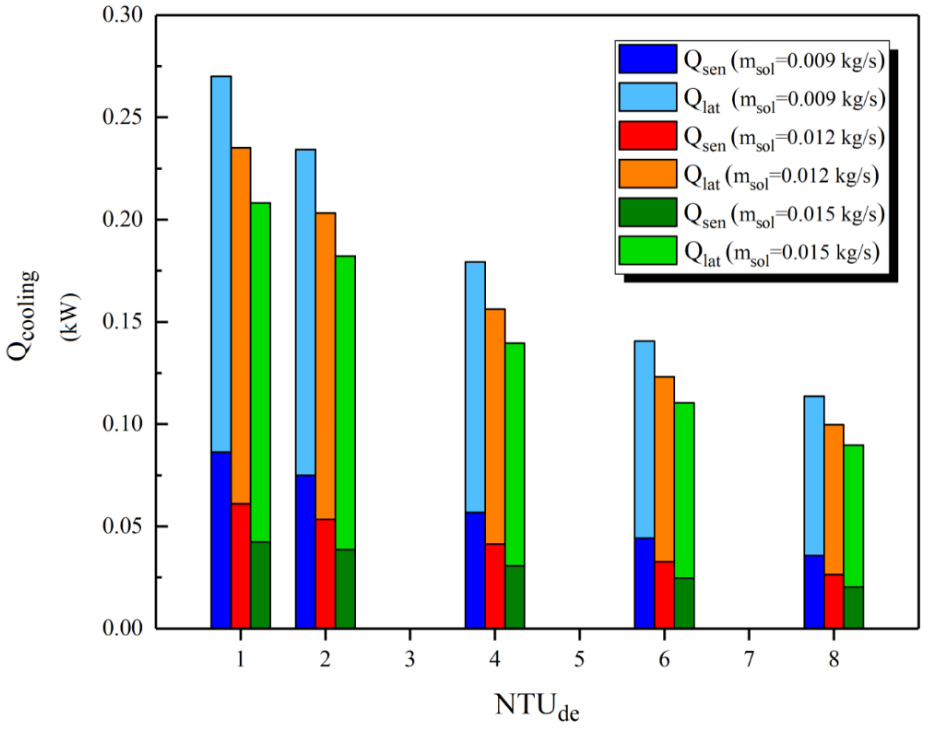


Fig 5- 8 Total cooling output $Q_{cooling}$ variations against NTU_{de} under various $\dot{m}_{sol}$

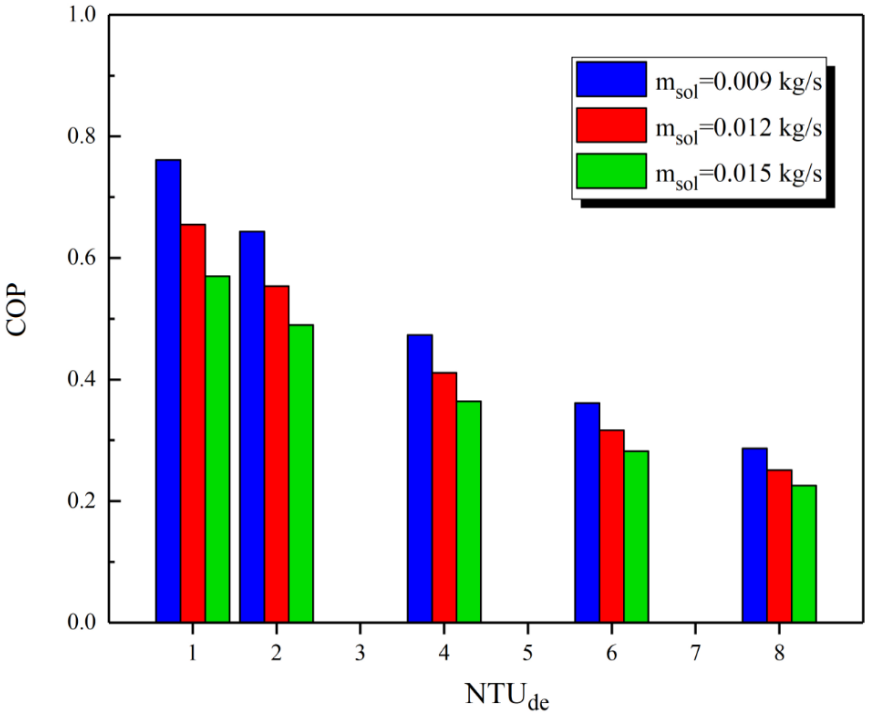


Fig 5- 9 COP variations against NTU_{de} under various $\dot{m}_{sol}$

As shown in Fig. 5-8, the latent cooling output Q_{lat} is significantly higher than the sensible cooling output Q_{sen} under all circumstances, in other words the latent cooling output accounts for the majority part of the total cooling out. For instance, under $\dot{m}_{sol} = 0.009$ kg/s and $NTU_{de} = 1$, the sensible cooling output is 0.086 kW while the latent cooling output is 0.184 kW, which is two times higher than the sensible cooling output. As mentioned in previous study [18], decreasing the solution inlet temperature could improve the cooling effect in the dehumidifier, however for the complete system in reality, sometimes it is not practical to cool the desiccant solution. That is the reason to set the desiccant solution temperature as 25℃ in this study. As the result, the dehumidifier outlet air temperature is too high to be supplied to conditioned space directly, so further cooling, such as indirect evaporative cooling, is required after dehumidification. Furthermore, under all solution flow rates, the sensible cooling output Q_{sen}, latent cooling output Q_{lat} and total cooling output Q_{tot} decrease considerably with NTU_{de}. For example, under $\dot{m}_{sol} = 0.009$ kg/s, when NTU_{de} increases from 1 to 8, Q_{sen} decreases from 0.086 kW to 0.036 kW, Q_{lat} decreases from 0.184 kW to 0.078 kW and Q_{tot} decreases from 0.270 kW to 0.114 kW. This is owing to significant decrease of $\dot{m}_{air,de}$ when increasing NTU_{de}. As discussed previously, although the dehumidification effectiveness is improved, the total cooling output is limited by dramatic decrease of the air flow rate. Similar results can be noticed from the variations of COP with NTU_{de} in Fig. 5-9. Under $\dot{m}_{sol} = 0.009, 0.012$ and $0.015\ kg/s$, when NTU_{de} increases from 1 to 8, the COP decreases from 0.761 to 0.287, 0.655 to 0.251 and 0.570 to 0.226 respectively. Based on the definition of NTU, for the dehumidifier or regenerator with the fixed geometry (fixed heat and mass transfer area) and solution type, NTU can be only changed by adjusting the air flow rate. Thus the moisture flux rate MFR, total cooling output $Q_{cooling}$ and COP would all reduce with NTU_{de} even though both the sensible and latent effectiveness of complete system can be improved.

5.6.2.2 Effects of regenerator side NTU_{re}

Similar to NTU_{de} effects, the influences of the regenerator side NTU_{re} are addressed in this section. The variations of $\varepsilon_{sen,sys}$, $\varepsilon_{lat,sys}$ and MFR with NTU_{re} under different solution mass flow rates are plotted in Figs 5-10 – 5-12.

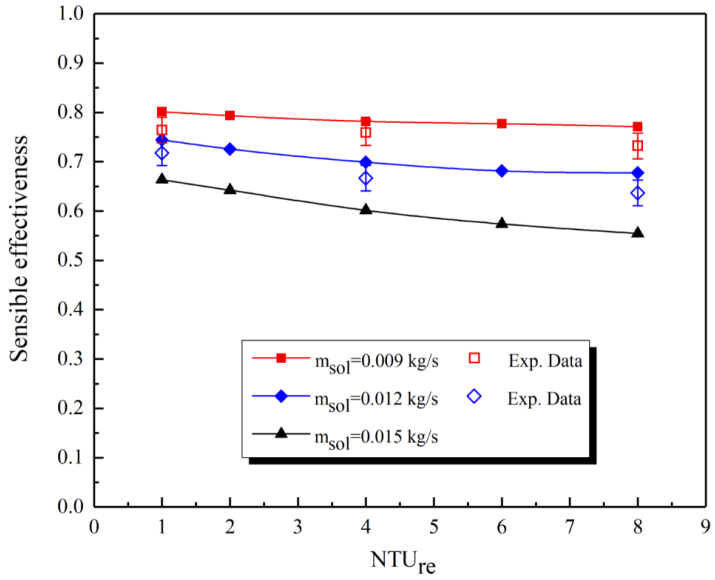


Fig 5- 10 System sensible effectiveness variations against NTU_{re} under various $\dot{m}_{sol}$

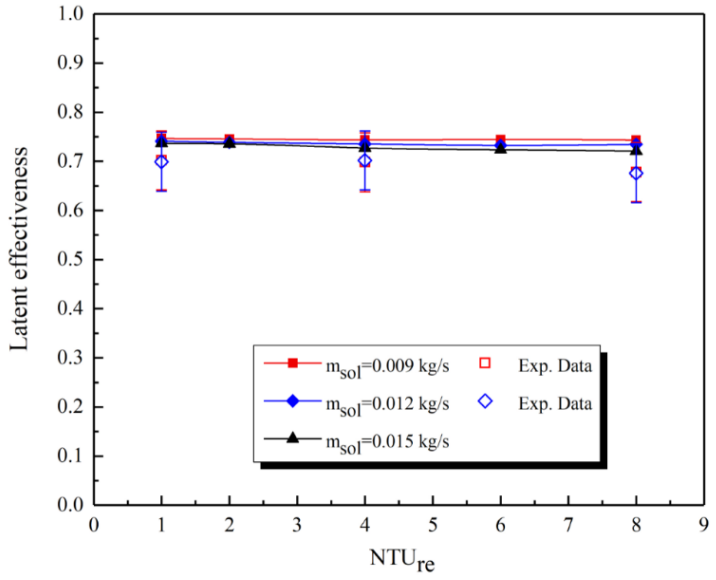


Fig 5- 11 System latent effectiveness variations against NTU_{re} under various $\dot{m}_{sol}$

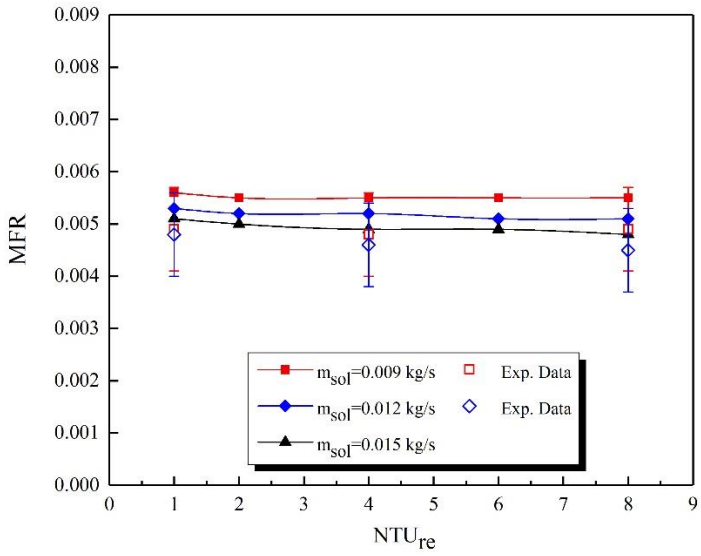


Fig 5- 12 Moisture flux rate variations against NTU_{re} under various $\dot{m}_{sol}$

According to Fig. 5-10, the influence of NTU_{re} on the system sensible effectiveness is different from that of NTU_{de}. The system sensible effectiveness decreases with NTU_{re}, and the decrease gradient is more noticeable when $\dot{m}_{sol}$ is relatively higher. Under $\dot{m}_{sol} = 0.009$ kg/s, $\varepsilon_{sen,sys}$ is decreased by 3.78% from 0.801 to 0.771 when NTU_{re} changes from 1 to 8, while it is decreased by 16.4% from 0.664 to 0.554 under $\dot{m}_{sol} = 0.015$ kg/s. However, the influence of NTU_{re} on the system sensible effectiveness is negligible compared with that of NTU_{de}. This is more obvious for the system latent effectiveness and MFR. It can be seen from Figs. 5-11 and 5-12 that neither $\varepsilon_{lat,sys}$ nor MFR has noticeable variation with NTU_{re}. For example, under $\dot{m}_{sol} = 0.009$ kg/s, $\varepsilon_{lat,sys}$ is only changed by 0.54% from 0.747 to 0.743 when NTU_{re} increases from 1 to 8. The effect of solution mass flow rate on $\varepsilon_{lat,sys}$ is negligible as well, when NTU_{re} changes from 1 to 8, $\varepsilon_{lat,sys}$ is reduced by 2.17% from 0.737 to 0.721 under $\dot{m}_{sol} = 0.015$ kg/s. The similar influence is for the moisture flux rate, for example when $\dot{m}_{sol} = 0.009, 0.012$ and 0.015 kg/s, MFR are decreased by 1.79%, 3.77% and 5.77% respectively. It is interesting that according to previous research [220] on influence

of NTU on the regenerator performance, NTU has considerable impact on the sensible and latent performance of the regenerator. This can be considered as a major difference between using the regenerator side effectiveness and system effectiveness. The major interests on the complete system are how much sensible and latent cooling the complete system can provide for a conditioned space during the dehumidification process. The NTU_{re}, which is adjusted by changing the air flow rate through the regenerator, has no obvious effect on the improvement of system sensible and latent cooling performance.

Furthermore, the variations of $Q_{cooling}$ and COP with NTU_{re} under different solution mass flow rates are given in Fig 5-13 and 5-14.

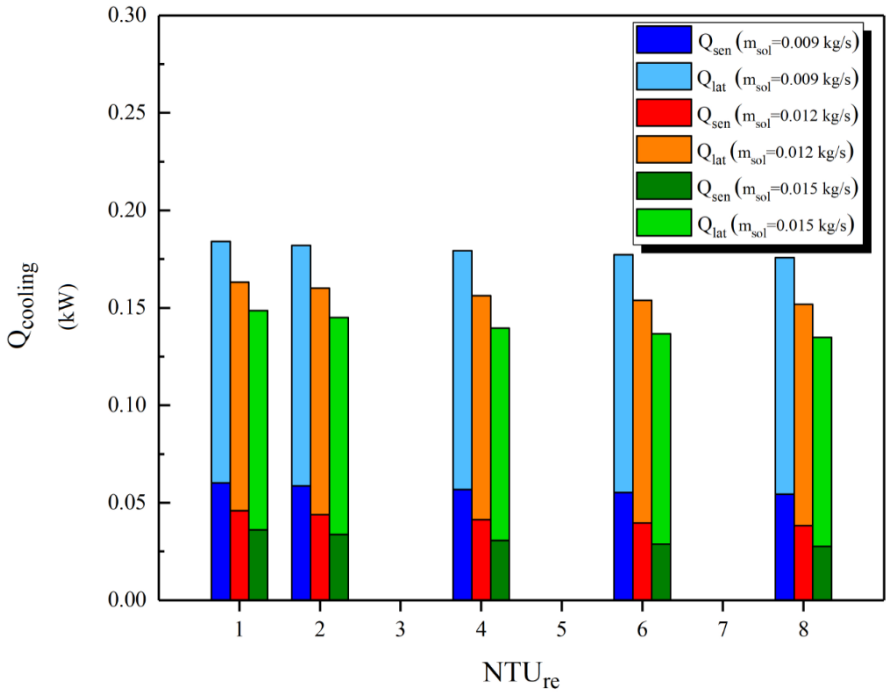


Fig 5- 13 Total cooling output $Q_{cooling}$ variations against NTU_{re} under various $\dot{m}_{sol}$

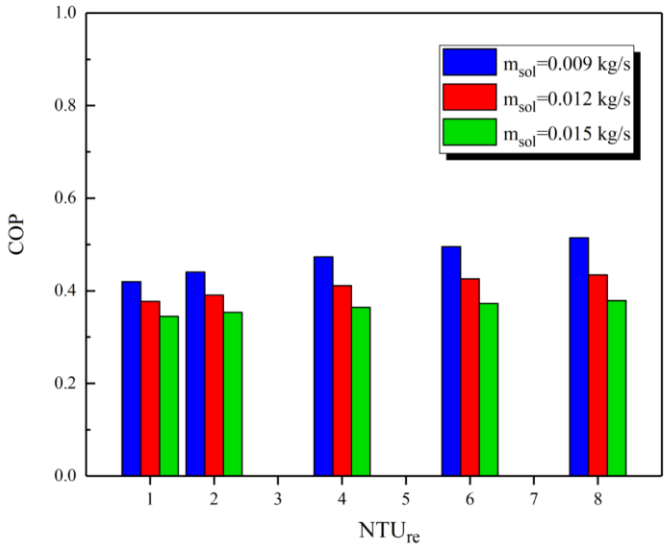


Fig 5- 14 COP variations against NTU_{re} under various $\dot{m}_{sol}$

Since the air mass flow rate through the dehumidifier remains constant, the sensible and latent cooling outputs are related to the system sensible and latent effectiveness directly, which are illustrated in Figs. 5-13 and 5-14. Under $\dot{m}_{sol} = 0.009$ kg/s, Q_{sen} decreases from 0.060 kW to 0.054 kW when NTU_{re} increases from 1 to 8, and this is caused by the decrease of $\varepsilon_{sen,sys}$. Similarly, since $\varepsilon_{lat,sys}$ and MFR are independent of NTU_{re}, Q_{lat} is relatively constant when NTU_{re} changes. For instance, under $\dot{m}_{sol} = 0.012$ kg/s, Q_{lat} only decreases by 5.3% from 0.113 to 0.107 when NTU_{re} increases from 1 to 8. It can be noticed that the latent cooling output again accounts for the majority of the total cooling output under all conditions. As the result, the total cooling output does not vary significantly with NTU_{re}. As $\dot{m}_{sol}$ is 0.009, 0.012 and 0.015 kg/s, the corresponding $Q_{cooling}$ decrease by 4.35%, 6.75% and 9.40% respectively when NTU_{re} increases from 1 to 8. NTU_{re} has positive effect on the system COP as displayed in Fig. 5-14. It is the fact that the total cooling output would decrease slightly with NTU_{re}, however the regeneration heat input would decrease as well. This is because increasing the air flow rate through the regenerator would significantly improve the regenerator latent effectiveness, as the result the regeneration of desiccant solution becomes easier and the regeneration energy input is reduced [220]. For $\dot{m}_{sol} = 0.009$ kg/s, with the increase of

NTU_{re} from 1 to 8, Q_{reg} reduces from 0.438 kW to 0.342 kW and COP increases from 0.420 to 0.514. Similarly, for $\dot{m}_{sol} = 0.015$ kg/s, Q_{reg} reduces from 0.431 kW to 0.356 kW and COP increases from 0.345 to 0.379 as NTU_{re} increases from 1 to 8.

5.6.2.3 Effects of mass flow rate ratio m^*

m^* is another important dimensionless parameter affecting system performance. It is defined in Eq. (3-33) as the ratio of solution mass flow rate over air mass flow rate. For the complete system, the solution mass flow rate is constant within the system since it is a closed loop. To address the influence of m^*, the air mass flow rates through the dehumidifier and regenerator are set equal. This is reasonable in practice since according to Fig. 5−3, the supply air flow rate from the dehumidifier and return air flow rate from conditioned space to the regenerator are the same. This setting is helpful for the balance of the air in the conditioned space. Following the same method, the variations of $\varepsilon_{sen,sys}$, $\varepsilon_{lat,sys}$ and MFR with m^* under different NTU values are plotted in Figs. 5−15 – 5−17.

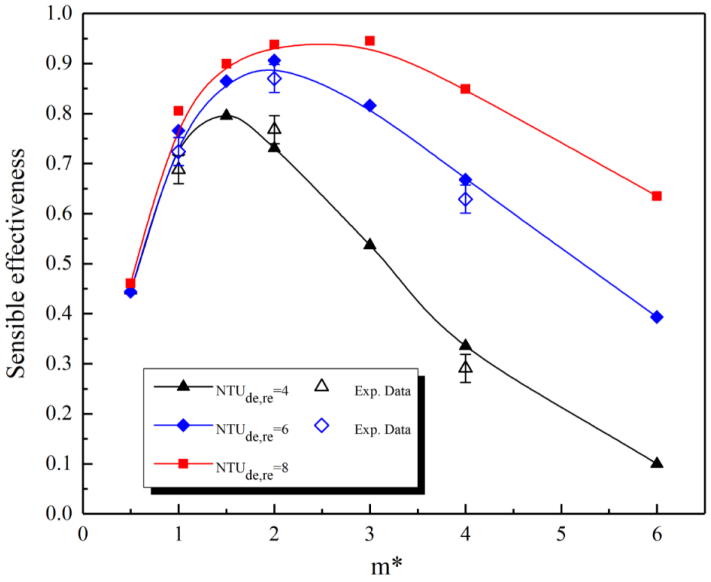


Fig 5- 15 System sensible effectiveness variations against m^* under various NTU

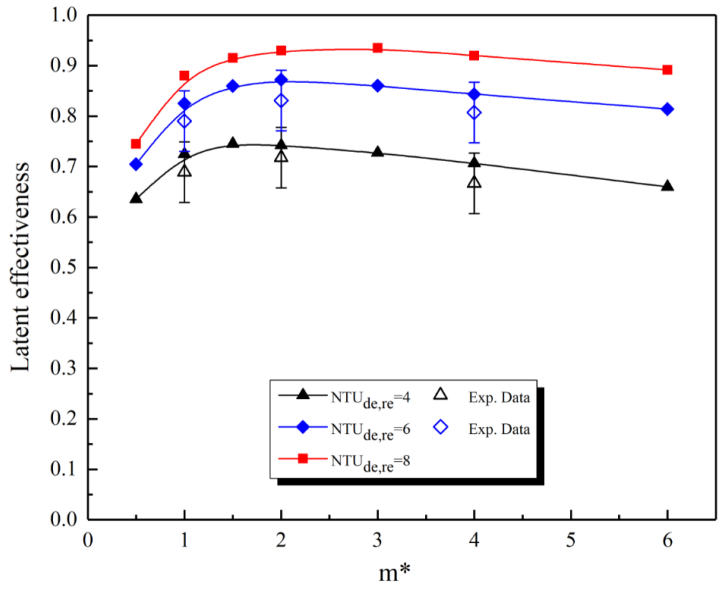


Fig 5- 16 System latent effectiveness variations against m^* under various NTU

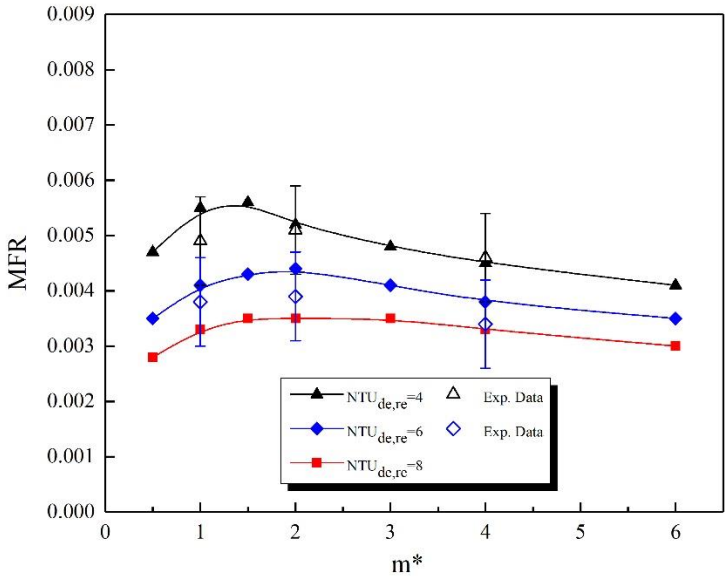


Fig 5- 17 Moisture flux rate variations against m^* under various NTU

It can be seen from Fig. 5−15 that the mass flow rate ratio has very strong impact on the system sensible effectiveness. Generally, it sharply increases with m^* at first, and then decreases gradually. Under $NTU_{de,re} = 4$, $\varepsilon_{sen,sys}$ increases from 0.446 to 0.796 when m^* changes from

0.5 to 1.5. When m^* keeps increasing to 6, $\varepsilon_{sen,sys}$ gradually decreases from 0.796 to 0.336. The variation trend is similar to that of $\varepsilon_{sen,sys}$ with $NTU_{de,re}$. Furthermore, the optimal mass flow rate ratio values, under which the system sensible effectiveness reaches its highest point, are different for different $NTU_{de,re}$. Under $NTU_{de,re} = 4$, $\varepsilon_{sen,sys}$ reaches its highest value of 0.796 when $m^* = 1.5$. By contrast, it reaches its highest value of 0.906 under $NTU_{de,re} = 6$ when $m^* = 2$, and 0.945 under $NTU_{de,re} = 8$ when $m^* = 3$. The variation of the system latent effectiveness with m^* is comparatively weaker than that of the system sensible effectiveness. Similar to the $\varepsilon_{sen,sys}$ variation, $\varepsilon_{lat,sys}$ increases with m^* before reaching its peak value, and then slowly decreases. The maximum values of $\varepsilon_{lat,sys}$ under $NTU_{de,re} = 4, 6$ and 8 are 0.745, 0.872 and 0.935, and their corresponding m^* are 1.5, 2 and 3 respectively. With regard to the moisture flux rate MFR as depicted in Fig. 5-17, it is found that MFR under high $NTU_{de,re}$ has low value. This has been explained in previous sections as high $NTU_{de,re}$ means low air mass flow rate. Even $\varepsilon_{sen,sys}$ and $\varepsilon_{lat,sys}$ would be improved, the total amount of moisture being absorbed would be reduced. Moreover, the variation of MFR with m^* has very similar trend as those of $\varepsilon_{sen,sys}$ and $\varepsilon_{lat,sys}$, it would decrease after reaching the peak value. The variation of MFR under $NTU_{de,re} = 8$ is comparatively weak compared with those under another $NTU_{de,re}$ values. It increases from 0.0028 to 0.0035 kg/kg dry air when m^* changes from 0.5 to 1.5, then it reduces to 0.003 kg/kg dry air when m^* reaches 6. Under $NTU_{de,re} = 6$, it peaks at $m^* = 2$ with the peak value of 0.0044 kg/kg dry air, and under $NTU_{de,re} = 4$, it peaks at $m^* = 1.5$ with the peak value of 0.0056 kg/kg dry air. To sum up, in practice when the air mass flow rate has been determined, there is no benefit by increasing the solution mass flow rate once it's beyond a specific value. To keep increasing the solution mass flow rate would dramatically reduce the system sensible effectiveness, its latent effectiveness and moisture flux rate would be restricted as well. Moreover, the high solution flow rate brings

more pump energy input to the system, which would drag down the COP, and this will be discussed later in this section. Then the variations of $Q_{cooling}$ and COP with m^* under different NTU values are shown in Fig 5-18 and 5-19.

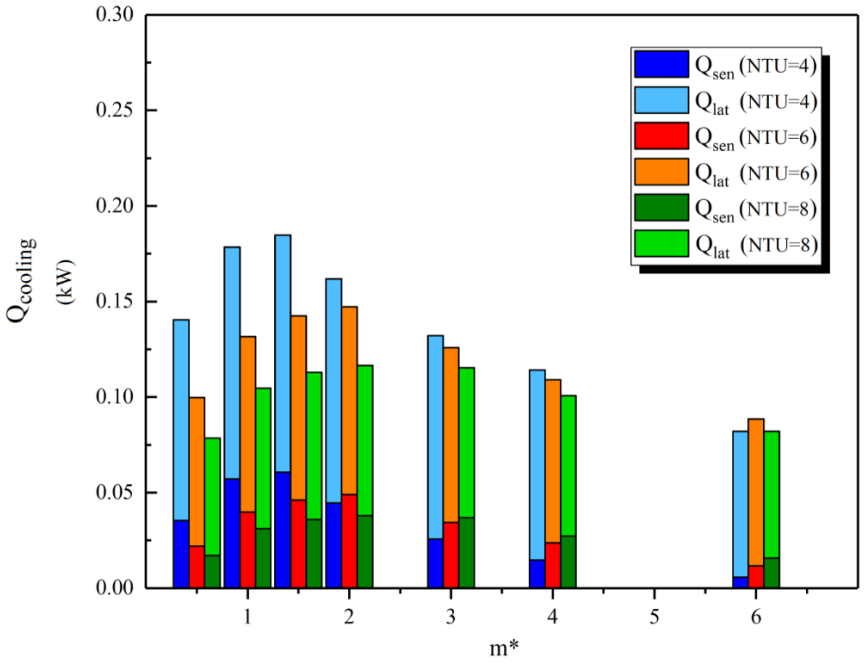


Fig 5- 18 Total cooling output $Q_{cooling}$ variations against m^* under various NTU

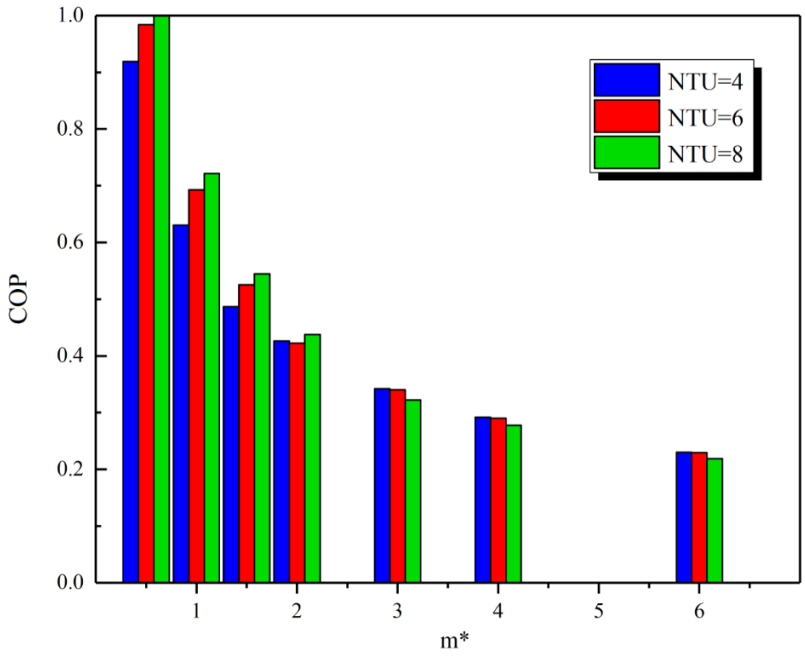


Fig 5- 19 COP variations against m^* under various NTU

Similar to Fig 5-8 and 5-13, Fig 5-18 clearly shows that the latent cooling output accounts for the majority of the total cooling output. The variation of $Q_{cooling}$ follows the similar trend of the system effectiveness's or moisture flux rate's. For $NTU = 4$, when m^* changes from 0.5 to 1.5, $Q_{cooling}$ increases from 0.140 kW to its maximum value of 0.185 kW. After that $Q_{cooling}$ decreases gradually to 0.114 kW. For $NTU = 6$, $Q_{cooling}$ peaks at 0.147 kW under $m^* = 2$, while for $NTU = 8$, it peaks at 0.117 kW under $m^* = 3$. In other words, the maximum total cooling outputs can be achieved at $m^* = 1.5$ under $NTU = 4$, at $m^* = 2$ under $NTU = 6$ and $m^* = 3$ under $NTU = 8$. However the COP would decline as m^* increases from 0.5 to 6, as shown in Fig. 5-19. Despite the variation of the cooling output with m^* is not in one direction, m^* has considerable effect on the denominator in Eq. (5-34). Since the dehumidifier and regenerator side $NTUs$ remain unchanged, so the fan power W_{fan} is constant. However m^* can be enhanced by increasing the solution flow rate in the closed solution loop, which would significantly increase the pump power W_{pump} and regeneration heat input Q_{reg}. For instance, under $NTU = 6$, Q_{reg} rises from 0.11 kW to 0.386 kW as m^* increases from 0.5 to 6. This also indicates that increasing m^* after excessing a critical value would not enhance the total cooling output, the system COP would be deteriorated as well.

5.6.3 Effects of solution inlet property

In this section, the effects of solution inlet property on the complete system are investigated. For the complete system, one of the controllable inputs is the solution inlet concentration in the dehumidifier $C_{sol,in}$. The variations of the effectiveness (sensible and latent effectiveness) and moisture flux rate with $C_{sol,in}$ are plotted in Fig. 5-20 when both NTU_{de} and NTU_{re} are set as

4, and m^* is set as 1, the changes of $Q_{cooling}$ and COP with $C_{sol,in}$ are given in Fig. 5-21 and Fig. 5-22 respectively.

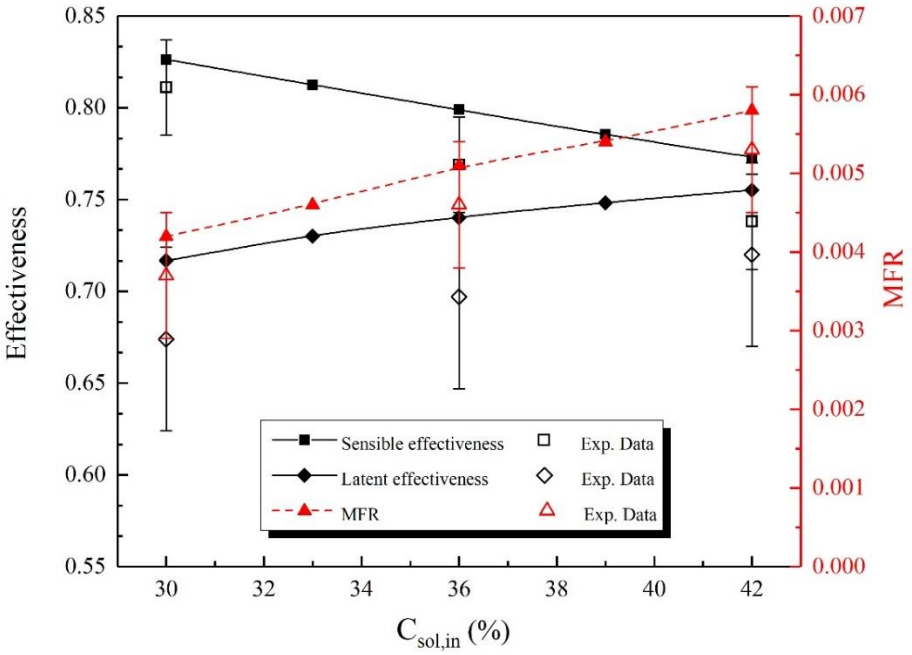


Fig 5- 20 Variations of effectiveness and moisture flux rate against $C_{sol,in}$

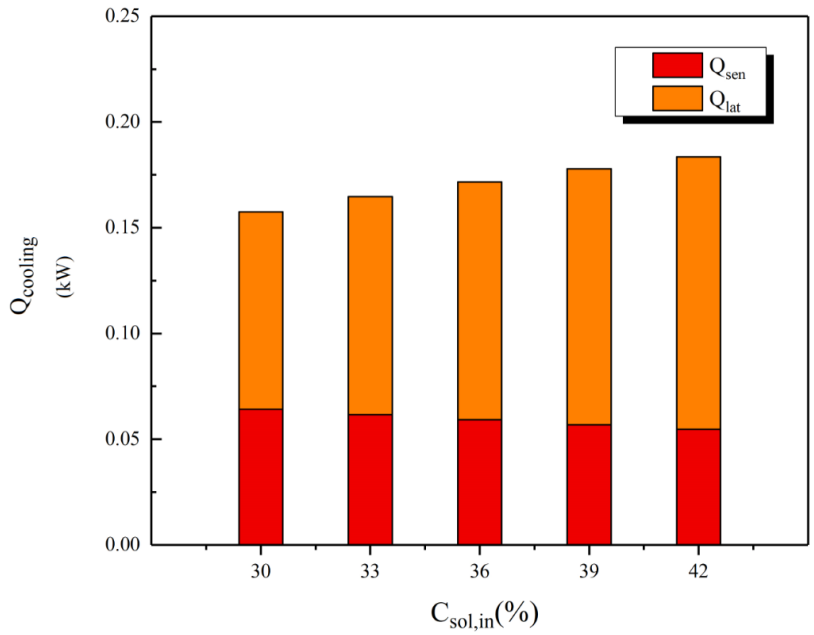


Fig 5- 21 Total cooling output $Q_{cooling}$ variations against $C_{sol,in}$

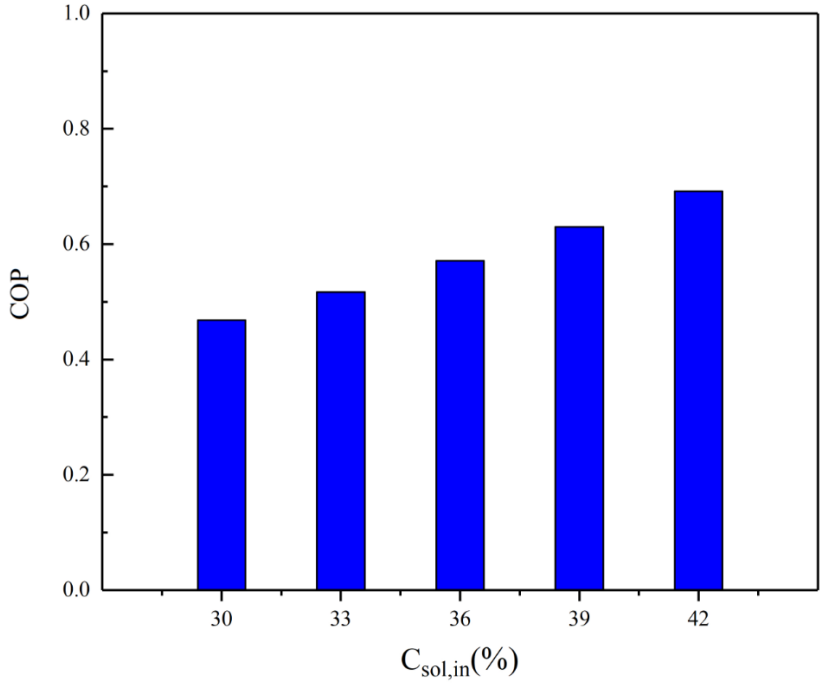


Fig 5- 22 COP variations against $C_{sol,in}$

As presented in Fig. 5-20, increasing the dehumidifier inlet solution concentration from 30% to 42% would improve the latent effectiveness from 0.717 to 0.755 and decrease the system sensible effectiveness from 0.826 to 0.773. Increasing the solution concentration will decrease the solution surface vapour pressure, as the result the solution absorption ability and the latent effectiveness are enhanced. Similarly, the moisture flux rate MFR is improved as well, it increases from 0.0042 to 0.0058 as $C_{sol,in}$ changes from 30% to 42%. In the meanwhile, the system sensible effectiveness decreases as the increased dehumidification ability will negatively affect the sensible effectiveness for more latent heat being released to the solution side. With regard to the cooling energy output, it can be seen in Fig. 5-21 that the sensible cooling output slightly decreases with $C_{sol,in}$, while the latent cooling output increases. Since only the solution inlet property is changed, both the solution and air mass flow rates remain constant, thus the variations of the sensible and latent cooling output have the direct

relationships with the sensible and latent effectiveness. So the sensible cooling output decreases from 0.064 kW to 0.055 kW, and the latent cooling output increases from 0.093 kW to 0.129 kW. As the result, the total cooling output $Q_{cooling}$ is improved slightly from 0.158 kW to 0.184 kW. As displayed in Fig. 5-22, $C_{sol,in}$ has considerable impact on the system COP. Although the total cooling output is improved, the change is almost negligible. Another important fact is that the regeneration energy Q_{reg} reduces with $C_{sol,in}$. For example, when $C_{sol,in}$ increases from 30% to 42%, Q_{reg} decreases by 21.36% from 0.337 kW to 0.265 kW. This is caused by the reduction of temperature difference between the inlet and outlet of the regenerator after rising the solution inlet concentration.

In real application, low solution temperature is not suitable to reduce energy consumption, thus increasing the solution inlet concentration in the dehumidifier is more applicable and would be a good way to improve the system dehumidification and energy performance. However, it should be mentioned that the use of highly concentrated solution may cause the solution crystallization, which would bring more problems such as mal-distribution, membrane fouling and high pumping pressure. Thus the operating condition should be assessed to avoid crystallization when using high concentration solution.

5.7 Summary

In this chapter, a complete membrane-based liquid desiccant dehumidification system that mainly contains a dehumidifier, a regenerator, a cold and a hot water supply units is investigated through performance evaluation and energy analysis. Heat and mass transfer in the dehumidifier and regenerator are studied by numerical simulation and experimental tests. The dehumidification performance is evaluated by the system sensible and latent effectiveness $\varepsilon_{sen,sys}$, $\varepsilon_{lat,sys}$ and moisture flux rate MFR, while its energy performance is assessed by the total cooling output $Q_{cooling}$ and coefficient of performance COP. The influences of main parameters are assessed respectively, which include the dehumidifier side NTU_{de}, regenerator side NTU_{re}, mass flow rate ratio $m^*$and solution inlet concentration in the dehumidifier $C_{sol,in}$. By comparing the numerical simulations and experimental data, it is shown that the highest relative errors are 13.29%, 12.72% and 12.96% for $\varepsilon_{sen,sys}$, $\varepsilon_{lat,sys}$ and MFR respectively. The main conclusions can be drawn as follows:

- The boundary conditions of the membrane surfaces in the dehumidifier and regenerator are neither uniform temperature nor uniform humidity ratio, and they change along the diagonal lines of the membranes.
- NTU_{de} and m^* are directly related to the solution and air mass flow rates in the dehumidifier. NTU_{de} and m^* have the most considerable impact on the system performance, while NTU_{re} and $C_{sol,in}$ have relatively weak influences.
- The system sensible and latent effectiveness can be improved by up to 0.62 and 0.65 respectively by increasing NTU_{de} from 1 to 6, however their increasing gradients hardly change when NTU_{de} exceeds its critical value $NTU_{de,crit}$ of 6 in this study.

- Although the system effectiveness increase with NTU_{de} , the total amount of moisture being absorbed, $Q_{cooling}$ and COP decrease with NTU_{de}. Thus there is no meaning to raise NTU_{de} over $NTU_{de,crit}$ for the performance improvement.
- The latent cooling output Q_{lat} is significantly (up to 3.92 times under $NTU_{de} = 1$ and $NTU_{re} = 4$) higher than the sensible cooling output Q_{sen}, so the process air should be further cooled after being dehumidified.
- The system effectiveness, moisture removal flux rate and cooling output increase with m^* initially, but then decrease. The corresponding m^* for the highest values are different for various NTU values (such as 1.5 for $NTU = 4$, 2 for $NTU = 6$ and 3 for $NTU = 6$ respectively). It is preferable to keep m^* at or below its critical value as further increasing m^* would reduce the system COP.
- Increasing the solution inlet concentration for the dehumidifier is more applicable to improve the system dehumidification and energy performance compared with reducing the solution temperature. However the problem of crystallization should be avoided when applying high concentration solution.

Chapter 6: Parametric analysis of mixed LiCl-$CaCl_2$ solution and optimum mixing ratio selection

6.1 Introduction

In Chapters 3 – 5 the performance of single dehumidifier, single regenerator and the complete system have been discussed using the pure LiCl as the working liquid. However, as stated in the literature review, compared with the single desiccant solution, some mixed desiccant solutions have the better dehumidification efficiency, lower material cost and energy consumption. The objective of this chapter is to investigate the effects of the mixed LiCl-$CaCl_2$ desiccant solution properties (i.e. temperature T_{sol}, concentration C_{sol} and mixing ratio of LiCl and $CaCl_2$) on the performance of a membrane-based liquid desiccant dehumidification system by numerical modelling and experimental tests. Section 6.2 introduces the calculation method for mixed liquid desiccant properties; Section 6.3 shows the numerical method for the dehumidification system; Section 6.4 introduces the performance evaluation indices; Section 6.5 illustrates the experimental set-up for the model validation; Section 6.6 validates the numerical model; Section 6.7 investigates the mixed solution system performance and Section 6.8 is the summary. By comparing with the experimental results, this chapter comes out a method to predict the system performance with the mixed solution by combining an electrolyte non-random two-liquid (NRTL) method and numerical modelling. It presents a comprehensive investigation on the effects of the mixed LiCl-$CaCl_2$ desiccant properties on the membrane-based liquid desiccant dehumidification system, and provides an approach for the optimum mixing ratio selection through the system performance and COP analyses.

6.2 Mixed liquid desiccant properties calculation

The predictions of the mixed desiccant properties (such as surface vapour pressure and specific humidity ratio) under different mixing ratios, temperatures and concentrations are of vital importance. As presented in the introduction section, the SMR method is only capable of predicting the mixed desiccant properties when its concentration is lower than 10%. By contrast, the NRTL method provides more accurate calculation for the mixed desiccant solution with over 30% concentration. The NRTL method uses only binary parameters to correlate and predict the deviation from ideality of aqueous multi-component electrolyte system over the entire ranges of temperature and concentration [169]. Thus the NRTL method is adopted in this study to calculate the mixed desiccant surface vapour pressure.

The vapour-liquid equilibrium relation for water in an electrolyte solution can be given as [167]:

$$a_w = \frac{P_{v,sol}}{P_{v,w}} \tag{6-1}$$

$$a_w = x_w f_w \tag{6-2}$$

Where a_w is activity of water; $P_{v,sol}$ and $P_{v,w}$ are vapour pressures of the solution and water respectively (Pa); x_w is mole concentration of water; f_w is activity coefficient of water.

The vapour pressure of water can be obtained by using August-Roche-Magnus equation [221] :

$$P_{v,w} = 0.61094 exp\left(\frac{17.625T}{T+243.04}\right) \tag{6-3}$$

Where $P_{v,w}$ is water vapour pressure (kPa); T is water temperature (℃).

The solution vapour pressure can be obtained once the activity of water is determined, which is the product of water mole concentration x_w and activity coefficient f_w. The calculation of f_w can be divided into two parts: long-range and short-range interaction contributions, as can be expressed as [167]:

$$lnf_w = lnf_w^{LRC} + lnf_w^{SRC} \tag{6-4}$$

The long-range interaction contribution f_w^{LRC} can be calculated by using Pitzer-Debye-Huckel function:

$$ln f_w^{LRC} = \left(\frac{1000}{M_w}\right)\frac{2A_\phi I_x^{3/2}}{1+\chi I_x^{1/2}} \quad (6\text{-}5)$$

Where M_w is molecular weight of water, which is 0.018 kg/mol; A_ϕ is Debye-Huckel constant for the osmotic coefficient, which is 0.391; I_x is ionic strength in mole fraction, which equals $0.5\sum x_i z_i^2$, where x_i is mole fraction of any species in the mixed desiccant solution, and z_i is corresponding absolute value of ionic charge ; χ is the closest approach parameter of the Pitzer-Debye-Huckel equation, which is 14.9.

For the LiCl-$CaCl_2$ desiccant, Eq. (6-5) can be derived to:

$$ln f_w^{LRC} = 5.829 \times \frac{x_{LiCl}+3x_{CaCl_2}}{1+14.9(x_{LiCl}+3x_{CaCl_2})^{1/2}} \quad (6\text{-}6)$$

The short-range interaction in LiCl-$CaCl_2$ electrolyte can be expressed as:

$$ln f_w^{SRC} = (-x_w)\frac{2A\tau_{LiCl,w}x_{LiCl}+4B\tau_{CaCl_2,w}x_{CaCl_2}}{\left(2Ax_{LiCl}+4Bx_{CaCl_2}+x_w\right)^2} + \frac{2A\tau_{LiCl,w}x_{LiCl}+4B\tau_{CaCl_2,w}x_{CaCl_2}}{1+(2A-2)x_{LiCl}+(4B-3)x_{CaCl_2}} + (x_{LiCl}A') \times$$

$$\frac{\tau_{w,LiCl}x_{LiCl}+2\left[C'(\tau_{w,LiCl}-\tau_{CaCl_2,LiCl})+2\tau_{w,LiCl}\right]x_{CaCl_2}}{\left[(1-2A')x_{LiCl}+(2C'+2-3A')x_{CaCl_2}+A'\right]} + \left(2B'x_{CaCl_2}\right) \times$$

$$\frac{\left[C(\tau_{w,CaCl_2}-\tau_{LiCl,CaCl_2})+\tau_{w,CaCl_2}\right]x_{LiCl}+2\tau_{w,CaCl_2}x_{CaCl_2}}{\left[(C+1-2B')x_{LiCl}+(2-3B')x_{CaCl_2}+B'\right]^2} + (x_{LiCl}A') \times$$

$$\frac{\tau_{w,LiCl}x_{LiCl}+2C'(\tau_{w,LiCl}-\tau_{CaCl_2,LiCl})x_{CaCl_2}}{\left(x_{LiCl}+2C'x_{CaCl_2}+A'x_w\right)^2} + (2B'x_{CaCl_2}) \times \frac{C(\tau_{w,CaCl_2}-\tau_{LiCl,CaCl_2})x_{LiCl}+2\tau_{w,CaCl_2}x_{CaCl_2}}{(Cx_{LiCl}+2x_{CaCl_2}+B'x_w)^2} \quad (6\text{-}7)$$

Where A, B, C, A', B' and C' represent:

$A = e^{(-0.2\tau_{LiCl,w})}$

$B = e^{(-0.2\tau_{CaCl_2,w})}$

$C = e^{(-0.2\tau_{LiCl,CaCl_2})}$

$A' = e^{(-0.2\tau_{w,LiCl})}$

$B' = e^{(-0.2\tau_{w,CaCl_2})}$

$C' = e^{(-0.2\tau_{CaCl_2,LiCl})}$

Where $\tau_{LiCl,w}$, $\tau_{CaCl_2,w}$, $\tau_{w,LiCl}$, $\tau_{w,CaCl_2}$, $\tau_{LiCl,CaCl_2}$ and $\tau_{CaCl_2,LiCl}$ are binary interaction energy parameters, which are given at 25℃ and listed in Table 6-1.

Table 6- 1 Parameters of binary interaction energy for mixed solution activity coefficient calculation (25℃) [167]

parameter	$\tau_{LiCl,w}$	$\tau_{CaCl_2,w}$	$\tau_{w,LiCl}$	$\tau_{w,CaCl_2}$	$\tau_{LiCl,CaCl_2}$	$\tau_{CaCl_2,LiCl}$
value	-5.1737	-5.2549	10.1242	10.5126	0	0

For the binary interaction energy parameters at different temperatures, the following correlation should be applied [167]:

$$\tau_{(T)} = \frac{298.15}{T+273.15}\tau_{(25℃)} \quad (6\text{-}8)$$

Where $\tau_{(25℃)}$ is binary interaction energy parameter at 25℃ as given in Table 6-1.

In Eq. (6-7), x_{LiCl} and x_{CaCl_2} are mole concentrations of LiCl and $CaCl_2$ respectively, and there exits such a relationship:

$$x_{LiCl} + x_{CaCl_2} + x_w = 1 \quad (6\text{-}9)$$

Then the mixed solution vapour pressure $P_{v,sol}$ can be obtained by solving Eqs. (6-1) - (6-9). Once $P_{v,sol}$ is obtained, the solution specific humidity ratio W_{sol} (kg/kg dry air) can be calculated by [214]:

$$W_{sol} = 0.62198\frac{P_{v,sol}}{P-P_{v,sol}} \quad (6\text{-}10)$$

Where P is atmospheric pressure (Pa).

The other mixed solution properties, for example density and specific heat capacity, are calculated using the simple mixing role (SMR) method. This method is explained as below:

Any property of mixed solution S containing solution a and solution b can be calculated by:

$$S = S_a\varphi_a + S_b\varphi_b \tag{6-11}$$

Where S_a and S_b are properties of each component, and φ_a and φ_b are mass fractions of each component, so there is:

$$\varphi_a + \varphi_b = 1 \tag{6-12}$$

6.3 Numerical modelling

The numerical modelling method used for the mixed solution dehumidification is the same as that used for the pure solution system as explained in Chapter 3, Section 3.2.

6.4 Performance evaluation indices

6.4.1 Effectiveness of dehumidifier

The effectiveness as a critical index applied for the performance evaluation of a heat and mass exchanger has been applied for performance evaluation in previous chapters. Thus in this chapter, sensible effectiveness (ε_{sen}) and latent effectiveness (ε_{lat}) are used for the dehumidifier performance evaluation:

$$\varepsilon_{sen} = \frac{T_{air,in} - T_{air,out}}{T_{air,in} - T_{sol,in}} \tag{6-13}$$

$$\varepsilon_{lat} = \frac{W_{air,in} - W_{air,out}}{W_{air,in} - W_{sol,in}} \tag{6-14}$$

Where $T_{air,out}$ is air outlet temperature (℃), and $W_{air,out}$ is air outlet humidity ratio (kg/kg dry air).

6.4.2 Moisture flux rate

The moisture removal rate (MRR) is an evaluation of the quantity of moisture absorbed by dry air from the weak liquid desiccant during regeneration, or the quantity of moisture in moist air absorbed by the strong liquid desiccant during dehumidification. For the dehumidifier, it is expressed as:

$$MRR = \dot{m}_{air}\left(W_{air,in} - W_{air,out}\right) \tag{6-15}$$

Afterward, the moisture flux rate (MFR) is presented:

$$MFR = \frac{MRR}{U_m A} = \frac{\dot{m}_{air}\left(W_{air,in} - W_{air,out}\right)}{U_m A} \tag{6-16}$$

MFR has been used for the performance evaluation of regenerator and the complete system in Chapter 4 and 5. It is the ratio of moisture removal rate MRR over the membrane overall mass transfer conductance. In this study the MFR is used for performance analysis rather than the MFF since compared with the MRR, the MFR is independent of the dehumidifier size and it is only related to inlet state.

6.4.3 Coefficient of performance (COP)

The COP of the membrane-based liquid desiccant dehumidification system can be defined as:

$$COP = \frac{Q_{sen} + Q_{lat}}{Q_{reg}} \tag{6-17}$$

Where Q_{sen}, Q_{lat} and Q_{reg} are sensible cooling output, latent cooling output and regeneration power input (kW) respectively, which can be calculated by:

$$Q_{sen} = \dot{m}_{air} c_{p,air} (T_{air,in} - T_{air,out}) \tag{6-18}$$

$$Q_{lat} = MRR \times h_{fg} = \dot{m}_{air} h_{fg} \left(W_{air,in} - W_{air,out}\right) \tag{6-19}$$

$$Q_{reg} = \dot{m}_{sol} c_{p,sol} (T_{reg} - T_{sol,out}) \tag{6-20}$$

Where $T_{sol,out}$ is solution temperature at the dehumidifier outlet (℃), T_{reg} is required solution temperature at the regenerator inlet (℃).

6.5 Experimental set-up

The experimental rig used for the mixed solution dehumidification system is the same as that used for the pure solution dehumidification system as illustrated in the previous Chapter. The schematic diagram of the system is shown in Fig 6-1.

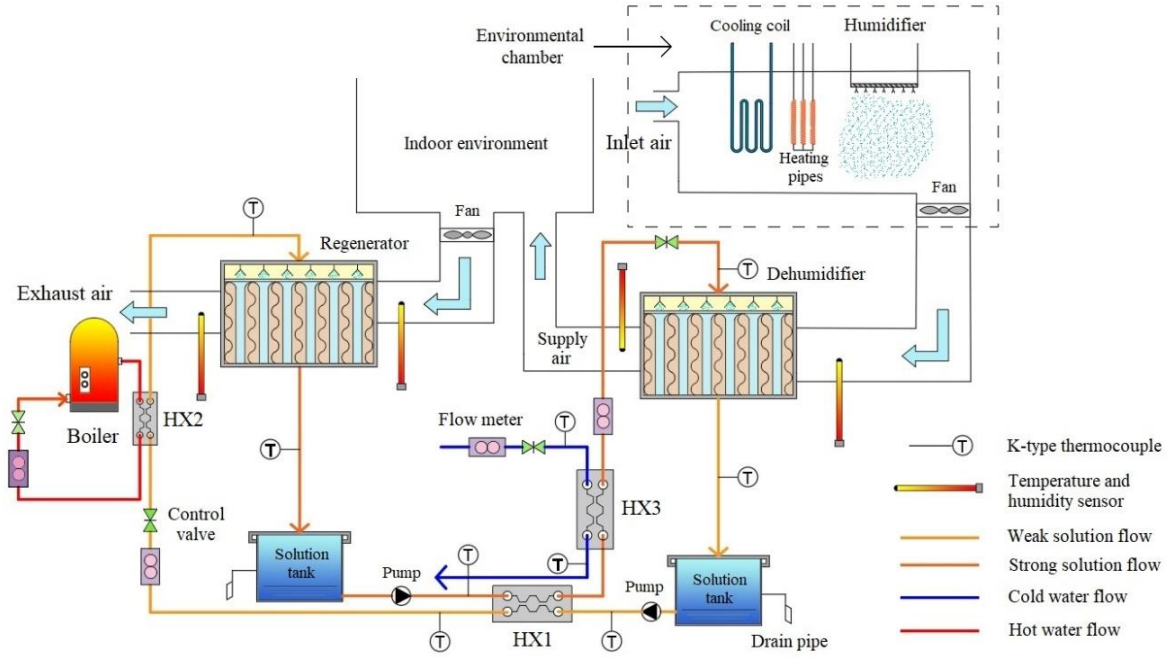


Fig 6- 1 Schematic diagram of the mixed solution dehumidification system

Detailed explanation of the operation of the experimental testing has been given in the previous chapter. It should be mentioned that to make the mixed solution with the specific mixing ratio and concentration, firstly the mixing ratio is achieved at a low concentration, then more LiCl and $CaCl_2$ are added to the mixed solution to increase its concentration. For example, to make a 1:1 mixed solution, the same amounts of LiCl and $CaCl_2$ are added into water to make a 30% mixed solution. Then the water remains unchanged, more LiCl and $CaCl_2$ with the same

amount are added into the solution to increase its concentration (e.g. 36% and 39%). This procedure is also used for the other mixing ratios.

6.6 Numerical model validation

The numerical model and NRTL method are validated by experimental data. The experiment process consists of two stages, and total 28 tests under different designed operating conditions have been completed in this study. At first, 15 tests are carried out to verify the sensible and latent effectiveness. The operating conditions, together with numerically obtained and experimentally collected values of the effectiveness are given in Table 6-2. Another 13 tests are conducted in the second stage to validate the moisture flux rate. The solution and air mass flow rates are kept constant through all the tests for the same m^* and NTU. The moisture flux rate comparisons between the numerical calculations and the experimental data are given in Table 6-3.

It can be seen in Table 6-2 that the simulation results of ε_{sen} and ε_{lat} generally are in accordance with the measurement data. The maximum discrepancies for ε_{sen} and ε_{lat} are 3.679% and 6.257% respectively. The maximum difference for the MFR is 15.510% as indicated in Table 6-3. As seen, generally the numerical model predicts the heat and moisture transfer in the dehumidifier well. The numerical modelling results are in good agreement with experimental data, and they have similar variation trends. This means the developed numerical model with the NRTL method predicts the system performance accurately and can predict the characteristics of this system rather successfully.

Table 6- 2 Sensible and latent effectiveness under various designed operating conditions, comparison of numerical and experimental results

Designed operating conditions						Comparisons					
$T_{sol,in}$ (℃)	$C_{sol,in}$ (%)	X_{LiCl}	X_{CaCl2}	m_{air} (kg/s)	m_{sol} (kg/s)	$\varepsilon_{sen,num}$	$\varepsilon_{sen,exp}$	Error (%)	$\varepsilon_{lat,num}$	$\varepsilon_{lat,exp}$	Error (%)
16	30	1	0	0.0495	0.099	0.8604	0.838	2.603	0.7012	0.687	2.025
16	30	2	1	0.0495	0.099	0.8555	0.825	3.565	0.7486	0.714	4.622
16	30	1	1	0.0495	0.099	0.8530	0.832	2.462	0.7807	0.739	5.341
16	30	1	2	0.0495	0.099	0.8504	0.829	2.516	0.8216	0.803	2.264
16	30	0	1	0.0495	0.099	0.8448	0.815	3.527	0.9454	0.894	5.437
16	36	1	0	0.0495	0.099	0.8479	0.818	3.526	0.7658	0.732	0.414
16	36	2	1	0.0495	0.099	0.8427	0.813	3.524	0.8046	0.785	2.436
16	36	1	1	0.0495	0.099	0.8399	0.809	3.679	0.8311	0.796	4.223
16	36	1	2	0.0495	0.099	0.8371	0.807	3.596	0.8658	0.818	5.521
16	36	0	1	0.0495	0.099	0.8310	0.808	2.768	0.9810	0.921	6.116
14	36	1	0	0.0495	0.099	0.8596	0.841	2.164	0.7738	0.760	1.783
14	36	2	1	0.0495	0.099	0.8548	0.830	2.901	0.8062	0.782	3.001
14	36	1	1	0.0495	0.099	0.8522	0.827	2.957	0.8282	0.799	3.526
14	36	1	2	0.0495	0.099	0.8496	0.826	2.778	0.8566	0.803	6.257
14	36	0	1	0.0495	0.099	0.8440	0.817	3.200	0.9486	0.893	5.861

Table 6- 3 Moisture flux rates under different designed operating conditions, comparison of numerical and experimental results

Designed operating conditions						Comparisons		
$T_{sol,in}$ (℃)	$C_{sol,in}$ (%)	X_{LiCl}	X_{CaCl2}	m_{air} (kg/s)	m_{sol} (kg/s)	MFR	MFR_{exp}	Error (%)
16	24	1	1	0.0495	0.099	0.00396	0.0037	6.575
16	30	1	1	0.0495	0.099	0.00485	0.0041	15.510
16	36	1	1	0.0495	0.099	0.00571	0.0053	7.209
16	42	1	1	0.0495	0.099	0.00640	0.0058	9.425
12	36	1	1	0.0495	0.099	0.00609	0.0054	11.393
14	36	1	1	0.0495	0.099	0.00591	0.0056	5.288
16	36	1	1	0.0495	0.099	0.00571	0.0053	7.209
18	36	1	1	0.0495	0.099	0.00549	0.0048	12.570
16	36	1	0	0.0495	0.099	0.00573	0.00572	0.175
16	36	2	1	0.0495	0.099	0.00572	0.0057	3.197
16	36	1	1	0.0495	0.099	0.00571	0.00569	3.809
16	36	1	2	0.0495	0.099	0.00570	0.00566	7.886
16	36	0	1	0.0495	0.099	0.00569	0.00565	7.150

6.7 Results and discussion

6.7.1 Specific humidity of the mixed desiccant solution

Instead of the surface vapour pressure, the equilibrium specific humidity of the mixed solution is adopted to evaluate solution capability to absorb vapour since it is more straight-forward. Based on Eqs. (6-1) - (6-10), the specific humidity of the mixed desiccant solution is related to its temperature, concentration and solute mixing ratio. The mixed solutions with concentration of 15%, 30% and 42% are used in this study, and five different mass fraction ratios between LiCl and $CaCl_2$ are adopted: 1:0 (pure LiCl solution), 2:1, 1:1, 1:2 and 0:1(pure $CaCl_2$ solution) for each concentration. The variations of the solution specific humidity with temperature for different mixing ratios under the three concentrations are plotted in Figs 6-2 – 6-4.

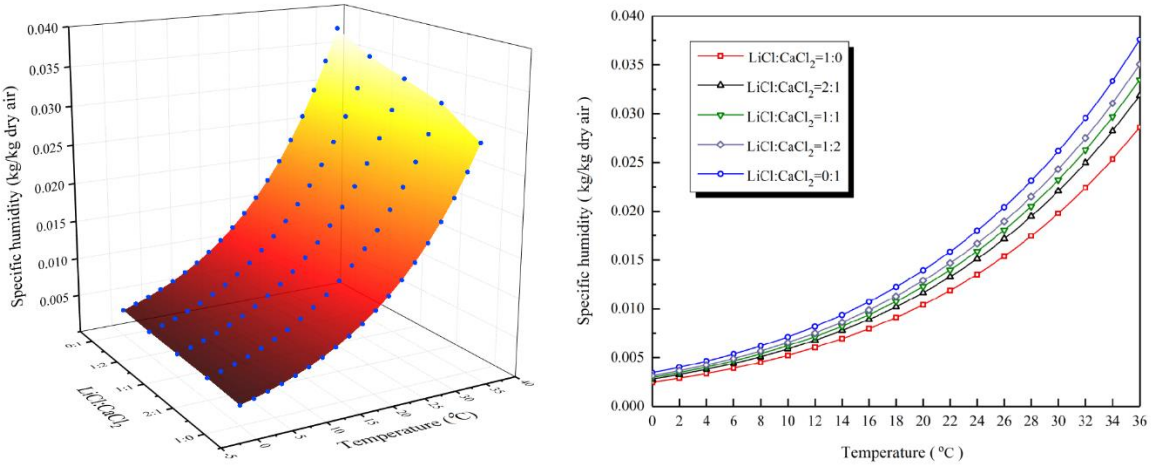


Fig 6- 2 Mixed solution specific humidity variations with temperature for different mixing ratios under $C_{sol} = 15\%$

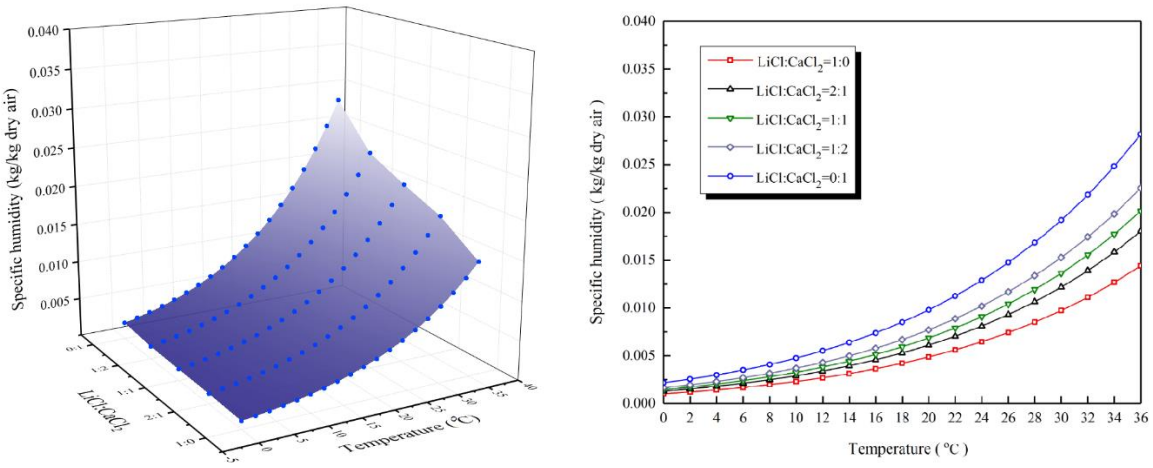


Fig 6- 3 Mixed solution specific humidity variations with temperature for different mixing ratios under $C_{sol} = 30\%$

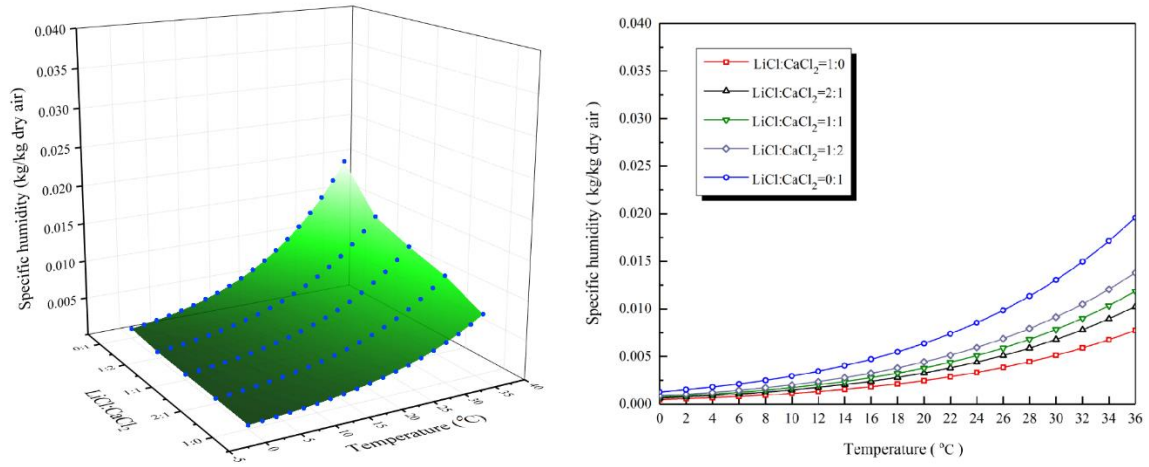


Fig 6- 4 Mixed solution specific humidity variations with temperature for different mixing ratios under $C_{sol} = 42\%$

As shown in these figures, the mixed solution specific humidity increases with its temperature. For the solution with the low concentration, its temperature influence is larger than that with the high concentration. For example, under $C_{sol} = 15\%$, the specific humidity of the 1:1 mixed solution is increased by 0.03051 (from 0.00297 to 0.03348) kg/kg when its temperature rises from 0℃ to 36℃. By contrast, it is increased by 0.0111 (from 0.00073 to 0.01183) kg/kg under

$C_{sol} = 42\%$. In contrast, increasing the solution concentration can enhance the dehumidification ability as well by reducing the solution specific humidity. Taking the 1:1 mixed solution as an example, its maximum specific humidity under C_{sol} of 15%, 30% and 42% are 0.0335, 0.0202 and 0.0118 kg/kg respectively. Apart from T_{sol} and C_{sol}, the mixing ratio is another important parameter influencing the solution specific humidity, which is the main focus of this paper. According to Figs 6-2 – 6-4, the solution specific humidity decreases with LiCl mass fraction at the given concentration and temperature, this is because pure $CaCl_2$ solution always has the higher specific humidity compared with pure LiCl solution. It is noticed that the influences of the solution temperature, concentration and mixing ratio are interacted with each other. Under the same concentration, the impact of the mixing ratio is insignificant when the solution temperature is relatively low. For example, under $C_{sol} = 42\%$, the specific humidity difference between LiCl and $CaCl_2$ solutions at 36℃ is 0.01185 kg/kg, while the difference is only 0.00213 kg/kg at 12℃. Furthermore, the influence of the mixing ratio increases with the solution concentration, which is illustrated in Fig 6-5. It can be seen that the specific humidity difference between LiCl and $CaCl_2$ solutions under 15% is much smaller than that under 42%, meaning the mixing ratio has more significant influence on the solution specific humidity under the high concentration. The solution with high concentration is preferred in dehumidification, increasing LiCl mass fraction leads to the significant performance improvement.

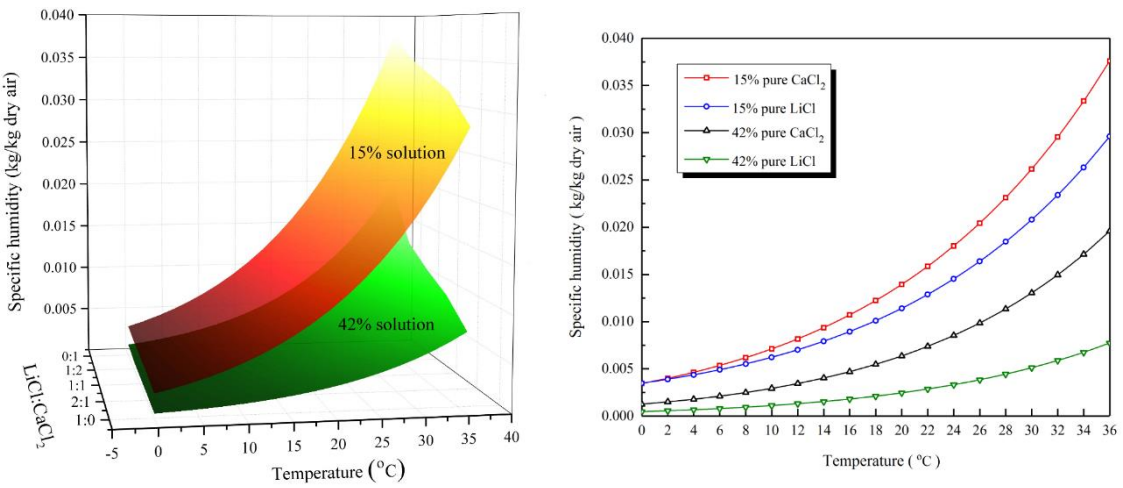


Fig 6- 5 Mixed solution specific humidity variations for pure LiCl and $CaCl_2$ solutions under different concentrations

6.7.2. Impact of the mixed solution property on cooling effect

To cool the supply air in the dehumidifier is of vital importance since the air with low temperature can save energy used for the subsequent cooling. The cooling effect is evaluated by the sensible effectiveness introduced in Section 6.4.1. The variations of the sensible effectiveness with the mixing ratio under various solution concentrations and temperatures are given in Figs 6-6 and 6-7.

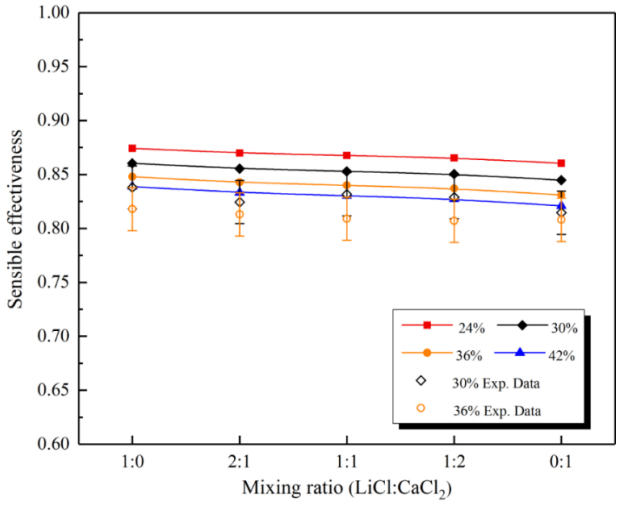


Fig 6- 6 Sensible effectiveness changes with the mixing ratio under different solution concentrations

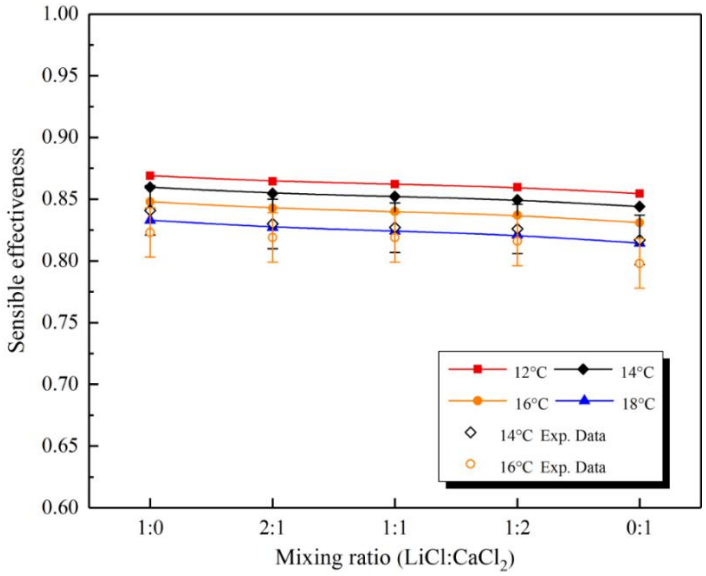


Fig 6- 7 Sensible effectiveness changes with the mixing ratio under different solution temperatures

It is noticed from these two figures that the sensible effectiveness increases with LiCl mass fraction in the mixed solution, but very weakly. For instance, for the 42% concentration solution, its sensible effectiveness only increases by 2.18% (from 0.8209 to 0.8388) when the mixing ratio ($LiCl:CaCl_2$) changes from 0:1 to 1:0. Similarly, at the solution temperature of 18℃, the sensible effectiveness also increases by 2.28% (from 0.8144 to 0.833) when the mixing ratio changes from 0:1 to 1:0. The dehumidification capacity increases with LiCl mass fraction as well, meaning more latent heat is released. However the sensible effectiveness increases slight rather than being deteriorated. A reasonable explanation for this is given as follows. The air temperature change is induced by two parts: sensible temperature decrease and temperature increase caused by the released latent heat. It can be expressed by:

$$\Delta T = \Delta T_{sen} - \Delta T_{lat} \tag{6-21}$$

Where ΔT is temperature change of the air; ΔT_{sen} is sensible temperature decrease caused by the temperature difference between the solution and air; ΔT_{lat} is temperature increase caused by the latent heat during dehumidification. It can be further derived as:

$$\Delta T = \Delta T_{sen} - \frac{Q_{lat}}{c_{p,sol}\dot{m}_{sol}} \tag{6-22}$$

Where Q_{lat} is latent heat released (kW), and it increases with LiCl mass fraction. However, in the meanwhile $c_{p,sol}$ is increased as well. As a result, $\frac{Q_{lat}}{c_{p,sol}\dot{m}_{sol}}$ is slightly decreased due to this combined effect and ΔT is enhanced. Then based on the definition of the sensible effectiveness, it is increased to a small extent.

The influence of the solution concentration on the sensible effectiveness is reflected in Fig 6-6. Under the same mixing ratio, increasing the solution concentration leads to the sensible effectiveness decrease. The sensible effectiveness at $C_{sol} = 24\%$ is the highest, while it is the lowest at $C_{sol} = 42\%$. As explained in the previous section, the higher solution concentration, the lower solution specific humidity. Thus the latent heat released during the dehumidification is increased, the cooling effect is reduced based on Eq. (6-22). With regard to the solution temperature, it has negative effect on the sensible effectiveness as well, as displayed in Fig 6-7. The highest sensible effectiveness is at 12℃, while it reaches the lowest at 18℃. This is easy to understand since increasing the solution temperature will significantly reduce the temperature difference between the solution and air, the heat transfer potential is decreased as well. This leads to the sensible effectiveness decrease.

6.7.3 Impact of the mixed solution property on dehumidification effect

Dehumidification is the key function of the heat and mass exchanger. Similar to cooling effect, the dehumidification effect is also closely related to the solution properties: concentration,

temperature and mixing ratio. The influences of the solution mixing ratio on the latent effectiveness under various concentrations are plotted in Fig 6-8.

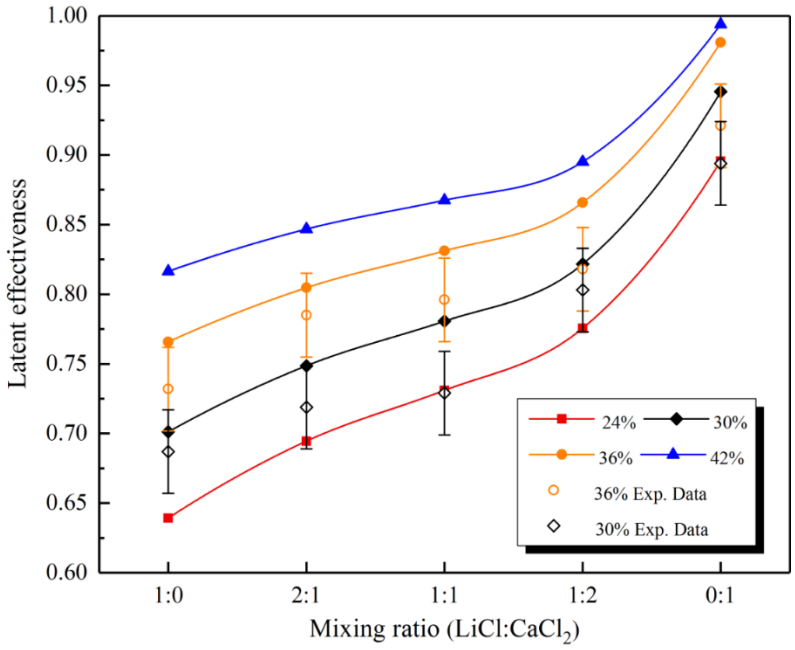


Fig 6- 8 Latent effectiveness changes with mixing ratio for different solution concentrations

Firstly, the impact of the solution concentration on the latent effectiveness is explored. As clearly illustrated in Fig 6-8, the higher solution concentration, the better the system dehumidification effect. For example, for the solution with a mixing ratio of 1:1, its latent effectiveness increases by 18.69% (from 0.7309 to 0.8675) when C_{sol} changes from 24% to 42%. For the 2:1 mixed solution, its latent effectiveness increases by 21.94% (from 0.6945 to 0.8467) when C_{sol} varies from 24% to 42%, and the similar cases are found for the other mixing ratios. This can be reflected by the variations of the moisture flux rate (MFR) and air outlet specific humidity ($W_{air,out}$) with the solution concentration as well.

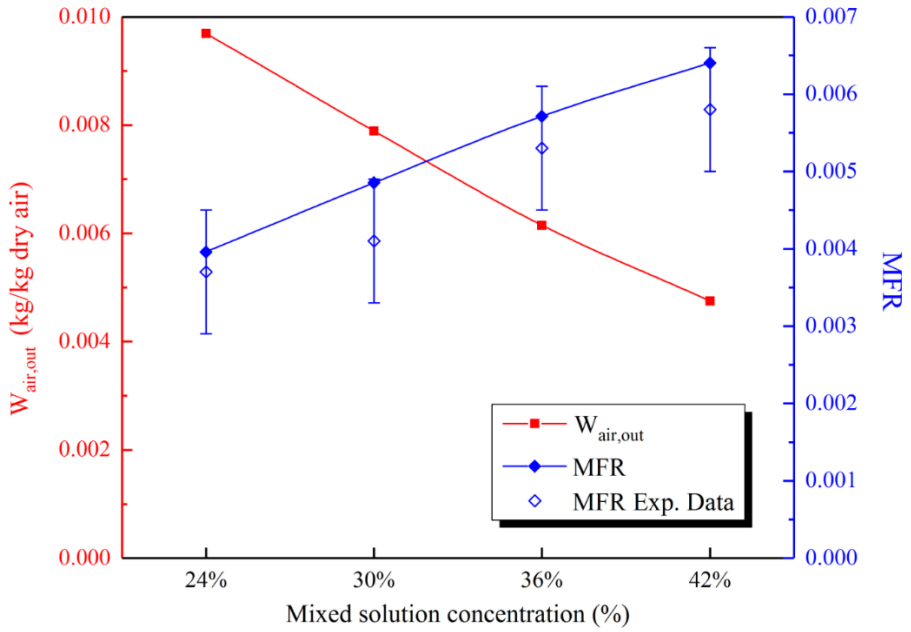


Fig 6- 9 Impact of solution concentration on MFR and $W_{air,out}$

The effects of the solution concentration on the MFR and $W_{air,out}$ are shown in Fig 6-9 for a mixing ratio of 1:1. It can been seen from this figure that the MFR increases by 61.7% (from 0.00396 to 0.0064) when the solution concentration varies from 24% to 42%. In the meanwhile $W_{air,out}$ reduces from 0.00969 kg/kg dry air to 0.00475 kg/kg dry air, meaning the dehumidification effect is considerably improved. This can be explained by the variation of the solution specific humidity with its concentration. As mentioned previously, the solution specific humidity decreases with its concentration. Therefore, the mass transfer potential between the solution and air is improved, so the MFR increases. As for the latent effectiveness, based on its definition given in Eq. (6-14), although the solution inlet specific humidity is decreased, the significant rise of the humidity difference between the inlet and outlet air still improves the latent effectiveness. As shown in Fig 6-8, the influence of the solution concentration becomes weak with $CaCl_2$ mass fraction in the mixed solution. For example, for pure LiCl solution, the latent effectiveness can be improved by 27.7% (from 0.6393 to 0.8164)

when the solution concentration varies from 24% to 42%. By contrast, for pure $CaCl_2$ solution, it is increased by 10.98% only (from 0.8955 to 0.9938).

Apart from the solution concentration, its temperature should be taken into consideration as well since it is closely related to the mixed solution surface vapour pressure. The changes of the latent effectiveness with the mixing ratio under different solution temperatures are plotted in Fig 6-10, while the variations of the MFR and $W_{air,out}$ with the solution temperature are shown in Fig 6-11.

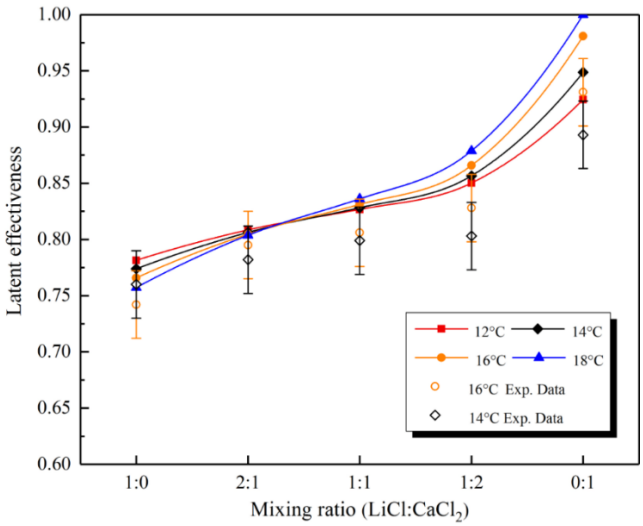


Fig 6- 10 Latent effectiveness changes with mixing ratio for different solution temperatures

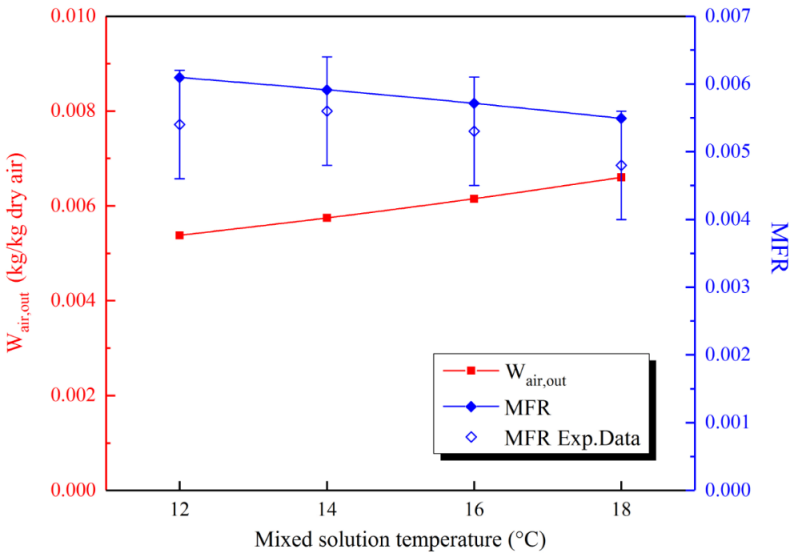


Fig 6- 11 Impacts of solution temperature on MFR and $W_{air,out}$

As indicated in Fig 6-10, the solution temperature has different effects on the latent effectiveness under different mixing ratios. For the LiCl:$CaCl_2$=1:0 solution, the latent effectiveness is high at low temperature. For the LiCl:$CaCl_2$=1:2 and 0:1 solutions, increasing the solution temperature can improve the latent effectiveness. For the LiCl:$CaCl_2$=2:1 and 1:1 solutions, the influence of the solution temperature on the latent effectiveness is negligible. For example, for the LiCl:$CaCl_2$=2:1 solution, the maximum difference of the latent effectiveness at the measured temperature range is only 0.0048 (the maximum value is 0.8085 at $T_{sol} = 12℃$ while the minimum value is 0.8037 at $T_{sol} = 18℃$). As explained previously, the lower solution temperature, the lower solution specific humidity, thus the mass transfer potential between the solution and air is increased. In the meanwhile, the solution inlet specific humidity is decreased, so the air humidity difference between the air at outlet and inlet is increased and the system dehumidification ability is improved. With referring to Eq. (6-14), both the numerator and denominator are increased, this combined effect would lead to different influences on the latent effectiveness. However, if only the amount of moisture being absorbed in the dehumidifier is considered, the system will benefit greatly from decreasing the solution temperature. This is reflected in Fig 6-11 as well, where the MFR and $W_{air,out}$ variations with the solution temperature for the solution with the mixing ratio of 1:1 are plotted. As can be seen from Fig 6-11 that the MFR is raised by 11% (from 0.00549 to 0.00609), and the $W_{air,out}$ is decreased by 18.52% (from 0.006598 to 0.005376 $\mathrm{kg/kg\ dry\ air}$) when the solution temperature reduces from 18℃ to 12℃.

Finally the influence of the mixing ratio on the dehumidification effect is investigated. For a better understanding of the mixing ratio effect, the MFR and $W_{air,out}$ variations with the mixing ratio are plotted in Fig 6-12.

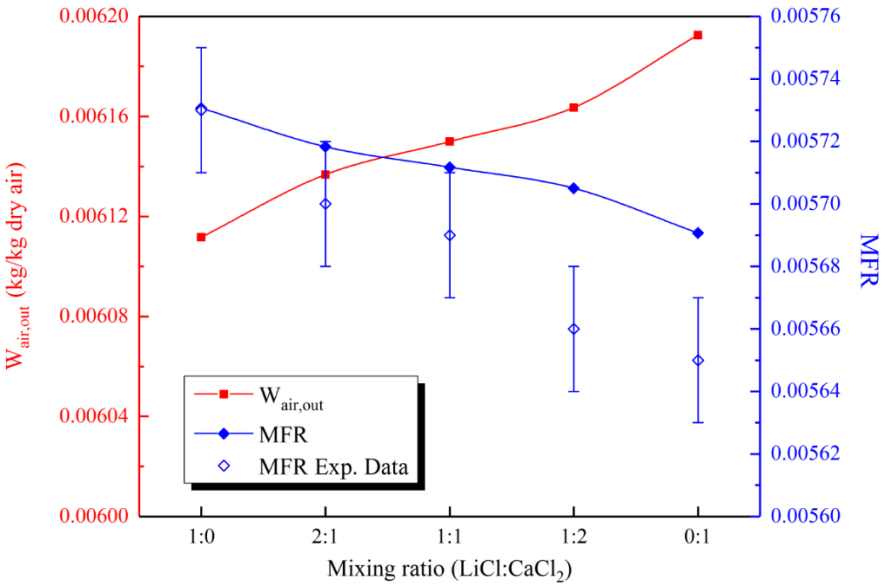


Fig 6- 12 Influences of solution mixing ratio on MFR and $W_{air,out}$

LiCl has been proved to have better moisture absorbing ability compared with $CaCl_2$, and this is in accordance with the results shown in Fig 6-12. In this figure, the mixed solution concentration and temperature are maintained at 36% and 16℃ respectively. When $CaCl_2$ mass fraction increases from 0 to 1, the MFR is reduced from 0.00573 to 0.00569, while the $W_{air,out}$ is increased from 0.00611 to 0.0062 kg/kg dry air. This is because the specific humidity ratio of pure $CaCl_2$ solution is always higher than that of pure LiCl solution under the same concentration and temperature. However, it should be pointed out that the mixing ratio has less impact on the dehumidification ability compared with the solution concentration and temperature. In Figs 6-9 and 6-11, the MFR can be improved by 61.7% and 11% respectively by increasing concentration from 24% to 42%, or reducing temperature from 18℃ to 12℃. By contrast it is only improved by 1.63% by increasing LiCl mass fraction from 0 to1. With regard to the latent effectiveness, both Fig 6-8 and Fig 6-10 reveal that the latent effectiveness increases with CaCl2 mass fraction. According to Eq. (6-14), the numerator would be decreased with $CaCl_2$ mass fraction, so less moisture is absorbed. However the solution inlet

specific humidity $W_{sol,in}$ is increased as well, which leads to the decrease of the denominator. This offsetting effect finally improves the latent effectiveness.

6.7.4 Impact of the solution mixing ratio on system COP

The previous sections are about impact of the main solution properties on the cooling and dehumidification effects. In this section, the system energy efficiency is evaluated by applying the COP analysis. According to Eq. (6-17), the COP is closely related to the system sensible and latent cooling outputs, and the heat input for regeneration. First of all, the regeneration heat input Q_{reg} is assessed.

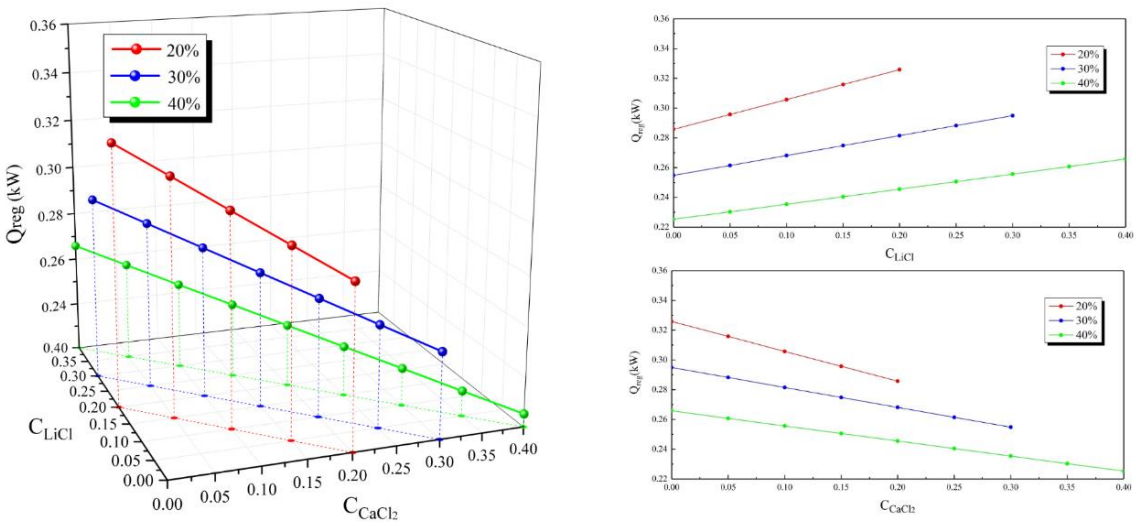


Fig 6- 13 Variations of Q_{reg} with contents of LiCl and $CaCl_2$ at 16℃

The relationship between Q_{reg} and the solute content at the mixed solution temperature $T_{sol,in} = 16℃$ is reflected in Fig 6-13. It is noticed that when the mixed solution concentration increases, Q_{reg} tends to decline. For instance, Q_{reg} varies from 0.286 to 0.326 kW for the 20% solution when LiCl mass fraction changes from 0 to 0.4, while it varies from 0.255 to 0.295 kW for the 30% solution, and from 0.225 to 0.266 kW for the 40% solution respectively. The system dehumidification effect is improved by applying the high concentration solution, as a

result more latent heat is released during this process, the solution outlet temperature is increased. For example, $T_{sol,out}$ for the 1:1 mixed solution at 20% concentration is 21.84℃, while it is 23.11℃ at 30% concentration and 24.31℃ at 40% concentration. Then based on Eq. (6-21), the temperature difference between $T_{sol,out}$ and T_{reg} is narrowed, meaning the less energy is required for regeneration. With referring to the influence of the solute content again, as shown in Fig 6-13, Q_{reg} reduces significantly with $CaCl_2$ mass fraction in the mixed solution. This seems to be inconsistent with the impact of the solution concentration, as increasing $CaCl_2$ can reduce the latent heat transfer, which reduces $T_{sol,out}$. However, it should also be noted that when $CaCl_2$ mass fraction is increased, the air cooling effect is reduced, thus $T_{air,out}$ will be increased. This combined effect leads to the rise of $T_{sol,out}$. Taking the 40% solution as an example, $T_{sol,out}$ increases gradually from 24.03 ℃ to 24.76 ℃ when C_{CaCl_2} varies from 0 to 0.4. So the heat input for regeneration is reduced.

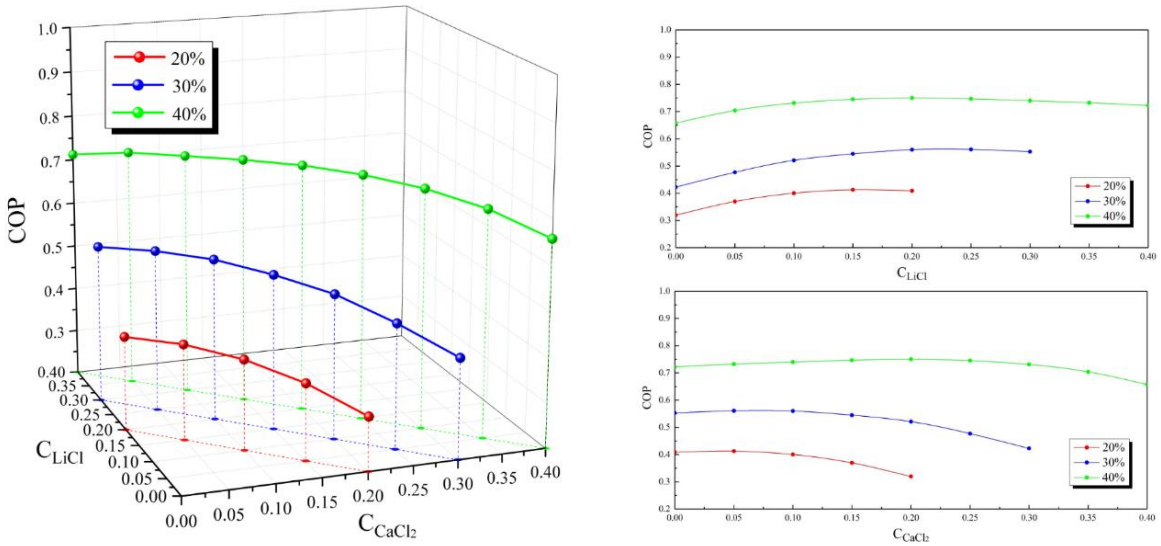


Fig 6- 14 Variations of COP with contents of LiCl and $CaCl_2$ at 16℃

Afterwards the relationships between the COP and solute content are plotted in Fig 6-14. Obviously the COP differences among various mass fractions are dramatic, and can be significantly increased by raising the solution concentration. The maximum COPs for the 20%,

30% and 40% solutions are 0.413, 0.56 and 0.749 respectively. The sensible heat output is decreased slightly with the solution concentration, this is due to more heat released during the dehumidification. The latent heat output is increased due to the better dehumidification effect, and Q_{reg} is reduced as discussed previously. So the dramatic difference of the COP between different concentrations is easily understood.

Then the influences of the solute contents on the system COP are explored. As discussed in Sections 6.7.2 and 6.7.3, increasing $CaCl_2$ mass fraction will reduce both the cooling and dehumidification effects due to the increased $T_{air,out}$ and reduced MFR. This is reflected in Fig 6-15 where $T_{air,out}$ increases from 17.95℃ to 18.57℃, and the MFR decreases from 0.0082 to 0.0063 when $CaCl_2$ mass fraction changes from 0 to 0.3. As a result, both Q_{sen} and Q_{lat} are reduced. In the meanwhile Q_{reg} is reduced as well due to the increased solution outlet temperature. This is also illustrated in Fig 6-15 that $T_{sol,out}$ increases from 22.83℃ to 23.61℃ when $CaCl_2$ mass fraction changes from 0 to 0.3.

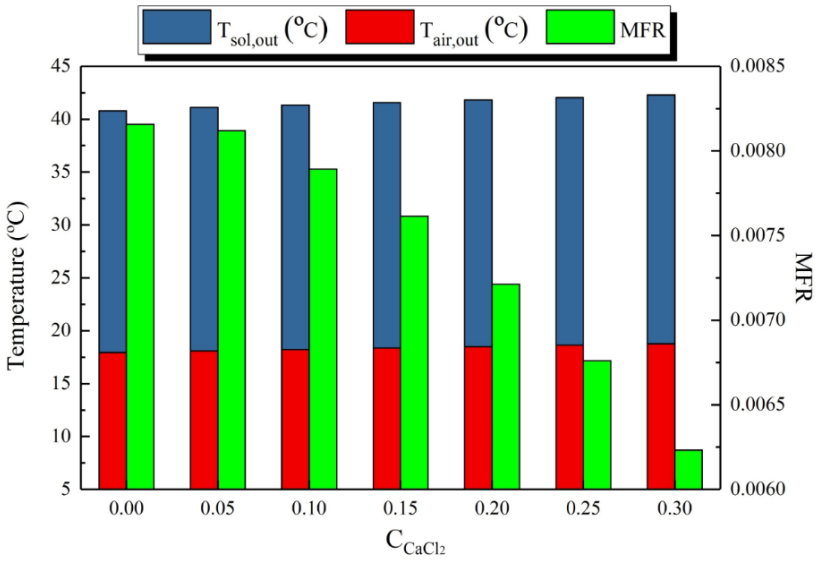


Fig 6- 15 Variations of $T_{sol,out}$, $T_{air,out}$ and MFR with $CaCl_2$ mass fraction

The variations of the total cooling output (the sum of the sensible and latent cooling output) and Q_{reg} with $CaCl_2$ mass fraction for the 30% solution are shown in Fig 6-16. It can be noticed that the total cooling output decreases from 0.163 to 0.108 kW as $CaCl_2$ mass fraction rises

from 0 to 0.3, while Q_{reg} decreases from 0.294 to 0.255 kW. As a result, the system COP initially increases with $CaCl_2$ mass fraction, then drops off afterwards.

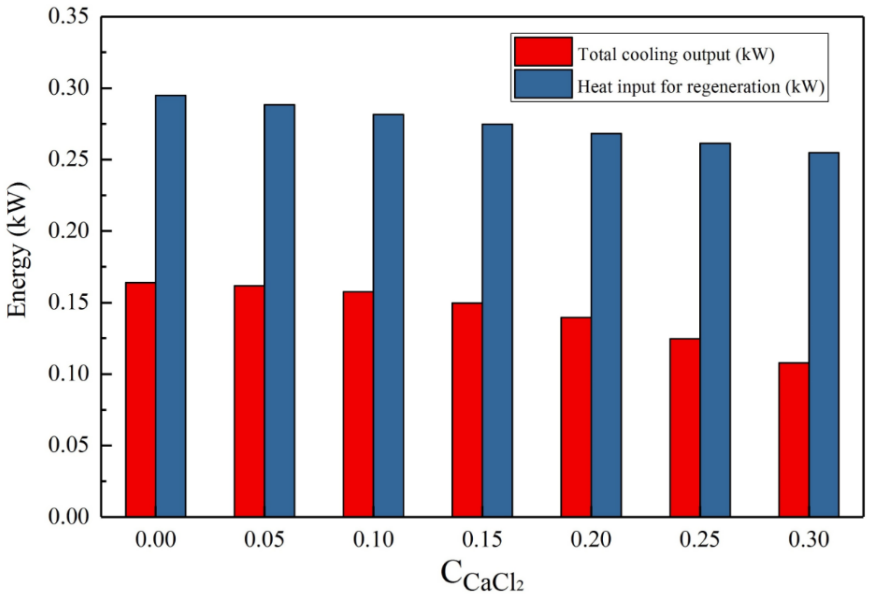


Fig 6- 16 Variations of total cooling output and Q_{reg} with $CaCl_2$ mass fraction for 30% desiccant solution

Compared with pure LiCl solution, the system COP can be improved by adopting the mixed solution. For the 20%, 30% and 40% solutions, the system COPs can be increased by 28.13%, 30.23% and 15.38% respectively compared with pure LiCl solution. For the 20% solution, the system COP peaks at 0.413 when LiCl:$CaCl_2$=3:1. But for the 30% solution, the COP peaks at 0.56 when LiCl:$CaCl_2$=2:1, while for the 40% solution, its COP peaks at 0.749 when LiCl:$CaCl_2$=1:1. Thus under different solution concentrations, the optimum mixing ratio for the highest COP is different, and the higher the solution concentration, the more $CaCl_2$ shall be added. This is useful for selecting the optimum mixing ratio under different concentrations. Currently the LiCl price in the UK is 40£/kg, while the $CaCl_2$ price is only 1.5£/kg. Considering the price difference between LiCl and $CaCl_2$, applying the mixed solution can not only increase the system efficiency but also save material cost as well.

6.8 Summary

In this chapter, the effects of the mixed LiCl-$CaCl_2$ desiccant properties on the performance of a membrane-based dehumidification system are analysed. The finite difference method is used to develop the governing equations in the numerical simulation, and the NRTL method is applied for the mixed solution property calculation. The experimental tests are carried out to validate the numerical modelling. The maximum discrepancies for ε_{sen} and ε_{lat} are 3.679% and 6.257% respectively, and the maximum difference for MFR is 15.510%. The optimum mixing ratio is identified based on the system COP analysis. The main conclusions are given as follows:

- The specific humidity of the mixed solution can be reduced by decreasing its temperature, increasing its concentration, and applying the solution with high LiCl content.
- The effects of the solution temperature, concentration and mixing ratio interact with each other. Under the same concentration, the mixing ratio influence is insignificant when the solution temperature is relatively low. The mixing ratio has more significant effect at the high concentration.
- The system cooling performance can be enhanced by applying the mixed solution with low concentration, temperature and $CaCl_2$ content, while its dehumidification capacity can be increased by using the strong and cool solution. Increasing LiCl content can improve the dehumidification effect, but its influence is relatively weak compared with the solution concentration and temperature effects.
- The regeneration heat Q_{reg} can be dramatically saved, and the high system COP can be achieved by increasing either the solution concentration or $CaCl_2$ content.

- Compared with the pure LiCl solution system, the mixed solution system COP can be raised up to 30.23% by increasing $CaCl_2$ content at a 30% solution concentration. The system COP initially increases with $CaCl_2$ content, then drops off.
- The optimum mixing ratio varies with the solution concentration. For the LiCl-$CaCl_2$ solution, the highest COPs appear at the mixing ratios of 3:1, 2:1 and 1:1 for 20%, 30% and 40% concentrations respectively. More $CaCl_2$ shall be added to the high concentration solution for achieving the better performance.

Chapter 7: Conclusions and future work

7.1 Introduction

The membrane-based liquid desiccant dehumidification air-conditioning system provides occupants with significant physical, environmental and economic benefits compared to the traditional air-conditioning systems. The main aim of the thesis is to develop and evaluate a novel membrane-based liquid desiccant dehumidification air-conditioning system, which includes two main units: dehumidifier and regenerator. These two units, and the integrated complete dehumidification system have been investigated. Moreover the effects of mixed LiCl-$CaCl_2$ solution on the system performance have been evaluated and a method for selecting optimum mixing ratio has been proposed. Both numerical and experimental methods have been adopted for a rigorous and analytical piece of work. Based on the simulation and experimental results, this thesis has proved the design concept of the membrane-based liquid desiccant dehumidification system, which thereby provides an evident contribution to new knowledge in the field of the desiccant dehumidification technology. To produce a coherent conclusion of the thesis, this chapter consists of two sections: section 7.2 summarises the main findings from each chapter by revisiting the thesis aim and objectives, and section 7.3 proposes the recommendations for future work.

7.2 Main conclusions

The preceding six chapters have sought to achieve the main aim of the thesis by accomplishing the thesis objectives as presented in Section 1.2. In this section, main findings of this thesis are presented.

1) The first objective: "*Literature review on technologies related to the liquid desiccant dehumidification system to give a comprehensive background and evaluation of current available literature on the topic. More importantly, to highlight the research gaps in the existing literature of the membrane-based liquid desiccant dehumidification system*" has been achieved in Chapter 2. Through extensive review of literatures on dehumidifier, regenerator, desiccant and membrane materials and mathematical modelling methods, it has been found that most of the investigations on the liquid desiccant dehumidification system are through experimental analysis. Limited numerical analyses focuse on the heat and mass transfer mechanism, or the system performance under limited conditions. Comprehensive parametric studies on the membrane-based dehumidifier and regenerator performance using finite difference method have not been explored widely yet. With regard to the complete dehumidification system, based on the literature review it was assumed that supply and exhaust side exchangers are coupled with aqueous salt solution flowing in a closed loop in most previous literatures. Furthermore, no previous work has been reported on the performance evaluation using mixed LiCl-$CaCl_2$ solution through numerical modelling.
2) The second objective: "*Numerical and experimental analysis of the membrane-based dehumidifier under various conditions and the performance evaluation based on the simulation and experimental results*" has been achieved in Chapter 3 through numerical modelling using finite difference method and experimental tests. It has been found that mass flow rate ratio $m^*$and number of heat transfer units NTU are two of the most important parameters influencing the dehumidifier effectiveness. Although all effectiveness increase with $m^*$and NTU, their increasing gradients hardly change when $m^*$and NTU exceed m^*_{crit} and NTU_{crit} respectively, which are 1 and 4 respectively in this study. Effects of m^* and NTU on the system performance are interacted with each

other: there is hardly benefit to the system performance improvement by increasing m^* at low NTU, especially for the latent effectiveness. By contrast, no obvious performance enhancement is achieved by increasing NTU at low m^*, especially for the sensible effectiveness. The sensible effectiveness is insensitive to both T_{sol} and C_{sol}, while the latent effectiveness increases significantly with C_{sol} at a high solution temperature. The system shows broad adaptability in different weather conditions by providing relative stable state supply air, in particular at high NTU.

3) The third objective: "*Numerical and experimental analysis of the membrane-based regenerator under different conditions and the performance evaluation based on the simulation and experimental results*" has been accomplished in Chapter 4 through numerical modelling by finite difference method and experimental tests. Membrane-based regenerator has the same structure as membrane-based dehumidifier, but with reversed heat and mass transfer directions and different working conditions. It has been found that similar to dehumidifier, NTU and m^* have the most significant effects on the regeneration performance, and their effects are interacted with each other. There is hardly benefit to the performance improvement by increasing NTU at low m^*(e.g. lower than 1). By contrast, no obvious performance enhancement is achieved by increasing m^* at low NTU (e.g. lower than 2). The increasing gradients of regenerator effectiveness hardly change when NTU and m^* exceed NTU_{crit} and m^*_{crit}, which are 4 and 2 respectively in this study. Neither $T_{air,in}$ nor $W_{air,in}$ has remarkable influence on the regeneration performance, though the solution re-concentration ability can be enhanced slightly by applying drier and warmer air. Regenerator can benefit from increased solution temperature as enhanced re-concentration (0.8% increase of MFR) and cooling effects (13.7% increase of TDR). However this means more cooling energy is required for the high temperature desiccant solution.

4) The forth objective: "*Development of a complete membrane-based liquid desiccant dehumidification system by integrating both dehumidifier and regenerator, and to investigate effects of various operating conditions on the complete system performance through simulation and experimental data*" have been achieved in Chapter 5. Through the experimental data and the numerical model for the complete membrane-based liquid desiccant dehumidification system including a dehumidifier, a regenerator, and hot and cooling water supply systems, it has been found that NTU_{de} and m^* have the most considerable impact on the complete system performance, while the influences of NTU_{re} and $C_{sol,in}$ are comparatively weak. The system overall sensible and latent effectiveness can be improved by increasing NTU_{de} before its critical value of 6. However the total amount of moisture being absorbed, total cooling output $Q_{cooling}$ and COP decrease with NTU_{de} for the reduced air mass flow rate. The critical values of m^* vary under different NTUs, and it is preferable to keep m^* at or below critical values as further increasing solution flow rate would reduce system COP. The latent cooling output Q_{lat} is normally two times higher than the sensible cooling output Q_{sen} under all circumstances. Considering it is not practical to pre-cool the desiccant solution, further cooling, such as indirect evaporative cooling is required after the dehumidification. Improving the solution inlet concentration is more applicable approach to improve the system dehumidification and energy performance compared with reducing solution temperature. However the problem of crystallization should be avoided when applying high concentration solution.

5) The fifth objective: "*Investigation on effects of mixed LiCl-$CaCl_2$ solution on the system performance, and to provide an optimum mixing ratio selection method based on the mathematical model and experimental data*" has been accomplished in Chapter 6 by combining finite difference method and electrolyte non-random two-liquid (NRTL)

method. It has been found that the system cooling performance can be enhanced by applying the mixed solution with low concentration, temperature and $CaCl_2$ content, while its dehumidification capacity can be increased by using the strong and cool solution. Increasing LiCl content can improve the dehumidification effect, but its influence is relatively weak compared with the solution concentration and temperature effects. The regeneration heat Q_{reg} can be dramatically saved, and the high system COP can be achieved by increasing either the solution concentration or $CaCl_2$ content. Compared with the pure LiCl solution system, the mixed solution system COP can be raised up to 30.23% by increasing $CaCl_2$ content at a 30% solution concentration. The system COP initially increases with $CaCl_2$ content, then drops off. The optimum mixing ratio varies with the solution concentration. For the LiCl-$CaCl_2$ solution, the highest COPs appear at the mixing ratios of 3:1, 2:1 and 1:1 for 20%, 30% and 40% concentrations respectively. More $CaCl_2$ shall be added to the high concentration solution for achieving the better performance.

The sixth objective: "*Recommendations for the future work*" is presented in next section.

7.3 Recommendations for future work

Based on the major findings as presented in the previous section, recommendations for the future work of the membrane-based liquid desiccant dehumidification system are presented as follows:

1) The work presented in Chapter 3 and Chapter 4 has discussed the impact of various operating parameters, such as dimensionless parameters, solution properties and air properties on the dehumidifier and regenerator performance. However, due to the limitations in research time and finance support, the impact of using different membrane materials has not been investigated yet. As discussed in Section 2.5.2, many advanced materials have been developed recently and using different types of membrane materials could bring significant system performance difference. Future research would focus on the detailed heat and mass transfer mechanism through more complex structure of advanced membrane materials.
2) The performance and energy analysis of the complete system have been presented in Chapter 5. However, only regeneration energy and system COP are used as criteria for energy analysis. For a more comprehensive performance evaluation, assessments with regard to exergy, economic and environment need to be discussed. More importantly, more analysis should be conducted in the future work regarding the difference of annual electricity consumption or annual CO_2 production between membrane-based liquid desiccant dehumidification system and traditional system.
3) The finite difference method is applied to analyse the heat and mass transfer in dehumidifier and regenerator. However, only temperature and concentration profiles are obtained from governing equations for investigation. For better understanding of

the system, velocity and pressure profiles should be calculated in the future by establishing more complex Naiver-Stokes equations and solved by applying CFD.

4) Due to limitation in time for the testing rig development, only the data at inlets and outlets are used for the numerical model validation. Though the entire temperature and concentration fields are obtained by numerical modelling, they are not validated entirely by experimental tests. Thus the future work would consider constructing dehumidifier and regenerator with better structure design that sensors could be placed inside solution and air channels.
5) The latent heat generated in the dehumidifier could negatively affect the system performance for the current design. So the cooling system of solution in the dehumidifier could be designed in the future.
6) The diluted solution is regenerated by an electrical boiler in this study. In the future, the low-grade energy sources such as solar thermal boiler or ground-source heat pump could be integrated to the dehumidification system to make the complete system more sustainable and improve the performance further.

References

1. Abdel-Salam, M.R.H., et al., *State-of-the-art in liquid-to-air membrane energy exchangers (LAMEEs): A comprehensive review.* Renewable and Sustainable Energy Reviews, 2014. 39: p. 700-728.
2. *British petroleum statistical review of world energy.* 2017.
3. Tverberg, G. *China: is peak coal part of its problem?* 2016; Available from: https://ourfiniteworld.com/2016/06/20/china-is-peak-coal-part-of-its-problem/.
4. Chowdhury, J.I., et al., *Reducing industrial energy demand in the UK: A review of energy efficiency technologies and energy saving potential in selected sectors.* Renewable and Sustainable Energy Reviews, 2018. 94: p. 1153-1178.
5. *World erengy outlook 2012: executive summary*. 2012; Available from: https://www.iea.org.
6. *Climate Change Act 2008*. 2008, Parliament of the United Kingdom: London.
7. Gupta, R. and M. Gregg, *Assessing energy use and overheating risk in net zero energy dwellings in UK.* Energy and Buildings, 2018. 158: p. 897-905.
8. *Europe 2020 target in: Europe 2020*. 2015, European Commission.
9. *Energy Supply and Consumption Revolution Strategy (2016-2030).* 2017, National Development and Reform Commission (NDRC): Beijing.
10. Wyon, D.P., *The effects of indoor air quality on performance and productivity.* Indoor Air, 2004. 14 Suppl 7: p. 92-101.
11. Omer, A.M., *Energy, environment and sustainable development.* Renewable and Sustainable Energy Reviews, 2008. 12(9): p. 2265-2300.
12. Kolokotsa, D., et al., *A roadmap towards intelligent net zero- and positive-energy buildings.* Solar Energy, 2011. 85(12): p. 3067-3084.

13. *The 2011 Building Energy Databook*, U.D.o. Energy, Editor. 2011: Washington DC.

14. Iain Macleay, K.H., Anwar Annut, *Digest of United Kingdom Energy Statistics* E.a.c. change, Editor. 2011: London.

15. Hao, X., et al., *Optimizing the pad thickness of evaporative air-cooled chiller for maximum energy saving.* Energy and Buildings, 2013. 61: p. 146-152.

16. Al-Abidi, A.A., et al., *Review of thermal energy storage for air conditioning systems.* Renewable and Sustainable Energy Reviews, 2012. 16(8): p. 5802-5819.

17. Pérez-Lombard, L., J. Ortiz, and C. Pout, *A review on buildings energy consumption information.* Energy and Buildings, 2008. 40(3): p. 394-398.

18. *Peoject for the Directorate Genral Transportation-Energy of the Commossion of the European Union, Final Report*, E.E.E.a.C.o.C.A. Conditioners), Editor. 2003.

19. Feng, Z., et al., *Impacts of humidification process on indoor thermal comfort and air quality using portable ultrasonic humidifier.* Building and Environment, 2018. 133: p. 62-72.

20. Cao, S.-J. and J. Meyers, *Influence of turbulent boundary conditions on RANS simulations of pollutant dispersion in mechanically ventilated enclosures with transitional slot Reynolds number.* Building and Environment, 2013. 59: p. 397-407.

21. Deng, Y., et al., *The impact of manufacturing parameters on submicron particle emissions from a desktop 3D printer in the perspective of emission reduction.* Building and Environment, 2016. 104: p. 311-319.

22. Spengler, J. and K. Sexton, *Indoor air pollution: a public health perspective.* Science, 1983. 221(4605): p. 9-17.

23. Dimitroulopoulou, C. *Ventilation in European dwellings: A review*. Building and Environment 2012 2012/01/01/ [cited 47; 109-125]. Available from: http://www.sciencedirect.com/science/article/pii/S0360132311002241.

24. Sundell, J. and T. Lindvall, *Indoor Air Humidity And Sensation Of Dryness As Risk Indicators Of Sbs.* Indoor Air, 1993. 3(4): p. 382-390.

25. Reinikainen, L.M. and J.J.K. Jaakkola, *Significance of humidity and temperature on skin and upper airway symptoms.* Indoor Air, 2003. 13(4): p. 344-352.

26. Wolkoff, P., *External eye symptoms in indoor environments.* Indoor Air, 2017. 27(2): p. 246-260.

27. Wolkoff, P., *"Healthy" eye in office-like environments.* Environment International, 2008. 34(8): p. 1204-1214.

28. Abelson, R., et al., *Asingle-center study evaluating the effect of the controlled adverse environment (CAE) model on tear film stability.* Clin. Ophthalmol., 2012. 6: p. 1865-1872.

29. Huang, S.-M. and L.-Z. Zhang, *Researches and trends in membrane-based liquid desiccant air dehumidification.* Renewable and Sustainable Energy Reviews, 2013. 28: p. 425-440.

30. Radhwan, A.M., H.N. Gari, and M.M. Elsayed, *Parametric study of a packed bed dehumidifier/regenerator using CaCl2 liquid desiccant.* Renewable Energy, 1993. 3(1): p. 49-60.

31. Dwyer, T. *Module 71: Liquid desiccants for dehumidification in building air conditioning systems*. 2014 [cited 2014 December]; Available from: https://www.cibsejournal.com/cpd/modules/2014-12/.

32. Huang, Y., et al., *Optimal energy-efficient predictive controllers in automotive air-conditioning/refrigeration systems.* Applied Energy, 2016. 184: p. 605-618.

33. Bai, H., et al., *State-of-art in modelling methods of membrane-based liquid desiccant heat and mass exchanger: A comprehensive review.* International Journal of Heat and Mass Transfer, 2018. 125: p. 445-470.

34. Afonso, C.F.A., *Recent advances in building air conditioning systems.* Applied Thermal Engineering, 2006. 26(16): p. 1961-1971.

35. Yu, B.F., et al., *Review of research on air-conditioning systems and indoor air quality control for human health.* International Journal of Refrigeration, 2009. 32(1): p. 3-20.

36. Zhang, L.Z., *Total heat recovery: heat and moisture recovery from ventilation air*. 2008, New York: Nova Science Publishers Inc.

37. Grossman, G. and A. Johannsen, *Solar cooling and air conditioning.* Progress in Energy and Combustion Science, 1981. 7(3): p. 185-228.

38. Burns, P.R., J.W. Mitchell, and W.A. Beckman, *SOLAR HYBRID DESICCANT COOLING SYSTEMS IN SUPERMARKET APPLICATIONS*, in *Intersol Eighty Five*, E. Bilgen and K.G.T. Hollands, Editors. 1986, Pergamon: Oxford. p. 700-706.

39. Ghadiri Moghaddam, D., R.W. Besant, and C.J. Simonson, *Solution-side effectiveness for a liquid-to-air membrane energy exchanger used as a dehumidifier/regenerator*. Applied Energy, 2014. 113: p. 872-882.

40. Jain, S. and P.K. Bansal, *Performance analysis of liquid desiccant dehumidification systems.* International Journal of Refrigeration, 2007. 30(5): p. 861-872.

41. Scalabrin, G. and G. Scaltriti, *A liquid sorption-desorption system for air conditioning with heat at lower temperature.* Journal of Solar Energy Engineering, Transactions of the ASME, 1990. 112(2): p. 70-75.

42. Chung, T.W. and H. Wu, *Comparison between spray towers with and without fin coils for air dehumidification using triethylene glycol solutions and development of the mass-transfer correlations.* Industrial and Engineering Chemistry Research, 2000. 39(6): p. 2076-2084.

43. Pesaran, A.A., et al. *Evaluation of a liquid desiccant-enhanced heat pipe air preconditioner*. in *ASHRAE Transactions*. 1995.

44. Zurigat, Y.H., M.K. Abu-Arabi, and S.A. Abdul-Wahab, *Air dehumidification by triethylene glycol desiccant in a packed column.* Energy Conversion and Management, 2004. 45(1): p. 141-155.

45. Martin, V. and D.Y. Goswami, *Effectiveness of heat and mass transfer processes in a packed bed liquid desiccant dehumidifier/regenerator.* HVAC and R Research, 2000. 6(1): p. 21-39.

46. Chung, T.W., *Predictions of moisture removal efficiencies for packed-bed dehumidification systems.* Gas Separation and Purification, 1994. 8(4): p. 265-268.

47. Babakhani, D. and M. Soleymani, *An analytical solution for air dehumidification by liquid desiccant in a packed column.* International Communications in Heat and Mass Transfer, 2009. 36(9): p. 969-977.

48. Factor, H.M. and G. Grossman, *A packed bed dehumidifier/regenerator for solar air conditioning with liquid desiccants.* Solar Energy, 1980. 24(6): p. 541-550.

49. Patnaik, S., T.G. Lenz, and G.O.G. Löf, *Performance studies for an experimental solar open-cycle liquid desiccant air dehumidification system.* Solar Energy, 1990. 44(3): p. 123-135.

50. Elsarrag, E., *Performance study on a structured packed liquid desiccant regenerator.* Solar Energy, 2006. 80(12): p. 1624-1631.

51. Pietruschka, D., et al., *Experimental performance analysis and modelling of liquid desiccant cooling systems for air conditioning in residential buildings.* International Journal of Refrigeration, 2006. 29(1): p. 110-124.

52. Zhang, L., et al., *Experimental analysis of mass transfer in adiabatic structured packing dehumidifier/regenerator with liquid desiccant.* International Journal of Heat and Mass Transfer, 2010. 53(13-14): p. 2856-2863.

53. Grossman, G., *Solar cooling, dehumidification and air conditioning.* Chapter in Encyclopedia of Energy, 2004. 5: p. 575-585.

54. Bansal, P., S. Jain, and C. Moon, *Performance comparison of an adiabatic and an internally cooled structured packed-bed dehumidifier.* Applied Thermal Engineering, 2011. 31(1): p. 14-19.

55. Yin, Y., et al., *Experimental study on a new internally cooled/heated dehumidifier/regenerator of liquid desiccant systems.* International Journal of Refrigeration, 2008. 31(5): p. 857-866.

56. Kessling, W., E. Laevemann, and C. Kapfhammer, *Energy storage for desiccant cooling systems component development.* Solar Energy, 1998. 64(4-6): p. 209-221.

57. Yoon, J.-I., et al., *Numerical study on heat and mass transfer characteristic of plate absorber.* Applied Thermal Engineering, 2005. 25(14): p. 2219-2235.

58. Liu, J., et al., *Experimental analysis of an internally-cooled/heated liquid desiccant dehumidifier/regenerator made of thermally conductive plastic.* Energy and Buildings, 2015. 99: p. 75-86.

59. Zhang, T., et al., *Experimental analysis of an internally-cooled liquid desiccant dehumidifier.* Building and Environment, 2013. 63: p. 1-10.

60. Liu, J., X. Liu, and T. Zhang, *Performance comparison of three typical types of internally-cooled liquid desiccant dehumidifiers.* Building and Environment, 2016. 103: p. 134-145.

61. Saman, W.Y. and S. Alizadeh, *An experimental study of a cross-flow type plate heat exchanger for dehumidification/cooling.* Solar Energy, 2002. 73(1): p. 59-71.

62. Lun, W., et al., *Experimental analysis of a novel internally-cooled dehumidifier with self-cooled liquid desiccant.* Building and Environment, 2018. 141: p. 117-126.

63. Zhang, L.-Z., *Heat and mass transfer in a cross-flow membrane-based enthalpy exchanger under naturally formed boundary conditions.* International Journal of Heat and Mass Transfer, 2007. 50(1): p. 151-162.

64. Zhang, L.-Z., C.-H. Liang, and L.-X. Pei, *Conjugate heat and mass transfer in membrane-formed channels in all entry regions.* International Journal of Heat and Mass Transfer, 2010. 53(5): p. 815-824.

65. Niu, J.L. and L.Z. Zhang, *Membrane-based Enthalpy Exchanger: material considerations and clarification of moisture resistance.* Journal of Membrane Science, 2001. 189(2): p. 179-191.

66. Zhang, L.Z. and J.L. Niu, *Effectiveness Correlations for Heat and Moisture Transfer Processes in an Enthalpy Exchanger With Membrane Cores.* Journal of Heat Transfer, 2002. 124(5): p. 922-929.

67. Ghadiri Moghaddam, D., et al., *Numerical model of a small-scale liquid-to-air membrane energy exchanger: Parametric study of membrane resistance and air side convective heat transfer coefficient.* Applied Thermal Engineering, 2013. 61(2): p. 245-258.

68. Moghaddam, D.G., et al., *Small-scale single-panel liquid-to-air membrane energy exchanger (LAMEE) test facility development, commissioning and evaluating the steady-state performance.* Energy and Buildings, 2013. 66: p. 424-436.

69. Abdel-Salam, A.H., G. Ge, and C.J. Simonson, *Performance analysis of a membrane liquid desiccant air-conditioning system.* Energy and Buildings, 2013. 62: p. 559-569.

70. Vali, A., et al., *Numerical model and effectiveness correlations for a run-around heat recovery system with combined counter and cross flow exchangers.* International Journal of Heat and Mass Transfer, 2009. 52(25): p. 5827-5840.

71. Fan, H., et al., *Performance of a Run-Around System for HVAC Heat and Moisture Transfer Applications Using Cross-Flow Plate Exchangers Coupled with Aqueous Lithium Bromide*. Vol. 12. 2006. 313-336.

72. Das, R.S. and S. Jain, *Experimental performance of indirect air-liquid membrane contactors for liquid desiccant cooling systems.* Energy, 2013. 57: p. 319-325.

73. Das, R.S. and S. Jain, *Performance characteristics of cross-flow membrane contactors for liquid desiccant systems.* Applied Energy, 2015. 141: p. 1-11.

74. Min, J. and M. Su, *Performance analysis of a membrane-based enthalpy exchanger: Effects of the membrane properties on the exchanger performance*. Vol. 348. 2010. 376-382.

75. Huang, S.-M., et al., *Fluid flow and heat mass transfer in membrane parallel-plates channels used for liquid desiccant air dehumidification.* International Journal of Heat and Mass Transfer, 2012. 55(9): p. 2571-2580.

76. Huang, S.-M., L.-Z. Zhang, and M. Yang, *Conjugate heat and mass transfer in membrane parallel-plates ducts for liquid desiccant air dehumidification: Effects of the developing entrances.* Journal of Membrane Science, 2013. 437: p. 82-89.

77. Incropera FP, D.D., *Introduction to Heat Transfer*. 3rd Edition ed. 1996, New York: John Wiley & Sons.

78. Vali, A., et al., *Numerical modeling of fluid flow and coupled heat and mass transfer in a counter-cross-flow parallel-plate liquid-to-air membrane energy exchanger.* International Journal of Heat and Mass Transfer, 2015. 89: p. 1258-1276.

79. Mahmud, K., et al., *Performance testing of a counter-cross-flow run-around membrane energy exchanger (RAMEE) system for HVAC applications.* Energy and Buildings, 2010. 42(7): p. 1139-1147.

80. Ghadiri Moghaddam, D., et al., *Steady-State Performance of a Small-Scale Liquid-to-Air Membrane Energy Exchanger for Different Heat and Mass Transfer Directions, and Liquid Desiccant Types and Concentrations: Experimental and Numerical Data.* Journal of Heat Transfer, 2013. 135(12): p. 122002-122002-13.

81. Namvar, R., et al., *+Transient characteristics of a liquid-to-air membrane energy exchanger (LAMEE) experimental data with correlations.* International Journal of Heat and Mass Transfer, 2012. 55(23): p. 6682-6694.

82. Huang, S.-M., M. Yang, and X. Yang, *Performance analysis of a quasi-counter flow parallel-plate membrane contactor used for liquid desiccant air dehumidification.* Applied Thermal Engineering, 2014. 63(1): p. 323-332.

83. Huang, S.-M., Z. Zhong, and M. Yang, *Conjugate heat and mass transfer in an internally-cooled membrane-based liquid desiccant dehumidifier (IMLDD).* Journal of Membrane Science, 2016. 508: p. 73-83.

84. Yang, Y., et al., *Heat and mass transfer in an adjacent internally-cooled membrane-based liquid desiccant dehumidifier (AIMLDD).* Energy Procedia, 2017. 142: p. 3990-3997.

85. Huang, S.-M., et al., *Laminar flow and heat transfer in a quasi-counter flow parallel-plate membrane channel in the solution side with cooling tubes.* International Journal of Heat and Mass Transfer, 2017. 105: p. 769-780.

86. Huang, S.-M., et al., *Performance analysis of an internally-cooled plate membrane liquid desiccant dehumidifier (IMLDD): An analytical solution approach.* International Journal of Heat and Mass Transfer, 2018. 119: p. 577-585.

87. Abdel-Salam, M.R.H., R.W. Besant, and C.J. Simonson, *Design and testing of a novel 3-fluid liquid-to-air membrane energy exchanger (3-fluid LAMEE).* International Journal of Heat and Mass Transfer, 2016. 92: p. 312-329.

88. Abdel-Salam, M.R.H., R.W. Besant, and C.J. Simonson, *Performance testing of a novel 3-fluid liquid-to-air membrane energy exchanger (3-fluid LAMEE) under desiccant solution regeneration operating conditions.* International Journal of Heat and Mass Transfer, 2016. 95: p. 773-786.

89. Qiu, D., et al., *Laminar flow and heat transfer in an internally-cooled hexagonal parallel-plate membrane channel (IHPMC).* Applied Thermal Engineering, 2017. 124: p. 767-780.

90. Zhang, L.-Z., *Heat and mass transfer in a quasi-counter flow membrane-based total heat exchanger.* International Journal of Heat and Mass Transfer, 2010. 53(23): p. 5478-5486.

91. Huang, S.-M., Y. Hong, and F.G.F. Qin, *Fluid flow and heat transfer in hexagonal parallel-plate membrane channels (HPMC): Effects of the channel heights and fluid parameters.* Applied Thermal Engineering, 2016. 93: p. 8-14.

92. Mansourizadeh, A. and A.F. Ismail, *Hollow fiber gas–liquid membrane contactors for acid gas capture: A review.* Journal of Hazardous Materials, 2009. 171(1): p. 38-53.

93. Stefano Bergero, A.C., *Experimental and theoretical analysis of air humidification/dehumidification processes using hydrophobic capillary contactors.* Applied Thermal Engineering, 2001. 21: p. 1119-35.

94. Zhang, L.-Z. and S.-M. Huang, *Coupled heat and mass transfer in a counter flow hollow fiber membrane module for air humidification.* International Journal of Heat and Mass Transfer, 2011. 54(5): p. 1055-1063.

95. MA, L., *Les lois de la transmission de chaleur par convection.* Annual Mines, 1928. 13: p. 201-99.

96. Graetz, L., *On the heat capacity of fluids.* Ann. Phys. Chem., 1885. 25: p. 337-357.

97. Kreulen, H., et al., *Microporous hollow fibre membrane modules as gas-liquid contactors. Part 1. Physical mass transfer processes: A specific application: Mass transfer in highly viscous liquids.* Journal of Membrane Science, 1993. 78(3): p. 197-216.

98. Yang, M.C. and E.L. Cussler, *Designing hollow-fiber contactors.* AIChE Journal, 1986. 32(11): p. 1910-1916.

99. Zhang, L.-Z., *An Analytical Solution to Heat and Mass Transfer in Hollow Fiber Membrane Contactors for Liquid Desiccant Air Dehumidification.* Journal of Heat Transfer, 2011. 133(9): p. 092001-092001-8.

100. Zhang, L.-Z., et al., *Conjugate heat and mass transfer in a hollow fiber membrane module for liquid desiccant air dehumidification: A free surface model approach.* International Journal of Heat and Mass Transfer, 2012. 55(13): p. 3789-3799.

101. Huang, S.-M., et al., *Conjugate transport phenomena in a counter flow hollow fiber membrane tube bank: Effects of the fiber-to-fiber interactions.* Journal of Membrane Science, 2013. 442: p. 8-17.

102. Zhang, L.-Z., S.-M. Huang, and L.-X. Pei, *Conjugate heat and mass transfer in a cross-flow hollow fiber membrane contactor for liquid desiccant air dehumidification.* International Journal of Heat and Mass Transfer, 2012. 55(25): p. 8061-8072.

103. Huang, S.-M., et al., *Turbulent Heat and Mass Transfer Across a Hollow Fiber Membrane Tube Bank in Liquid Desiccant Air Dehumidification.* Journal of Heat Transfer, 2012. 134(8): p. 082001-082001-10.

104. Huang, S.-M., L.-Z. Zhang, and L.-X. Pei, *Transport Phenomena in a Cross-Flow Hollow Fibre Membrane Bundle Used for Liquid Desiccant Air Dehumidification.* Indoor and Built Environment, 2013. 22(3): p. 559-574.

105. Zhang, L.-Z., S.-M. Huang, and W.-B. Zhang, *Turbulent heat and mass transfer across a hollow fiber membrane bundle considering interactions between neighboring fibers.* International Journal of Heat and Mass Transfer, 2013. 64: p. 162-172.

106. Dindore, V.Y. and G.F. Versteeg, *Gas–liquid mass transfer in a cross-flow hollow fiber module: Analytical model and experimental validation.* International Journal of Heat and Mass Transfer, 2005. 48(16): p. 3352-3362.

107. Wickramasinghe, S.R., M.J. Semmens, and E.L. Cussler, *Mass transfer in various hollow fiber geometries.* Journal of Membrane Science, 1992. 69(3): p. 235-250.

108. Ouyang, Y.-W. and L.-Z. Zhang, *Conjugate heat and mass transfer in a skewed flow hollow fiber membrane bank used for liquid desiccant air dehumidification.* International Journal of Heat and Mass Transfer, 2016. 93: p. 23-40.

109. Ouyang, Y.-w., Z.-X. Li, and L.-Z. Zhang, *Oblique fluid flow and heat transfer across a hollow fiber membrane bank under uniform temperature conditions.* Journal of Membrane Science, 2014. 470: p. 524-534.

110. Huang, S.-M., et al., *Heat and mass transfer deteriorations in an elliptical hollow fiber membrane tube bank for liquid desiccant air dehumidification.* Applied Thermal Engineering, 2013. 57(1): p. 90-98.

111. Huang, S.-M. and M. Yang, *Longitudinal fluid flow and heat transfer between an elliptical hollow fiber membrane tube bank used for air humidification.* Applied Energy, 2013. 112: p. 75-82.

112. Huang, S.-M. and M. Yang, *Heat and mass transfer enhancement in a cross-flow elliptical hollow fiber membrane contactor used for liquid desiccant air dehumidification.* Journal of Membrane Science, 2014. 449: p. 184-192.

113. Huang, S.-M., et al., *Laminar flow and heat transfer between a regularly distributed elliptical hollow fiber membrane tube bank.* International Journal of Heat and Mass Transfer, 2016. 102: p. 1044-1049.

114. Moulin, P., et al., *Mass transfer improvement by secondary flows: Dean vortices in coiled tubular membranes.* Journal of Membrane Science, 1996. 114(2): p. 235-244.

115. Dean, W.R., *LXXII. The stream-line motion of fluid in a curved pipe (Second paper).* The London, Edinburgh, and Dublin Philosophical Magazine and Journal of Science, 1928. 5(30): p. 673-695.

116. Dean, W.R., *XVI. Note on the motion of fluid in a curved pipe.* The London, Edinburgh, and Dublin Philosophical Magazine and Journal of Science, 1927. 4(20): p. 208-223.

117. Liu, L., et al., *Mass transfer enhancement in coiled hollow fiber membrane modules.* Journal of Membrane Science, 2005. 264(1): p. 113-121.

118. Fumo, N. and D.Y. Goswami, *Study of an aqueous lithium chloride desiccant system: air dehumidification and desiccant regeneration.* Solar Energy, 2002. 72(4): p. 351-361.

119. Longo, G.A. and A. Gasparella, *Experimental analysis on desiccant regeneration in a packed column with structured and random packing.* Solar Energy, 2009. 83(4): p. 511-521.

120. Liu, X.H., et al., *Combined cogeneration and liquid-desiccant system applied in a demonstration building.* Energy and Buildings, 2004. 36(9): p. 945-953.

121. Chen, X.Y., et al., *Field study on independent dehumidification air-conditioning system - I: Performance of liquid desiccant dehumidification system*. Vol. 111. 2005. 271-276.

122. Kim, M.-H., J.-Y. Park, and J.-W. Jeong, *Simplified model for packed-bed tower regenerator in a liquid desiccant system.* Applied Thermal Engineering, 2015. 89: p. 717-726.

123. Liu, X.H., et al., *Experimental investigation of the heat and mass transfer between air and liquid desiccant in a cross-flow regenerator.* Renewable Energy, 2007. 32(10): p. 1623-1636.

124. Bouzenada, S., et al., *Experimental Study on dehumidification/regeneration of Liquid Desiccant: LiBr Solution.* Procedia Computer Science, 2014. 32: p. 673-680.

125. Shen, S., et al., *Investigation of liquid desiccant regenerator with heat recovery heat pipe system.* Energy and Buildings, 2017. 146: p. 353-363.

126. Shen, S., et al., *Investigation of liquid desiccant regenerator with fixed-plate heat recovery system.* Energy, 2017. 137: p. 172-182.

127. Yang, Z., et al., *Experimental study on mass transfer performances of the ultrasonic atomization liquid desiccant dehumidification system.* Energy and Buildings, 2015. 93: p. 126-136.

128. Yang, Z., et al., *Performance investigation on the ultrasonic atomization liquid desiccant regeneration system.* Applied Energy, 2016. 171: p. 12-25.

129. Nada, S.A., *Air cooling-dehumidification/desiccant regeneration processes by a falling liquid desiccant film on finned-tubes for different flow arrangements.* International Journal of Thermal Sciences, 2017. 113: p. 10-19.

130. Cheng, Q. and X. Zhang, *Review of solar regeneration methods for liquid desiccant air-conditioning system.* Energy and Buildings, 2013. 67: p. 426-433.

131. Alosaimy, A.S. and A.M. Hamed, *Theoretical and experimental investigation on the application of solar water heater coupled with air humidifier for regeneration of liquid desiccant.* Energy, 2011. 36(7): p. 3992-4001.

132. Kabeel, A.E., *Augmentation of the performance of solar regenerator of open absorption cooling system.* Renewable Energy, 2005. 30(3): p. 327-338.

133. Li, X.-W. and X.-S. Zhang, *Photovoltaic–electrodialysis regeneration method for liquid desiccant cooling system.* Solar Energy, 2009. 83(12): p. 2195-2204.

134. Cheng, Q., Y. Xu, and X.-S. Zhang, *Experimental investigation of an electrodialysis regenerator for liquid desiccant.* Energy and Buildings, 2013. 67: p. 419-425.

135. Li, X.-W., X.-S. Zhang, and S. Quan, *Single-stage and double-stage photovoltaic driven regeneration for liquid desiccant cooling system.* Applied Energy, 2011. 88(12): p. 4908-4917.

136. Cheng, Q., X.-S. Zhang, and X.-W. Li, *Double-stage photovoltaic/thermal ED regeneration for liquid desiccant cooling system.* Energy and Buildings, 2012. 51: p. 64-72.

137. Yang, Q., X.-W. Li, and A.-M. Fang, *Photovoltaic capacitive deionization regeneration method for liquid desiccant cooling system.* Applied Thermal Engineering, 2017. 117: p. 204-212.

138. Duong, H.C., et al., *Liquid desiccant lithium chloride regeneration by membrane distillation for air conditioning.* Separation and Purification Technology, 2017. 177: p. 121-128.

139. Ge, G., et al., *Comparison of experimental data and a model for heat and mass transfer performance of a liquid-to-air membrane energy exchanger (LAMEE) when used for air dehumidification and salt solution regeneration.* International Journal of Heat and Mass Transfer, 2014. 68: p. 119-131.

140. Datta, N., et al., *Experimental investigation of multi-effect regenerator for desiccant dehumidifier: Effects of various regeneration temperatures and solution flow rates on system performances.* International Journal of Refrigeration, 2017. 76: p. 7-18.

141. London, A.L. and W.M. Kays, *The liquid-coupled indirect-transfer regenerator for gas-turbine plants.* Trans. ASME, 1951. 73(73): p. 529-542.

142. Forsyth, B.I. and R.W. Besant, *The design of a run-around heat recovery system.* ASHRAE Trans, 1988. 94(2): p. 511-531.

143. Forsyth, B.I. and R.W. Besant, *The performance of a run-around heat recovery system using aqueous glycol as a coupling liquid.* ASHRAE Transactions, 1988. 94(2): p. 532-545.

144. Hemingson, H.B., C.J. Simonson, and R.W. Besant, *Steady-state performance of a run-around membrane energy exchanger (RAMEE) for a range of outdoor air conditions.* International Journal of Heat and Mass Transfer, 2011. 54(9): p. 1814-1824.

145. Ge, G., et al., *Analytical model based performance evaluation, sizing and coupling flow optimization of liquid desiccant run-around membrane energy exchanger systems.* Energy and Buildings, 2013. 62: p. 248-257.

146. Seyed-Ahmadi, M., et al., *Transient behavior of run-around heat and moisture exchanger system. Part I: Model formulation and verification.* International Journal of Heat and Mass Transfer, 2009. 52(25): p. 6000-6011.

147. Seyed-Ahmadi, M., et al., *Transient behavior of run-around heat and moisture exchanger system. Part II: Sensitivity studies for a range of initial conditions.* International Journal of Heat and Mass Transfer, 2009. 52(25): p. 6012-6020.

148. Patel, H., et al., *Contaminant transfer in run-around membrane energy exchangers.* Energy and Buildings, 2014. 70: p. 94-105.

149. Mølhave, L., *Volatile Organic Compounds, Indoor Air Quality and Health.* Indoor Air, 1991. 1(4): p. 357-376.

150. Rasouli, M., et al., *Energetic, economic and environmental analysis of a health-care facility HVAC system equipped with a run-around membrane energy exchanger.* Energy and Buildings, 2014. 69: p. 112-121.

151. Rafique, M.M., P. Gandhidasan, and H.M.S. Bahaidarah, *Liquid desiccant materials and dehumidifiers – A review.* Renewable and Sustainable Energy Reviews, 2016. 56: p. 179-195.

152. Elsarrag, E., *Dehumidification of Air by Chemical Liquid Desiccant in a Packed Column and Its Heat and Mass Transfer Effectiveness.* HVAC&R Research, 2006. 12(1): p. 3-16.

153. Ahmed, S.Y., P. Gandhidasan, and A.A. Al-Farayedhi, *Thermodynamic analysis of liquid desiccants.* Solar Energy, 1998. 62(1): p. 11-18.

154. Zuber, A., et al., *Thermodynamic properties of 1:1 salt aqueous solutions with the electrolattice equation of state.* Oil and Gas Science and Technology, 2013. 68(2): p. 255-270.

155. Sun, J., X.L. Gong, and M.H. Shi, *Study on vapor pressure of liquid desiccants solution.* J Refrig, 2004. 5(1): p. 87-95.

156. Morillon, V., et al., *Water vapour pressure above saturated salt solutions at low temperatures.* Fluid Phase Equilibria, 1999. 155(2): p. 297-309.

157. L.McNelly, *Thermodynamic properties of aqueous solutions of lithium bromide.* ASHRAE Trans, 1979(85): p. 412-434.

158. Kaita, Y., *Thermodynamic properties of lithium bromide-water solutions at high temperatures.* International Journal of Refrigeration, 2001. 24(5): p. 374-390.

159. Lazzarin, R.M., A. Gasparella, and G.A. Longo, *Chemical dehumidification by liquid desiccants: theory and experiment.* International Journal of Refrigeration, 1999. 22(4): p. 334-347.

160. Liu, X.H., X.Q. Yi, and Y. Jiang, *Mass transfer performance comparison of two commonly used liquid desiccants: LiBr and LiCl aqueous solutions.* Energy Conversion and Management, 2011. 52(1): p. 180-190.

161. Koronaki, I.P., et al., *Thermodynamic analysis of a counter flow adiabatic dehumidifier with different liquid desiccant materials.* Applied Thermal Engineering, 2013. 50(1): p. 361-373.

162. Elmer, T., et al., *An experimental study of a novel integrated desiccant air conditioning system for building applications.* Energy and Buildings, 2016. 111: p. 434-445.

163. Atkinson, S., *Vapour absorbent compositions comprising potassium formate, US patent 5846450.* 1998.

164. Lin, J., et al., *Thermodynamic analysis of a hybrid membrane liquid desiccant dehumidification and dew point evaporative cooling system.* Energy Conversion and Management, 2018. 156: p. 440-458.

165. Ertas, A., E.E. Anderson, and I. Kiris, *Properties of a new liquid desiccant solution—Lithium chloride and calcium chloride mixture.* Solar Energy, 1992. 49(3): p. 205-212.

166. Nielsen, L.E., *Predicting the properties of mixtures: Mixture rules in science and engineering* 1978, New York: Marcel Dekker.

167. Chen, C.-C. and L.B. Evans, *A local composition model for the excess Gibbs energy of aqueous electrolyte systems.* AIChE Journal, 1986. 32(3): p. 444-454.

168. Chen, C.-C., et al., *Local composition model for excess Gibbs energy of electrolyte systems. Part I: Single solvent, single completely dissociated electrolyte systems.* AIChE Journal, 1982. 28(4): p. 588-596.

169. Yao, Y., Y. Yu, and Z. Zhu, *Experimental investigations on surface vapor pressure models for LiCl–CaCl2 desiccant solutions.* Solar Energy, 2016. 126: p. 1-13.

170. ZY Zhu, Y.Y., *Verification and research on the vapour pressure of mixed LiCl-CaCl2 solution.* Journal of Refrigeration 2015. 36(6): p. 52-56.

171. Zhao, X., X. Li, and X. Zhang, *Selection of optimal mixed liquid desiccants and performance analysis of the liquid desiccant cooling system.* Applied Thermal Engineering, 2016. 94: p. 622-634.

172. Xiu-Wei, L., et al., *Research on ratio selection of a mixed liquid desiccant: Mixed LiCl–CaCl2 solution.* Solar Energy, 2008. 82(12): p. 1161-1171.

173. Li, X.-W., et al., *Research on ration selection of mixed absorbent solution for membrane air-conditioning system.* Energy Conversion and Management, 2015. 89: p. 111-119.

174. Li, X.-W., et al., *Progress in selecting desiccant and dehumidifier for liquid desiccant cooling system.* Energy and Buildings, 2012. 49: p. 410-418.

175. Techajunta, S., S. Chirarattananon, and R.H.B. Exell, *Experiments in a solar simulator on solid desiccant regeneration and air dehumidification for air conditioning in a tropical humid climate.* Renewable Energy, 1999. 17(4): p. 549-568.

176. Li Xin, L.Z., Wei Lifei, Xiao Jing,Xiao Limin, *Review on the Materials of Dehumidification.* Chemical Industry and Engineering Progress, 2004. 8: p. 811-815.

177. Jia, C.X., et al., *Experimental comparison of two honeycombed desiccant wheels fabricated with silica gel and composite desiccant material.* Energy Conversion and Management, 2006. 47(15-16): p. 2523-2534.

178. González, J.C., M. Molina-Sabio, and F. Rodríguez-Reinoso, *Sepiolite-based adsorbents as humidity controller.* Applied Clay Science, 2001. 20(3): p. 111-118.

179. Chua, K.J., *Heat and mass transfer of composite desiccants for energy efficient air dehumidification: Modelling and experiment.* Applied Thermal Engineering, 2015. 89: p. 703-716.

180. Chua, K.J., S.K. Chou, and M.R. Islam, *Integrating Composite Desiccant and Membrane Dehumidifier to Enhance Building Energy Efficiency.* Energy Procedia, 2017. 143: p. 186-191.

181. Zhang, X.-R., et al., *One-step fabrication and analysis of an asymmetric cellulose acetate membrane for heat and moisture recovery.* Journal of Membrane Science, 2011. 366(1): p. 158-165.

182. Zhang, L.-Z., et al., *Synthesis and characterization of a PVA/LiCl blend membrane for air dehumidification.* Journal of Membrane Science, 2008. 308(1): p. 198-206.

183. Zhang, L.-Z., *Progress on heat and moisture recovery with membranes: From fundamentals to engineering applications.* Energy Conversion and Management, 2012. 63: p. 173-195.

184. Jansen AE, F.P., *Method for gas absorption across a membrane,* U. Patent, Editor. 1998.

185. Gabelman, A. and S.-T. Hwang, *Hollow fiber membrane contactors.* Journal of Membrane Science, 1999. 159(1): p. 61-106.

186. Woods, J., et al., *Modeling of a membrane-based absorption heat pump.* Journal of Membrane Science, 2009. 337(1): p. 113-124.

187. Li, K. and W.K. Teo, *An Ultrathin Skinned Hollow Fibre Module for Gas Absorption at Elevated Pressures.* Chemical Engineering Research and Design, 1996. 74(8): p. 856-862.

188. Karoor, S. and K.K. Sirkar, *Gas Absorption Studies in Microporous Hollow Fiber Membrane Modules.* Industrial and Engineering Chemistry Research, 1993. 32(4): p. 674-684.

189. Lee, Y., et al., *Analysis of CO2 removal by hollow fiber membrane contactors.* Journal of Membrane Science, 2001. 194(1): p. 57-67.

190. Yang, B., et al., *A review of membrane-based air dehumidification.* Indoor and Built Environment, 2015. 24(1): p. 11-26.

191. Zhang, L.-Z., *Numerical study of heat and mass transfer in an enthalpy exchanger with a hydrophobic-hydrophilic composite membrane core.* Numerical Heat Transfer, Part A: Applications, 2007. 51(7): p. 697-714.

192. Zhang, L.-Z., *Coupled heat and mass transfer through asymmetric porous membranes with finger-like macrovoids structure.* International Journal of Heat and Mass Transfer, 2009. 52(3): p. 751-759.

193. Pei, L., W. Zhao, and L. Zhang, *Preparation and characterization of porous poly(vinylidene fluoride) membranes for dehumidification with poly(ethylene glycol) as an additive.* Journal of Applied Polymer Science, 2010. 118(5): p. 2696-2703.

194. Liu, X.H., K.Y. Qu, and Y. Jiang, *Empirical correlations to predict the performance of the dehumidifier using liquid desiccant in heat and mass transfer.* Renewable Energy, 2006. 31(10): p. 1627-1639.

195. Liu, X.-H., Y. Jiang, and K.-Y. Qu, *Analytical solution of combined heat and mass transfer performance in a cross-flow packed bed liquid desiccant air dehumidifier.* International Journal of Heat and Mass Transfer, 2008. 51(17): p. 4563-4572.

196. Khan, A.Y. and H.D. Ball. *Development of a generalized model for performance evaluation of packed-type liquid sorbent dehumidifiers and regenerators*. in *ASHRAE Transactions*. 1992.

197. Chen, X.Y., et al., *Analytical solution of adiabatic heat and mass transfer process in packed-type liquid desiccant equipment and its application.* Solar Energy, 2006. 80(11): p. 1509-1516.

198. Chengqin, R., J. Yi, and Z. Yianpin, *Simplified analysis of coupled heat and mass transfer processes in packed bed liquid desiccant-air contact system.* Solar Energy, 2006. 80(1): p. 121-131.

199. Stevens, D.I., J.E. Braun, and S.A. Klein, *An effectiveness model of liquid-desiccant system heat/mass exchangers.* Solar Energy, 1989. 42(6): p. 449-455.

200. Babakhani, D. and M. Soleymani, *Simplified analysis of heat and mass transfer model in liquid desiccant regeneration process.* Journal of the Taiwan Institute of Chemical Engineers, 2010. 41(3): p. 259-267.

201. Sadasivam, M. and A.R. Balakrishnan, *Effectiveness-NTU method for design of packed bed liquid desiccant dehumidifiers.* Chemical Engineering Research and Design, 1992. 70(A6): p. 572-577.

202. Ramesh K. Shah, D.P.S., *Fundamental of heat exchanger design*. 2003, New York: John Wiley & Sons. 976.

203. Nasif MS, M.G., Behnia M, *Heat and Mass Transfer in Air to Air Enthalpy Heat Exchangers*, in *6th International Conference on Heat Transfer, Fluid Mechanics and Thermodynamics*. 2005: Matsushima, Japan.

204. Gandhidasan, P., M. Rifat Ullah, and C.F. Keftleborough, *Analysis of heat and mass transfer between a desiccant-air system in a packed tower.* Journal of Solar Energy Engineering, Transactions of the ASME, 1987. 109(2): p. 89-93.

205. Oberg, V. and D.Y. Goswami, *Experimental study of the heat and mass transfer in a packed bed liquid desiccant air dehumidifier.* Journal of Solar Energy Engineering, Transactions of the ASME, 1998. 120(4): p. 289-297.

206. Liu, X.H., Y. Jiang, and K.Y. Qu, *Heat and mass transfer model of cross flow liquid desiccant air dehumidifier/regenerator.* Energy Conversion and Management, 2007. 48(2): p. 546-554.

207. Shah, R.K. and A.L. London, *Chapter VII - Rectangular Ducts*, in *Laminar Flow Forced Convection in Ducts*, R.K. Shah and A.L. London, Editors. 1978, Academic Press. p. 196-222.

208. Kays WM, C.M., *Convective heat and mass transfer*. third edition ed. 1990, New York: McGraw-Hill.

209. Hewitt, G.F., *Heat exchanger design handbook*. 2008: Begell House Inc. Publishers.

210. Namvar, R., et al., *Transient heat and moisture transfer characteristics of a liquid-to-air membrane energy exchanger (LAMEE) model verification and extrapolation.* International Journal of Heat and Mass Transfer, 2013. 66: p. 757-771.

211. Happel, J., *Viscous flow relative to arrays of cylinders.* AIChE Journal, 1959. 5(2): p. 174-177.

212. !!! INVALID CITATION !!! [].

213. Frank P. Incropera, D.P.D., Theodore L. Bergman, Adrienne S. Lavine *Principles of Heat and Mass Transfer* seventh edition ed. 2012 Jogn Wiley & Sons, Inc.

214. *2013 ASHRAE handbook : fundamentals*. 2013: Atlanta, GA: ASHRAE.

215. Cisternas, L.A. and E.J. Lam, *An analytic correlation for the vapour pressure of aqueous and non-aqueous solutions of single and mixed electrolytes. Part II. Application and extension.* Fluid Phase Equilibria, 1991. 62(1): p. 11-27.

216. American society of heating, r., and air-conditioning engineers, *ANSI/ASHRAE STANDARD 84-2013, Method of test for air-to-air heat/energy exchangers*. 2013: Atlanta

217. Conde, M.R., *Properties of aqueous solutions of lithium and calcium chlorides: formulations for use in air conditioning equipment design.* International Journal of Thermal Sciences, 2004. 43(4): p. 367-382.

218. Simonson, C.J. and R.W. Besant, *Energy wheel effectiveness: part I—development of dimensionless groups.* International Journal of Heat and Mass Transfer, 1999. 42(12): p. 2161-2170.

219. Taylor, J.R., *An Introduction to Error Analysis: The Study of Uncertainties in Physical Measurements*. 2nd Edition ed. 1997, Sausalito, California University Science Books.

220. Bai, H., et al., *Performance evaluation of a membrane-based flat-plate heat and mass exchanger used for liquid desiccant regeneration.* Applied Thermal Engineering, 2018. 139: p. 569-584.

221. Alduchov, O.A. and R.E. Eskridge, *Improved Magnus Form Approximation of Saturation Vapor Pressure.* Journal of Applied Meteorology, 1996. 35(4): p. 601-609.

Appendices

Appendix A: Normalization Methods for Governing Equations of Numerical Modelling

In this appendix, the normalization methods for governing equations are presented. Dehumidifier is taken as the example.

1. Solution side energy equation normalization

The governing equation of energy conservation in the solution side is:

$$\left(\frac{\dot{m}_{sol}}{L}\cdot\frac{\partial T_{sol}}{\partial y}\cdot C_{p,sol}\right)\cdot dxdy=\left[U(T_{air}-T_{sol})+h_{fg}\cdot U_m\left(W_{air}-W_{sol,mem}\right)\right]dxdy$$

Then we define some dimensionless parameters:

$$h^*=\frac{W_{sol,in}-W_{air,in}}{T_{sol,in}-T_{air,in}}\frac{h_{fg}}{c_{p,air}}$$

$$Cr=\frac{\left(\dot{m}c_p\right)_{air}}{\left(\dot{m}c_p\right)_{sol}}$$

$$NTU=\frac{UA}{\left(\dot{m}c_p\right)_{air}}$$

$$NTU_m=\frac{U_mA}{\dot{m}_{air}}$$

$$x^*=\frac{x}{L}$$

$$y^*=\frac{y}{H}$$

$$T^*=\frac{T-T_{air,in}}{T_{sol,in}-T_{air,in}}$$

$$W^*=\frac{W-W_{air,in}}{W_{sol,in}-W_{air,in}}$$

$$m^* = \frac{\dot{m}_{sol}}{\dot{m}_{air}}$$

Then the governing equation can be derived as:

$$\frac{\dot{m}_{sol}}{L} \cdot \frac{\partial T_{sol}}{\partial y} \cdot C_{p,sol} = \frac{(\dot{m}c_p)_{air} NTU}{LH} (T^*_{air} - T^*_{sol})\left(T_{sol,in} - T_{air,in}\right) + h_{fg} \frac{\dot{m}_{air} NTU_m}{LH} (W_{air}{}^* -$$

$$W_{sol,mem}{}^*)(W_{sol,in} - W_{air,in})$$

Times $\frac{LH}{(\dot{m}c_p)_{sol}}$ for both sides:

$$\frac{\partial T_{sol}}{\partial y^*} = NTUCr\left(T_{sol,in} - T_{air,in}\right)(T^*_{air} - T^*_{sol}) + h_{fg} \frac{Cr}{C_{p,air}} NTU_m\left(W_{air}{}^* - W_{sol,mem}{}^*\right)$$

$$\left(W_{sol,in} - W_{air,in}\right)$$

Substitute $h_{fg} = h^* C_{p,air} \frac{(T_{sol,in} - T_{air,in})}{(W_{sol,in} - W_{air,in})}$ into the above equation:

$$\frac{\partial T_{sol}}{\partial y^*} - NTU_m h^* Cr\left(W_{air}{}^* - W_{sol,mem}{}^*\right) - NTUCr(T_{air}{}^* - T_{sol}{}^*) = 0$$

2. Solution side mass equation normalization

The governing equation of moisture conservation in the solution side is:

$$\frac{\dot{m}_{desi}}{L} \cdot \frac{\partial X_{sol}}{\partial y} \cdot dxdy - U_m \cdot \left(W_{air} - W_{sol,men}\right)dxdy = 0$$

Then we define:

$$W_0 = W_{sol,in} - W_{air,in}$$

$$X_{sol} = \frac{\dot{m}_{moisture}}{\dot{m}_{desi}}$$

Then the governing equation can be derived as:

$$\frac{\dot{m}_{desi}}{L} \cdot \frac{\partial X_{sol}}{\partial y} - \frac{\dot{m}_{air} NTU_m}{LH}\left(W_{air}{}^* - W_{sol,mem}{}^*\right)W_0 = 0$$

$$\dot{m}_{desi} \frac{\partial X_{sol}}{\partial y^*} - \dot{m}_{air} NTU_m \, W_0\left(W_{air}{}^* - W_{sol,mem}{}^*\right) = 0$$

$$\frac{\partial X_{sol}}{\partial y^*} - NTU_m \frac{1}{m^*} W_0 (1 + X_{sol})({W_{air}}^* - {W_{sol,mem}}^*) = 0$$

3. Air side energy equation normalization

The governing equation of energy conservation in the air side is:

$$\frac{\dot{m}_{air}}{H} \cdot \frac{\partial T_{air}}{\partial x} \cdot C_{p,air} + U(T_{air} - T_{sol}) = 0$$

Then the governing equation can be derived as:

$$\frac{\dot{m}_{air}}{H} C_{p,air} \frac{\partial T_{air}}{\partial x} + \frac{\left(\dot{m}c_p\right)_{air} NTU}{LH} (T_{air}^* - T_{sol}^*)\left(T_{sol,in} - T_{air,in}\right) = 0$$

$$\frac{\partial {T_{air}}^*}{\partial x^*} + NTU({T_{air}}^* - {T_{sol}}^*) = 0$$

4. Air side mass equation normalization

The governing equation of moisture conservation in the air side is:

$$\frac{\dot{m}_{air}}{H} \frac{\partial W_{air}}{\partial x} + U_m \cdot \left(W_{air} - W_{sol,men}\right) = 0$$

Then the governing equation can be derived as:

$$\frac{\dot{m}_{air}}{H} \frac{\partial W_{air}}{\partial x} + \frac{\dot{m}_{air} NTU_m}{LH} \left({W_{air}}^* - {W_{sol,mem}}^*\right) W_0 = 0$$

$$\frac{\partial {W_{air}}^*}{\partial x^*} + NTU_m \left({W_{air}}^* - {W_{sol,mem}}^*\right) = 0$$

5. Membrane surface heat transfer boundary equation normalization

The heat transfer boundary equation through the membrane is:

$$h_{sol}\left(T_{sol,mem} - T_{sol}\right) = U\left(T_{air} - T_{sol,mem}\right) + h_{fg} U_m \left(W_{air} - W_{sol,mem}\right)$$

Then we define:

$$NTU_{sol} = \frac{h_{sol} A}{\left(\dot{m}c_p\right)_{air}}$$

Then the governing equation can be derived as:

$$\frac{NTU_{sol}\left(\dot{m}c_p\right)_{air}}{LH}\left(T_{sol,mem}{}^{*}-T_{sol}{}^{*}\right)\left(T_{sol,in}-T_{air,in}\right)=\frac{\left(\dot{m}c_p\right)_{air}NTU}{LH}$$

$$\left(T_{air}{}^{*}-T_{sol,mem}{}^{*}\right)\left(T_{sol,in}-T_{air,in}\right)+\frac{h^{*}(T_{sol,in}-T_{air,in})c_{p,air}}{W_{sol,in}-W_{air,in}}\cdot\frac{\dot{m}_{air}NTU_m}{LH}\left(W_{air}{}^{*}\right.$$

$$\left.-W_{sol,mem}{}^{*}\right)\left(W_{sol,in}-W_{air,in}\right)$$

$$NTU_{sol}\left(T_{sol,mem}{}^{*}-T_{sol}{}^{*}\right)=NTU\left(T_{air}{}^{*}-T_{sol,mem}{}^{*}\right)+NTU_m h^{*}\left(W_{air}{}^{*}-W_{sol,mem}{}^{*}\right)$$

6. Membrane surface mass transfer boundary equation normalization

The mass transfer boundary equation through the membrane is:

$$U_m\left(W_{air}-W_{sol,mem}\right)=h_{m,sol}\left(C_{sol}-C_{sol,mem}\right)$$

Then we define:

$$NTU_{m.sol}=\frac{h_{m,sol}A}{\dot{m}_{air}}$$

Then the governing equation can be derived as:

$$\frac{\dot{m}_{air}NTU_m}{LH}\left(W_{air}{}^{*}-W_{sol,mem}{}^{*}\right)\left(W_{sol,in}-W_{air,in}\right)=\frac{\dot{m}_{air}NTU_{m,sol}}{LH}\left(C_{sol}-C_{sol,mem}\right)$$

$$NTU_m W_0\left(W_{air}{}^{*}-W_{sol,mem}{}^{*}\right)=NTU_{m.sol}\left(C_{sol}-C_{sol,mem}\right)$$

Appendix B: Matlab Script for Dehumidifier or Regenerator Simulation

```
clear

%inlet conditions
T_sol_in=25;   %solution inlet temperature (C) (input value)
C_sol_in=0.39; %solution inlet mass concentration (%) (input value)
X_sol_in=(1-C_sol_in)/C_sol_in;  %solution inlet mass ratio between water
and salt (%)
W_sol_in=psychro_LiCl(T_sol_in,C_sol_in);  %solution inlet humidity ratio
(kg/kg)

T_air_in=30;   %air inlet temperature (C) (input value)
RH_air_in=70;  %air inlet relative humidity (%)  (input value)
W_air_in=humidityratio_air(T_air_in,RH_air_in);  %air inlet humidity ratio
(kg/kg)

NTU=12;    %NTU (input value)


m_mass_flow_ratio=2;   %solution mass flow rate over air mass flow rate
(input value)
m_star=1/m_mass_flow_ratio; %air mass flow rate over solution mass flow
rate

rou_air=1.29;  %air density (kg/m3)01
rou_sol=1247;  %solution density (kg/m3)


%geometric peroperties
number_of_channels=11;  %number of channels
L=0.41;     %length of dehumidfiier unit (m)
H=0.21;     %height of dehumidifier unit (m)
d_air=7.7e-3;   %air channel thickness (m)
d_sol=4.3e-3;   %solution channel thickness (m)
L_air=(4*d_air*H)/(2*(d_air+H));  %air channel hydrolic diameter (m)
L_sol=(4*d_sol*H)/(2*(d_sol+H));  %solution channel hydrolic diameter (m)
A=L*H*(number_of_channels*2-1);   %total heat and mass transfer area (m2)


%heat transfer coefficients
Nu_air=6.58;  %air side Nusselt number
k_air=0.03;   %air side heat conductivity (W/mK)
h_air=(Nu_air*k_air)/L_air;  %air side convective heat transfer coefficient
(W/m2K)

Nu_sol=7.74;  %solution side Nusselt number
k_sol=0.53;   %solution side heat conductivity (W/mK)
h_sol=(Nu_sol*k_sol)/L_sol;  %solution side convective heat transfer
coefficient (W/m2K)

%mass transfer coefficient
Sh_air=6.7;     %air side Sherwood number
```

```
D_air=2.46e-5;  %air side diffusivity
h_m_air=((Sh_air*D_air)/L_air)*rou_air;   %air side convective mass
transfer coefficient (kg/m2K)

Sh_sol=6.7;      %solution side Sherwood number ??
D_sol=0.892e-2;  %solution side diffusivity ??
h_m_sol=((Sh_sol*D_sol)/L_sol)*rou_sol;   %solution side convective mass
transfer coefficnet (kg/m2K)


%membrane properties
delta_mem=0.0005;    %membrane thickness (m)
k_mem=0.3;           %membrane heat conductivity (W/mK)
k_m_mem=3.87e-6;     %membrane mass conductivity (kg/mK)

%other peroperties
cp_air=1.02;                %air specific heat capacity (kJ/kgK)
cp_sol=3.2;                 %solution specific capacity (kJ/kgK)
h_fg=2450;                  %condensation heat of water (J/kg)
Cr=m_star*(cp_air/cp_sol);  %thermal capacity ratio

%NTU and NTUm
U=(1/h_air+delta_mem/k_mem+1/h_sol)^-1; %overall heat transfer coefficient
(W/m2K)
U_m=(delta_mem/k_m_mem+1/h_m_air)^-1;   %overall mass transfer coefficient
(kg/m2s)
m_air=(U*A)/(NTU*1000*cp_air);          %inlet air mass flow rate(kg/s)
NTU_m=(U_m*A)/m_air;                    %NTUm
NTU_sol=(h_sol*A)/(m_air*cp_air*1000);  %solution side NTU
NTU_m_sol=(h_m_sol*A)/m_air;            %solution side NTUm

m_sol=m_air*m_mass_flow_ratio;          %solution mass flow rate (kg/s)
m_salt=m_sol/(1+X_sol_in);              %salt mass flow rate (kg/s)

%matrixing and assign initial values
n=100;      %number of grids in y direction
m=200;      %number of grids in x direction
dx=1/(m-1); %grid length in x direction
dy=1/(n-1); %grid length in y direction

z=ones(n,m);
error1=10;error2=10;error3=10;error4=10;error5=10;

T_air=T_air_in*z;     %assign initial values for air inlet temperature
T_sol=T_sol_in*z;     %assign initial values for solution inlet temperature
W_air=W_air_in*z;     %assign initial values for air inlet humidity ratio
X_sol=X_sol_in*z;     %assign initial values for solution inlet mass ratio
W_sol_mem=W_sol_in*z; %assign initial values for solution membrane humidity
ratio

W0=W_sol_in-W_air_in;                                    %define the
dimentionless parameter W0
T_non_air=(T_air-T_air_in)/(T_sol_in-T_air_in);          %normalization
of air temperature
T_non_sol=(T_sol-T_air_in)/(T_sol_in-T_air_in);          %normalization
of solution temperature
W_non_air=(W_air-W_air_in)/W0;                           %normalization
of air humidity ratio
```

```
W_non_sol_mem=(W_sol_mem-W_air_in)/W0;                    %normalization
of solution membrane humidity ratio
h=((W_sol_in-W_air_in)/(T_sol_in-T_air_in))*(h_fg/cp_air); %normalization
of h*


%start the loop
while (error1>1e-10)||(error2>1e-10)||(error3>1e-10)||(error4>1e-10);


%the solution side mass equation
 X_sol_f=X_sol;
 for a=1:n-1;
    for b=1:m;
        X_sol(1,b)=X_sol_in;  %boundary condition
        X_sol(a+1,b)=(X_sol(a,b)+dy*m_star*W0*NTU_m*((W_non_air(a+1,b))-
W_non_sol_mem(a+1,b))./(1-dy*m_star*W0*NTU_m*(W_non_air(a+1,b)-
W_non_sol_mem(a+1,b)));
    end
 end
 error1=sum(sum(abs(X_sol-X_sol_f)./(X_sol)));
 C_sol=1./(1+X_sol);


 %the solution side energy equation
 T_sol_f=T_sol;
 for c=1:n-1;
     for d=1:m;
         T_non_sol(1,d)=1;   %boudary condition
         T_non_sol(c+1,d)=(T_non_sol(c,d)+dy*NTU_m*h*Cr*(W_non_air(c+1,d)-
W_non_sol_mem(c+1,d))+dy*Cr*NTU*T_non_air(c+1,d))/(1+dy*NTU*Cr);
     end
 end
 T_sol=T_non_sol*(T_sol_in-T_air_in)+T_air_in;
 error2=sum(sum(abs(T_sol-T_sol_f)./(T_sol)));


 %the air side mass equation
 W_air_f=W_air;
 for e_=1:n;
     for f=1:m-1;
         W_non_air(e_,1)=0;   %boundary condition

W_non_air(e_,f+1)=(W_non_air(e_,f)+dx*NTU_m*W_non_sol_mem(e_,f+1))./(1+dx*N
TU_m);
     end
 end
 W_air=W_non_air*W0+W_air_in;
 error3=sum(sum(abs(W_air-W_air_f)./(W_air)));


 %the air side energy equation
 T_air_f=T_air;
 for g=1:n;
     for h_=1:m-1;
         T_non_air(g,1)=0;    %boundary condition

T_non_air(g,h_+1)=(T_non_air(g,h_)+dx*NTU*T_non_sol(g,h_+1))./(1+dx*NTU);
     end
```

```
 end
 T_air=T_non_air*(T_sol_in-T_air_in)+T_air_in;
 error4=sum(sum(abs(T_air-T_air_f)./(T_air)));

 error5=10;


         while (error5>1e-10)

             W_non_sol_mem_f=W_non_sol_mem;
             C_sol_mem=C_sol-((NTU_m*W0*(W_non_air-
W_non_sol_mem))./(NTU_m_sol));  %solve membrane mass equation
             T_non_sol_mem=(NTU*T_non_air+NTU_m*h*(W_non_air-
W_non_sol_mem)+NTU_sol*T_non_sol)./(NTU_sol+NTU);
             T_sol_mem=T_non_sol_mem*(T_sol_in-T_air_in)+T_air_in;

             %obtain the new membrane humidity ratio
             W_sol_mem=psychro_LiCl(T_sol_mem,C_sol_mem);
             W_non_sol_mem=(W_sol_mem-W_air_in)/W0;

             error5=sum(sum(abs(W_non_sol_mem-
W_non_sol_mem_f)./(W_non_sol_mem)));

         end
end

T_air_out=mean(T_air(:,m));
W_air_out=mean(W_air(:,m));
T_sol_out=mean(T_sol(n,:));
X_sol_out=mean(X_sol(n,:));
C_sol_out=1./(1+X_sol_out);

effec_sen_air=(T_air_in-T_air_out)/(T_air_in-T_sol_in);      %calculate the
air side sensible effectiveness
effec_lat_air=(W_air_in-W_air_out)/(W_air_in-W_sol_in);      %calcualte the
air side latent effectiveness
effec_tot_air=(effec_sen_air+h*effec_lat_air)/(1+h);         %calculate the
air side total effectiveness

effec_sen_sol=(m_sol*cp_sol*(T_sol_out-T_sol_in)-m_salt*h_fg*(X_sol_out-
X_sol_in))/(m_air*cp_air*(T_air_in-T_sol_in));  %calculate the solution
side sensible effectiveness
effec_lat_sol=(m_salt*h_fg*(X_sol_out-X_sol_in))/(m_air*h_fg*(W_air_in-
W_sol_in));                                          %calculate the solution
side latent effectiveness
effec_tot_sol=(m_sol*cp_sol*(T_sol_out-T_sol_in))/(m_air*cp_air*(T_air_in-
T_sol_in)+m_air*h_fg*(W_air_in-W_sol_in));    %calculate the solution side
total effectiveness

MRR=m_air*(W_air_in-W_air_out);        %calculate the moisture romoval rate
```

```
function output=psychro_LiCl(T_sol_in,C_sol_in)
output=(0.62198.*Pv(T_sol_in,C_sol_in))./(101325-Pv(T_sol_in,C_sol_in))

 function output1=Pv(T_sol_in,C_sol_in);
 output1=(10.^(0.73*I(C_sol_in).*(A(C_sol_in)-
B(C_sol_in)./((T_sol_in)+273.15-39.53))+(C(C_sol_in)-
D(C_sol_in)./((T_sol_in)+273.15-39.53))))*1000;

   function output2=I(C_sol_in);
   output2=(400/17)*(C_sol_in./(1-C_sol_in));
   end
    function output3=A(C_sol_in);
      output3=-0.021302+3.60591e-4*I(C_sol_in)+0.018/2303;
    end
    function output4=B(C_sol_in);
      output4=-5.390915+1.382982*I(C_sol_in)-0.031185*I(C_sol_in).^2;
    end
    function output5=C(C_sol_in);
      output5=7.192959-3.99334e-3*I(C_sol_in)-1.11614e-
4*I(C_sol_in).^2+(0.018*I(C_sol_in).*(1-2))./2303;
    end
    function output6=D(C_sol_in);
      output6=1730.2857-0.138481*I(C_sol_in)+0.027511*I(C_sol_in).^2-
1.79277e-3*I(C_sol_in).^3;
    end
 end
end



function W_air_in=humidityratio_air(T_air_in,RH_air_in)
W_air_in=((6.112*exp((17.67*T_air_in)/(T_air_in+243.5))*RH_air_in*2.1674)/(
273.15+T_air_in))/(1.2*1000)
```

Appendix C: Matlab Script for the Complete System Simulation

```
clear

%basic inlet conditions

m_sol_de=0.009;                    %assign solution mass flow rate in
dehumidifier (kg/s)
m_sol_re=0.009;                    %assign solution mass flow rate in
regenerator (kg/s)

NTU_de=1;                          %assign NTU in dehumidfiier
NTU_re=4;                          %assign NTU in regenerator

rou_air=1.29;                      %air density (kg/m3)
rou_sol=1247;                      %solution density (kg/m3)
cp_air=1.02;                       %air specific heat capacity (kJ/kgK)
cp_sol=3.2;                        %solution specific heat capacity
(kJ/kgK)
cp_water=4.187;                    %water specific heat capacity (KJ/kgK)
h_fg=2450;                         %condensation heat of water (J/kg)

A=1.8081;                          %total heat and mass transfer area (m2)

%heat and mass transfer coefficient

L_air=0.0149;                                              %air channel
hydrolic diameter (m)
L_sol=0.0084;                                              %solution
channel hydrolic diameter (m)

Nu_air=6.58;                                               %air side
Nusselt number
k_air=0.03;                                                %air side heat
conductivity (W/mK)
h_air=(Nu_air*k_air)/L_air;                                %air side
convective heat transfer coefficient (W/m2K)

Nu_sol=7.74;                                               %solution side
Nusselt number
k_sol=0.53;                                                %solution side
heat conductivity (W/mK)
h_sol=(Nu_sol*k_sol)/L_sol;                                %solution side
convective heat transfer coefficient (W/m2K)

Sh_air=6.7;                                                %air side
Sherwood number
D_air=2.46e-5;                                             %air side
diffusivity
h_m_air=((Sh_air*D_air)/L_air)*rou_air;                    %air side
convective mass transfer coefficient (kg/m2K)

Sh_sol=6.7;                                                %solution side
Sherwood number
D_sol=0.892e-2;                                            %solution side
diffusivity
```

```
h_m_sol=((Sh_sol*D_sol)/L_sol)*rou_sol;                    %solution side
convective mass transfer coefficnet (kg/m2K)


%membrane properties
delta_mem=0.0005;                                          %membrane
thickness (m)
k_mem=0.3;                                                 %membrane heat
conductivity (W/mK)
k_m_mem=3.87e-6;                                           %membrane mass
conductivity (kg/mK)

%NTU and NTUm; m_air and m_sol;m* and Cr*
U=(1/h_air+delta_mem/k_mem+1/h_sol)^-1;                    %overall heat
transfer coefficient (W/m2K)
U_m=(delta_mem/k_m_mem+1/h_m_air)^-1;                      %overall mass
transfer coefficient (kg/m2s)

m_air_de=(U*A)/(NTU_de*1000*cp_air);                       %inlet air mass
flow rate in dehumidifier (kg/s)
m_air_re=(U*A)/(NTU_re*1000*cp_air);                       %inlet air mass
flow rate in regenerator (kg/s)

NTU_m_de=(U_m*A)/m_air_de;                                 %NTUm in
dehumidifier
NTU_m_re=(U_m*A)/m_air_re;                                 %NTUm in
regenerator

NTU_sol_de=(h_sol*A)/(m_air_de*cp_air*1000);               %solution side
NTU in dehumidifier
NTU_sol_re=(h_sol*A)/(m_air_re*cp_air*1000);               %solution side
NTU in regenerator

NTU_m_sol_de=(h_m_sol*A)/m_air_de;                         %solution side
NTUm in dehumidifier
NTU_m_sol_re=(h_m_sol*A)/m_air_re;                         %solution side
NTUm in regenerator

m_mass_flow_ratio_de=m_sol_de/m_air_de;
m_mass_flow_ratio_re=m_sol_re/m_air_re;
m_star_de=1/m_mass_flow_ratio_de;
m_star_re=1/m_mass_flow_ratio_re;

Cr_de=m_star_de*(cp_air/cp_sol);                           %thermal
capacity ratio in dehumidifier
Cr_re=m_star_re*(cp_air/cp_sol);                           %thermal
capacity ratio in regenerator


% !!! inlet conditions in dehumidifier and regenerator

T_air_in_de(1)=30;      %air inlet temperature in dehumidifier (C)
W_air_in_de(1)=0.015;   %air inlet specific humidity in dehumidifier
(kg/kg)

T_air_in_re(1)=28;      %air inlet temperature in regenerator (C)
W_air_in_re(1)=0.012;   %air inlet specific humidity in regenerator (kg/kg)
```

```
T_sol_in_de(1)=25;      %solution inlet temperature in dehumidifier (C)
C_sol_in_de(1)=0.39;    %solution inlet mass concentration in dehumidifier

T_sol_in_re(1)=47.0905;      %solution inlet temperature in dehumidifier
(C)
C_sol_in_re(1)=0.3865;       %solution inlet mass concentration in
dehumidifier (%)

n=30;                                        %number of grids in y direction
m=60;                                        %number of grids in x direction
dx=1/(m-1);                                  %grid length in x direction
dy=1/(n-1);                                  %grid length in y direction
z=ones(n,m);                                 %define the matrix


%three heat exchangers,boiler and coolin water simulation

effect_1=0.7;                                                %effectiveness of
heat exchanger 1(solution exchanger)
effect_2=0.7;                                                %effectiveness of
heat exchanger 2(cooling water)
effect_3=0.7;                                                %effectiveness of
heat exchanger 3(hot water)

T_coldwater_in=10;                                           %cold water inlet
temperature (C)
m_coldwater=0.006;                                           %cold water mass
flow rate (kg/s)

T_hotwater_in=60;                                            %hot water inlet
temperature (C)
m_hotwater=0.006;                                            %hot water mass
flow rate (kg/s)




%start the loop


%matrixing and assign initial values


error_C_de=10;error_C_re=10;error_T_de=10;error_T_re=10;

i=1;

while error_C_de>0.05||error_C_re>0.05||error_T_de>0.05||error_T_re>0.05

error1=10;error2=10;error3=10;error4=10;error5=10;error6=10;error7=10;error
8=10;error9=10;error10=10;

W_air_in_de(i)=W_air_in_de(1);       %air inlet humidity ratio in
dehumidifier (kg/kg)
W_air_in_re(i)=W_air_in_re(1);       %air inlet humidity ratio in
regenerator (kg/kg)
```

```
X_sol_in_de(i)=(1-
C_sol_in_de(i))/C_sol_in_de(i);                          %solution inlet mass
ratio between water and salt in dehumidifier (%)
X_sol_in_re(i)=(1-
C_sol_in_re(i))/C_sol_in_re(i);                          %solution inlet mass
ratio between water and salt in dehumidifier (%)
W_sol_in_de(i)=psychro_LiCl(T_sol_in_de(i),C_sol_in_de(i));             %so
lution inlet humidity ratio in dehumidifier (kg/kg)
W_sol_in_re(i)=psychro_LiCl(T_sol_in_re(i),C_sol_in_re(i));             %so
lution inlet humidity ratio in dehumidifier (kg/kg)


T_air_de=T_air_in_de(i)*z;                                          %assign
initial values for air inlet temperature in dehumidifier
T_air_re=T_air_in_re(i)*z;                                          %assign
initial values for air inlet temperature in regenerator

T_sol_de=T_sol_in_de(i)*z;                                          %assign
initial values for solution inlet temperature in dehumidifier
T_sol_re=T_sol_in_re(i)*z;                                          %assign
initial values for solution inlet temperature in regenerator

W_air_de=W_air_in_de(i)*z;                                          %assign
initial values for air inlet humidity ratio in dehumidfiier
W_air_re=W_air_in_re(i)*z;                                          %assign
initial values for air inlet humidity ratio in regenerator

X_sol_de=X_sol_in_de(i)*z;                                          %assign
initial values for solution inlet mass ratio in dehumidifier
X_sol_re=X_sol_in_re(i)*z;                                          %assign
initial values for solution inlet mass ratio in dehumidifier

W_sol_mem_de=W_sol_in_de(i)*z;                                      %assign
initial values for solution membrane humidity ratio in dehumidifier
W_sol_mem_re=W_sol_in_re(i)*z;                                      %assign
initial values for solution membrane humidity ratio in regenerator


%normalization
W0_de=W_sol_in_de(i)-
W_air_in_de(i);                                                          %defi
ne the dimentionless parameter W0 in dehumidifier
W0_re=W_sol_in_re(i)-
W_air_in_re(i);                                                          %defi
ne the dimentionless parameter W0 in regenerator

T_non_air_de=(T_air_de-T_air_in_de(i))/(T_sol_in_de(i)-
T_air_in_de(i));                    %normalization of air temperature in
dehumidifier
T_non_air_re=(T_air_re-T_air_in_re(i))/(T_sol_in_re(i)-
T_air_in_re(i));                    %normalization of air temperature in
regenerator

T_non_sol_de=(T_sol_de-T_air_in_de(i))/(T_sol_in_de(i)-
T_air_in_de(i));                    %normalization of solution temperature
in dehumidifier
T_non_sol_re=(T_sol_re-T_air_in_re(i))/(T_sol_in_re(i)-
T_air_in_re(i));                    %normalization of solution temperature
in regenerator
```

```
W_non_air_de=(W_air_de-
W_air_in_de(i))/W0_de;                                          %normal
ization of air humidity ratio in dehumidifier
W_non_air_re=(W_air_re-
W_air_in_re(i))/W0_re;                                          %normal
ization of air humidity ratio in regenerator

W_non_sol_mem_de=(W_sol_mem_de-
W_air_in_de(i))/W0_de;                                  %normalization
of solution membrane humidity ratio in dehumidifier
W_non_sol_mem_re=(W_sol_mem_re-
W_air_in_re(i))/W0_re;                                  %normalization
of solution membrane humidity ratio in regenerator

h_de=((W_sol_in_de(i)-W_air_in_de(i))/(T_sol_in_de(i)-
T_air_in_de(i)))*(h_fg/cp_air);      %normalization of h* in dehumidifier
h_re=((W_sol_in_re(i)-W_air_in_re(i))/(T_sol_in_re(i)-
T_air_in_re(i)))*(h_fg/cp_air);      %normalization of h* in regenerator


%solve heat and mass transfer in dehumidifier
while (error1>1e-10)||(error2>1e-10)||(error3>1e-10)||(error4>1e-10);

 %the solution side mass equation in dehumidifier
 X_sol_f_de=X_sol_de;
 for a=1:n-1;
    for b=1:m;
        X_sol_de(1,b)=X_sol_in_de(i);  %boundary condition

X_sol_de(a+1,b)=(X_sol_de(a,b)+dy*m_star_de*W0_de*NTU_m_de*((W_non_air_de(a
+1,b))-W_non_sol_mem_de(a+1,b))./(1-
dy*m_star_de*W0_de*NTU_m_de*(W_non_air_de(a+1,b)-W_non_sol_mem_de(a+1,b)));
    end
 end
 error1=sum(sum(abs(X_sol_de-X_sol_f_de)./(X_sol_de)));
 C_sol_de=1./(1+X_sol_de);


 %the solution side energy equation in dehumidifier
 T_sol_f_de=T_sol_de;
 for c=1:n-1;
     for d=1:m;
         T_non_sol_de(1,d)=1;   %boudary condition

T_non_sol_de(c+1,d)=(T_non_sol_de(c,d)+dy*NTU_m_de*h_de*Cr_de*(W_non_air_de
(c+1,d)-
W_non_sol_mem_de(c+1,d))+dy*Cr_de*NTU_de*T_non_air_de(c+1,d))/(1+dy*NTU_de*
Cr_de);
     end
 end
 T_sol_de=T_non_sol_de*(T_sol_in_de(i)-T_air_in_de(i))+T_air_in_de(i);
 error2=sum(sum(abs(T_sol_de-T_sol_f_de)./(T_sol_de)));


 %the air side mass equation in dehumidifier
 W_air_f_de=W_air_de;
 for e_=1:n;
     for f=1:m-1;
```

```
        W_non_air_de(e_,1)=0;   %boundary condition

W_non_air_de(e_,f+1)=(W_non_air_de(e_,f)+dx*NTU_m_de*W_non_sol_mem_de(e_,f+
1))./(1+dx*NTU_m_de);
     end
 end
 W_air_de=W_non_air_de*W0_de+W_air_in_de(i);
 error3=sum(sum(abs(W_air_de-W_air_f_de)./(W_air_de)));


 %the air side energy equation in dehumidifier
 T_air_f_de=T_air_de;
 for g=1:n;
     for h_=1:m-1;
         T_non_air_de(g,1)=0;    %boundary condition

T_non_air_de(g,h_+1)=(T_non_air_de(g,h_)+dx*NTU_de*T_non_sol_de(g,h_+1))./(
1+dx*NTU_de);
     end
 end
 T_air_de=T_non_air_de*(T_sol_in_de(i)-T_air_in_de(i))+T_air_in_de(i);
 error4=sum(sum(abs(T_air_de-T_air_f_de)./(T_air_de)));

 error5=10;


        while (error5>1e-10)

            W_non_sol_mem_f_de=W_non_sol_mem_de;
            C_sol_mem_de=C_sol_de-((NTU_m_de*W0_de*(W_non_air_de-
W_non_sol_mem_de))./(NTU_m_sol_de));  %solve membrane mass equation in
dehumidifier

T_non_sol_mem_de=(NTU_de*T_non_air_de+NTU_m_de*h_de*(W_non_air_de-
W_non_sol_mem_de)+NTU_sol_de*T_non_sol_de)./(NTU_sol_de+NTU_de);
            T_sol_mem_de=T_non_sol_mem_de*(T_sol_in_de(i)-
T_air_in_de(i))+T_air_in_de(i);

            %obtain the new membrane humidity ratio in dehumidifier
            W_sol_mem_de=psychro_LiCl(T_sol_mem_de,C_sol_mem_de);
            W_non_sol_mem_de=(W_sol_mem_de-W_air_in_de(i))/W0_de;

            error5=sum(sum(abs(W_non_sol_mem_de-
W_non_sol_mem_f_de)./(W_non_sol_mem_de)));

        end
end

T_air_out_de(i)=mean(T_air_de(:,m));                              %calculat
e the air outlet temperature in dehumidifier
W_air_out_de(i)=mean(W_air_de(:,m));                              %calculat
e the air outlet humidity ratio in dehumidifier
T_sol_out_de(i)=mean(T_sol_de(n,:));                              %calculat
e the solution outlet temperature in dehumidifier
X_sol_out_de(i)=mean(X_sol_de(n,:));                              %calculat
e the solution outlet mass ratio in dehumidifier
C_sol_out_de(i)=1/(1+X_sol_out_de(i));                            %calculat
e the solution outlet concentration in dehumidifier
```

```
%solve heat and mass transfer in regenerator
while (error6>1e-10)||(error7>1e-10)||(error8>1e-10)||(error9>1e-10);

 %the solution side mass equation in regenerator
 X_sol_f_re=X_sol_re;
 for a=1:n-1;
    for b=1:m;
        X_sol_re(1,b)=X_sol_in_re(i);  %boundary condition

X_sol_re(a+1,b)=(X_sol_re(a,b)+dy*m_star_re*W0_re*NTU_m_re*((W_non_air_re(a
+1,b))-W_non_sol_mem_re(a+1,b))./(1-
dy*m_star_re*W0_re*NTU_m_re*(W_non_air_re(a+1,b)-W_non_sol_mem_re(a+1,b)));
    end
 end
 error6=sum(sum(abs(X_sol_re-X_sol_f_re)./(X_sol_re)));
 C_sol_re=1./(1+X_sol_re);


 %the solution side energy equation in regenerator
 T_sol_f_re=T_sol_re;
 for c=1:n-1;
     for d=1:m;
         T_non_sol_re(1,d)=1;   %boudary condition

T_non_sol_re(c+1,d)=(T_non_sol_re(c,d)+dy*NTU_m_re*h_re*Cr_re*(W_non_air_re
(c+1,d)-
W_non_sol_mem_re(c+1,d))+dy*Cr_re*NTU_re*T_non_air_re(c+1,d))/(1+dy*NTU_re*
Cr_re);
     end
 end
 T_sol_re=T_non_sol_re*(T_sol_in_re(i)-T_air_in_re(i))+T_air_in_re(i);
 error7=sum(sum(abs(T_sol_re-T_sol_f_re)./(T_sol_re)));


 %the air side mass equation in regenerator
 W_air_f_re=W_air_re;
 for e_=1:n;
     for f=1:m-1;
         W_non_air_re(e_,1)=0;   %boundary condition

W_non_air_re(e_,f+1)=(W_non_air_re(e_,f)+dx*NTU_m_re*W_non_sol_mem_re(e_,f+
1))./(1+dx*NTU_m_re);
     end
 end
 W_air_re=W_non_air_re*W0_re+W_air_in_re(i);
 error8=sum(sum(abs(W_air_re-W_air_f_re)./(W_air_re)));


 %the air side energy equation in regenerator
 T_air_f_re=T_air_re;
 for g=1:n;
     for h_=1:m-1;
         T_non_air_re(g,1)=0;    %boundary condition

T_non_air_re(g,h_+1)=(T_non_air_re(g,h_)+dx*NTU_re*T_non_sol_re(g,h_+1))./(
1+dx*NTU_re);
     end
 end
 T_air_re=T_non_air_re*(T_sol_in_re(i)-T_air_in_re(i))+T_air_in_re(i);
```

```
 error9=sum(sum(abs(T_air_re-T_air_f_re)./(T_air_re)));

 error10=10;


         while (error10>1e-10)

             W_non_sol_mem_f_re=W_non_sol_mem_re;
             C_sol_mem_re=C_sol_re-((NTU_m_re*W0_re*(W_non_air_re-
W_non_sol_mem_re))./(NTU_m_sol_re));  %solve membrane mass equation in
regenerator

T_non_sol_mem_re=(NTU_re*T_non_air_re+NTU_m_re*h_re*(W_non_air_re-
W_non_sol_mem_re)+NTU_sol_re*T_non_sol_re)./(NTU_sol_re+NTU_re);
             T_sol_mem_re=T_non_sol_mem_re*(T_sol_in_re(i)-
T_air_in_re(i))+T_air_in_re(i);

             %obtain the new membrane humidity ratio in dehumidifier
             W_sol_mem_re=psychro_LiCl(T_sol_mem_re,C_sol_mem_re);
             W_non_sol_mem_re=(W_sol_mem_re-W_air_in_re(i))/W0_re;

             error10=sum(sum(abs(W_non_sol_mem_re-
W_non_sol_mem_f_re)./(W_non_sol_mem_re)));

         end
end

T_air_out_re(i)=mean(T_air_re(:,m));                %calculate the air
outlet temperature in regenerator
W_air_out_re(i)=mean(W_air_re(:,m));                %calculate the air
humidiity ratio in regenerator
T_sol_out_re(i)=mean(T_sol_re(n,:));                %calculate the solution
outlet temperature in regenerator
X_sol_out_re(i)=mean(X_sol_re(n,:));                %calculate the solution
outlet mass ratio in regenerator
C_sol_out_re(i)=1/(1+X_sol_out_re(i));              %calcualte tje solution
outlet concentration in regenerator

T1(i)=T_sol_out_re(i)-
((effect_1*min(m_sol_de*cp_sol,m_sol_re*cp_sol)*(T_sol_out_re(i)-
T_sol_out_de(i)))/(m_sol_de*cp_sol));
T2(i)=((effect_1*min(m_sol_de*cp_sol,m_sol_re*cp_sol)*(T_sol_out_re(i)-
T_sol_out_de(i)))/(m_sol_re*cp_sol))+T_sol_out_de(i);

T_sol_in_de(i+1)=T1(i)-
((effect_2*min(m_sol_de*cp_sol,m_coldwater*cp_water)*(T1(i)-
T_coldwater_in))/(m_sol_de*cp_sol));
C_sol_in_de(i+1)=C_sol_out_re(i);                   %assign new solution
inlet concentration in dehumidifier
T_sol_in_re(i+1)=((effect_3*min(m_sol_re*cp_sol,m_hotwater*cp_water)*(T_hot
water_in-T2(i)))/(m_sol_re*cp_sol))+T2(i);
C_sol_in_re(i+1)=C_sol_out_de(i);

T_air_in_de(i+1)=T_air_in_de(i);                    %assign new air inlet
temperature in dehumidifier
T_air_in_re(i+1)=T_air_in_re(i);                    %assign new air inlet
temperature in regenerator
```

```
W_air_in_de(i+1)=W_air_in_de(i);
%calculate new air inlet humidity ratio in dehumidifier (kg/kg)
W_air_in_re(i+1)=W_air_in_de(i);
%calculate new air inlet humidity ratio in regenerator (kg/kg)
X_sol_in_de(i+1)=(1-
C_sol_in_de(i+1))/C_sol_in_de(i+1);                    %calculate new
solution inlet mass ratio between water and salt in dehumidifier (%)
X_sol_in_re(i+1)=(1-
C_sol_in_re(i+1))/C_sol_in_re(i+1);                    %calculate new
solution inlet mass ratio between water and salt in dehumidifier (%)
W_sol_in_de(i+1)=psychro_LiCl(T_sol_in_de(i+1),C_sol_in_de(i+1));
%calculate new solution inlet humidity ratio in dehumidifier (kg/kg)
W_sol_in_re(i+1)=psychro_LiCl(T_sol_in_re(i+1),C_sol_in_re(i+1));
%calculate new solution inlet humidity ratio in dehumidifier (kg/kg)


error_T_de=abs(T_sol_in_de(i+1)-T_sol_in_de(i));
error_T_re=abs(T_sol_in_re(i+1)-T_sol_in_re(i));
error_C_de=abs(C_sol_in_de(i+1)-C_sol_in_de(i));
error_C_re=abs(C_sol_in_re(i+1)-C_sol_in_re(i));

i=i+1;

end

m_salt_re=m_sol_re./(1+X_sol_in_re(1));

effect_sen=(T_air_in_de-T_air_out_de(i-1))/(T_air_in_de-T_sol_in_de);
effect_lat=(W_air_in_de-W_air_out_de(i-1))/(W_air_in_de-W_sol_in_de);

MRR=m_air_de*(W_air_in_de(1)-W_air_out_de(i-1));
MAD=m_salt_re*(X_sol_in_re(1)-X_sol_out_re(i-1));
MFR_de=MRR/(U_m*A);
MFR_re=MAD/(U_m*A);

Q_sen=m_air_de*cp_air*(T_air_in_de-T_air_out_de(i-1));
Q_lat=m_air_de*h_fg*(W_air_in_de-W_air_out_de(i-1));
Q_reg=m_sol_de*cp_sol*(T_sol_in_re(i-1)-T2(i-1));
COP=(Q_sen+Q_lat)/Q_reg;
```

Appendix D: Matlab Script for the Mixed LiCl-$CaCl_2$ Solution Properties Calculation

```
function output=psychro_mix(T_sol_in,X_LiCl_in,X_CaCl2_in)
output=(0.62198.*Pv_s(T_sol_in,X_LiCl_in,X_CaCl2_in))./(101325-
Pv_s(T_sol_in,X_LiCl_in,X_CaCl2_in))

 function output1=Pv_s(T_sol_in,X_LiCl_in,X_CaCl2_in)
 output1=Pv_w(T_sol_in)*alfa_w(T_sol_in,X_LiCl_in,X_CaCl2_in)

     function output2=Pv_w(T_sol_in)
         output2=0.61094*exp((17.625*T_sol_in)/(T_sol_in+243.04))*1000
     end
     function output3=alfa_w(T_sol_in,X_LiCl_in,X_CaCl2_in)

output3=X_w(X_LiCl_in,X_CaCl2_in)*f_w(T_sol_in,X_LiCl_in,X_CaCl2_in)
         function output4=X_w(X_LiCl_in,X_CaCl2_in)
             output4=1-X_LiCl_in-X_CaCl2_in
         end
         function output5=f_w(T_sol_in,X_LiCl_in,X_CaCl2_in)

output5=exp(LRC(X_LiCl_in,X_CaCl2_in)+SRC(T_sol_in,X_LiCl_in,X_CaCl2_in))
             function output6=LRC(X_LiCl_in,X_CaCl2_in)

output6=5.829*((X_LiCl_in+3*X_CaCl2_in)/(1+14.9*((X_LiCl_in+3*X_CaCl2_in)^0
.5)))
             end
             function output7=SRC(T_sol_in,X_LiCl_in,X_CaCl2_in)

output7=A(T_sol_in,X_LiCl_in,X_CaCl2_in)+B(T_sol_in,X_LiCl_in,X_CaCl2_in)+C
(T_sol_in,X_LiCl_in,X_CaCl2_in)+D(T_sol_in,X_LiCl_in,X_CaCl2_in)+E(T_sol_in
,X_LiCl_in,X_CaCl2_in)+F(T_sol_in,X_LiCl_in,X_CaCl2_in)
                 function output8=A(T_sol_in,X_LiCl_in,X_CaCl2_in)
                     output8=(2*exp(-0.2*((298.15/(T_sol_in+273.15))*(-
5.1737)))*((298.15/(T_sol_in+273.15))*(-5.1737))*X_LiCl_in+4*exp(-
0.2*((298.15/(T_sol_in+273.15))*(-5.2549)))*((298.15/(T_sol_in+273.15))*(-
5.2549))*X_CaCl2_in)/(1+(2*exp(-0.2*((298.15/(T_sol_in+273.15))*(-
5.1737)))-2)*X_LiCl_in+(4*exp(-0.2*((298.15/(T_sol_in+273.15))*(-5.2549)))-
3)*X_CaCl2_in)
                 end
                 function output9=B(T_sol_in,X_LiCl_in,X_CaCl2_in)
                     output9=((X_LiCl_in*exp(-
0.2*(298.15*10.1242/(T_sol_in+273.15))))*(X_LiCl_in+6*(X_CaCl2_in))*(298.15
*10.1242/(T_sol_in+273.15)))/((1-2*exp(-
0.2*(298.15*10.1242/(T_sol_in+273.15))))*X_LiCl_in+(4-3*exp(-
0.2*(298.15*10.1242/(T_sol_in+273.15))))*X_CaCl2_in+exp(-
0.2*(298.15*10.1242/(T_sol_in+273.15))))
                 end
                 function output10=C(T_sol_in,X_LiCl_in,X_CaCl2_in)
                     output10=((2*X_CaCl2_in*exp(-
0.2*(298.15*10.5126/(T_sol_in+273.15))))*(298.15*10.5126/(T_sol_in+273.15))
*(2*X_LiCl_in+2*X_CaCl2_in))/(((2-2*exp(-
0.2*(298.15*10.5126/(T_sol_in+273.15))))*X_LiCl_in+(2-3*exp(-
0.2*(298.15*10.5126/(T_sol_in+273.15))))*X_CaCl2_in+exp(-
0.2*(298.15*10.5126/(T_sol_in+273.15))))^2)
                 end
```

```
                function output11=D(T_sol_in,X_LiCl_in,X_CaCl2_in)
                    output11=((X_LiCl_in*exp(-
0.2*(298.15/(T_sol_in+273.15)*10.1242)))*(((298.15/(T_sol_in+273.15))*10.12
42)*(X_LiCl_in+2*X_CaCl2_in)))/((X_LiCl_in+2*X_CaCl2_in+exp(-
0.2*(298.15/(T_sol_in+273.15)*10.1242))*(1-X_LiCl_in-X_CaCl2_in))^2)
                end
                function output12=E(T_sol_in,X_LiCl_in,X_CaCl2_in)
                    output12=((2*exp(-
0.2*(298.15/(T_sol_in+273.15))*10.5126)*X_CaCl2_in)*(298.15/(T_sol_in+273.1
5)*10.5126)*(X_LiCl_in+2*X_CaCl2_in))/((X_LiCl_in+2*X_CaCl2_in+exp(-
0.2*(298.15/(T_sol_in+273.15))*10.5126)*(1-X_LiCl_in-X_CaCl2_in))^2)
                end
                function output13=F(T_sol_in,X_LiCl_in,X_CaCl2_in)
                    output13=(-(1-X_LiCl_in-X_CaCl2_in))*(2*exp(-
0.2*(298.15/(T_sol_in+273.15))*(-5.1737))*((298.15/(T_sol_in+273.15))*(-
5.1737))*X_LiCl_in+4*exp(-0.2*(298.15/(T_sol_in+273.15))*(-
5.2549))*((298.15/(T_sol_in+273.15))*(-5.2549))*X_CaCl2_in)/((2*exp(-
0.2*(298.15/(T_sol_in+273.15))*(-5.1737))*X_LiCl_in+4*exp(-
0.2*(298.15/(T_sol_in+273.15))*(-5.2549))*X_CaCl2_in+(1-X_LiCl_in-
X_CaCl2_in))^2)
                end
            end
        end
    end
 end
end
```